Zirconia/Titania Catalysts for Carbon Dioxide Utilisation

By Emad Naji Al-Shafei

A thesis submitted to the University of Huddersfield in partial fulfilment of the requirement for the degree of Doctor of Philosophy

Department of Chemical and Biological Sciences

The University of Huddersfield

2015

University of Huddersfield Repository

Al-Shafei, Emad

Zirconia/titania catalysts for carbon dioxide utilisation

Original Citation

Al-Shafei, Emad (2015) Zirconia/titania catalysts for carbon dioxide utilisation. Doctoral thesis, University of Huddersfield.

This version is available at http://eprints.hud.ac.uk/xxxxx/

CONFERENCE PRESENTATIONS

1. "Dehydrogenation of propane to olefins using CO_2", **Emad Naji Al-Shafei**, Ki-Hyouk Choi, Sai Katikaneni, Rashid Al-Othman and Rob Brown, the 9th Middle East Refining & Petrochemicals Conference and Exhibition (PetroTech 2014), Bahrain, 18-21 May 2014.

2. "CO_2 Utilization: Acetic acid from direct reaction of CO_2", **Emad Naji Al-Shafei**, Ki-Hyouk Choi, Sai Katikaneni, and Rob Brown, H. Golshekan, Ninth (9th) International Chemistry in Industry Conference and Exhibition (CHEMINDIX 2013). Bahrain, 2-6 November 2013.

3. "Direct reaction of CO_2 with C-H bond activation of methane to produce chemicals", **Emad N. Al-Shafei**, Sai P. Katikaneni, Ki-Hyouk Choi and Rob Brown, Catalysts in Petroleum Refining & Petrochemicals 1-2 Dec 2014 (KFUPM, Dhahran, KSA).

4. "Direct carbon-carbon reaction of CO_2 with methane and ethane to produce chemicals", **Emad N. Al-Shafei**, Sai P. Katikaneni, Ki-Hyouk Choi and Rob Brown, The International Conference on Carbon Dioxide Utilization (ICCDU) July 5th to 9th 2015 – Singapore.

ABSTRACT

Reaction and conversion of CO_2 to chemicals is a challenging area of research. The objective of this work is to study and investigate the use of mixed metal oxide Zr/Ti oxide and related catalysts for the conversion and utilisation of CO_2. The first reaction studied was propane dehydrogenation using CO_2 to produce propene. Then, the study extended to investigate the direct reaction of CO_2 as whole molecule with methane, ethane, acetylene, ethylene and propane to synthesis carboxylic acids.

The catalysts were prepared in several ways. Four methods were based on co-precipitation of the mixed catalyst from solutions of zirconium (IV) oxynitrate hydrate and titanium (IV) chloride. Other methods involved impregnation, based on titanium (IV) oxide. Catalysts were characterised by nitrogen adsorption, by powder X-ray diffraction, by ammonia temperature programmed desorption and, ultimately, in terms of catalytic activities.

The powder X-ray diffraction patterns of the impregnated titania-rich Zr/Ti oxide catalysts showed that ZrO_2 dissolved in the solid anatase phase of titania. At higher concentrations, the ZrO_2 appeared as a separate tetragonal phase. Low zirconia content Zr/Ti oxide catalysts showed significantly increased surface areas and higher acidities than the individual oxides. A range of other metal oxides were added as third metal oxides in these mixtures, but none had significant impacts on surface areas or on surface acidities.

Propane dehydrogenation is thermodynamically limited. The only possible route is a radical mechanism for H_2 removal via a surface process. The catalytic activities at low CO_2:propane ratio showed that Zr/Ti oxide exhibited the higher activity than single oxides, but activities were all too low to be of economic significance.

In contrast, using higher CO_2:propane ratio improved the propene yield and selectivity to values comparable to those achieved with the industrial chromium based catalyst.

The catalyst showed selectivity to C-H bond breaking to form propene over C-C bond breaking to make ethene. The study demonstrated that CO_2 was utilised mainly for the reverse water gas shift reaction (RWGS) to remove hydrogen from the catalyst surface.

The study showed that the Zr/Ti oxide catalysts exhibited higher stability compared to the industrial catalysts at slightly higher gas space velocity. Thermogravimetric analysis showed that Zr/Ti oxide catalyst assists coke gasification in the presence of CO_2 at 600 ^{o}C.

The other mixed oxide catalysts generally showed lower surface acidities and higher selectivities to C-C bond breaking products over the desired propene product.

The second study was the direct reaction of CO_2 with CH_4 to produce acetic acid. Again, this reaction is thermodynamically unfavourable and the only possible route must involve a radical species by which reactants are concentrated on the catalyst surface. Evidence of methyl surface species formation in the presence of methane was indeed found over the Zr/Ti oxide catalyst. With CO_2 methane reacted with CO_2 to form acetic acid over Zr/Ti oxide catalysts. The C-C insertion mechanism is proposed by which methyl surface species formed on the catalyst and reacted with CO_2. This was followed by hydrogenation to form acetic acid.

Reactions of CO_2 with ethane, ethylene, acetylene and propene were also studied, in the hope of observing direct insertion to produce the corresponding carboxylic acid. In fact, lower acids were formed in all cases, suggesting a radical mechanism involving C-C bond breaking over Zr/Ti oxide catalyst.

Interestingly, acetic acid was formed with all these precursor hydrocarbons, and it appears that it occurs via C≡C, C=C, C-C and C-H bond breaking.

DEDICATION

I would like to dedicate my work to my loving wife, Dr. Eman and my sons Ahmed, Aqeel, Ali and daughter Sarah.

and

I would like also to dedicate my work to my father Naji and mother Salma for their pray and support. The achievement that I had is a result of their excellence parenting.

ACKNOWLEDGEMENTS

TABLE OF CONTENTS

CHAPTER 1

OBJECTIVE, BACKGROUND AND LITERATURE REVIEW

Table of content

1.1 Introduction

1.1.1 Background

Carbon dioxide is one of the major worldwide environmental concerns due to its emission that exceeds 10 gigatonne/year to the atmosphere according to the United Nations Framework Convention on Climate Change (UNFCCC)[1-2]. The CO_2 level in the atmosphere has increased to reach 386 ppm in 2013 according to the historic atmosphere analysis[3].

Utilisation of CO_2 is one of the major challenges for CO_2 research. The reactions of CO_2 are mostly endothermic because of the stability of CO_2. Therefore, a substantial input of energy is required. In addition, suitable catalysts are important in order to react CO_2 in organic synthesis[4].

There are several ways in which CO_2 can react:

1- CO_2 reacts as a whole molecule (**section 1.1.2**).
2- CO_2 reacts through dissociating to CO and an O atom. The CO reacts to form the product (**section 1.1.3**).
3- CO_2 reacts by dissociating to a C atom and O_2. The C atom reacts with H atoms in order to form the product (**section 1.1.4**).

1.1.2 Whole molecule CO_2 reaction

The following are examples of CO_2 reacting as a whole molecule (Table 1.1):

Table 1.1. CO_2 reaction as a whole molecule

Chemical	Reaction and equation
Urea	Urea reaction proceeds first between a carbon on CO_2 and nitrogen on NH_3. The reaction is exothermic at high pressure of 240 bar and 185-190 ^oC to form ammonium carbamate as equation (1.1) [5]. $2NH_3 + CO_2 \rightarrow H_2NCOONH_4$ ...... Eq. (1.1) Then ammonium carbamate decomposes endothermically to form urea and water at reduced pressure (equation 1.2): $2NH_3 + CO_2 \rightarrow H_2NCOONH_4 \rightarrow H_2NCONH_2 + H_2O$ ..... Eq. (1.2)[5]
Salicylic acid	Phenol reacts with a whole molecule of CO_2 in the presence of NaOH at a pressure of ~100 bar and at 110 ^oC. The C atom of CO_2 reacts with phenol. The reaction produces sodium salicylate. Then, under strong acidic conditions, salicylic acid is formed (equation 1.3) [6]. Eq. (1.3)
Ethene carbonate	Ethene carbonate is made from ethene oxide and CO_2 (equation (1.4)). The process has been commercialized by BASF. The reaction occurs between an O atom of CO_2 and a C atom of ethene oxide. Then ring closure by C atom of CO_2 with the O atom of ethane oxide forms the cyclic ethene carbonate[7]. ..... Eq. (1.4)

Propene carbonate	Propene carbonate forms by reaction between CO_2 and propene oxide (equation (1.5)). In addition, propene glycol also reacts with CO_2 to from propene carbonate (equation 1.6) [8].
	
	  ..... Eq. (1.5)
	
	  ...Eq. (1.6)

Dimethyl carbonate and diethyl carbonate	Dimethyl carbonate and diethyl carbonate formation are discussed widely. CO_2 reacts with methanol or ethanol at 110-200 °C and a pressure of 10 - 80 bar (equations 1.7[9] and 1.8[10]):
	
	  ..... Eq. (1.7)
	
	  .. Eq. (1.8)

Formic acid via an electrochemical route	CO_2 is reduced electrochemically to CO_2^{2-} which reacts with hydrogen cations (H^+) from water to form formic acid (equation 1.9) [11]. $CO_{2\ (g)} + 2H^+_{(aq)} + 2e^- \rightarrow HCOOH_{(aq)}$ ..... Eq. (1.9)

1.1.3 Reaction by dissociation of CO_2 to CO and O atom

Table 1.2 lists the common chemical reactions that follow dissociation of CO_2 to CO and an O atom:

Table 1.2. CO_2 reaction as CO and O

Chemical	Reaction and equation
Dry reforming of CO_2	Dry reforming of CO_2 with CH_4 occurs over suitable catalysts as illustrated in equation (1.10). $$CO_2 + CH_4 \rightarrow 2CO + 2H_2 \ ..... \ Eq. \ (1.10)$$
Reverse water gas-shift (RWGS)	At high temperature over selected catalysts, CO_2 reacts with H_2 to produce CO and H_2O (equation 1.11[12]). $$CO_2 + H_2 \rightarrow CO + H_2O \ ..... \ Eq. \ (1.11)$$
Hydrogenation of CO_2 to methanol	On Zn-Cu catalyst CO_2 reacts with H_2 at a pressure of over 20 bar and 250-350 ^oC (equation 1.12[13]). The hydrogenation of CO_2 has been commercialized by BP Chemicals. $$CO_2 + 3H_2 \rightarrow CH_3OH + H_2O \ ..... \ Eq. \ (1.12)$$
Dehydrogenation of propane by CO_2	CO_2 has been studied as a mild oxidant for propane and ethane as an alternative to using oxygen (equation 1.13[14]). $$C_3H_8 + CO_2 \rightarrow C_3H_6 + CO + H_2O \ ..... \ Eq. \ (1.13)$$
Electrochemical route: CO and methanol	CO_2 can be reduced electrochemically to CO and reacted with H^+ in water to produce CO or methanol (equation 1.14[15] and 1.15 [16]). $CO_{2 \ (g)} + 2H^+_{(aq)} + 2e^- \rightarrow CO_{(g)} + H_2O_{(l)}$, $E^o = $ -0.52 V Eq. (1.14) or $2CO_{2 \ (g)} + 6H^+_{(aq)} + 6e^- \rightarrow CH_3OH_{(l)} + H_2O_{(l)}$, $E^o = $ -0.38 V Eq.(1.15)

1.1.4 Reaction by dissociation of CO_2 to C and O_2

Several researchers have studied CO_2 utilisation in which the CO_2 molecule dissociates to a C atom and O_2. Table 1.3 lists the common reactions:

Table 1.3. CO_2 reaction as to C and O_2

Chemical	Reaction and equation
Hydrogenation of CO_2 to methane	CO_2 reacts with H_2 gas over Cu/ZrO_2 catalyst at 450-750 ^oC to form methane (equation 1.16[17]). $$CO_2 + 4H_2 \rightarrow CH_4 + 2H_2O \ ..... \ Eq. \ (1.16)$$
Electrochemical route: CO_2 to ethylene	Using polymer electrolyte membrane (PEM) CO_2 can be reduced in the presence of H^+ cations to form ethylene (equation 1.17)[16,18-19]. $$2CO_{2(g)} + 12H^+_{(aq)} + 12e^- \rightarrow C_2H_{4 \ (g)} + 4H_2O_{(l)}, \ E^o = -0.169 \ V$$ $$.... \ Eq. \ (1.17)$$

1.1.5 Carbon dioxide interaction with solid surface

CO_2 has closed shells according to the octet rule. The C atom is sp hybridized and the CO_2 molecule exhibits strong bonds[19]. Scibioh *et al.* [20] described the adsorption of CO_2 on transition metal catalysts pointing out the complexity of the process. Markovits *et al.* [21] described CO_2 in term of weakly basic oxygen atoms and an acidic carbon atom. A study of the interaction between CO_2 and some transition metal surfaces showed that the CO_2 molecule adsorption has several feasible modes of coordination as shown in Figure 1.1[19],[22].

Figure 1.1. Modes of coordination of CO_2[19]

1.1.6 ZrO$_2$ and TiO$_2$ Catalyst

Several studies discussed the unique composition of mixed oxide catalysts formed between ZrO_2 and TiO_2[25]. The catalysts are reported to have better catalytic activity for several CO_2 reactions due to the acidic and basic properties of the Zr–O–Ti catalytic system compared to the single oxides, TiO_2 or ZrO_2[23-25].

Manríquez *et al.*[24] studied the bifunctional acid-base characteristic of mixed oxide ZrO_2-TiO_2. They studied the mixed oxides by FTIR to study CO_2 adsorption on ZrO_2-TiO_2 catalysts calcined at 400 ^{o}C to probe basic sites independent. . The catalysts 90% TiO_2 – 10% ZrO_2 and 10% TiO_2 – 90% ZrO_2 showed monodentate (1578-1359 cm^{-1}) and bidentate (1672, 1243, 1053 cm^{-1}) binding of CO_2 (Figure 1.2), characteristic of significantly basic sites on the ZrO_2-TiO_2 catalysts.

Figure 1.2 . The main types of CO_2 coordination on ZrO_2-TiO_2 detected by FTIR[24]

The acidity of these ZrO_2-TiO_2 catalyst was determined by temperature programmed desorption of ammonia (NH_3-TPD) and FTIR of adsorption pyridine (Manríquez *et al.* [24]). The results of NH_3-TPD are summarized in Table 1.4. It can be seen that the mixed oxides exhibit much more acidity than the individual oxides. Pyridine FTIR experiment demonstrated the presence of acidic Lewis sites and no acidic Brønsted sites on to the mixed oxides catalyst. The study concluded that binary oxides ZrO_2-TiO_2 has both acidic and basic sites[24]. The study also showed that the acid strength of the catalysts was reduced by high temperature calcination.

Table 1.4. NH3-TPD desorption result of ZrO_2-TiO_2 calcined at 400 [24]

Catalysts	µmol NH_3/g calculated from the ammonia thermodesorption curves
TiO_2	173
TiO_2-ZrO_2 (90-10)	1326
TiO_2-ZrO_2 (50-50)	1456
ZrO_2	138

The crystalline structure has been studied by powder X-ray diffraction (XRD) of the single oxides ZrO_2 and TiO_2, and the mixed oxides. For example, Santos *et al.* [26] studied the XRD of ZrO_2/TiO_2 in molar ratio 1:1 after calcination at 500, 600 and 700 ℃. A mixture of amorphous and orthorhombic phases of ZrO_2/TiO_2 was detected at 500 and 600 ℃, whereas a pure orthorhombic phase of was detected on calcination at 700 ℃.

Neppolian *et al.*[27], Vishwanatha *at al.*[28] and Pérez-Hernández *et al.*[25] studied different weight loadings of ZrO_2 on TiO_2, from 5%, 12%, 33% to 50% [27]. In addition, they studied doping TiO_2 on ZrO_2 at levels of 5%, 10%, 20%, 30% to 40%. All catalysts were prepared by the sol–gel method. The calcination temperature was 500 ℃. Powder XRD results are summarised below.

- 5 wt% TiO_2 doped on ZrO_2 showed XRD peaks of tetragonal ZrO_2 and no anatase peaks of TiO_2.
- 10% TiO_2 doped in ZrO_2 showed the same, with no evidence of a pure TiO_2 phase and only peaks of tetragonal ZrO_2.
- At 20% TiO_2 loading anatase peaks started to appear with tetragonal peaks of ZrO_2.
- When doping ZrO_2 on TiO_2, tetragonal ZrO_2 reflections were visible at all loadings from 5 to 33%, along with anatase reflections.

Catalytic activities of these ZrO_2/TiO_2 catalysts for methane coupling reactions to form ethane and ethene (no CO_2) were reported. (1.18) [29-31]. This reaction requires C-H bond breaking to form methyl ($CH_{3(ads)}$) and methylene ($CH_{2(ads)}$) surface species on the catalyst surface. The fact that these catalysts can promote surface species formation may be relevant to reactions that involve CO_2.

$$4CH_4 \rightarrow CH_3\text{-}CH_3 + CH_2=CH_2 +3H_2 \qquad \text{(eq. 1.18)}$$

Reddy and Khan review, ZrO_2/TiO_2 catalysts used for several reactions for isomerisation of methyl cyclohexene oxide, non-oxidative dehydrogenation cyclohexane and ethylbenzene, the epoxidation of cyclooctane, and the synthesis of chlorobenzene [32]. The TiO_2–ZrO_2 catalyst has been used for the dehydrocyclization reaction of C6–C8 n-paraffins. The catalyst was shown to exhibit both acidity and basicity in these reactions [33].

In other related work, catalysts have been prepared by adding a third oxide or other compound to ZrO_2-TiO_2. Activities of these in various reactions are also relevant to their potential use in CO_2 reactions. Sulphated ZrO_2-TiO_2 oxides are used for cumene synthesis by isopropylation of benzene with isopropanol [34].

B_2O_3/TiO_2–ZrO_2 catalysts are active in the production of lactams from oximes, which requires surface acidity. The acidity of these B_2O_3 catalysts was shown to be dependent on the catalyst calcination temperature [35].

In the presence of CO_2, catalysts based on TiO_2 with metal oxide dopant such as Rh, Ru, Pd, Pt, Ir, and K have been used for dry reforming to produce CO and H_2 [36]. A methanation reaction (hydrogenation of CO_2 to CH_4) has been reported over ZrO_2 doped with NiO (equation 1.19) [37]. Methanation (hydrogenation of CO_2 to methanol) has also been reported on CuO/ZrO_2 catalysts (Eq. 1.20)[13].

$$CO_2 +4H_2 \rightarrow CH_4 + 2H_2O, \quad \Delta H_{298} \text{ -165 kJ mol-1} \qquad \text{(eq. 1.19)}$$

$$CO_2 + 3H_2 \rightarrow CH_3OH + H_2O \ \ ..... \ Eq. \ (1.20)$$

Several CO_2 reactions have used ZrO_2 as a main metal oxide component of the catalysts. Dimethyl carbonate (DMC) from CO_2 and methanol synthesis utilises ZrO_2 and CeO at 100-200 ^oC and 2.5 MPa (equation 1.7)[9]. Also, the catalyst $CuO–TiO_2–ZrO_2$ was used for the synthesis of dimethyl ether (DME) from CO_2 at 350 ^oC and 4 MPa [38].

Dehydrogenation reactions have been reported with CO_2, and sometimes without CO_2, over catalysts based on ZrO_2, TiO_2 and $TiO_2–ZrO_2$[39-40]. CO_2 was used for oxidative dehydrogenation of ethylbenzene to styrene at 660 ^oC. The CO_2 acted as a soft oxidant over $TiO_2–ZrO_2$ and $CeO_2/TiO_2–ZrO_2$, $V_2O_5/TiO_2–ZrO_2$, $CeO_2–V_2O_5/TiO_2–ZrO_2$[39] and 3% K_2O/TiO_2-ZrO_2[40]. The $TiO_2–ZrO_2$ catalyst showed activity and stability for 10 hours [39-40]. However, they emphasised that it might be the CO_2 itself that gives the catalyst high stability. The proposed mechanism involves the simple dehydrogenation of ethylbenzene on the catalyst surface followed by CO_2 reacting with H atoms on the catalysts surface via a reverse water gas shift reaction (RWGS) as shown in equations (1.21 and 1.22) [39-40]:

Dehydrogenation: $C_6H_5CH_2CH_3 \rightarrow C_6H_5CH=CH_2 + 2H_{(ads)}$ equation (1.21)

RWGS: $2H_{(ads)} + CO_2 \rightarrow CO + H_2O$ equation (1.22)

CO_2 has been used for the dehydrogenation of p-ethyltoluene to p-methylstyrene over $TiO_2–ZrO_2$ and K_2O doped on $TiO_2–ZrO_2$. The reaction showed 85% selectivity to p-methylstyrene but low conversion of CO_2 of 11% [41].

Several papers report CO_2 utilisation for propane dehydrogenation using ZrO_2 and TiO_2 support catalysts. Xu *et al.* [42] described TiO_2 and ZrO_2 supported gallium oxide. But propane dehydrogenation in the presence of CO_2 gave only 22% propene yield. Catalytic stability was poor and dry reforming dominated.

CO_2 has been utilised for oxidative dehydrogenation (ODH) of n-butane at 600 ^oC over the mixed metal oxides $VO_x/CeO_2–ZrO_2$, $VO_x/TiO_2–ZrO_2$ and $CeO_2–ZrO_2$[43]. The paper suggested the CO_2 role was as a soft oxidant for butane gas and CO_2 dissociated to CO and O which was responsible for re-oxidation of the catalyst after reaction[43].

Several papers discussed the dehydrogenation of ethane with CO_2 using Cr, Ga, Mn, Co, Fe and Ce oxides doped on TiO_2 or ZrO_2 [44-46]. They reported that the dopants on ZrO_2 exhibited strong acidity and/or basicity and these dopants were in general fully dispersed on the tetragonal ZrO_2 phase [44],[47].

The overall conclusion found that ZrO_2, TiO_2 and especially a ZrO_2-TiO_2 mixture, could potentially show activity in a dehydrogenation reaction with CO_2. Evidence of high acidity, basicity and bifunctional reactivity might be expected to lead to high activity in these reactions. However, to date, these catalysts have not been fully studied for the use of CO_2 for propane dehydrogenation.   This reaction is studied in the work described in this thesis (**Chapter 3**).   The presence of both acidity and basicity, certainly on ZrO_2/TiO_2 catalysts, may also be important for the direct reaction of CO_2 with methane and other hydrocarbons to synthesise acetic acid. This reaction is studied in the work reported in **Chapter 4**.

1.2 Objectives

The main objective of the work described in this thesis is to study the conversion and utilisation of CO_2 for the formulation of valuable hydrocarbons using heterogeneous catalysts of mixed zirconia–titania. This research studies the CO_2 reaction for the dehydrogenation of propane to propene (**chapter 3**). In addition, the study explores the CO_2 reaction with methane, ethane, ethylene, acetylene and propane gases to formulate acetic acid (**chapter 4**). The following are the detailed research objectives:

1. **The first objective** is to study the CO_2 utilisation for olefin synthesis through the dehydrogenation of propane to propene (**chapter 3**). The research will explore the following:

- the activities of mixed binary and ternary metal oxide catalysts based on zirconia–titania (ZrO_2-TiO_2) and on titania (TiO_2) towards the dehydrogenation of propane,
- the catalytic stability of these in the conversion of propane.
- the effect of reactant composition (CO_2/propane ratio) on the yield of propene,
- the effect of the reactor temperature on the selectivity to propene,
- competing reactions, such dry reforming and the reverse water gas shift reaction,
- the characterization of these catalysts and the relationship between their activities and their structure/surface properties.

2. **The second objective** is to study the direct reaction of CO_2 with methane, ethane, ethylene, acetylene and propane gases to make acetic acid (**chapter 4**). The study will investigate and develop a series of binary and ternary heterogeneous catalysts for the direct reaction of CO_2 as follows:

- the effect of catalyst preparation methods,
- the effect of reactant gas composition,
- the activities of the catalysts towards C-C and C-H bond breaking in the presence of CO_2.
- the reaction mechanism of direct reaction of CO_2 with hydrocarbons,
- the characterization of these catalysts and the relationship between their activities and their structure/surface properties.

1.3 Dehydrogenation of propane by CO_2

The detailed results and finding of the propane dehydrogenation by CO_2 are shown in **chapter 3**.

1.3.1 Introduction

Propene (propylene) is one of the main basic petrochemical feedstock and the demand has increased sharply to the point that it exceeds ethene (ethylene) demand in this decade. Propene is used in the synthesis of many polymers, such as polypropene, polyacrylonitrile, and important propene derivatives are used to form cumene, acrylonitrile for acrylic fibers, isopropyl alcohol, acrylic acid for acrylates and propene oxide for polyethers or propene glycols [48-50].

1.3.2 Conventional method of making propene

Propene is a co-product from steam cracking plants. It is estimated that 68% of all propene comes from this source. However, it is invariably produced in lower abundance than ethene with and propene/ethene ratios are typically from 0.019 to 0.632 [51]. The steam cracking plants are not very selective as seen in Table (1.5). The conditions used in the plant can be adjusted to control propene yield to a limited extent. The propene yield is normally between 0.15 and 16% at 750 °C as shown in Table 1.5. It is also worth mentioning another current source of propene and that is as a product from fluid catalytic cracking (FCC) although, again, it is only ever a minor product (perhaps 15% yield from a naphtha source) [51].

Table 1.5. Steam cracking of different feeds stock and propene yield [51]

Feed of steam cracking plant	Propene yield %	Propene / Ethene ratio
Ethane gas feed	1.5 %	0.019
Propane gas	14 %	0.294
n-butane gas	16 %	0.364
Light naphtha	15 - 16%	0.421
Gas oil	15 -16 %	0.632

1.3.3 On-purpose propene plants

Higher propene yields can be achieved using "on-purpose" propene plants. These use mainly propane dehydrogenation and metathesis routes. According to a report published by Nexant in 2007, the growth of propane dehydrogenation plants could result in an increase in propene production by five times [51].

1.3.4 Commercial propane dehydrogenation (PDH)

Propane dehydrogenation is an endothermic equilibrium reaction. At reaction temperatures of 550-650 °C, there are thermodynamic limitations to PDH. Several methods have been used to overcome these thermodynamic limitations by addition of oxygen gas mixes with propane [52] or use of oxidative catalysts [51].

The petrochemical industry uses two types of PDH plant for propene production.

1. **Oxidative propene plant:** Lumms, Linde-BASF and Sanamporgetti-Yarsintez use an oxidative catalyst for propane dehydrogenation to propene, based on chromium oxide doped on an alumina support. These catalysts require regenerating after half an hour using steam and air to remove coke and to increase the chromium oxidation state back to its original value as shown in equation (1.23) and (1.24). The plant operates at 550-700 °C, for both the reaction and the catalyst regeneration step, and the space velocity of the reaction is low, between 0.8-2 h^{-1}. The yield of propene from the oxidative method is 30-35% and propane conversion is 35-45% [51].

Oxidation by Cr(V, VI)O$_x$ of C$_3$H$_8$: $C_3H_8 \xrightarrow[\text{In absence of air}]{550-600\,C} C_3H_6 + H_2O$ ..eq (1.23)

Regeneration Cr(III, IV)O$_x$: $Cr^{3+,4+}O_x \xrightarrow[\text{In presence of air}]{550-700\,C} Cr(V, VI)O_x$ ..eq (1.24)

2. **Non-oxidative plant:** UOP and Krupp Uhde use platinum mixed with oxides of zinc or tungsten doped on alumina. The space velocity is slightly

higher at 2-6 h^{-1} and the propene yield is 30%. The Pt-W or Pt-Zn catalyst works by abstraction of hydrogen from propane on the catalyst surface at 550-700 °C as shown in equation (1.25). But the catalyst deactivates quickly by coking [53].

$$C_3H_8 \xrightarrow{550-700\ C} C_3H_6 + H_2 \quad ....eq\ (1.25)$$

Both routes involve low catalytic stability, propene yield is limited to 30-35%, deactivation occurs in less than half an hour and they require low space velocities. Many researchers have tried to address the problem of catalyst deactivation by introducing O_2 [52] or CO_2 [48] to have in-situ catalyst regeneration.

1.3.5 Literature review of research into propane dehydrogenation by CO_2

The dehydrogenation of propane by CO_2 has been studied by many researchers to assist the regeneration of the catalysts and also as part of a non-oxidative route [49]. The use of CO_2 for these reactions, rather than oxygen, has advantage of low cost. Because reactions tend to generate less heat with CO_2, and CO_2 is a mild oxidant, there are also advantage in avoiding hot spots on solid catalysts [48],[50],[54].

Propane dehydrogenation is divided into:

1. **Oxidative propane dehydrogenation by CO_2,**
2. **Non-oxidative propane dehydrogenation by CO_2.**

1. **Oxidative propane dehydrogenation via CO_2:** Dehydrogenation proceeds by donation of an O atom from the chromium oxide catalyst to propane to form propene, CO and water [48],[50]. CO_2 is reported to then re-activate chromium oxide via redox cycling mechanisms from Cr(III, IV)O_x to Cr(V, VI)O_x by oxygen addition, producing CO (equation 1.26) [48]. In fact, several metal oxides, such as those of Fe, V, Ce and Mn, can also take part in the oxidative reaction of propane [54].

Cr(III, IV)O$_x$ regeneration by CO$_2$: Cr(III, IV)O$_x$ +CO$_2$ $\xrightarrow{550-600\,C}$ Cr(V, VI)O$_x$ + CO .eq (1.26)

2. **Non-oxidative propane dehydrogenation via CO$_2$:** it proceeds in two steps to achieve the complete dehydrogenation cycle, maintaining the catalyst surface activity.

   - First the propane couples on the catalyst surface and is dehydrogenated as shown in the equation (1.27).
   - Then CO$_2$ removes H$_2$ from the catalyst surface (equation (1.28)).

The overall non-oxidative reaction is in equation (1.29)[48]. Kuśtrowski et al.[49] emphasized that the RWGS reaction removes hydrogen from the surface and that makes catalytic sites available for further dehydrogenation of propane [55-56]. This RWGS reaction is key to ensuring that the overall reaction proceeds (equation (1.28)). It is also important to note that, in addition, CO$_2$ can play another role by reducing the coke on the catalyst surface by a coke gasification reaction as shown in equation (1.30).

Propane dehydrogenation on catalyst surface:	C$_3$H$_8$ → C$_3$H$_6$ + H$_{2(ads)}$	Eq. 1.27
Consumed H atoms by RWGS from catalysts:	CO$_2$ + 2H$_{(ads)}$ → CO + H$_2$O	Eq. 1.28
Overall dehydrogenation by CO$_2$:	C$_3$H$_8$ + CO$_2$ → C$_3$H$_6$ + CO + H$_2$O	Eq. 1.29
Coke gasification:	CO$_2$ + C$_{(coke)(ads)}$ → 2CO	Eq. 1.30

The following is a more detailed discussion of the main papers describing the two reaction types responsible for dehydrogenation of propane by CO$_2$.

1.3.5.1 Oxidative propane dehydrogenation via CO₂

Michorczyk *et al.* published several papers using CrO_x and FeO_x catalysts doped on silica and alumina for propane dehydrogenation by CO_2. They used a reaction temperature of 600 °C and a CO_2/propane ratio of 3:1[57]. Low propene yields of around 10% were measured over both catalysts, although this accounted for most of the propane conversion. Both catalysts were deactivated quickly and coke deposition was reported[57].

Higher propene yields were reported by Botavina *et al.* [58] over 6% Cr_2O_3 on SiO_2 at 600 °C with CO_2/propane of 3:1 but activity halved after 5 hours. Conclusions were reached on the importance of the oxidation state of the chromium needed for catalysis. (i.e Cr(V, VI)).

Another study was performed by UOP on the effect of CO_2/propane ratios, from 0:1 to 3:1 on 5% $Cr(V,VI)O_x$ impregnated on SiO_2 at a temperature of 600 °C and space velocity of 4 h^{-1}. The propene yield and selectivity increased with increasing CO_2 concentration[55].

Shishido *et al.* [59] studied the role of chromium oxide as a catalyst impregnated on silica and alumina. They found that under oxidative conditions, there was some loss in activity, with the propene yield only falling from 16% to 14% over 3 h at 550 °C. This compared with a fall to 11.5% over 2 h in the absence of CO_2. They concluded that CO_2 is responsible for the regeneration of the higher oxidation state chromium centres that are the catalytically active sites.

Kuśtrowski *et al.* [49] studied chromium oxide on activated carbon under oxidative conditions and again found that the catalyst deactivated quickly. Takehira *et al.* [54] studied the oxides of Cr, Fe, V, Mn, and Co supported on MCM-41. CrO_x-MCM-41 (Si/Al ratio of 50) was reported stable for propane dehydrogenation by CO_2 for 3 hours. After catalyst regeneration (by air), the conversion was reduced from 20% to 15%[60]. In

another study, an MSU-1 (a type of mesoporous molecular sieve)was used as a support for CrO_x Liu *et al.* [60] at 600 ^{o}C (gas ratio CO_2/propane 3:1) and propane conversion of 8% with propene selectivity at 82-92% was stable for more than three hours.

Zhu *et al.* reported Cr oxide on MFI zeolite to be a very stable catalyst for propane dehydrogenation, giving propane conversion at 30%, which gradually decreased to 8% with high selectivity to propene over 66 hours using CO_2, at space velocity 1.1 h^{-1} [61]. The authors suggested the active species Cr(III, VI) was responsible not Cr(V, VI).

The overall conclusion is that in oxidative propane dehydrogenation, CO_2 performs important role is to re-oxidise chromium to the active oxidation state. But the RWGS reaction and formation of by-product H_2 is observed and it is not clear identified role for oxidative catalyst. In addition, they reported formation of CH_4, ethane and ethene is evidence of C-C bond breaking of propane associated with oxidative dehydrogenation (more discussion in **section 1.3.6**).

1.3.5.2 Non-oxidative propane dehydrogenation via CO$_2$

Non-oxidative propane dehydrogenation via CO_2 has also been reported. Dury *et al.*[62] discussed Ni-Mo oxide catalysts. In addition, three papers were published by Fudan University in China on this topic. They conducted experiments on non-oxidative and oxidative catalysts [63-65]. The first study, which was published in 2010, was on non-oxidative catalysts made up of mixed metal oxides with In_2O_3 for propane dehydrogenation by CO_2. The catalyst 20% In_2O_3 on Al_2O_3 showed the highest propene yield at 25% for 12 hours (gas ratio CO_2/N_2/propane 4:35:1 at 600 ^{o}C)[64]. The selectivity to propene was >75% and the catalysts could be regenerated effectively. The mechanism involved propane coupling on the catalyst surface and CO_2 reacting with adsorbed H atoms on the surface via the reverse water gas shift reaction[63].

The study was extended to In_2O_3 supported on SiO_2, Al_2O_3 and ZrO_2[65]. Interestingly the In_2O_3-Al_2O_3 had the highest propene yield. NH_3-TPD and CO_2-TPD measurements showed the In-Zr catalyst to have the highest concentration strong acid and base sites. It appears that the moderate strength acid and basic sites of In_2O_3-Al_2O_3 provide optimum activity [65].

Another non-oxidative catalyst ZnO/ZSM-5 was studied by Fudan University for the dehydrogenation of propane via CO_2 [50],[66]. There appeared to be some dependence of activity on the acidity of the zeolite, showing variation with the Si/Al ratio of the zeolite, again with the medium acidity support resulting in optimum activity [66-67]. The authors proposed a mechanism involving propane coupling as the $C_3H_7^-$ anion (Figure 1.2) and they emphasized that the presence of CO_2 improved the catalyst surface stability and catalytic stability by ensuring effective removal of adsorbed H_2 from the surface by the reverse water gas shift (RWGS) reaction.

$$^-H_7C_3 \quad H^+ \qquad\qquad ^-H \quad H^+$$
$$| \quad\quad | \qquad\qquad\quad | \quad\quad |$$
$$Zn^{2+}O^{2-} + C_3H_8 \;\rightarrow\; Zn^{2+}O^{2-} \;\rightarrow\; Zn^{2+}O^{2-} + C_3H_6$$

Figure 1.2. The suggested mechanism of dehydrogenation reaction via coupling of propane[50]

Another non-oxidative catalyst for propane dehydrogenation with CO_2 reported by Xu *et al.* [68] was gallium oxide doped on TiO_2, Al_2O_3, ZrO_2, SiO_2, and MgO. They characterized the catalysts by XRD, XPS, and TPR-CO_2. The XPS suggested the dehydrogenation is effected via a heterolytic dissociation reaction pathway (Figure 1.3) and that adsorbed H_2 is then removed by reaction with CO_2 (via RWGS). This proposed reaction mechanism is different from that described by Zhang *et al.*[50] and shown in Figure 1.2 in that the propane coupling is via the alkyl cation rather than the alkyl anion.

$$\overset{\overset{\displaystyle H^-\quad C_3H_7{}^+}{\displaystyle |\qquad |}}{Ga^{x+}O^{2-}-M^{y+}+C_3H_8} \rightarrow \overset{\overset{\displaystyle {}^-H\quad H^+}{\displaystyle |\qquad |}}{Ga^{x+}O^{2-}-M^{y+}+} \rightarrow Ga^{x+}O^{2-}-M^{y+}+\ C_3H_6$$

Figure 1.3. The proposed mechanism of the heterolytical dissociation of C_3H_8 on Ga_2O_3[68]

Despite relatively promising results in terms of propane conversion and propene selectivity for the catalysts described above, it is very important to note that they have invariably been used with reactant feeds in which propane has been very dilute, typically 5% or less, and these levels are of little practical value for commercial application.

Several workers, including Michorczyk et al.[48], have shown that there are always byproducts from both oxidative and non-oxidative propane dehydrogenation reactions. For instance, they observed the non-oxidative pathway usually led to some C-C bond breaking of propane to form methane, ethane, ethylene and (hydrogenation of ethylene to ethane) as shown in equations (1.31), (1.32), and (1.33) [48].

Cracking of propane to ethane and methane by non-oxidative pathway by Cr^{3+}

$$C_3H_6 \xrightarrow{+H_2} C_2H_4 + CH_4 \qquad\qquad \text{Eq. (1.31)}$$

Non-oxidative pathway of ethylene to ethane by Cr^{3+}

$$C_2H_4 \xrightarrow{+H_2} C_2H_6 \qquad\qquad \text{Eq. (1.32)}$$

Non-oxidative pathway of ethylene to methane by Cr^{3+}

$$C_2H_4 \xrightarrow{+2H_2} 2CH_4 \qquad\qquad \text{Eq. (1.33)}$$

1.3.6 Summary of current knowledge of catalysts for propane dehydrogenation by CO_2

In general, to date, the major problems associated with oxidative catalysts have been their low been shown low catalytic stabilities and their rapid deactivation. For the most widely used catalysts based on chromium oxide, redox cycling during reaction has been crucial to retaining useful activity. Chromium oxide on some supports, such as SBA-15 and MCM-41, have shown slightly better catalytic stability but they have tended to result in low propene yields. The chromium oxide catalysts can also participate in the non-oxidative pathway (via $Cr(III, IV)O_x$), but the non-oxidative pathway generally favours more cracking propane to methane, ethane, and ethylene.

The non-oxidative catalysts In_2O_3-Al_2O_3 and ZnO/ZSM-5 for propane dehydrogenation via CO_2 show better catalytic stability. Propene yield tends to increase with the increase of CO_2 partial pressure. It seems likely that the moderate strength acid and possibly moderate strength base sites of In_2O_3-Al_2O_3 are responsible for both high propane conversion and high selectivity to propene. Moderate acidity is also thought to be the key to high conversion and selectivity exhibited by ZnO/ZSM-5.

The non-oxidative catalysts for propane dehydrogenation by CO_2 are still not very well understood. Questions are:

- How does CO_2 promote the reaction?
- What is the role of the catalyst to increase dehydrogenation of propane gas?
- How do we overcome dry reforming which can occur in the presence of CO_2?
- Can catalysts be developed to show adequate activity/selectivity using practically useful propane concentrations in the reactant feed.

Therefore, this study is hoping to evaluate in depth the role of non-oxidative via CO_2 by using heterogeneous catalysts based on ZrO_2-TiO_2 due to the evidence of high acidity

and basicity of catalytic surface (**section 1.1.5**). In addition to ZrO_2-TiO_2, several catalysts selection criteria is investigated based on the following:

- Binary mixed metal oxides with TiO_2, specifically metal oxides as follows:
  - Metals from Group 3 (Al, Ga, Tl) have been used because they are in the same group as indium and indium oxide blends with Al_2O_3 have been shown to be active [64].
  - Metal from Group 10B (Pt) have been used because Pt metal is known to assist non-oxidative PDH [69].
  - Metal from Groups 9B and 12B (Co, Rh, Ir and Cu) have been studied because these metals are well known for dehydrogenation of ethane [70], [72].
  - Metals from Groups 5B, 6B 7B and 8B (V, Nb and Fe) have been studied because these metals are well known for dehydrogenation of ethylbenzene and propane[71],[54].
  - Metal from Group 5B (Hf) from same metal group of Ti and Zr have been tested.
  - Uranium and thorium have been studied because these metal oxides have the potential of p-type conductivity which, in principle, could lead to the generation of oxygen surface species. They have been used for dehydrogenation of ethane [72].

1.4 Direct reaction of CO_2 with methane, ethane, ethene, acetylene and propane

A study of direct reaction of CO_2 with methane, ethane, ethylene, acetylene and propane is described in **chapter 4**.

1.4.1 Background

Relatively few papers have been published on the direct reaction of CO_2 as a whole molecule with methane[73-77]and ethane[78] to form acetic acid. Catalysts such as

Pt/Al_2O_3[73], Pd/carbon [73], Cu/Co, Pd/SiO_2, and V_2O_5-$PdCl_2/Al_2O_3$ at temperatures between 150 and 450 °C have been used [75-77]. There are also reports of the reaction of CO_2 with ethane in the presence of O_2 to produce acetic acid over LaMoV oxides[78].

1.4.2 Motivation

CO_2 and CH_4 are low cost and abundant raw materials. Reaction of CO_2 with natural gas, such as, methane ethane or propane, is considered a challenging research area.

1.4.3 Methane

Methane is the most abundant and main component of natural gas. Steam or dry reforming of methane is the main source of hydrogen and carbon monoxide – syngas – which is used for synthesis of basic chemicals such as methanol, formaldehyde and Fischer–Tropsch products [79]. Methane is the least reactive alkane so methane utilisation is challenging [79]. Several research groups have studied the methods for the direct conversion of methane to valuable chemicals by methane oxidation coupling to ethylene and ethane, methane oxyhalogenation and methane aromatization [80-81].

Methane gas is acidic and hydrogen atoms are acidic and have a small positive charge (δ^+) and the carbon atom is basic with a small negative charge (δ^-). This contrast to CO_2 in which the carbon atom is slightly acidic (δ^+) and the oxygen atoms are basic (δ^-).

Erdöhelyi *et al.*[82] illustrated the general principle of activating methane in the presence of CO_2. They showed that methane adsorbs on a rhodium catalyst as methyl and hydrogen surface species. As before, the role of the CO_2 is to clear the surface of adsorbed hydrogen by a reverse water gas shift reaction. The methyl surface species can react by several routes, to produce ethane or by further decomposition as shown in equations (1.34) (1.35) and (1.36).

$$CH_4 \rightarrow CH_{3(ads)} + H_{(ads)} \qquad \text{eq. (1.34)}$$

$$CH_{3(ads)} \rightarrow CH_{2(ads)} + H_{(ads)} \qquad \text{eq. (1.35)}$$

$$CH_{2(ads)} \rightarrow CH_{(ads)} + H_{(ads)} \qquad \text{eq. (1.36)}$$

1.4.4 Synthesising Acetic acid

Acetic acid is an important chemical and the annual production is more than 7 million tons. A large amount of acetic acid produced is converted to vinyl acetate for use in paints, adhesives and paper coating. The current method of synthesising acetic acid is mainly (60% of world production) by carbonylation of methanol by reaction with CO as shown in equation (1.37) [83]. Another route is the direct oxidation of butane by O_2 (equation 1.38) and the oxidation of acetaldehyde (equation 1.39) [84].

Eq. (1.37)

Eq. (1.38)

Eq. (1.39)

The BASF process involves carbonylation of methanol with CO over a CoI_2 catalyst. The process uses severe conditions, and one the highest pressures currently employed in any petrochemical plant, of about 700 bar. The temperature is moderate at 250 °C. The process produces of 45 wt% acetic acid, 35 wt% H_2O, and 20 wt% esters. Purification requires several distillation towers for degassing, catalyst separation, water washing, drying, and scrubbing.

The direct oxidation of naphtha, NGL gas, butane, ethene, and acetaldehyde contribute about 25-35% of acetic acid world production. Several people have attempted the very attractive route to acetic acid by oxidation of ethane by O_2. The reaction is usually based on mixed Mo with V oxides at high pressure and at 250 - 450 °C [85-86].

1.4.6 Literature review of direct reaction between CO_2 with methane

Examples of reports of reaction between CO_2 and CH_4 to produce acetic acid are shown in Table 1.8.

Table 1.8. Research groups studied CO_2 reaction with CH_4

No	Title of paper	Author
1	Direct catalytic formation of acetic acid from CO_2 and methane, Catalysis Today 88 (2003) 83–90 [73]	Esther M. Wilcox, George W. Roberts, James J. Spivey (USA)
2	Direct utilisation of carbon dioxide in chemical synthesis: vinyl acetate via methane carboxylation, Catalyst communication 9, (2008) 685-689 [74]	James J. Spivey, Esther M. Wilcox, George W. Roberts (USA)
3	Possibility of direct conversion of CH_4 and CO_2 to high value products, Journal of Natural Gas Chemistry 13 (2004) 113-115 [75]	W. Huang, K.-C. Xie, J.-P. Wang, Z.-H. Gao, L.-H. Yin, and Q.-M. Zhu (CHINA)
4	Direct Synthesis of Acetic Acid from CH_4 and CO_2 in the presence of O_2 over a V_2O_5-$PdCl_2$/Al_2O_3 Catalyst, Journal of Natural Gas Chemistry 13 (2004) 113-115 [76]	Wei Huang, Cuihong Zhang, Lihua Yin, Kechang Xie, (CHINA)
5	Direct synthesis of acetic acid from CH_4 and CO_2 by a step-wise route over Pd/SiO_2 and Rh/SiO_2 catalysts, Fuel Processing Technology 88 (2007) 319–324 [77]	Yi-Hui Ding, Wei Huang, Yong-Gang Wang
6	The interaction mechanism of CO_2 with CH_3 and H on Cu (1 1 1) surface in synthesis of acetic acid from CH_4/CO_2: A DFT study, Applied Catalysis A: General 443– 444 (2012) 50– 58 [87]	Riguang Zhang, Luzhi Song, Hongyan Liu, Baojun Wang
7	Preparation of La-Mo-V mixed-oxide systems and their application in the direct synthesis of acetic acid Journal of Natural Gas Chemistry 17(2008)213–224 [78]	Hamid Reza Arandiyan and Matin Parvari

Wilcox *et al.* [73] used 5% Pd/carbon and 5% Pt/Al_2O_3 catalysts and detected acetate on the catalysts' surfaces. Spivey *et al.* [74] formed vinyl acetate by reacting CO_2, CH_4 and acetylene on 5% Pt/Al_2O_3 mixed with $Zn(CH_3COO)_2$/C catalyst. They explained that the reaction proceeded into two steps, forming acetic acid on the Pt/Al_2O_3, which then reacts with acetylene on the zinc catalyst.

Four papers were published by a group from Taiyuan University of Technology that investigated reactions of CO_2 with CH_4 to form acetic acid at 100–450 ^{o}C. They proposed

a C-C mechanism in which CO_2 first reacts with CH_3 surface species on the catalyst surface.   They used Cu-Co oxides [75] and in a   second study, V_2O_5-$PdCl_2$/Al_2O_3 catalysts[76]. They also studied the synthesis of acetic acid from CH_4 and CO_2 using Pd and Rh[77]. In the first stage, CH_4 was adsorbed and thought to dissociate on the metal surface. CO_2 was then thought to react with introduced to react with the adsorbed species to form acetic acid. The results showed 2% Pd/SiO_2 catalyst was active at 170-200 ^oC. Formic acid was the only by-product over the Pd catalyst [77].

Workers at Taiyuan University of Technology performed DFT computational studies on the interaction between CO_2 and CH_4 on a copper-cobalt catalyst[74-75],[87].   They concluded that reaction between Co-$CH_{3(ads)}$ and Cu-$CO_{2(ads)}$ to form CH_3COO-Cu is the most favourable reaction route with an activation barrier of   85.2 kJ mol^{-1} [87]. An adsorbed hydrogen reaction then reacts to form acetic acid which desorbs as shown in equations (1.43), (1.44) and (1.45) [87].

$$CH_4 \rightarrow CH_{3\ (ads)} + H_{(ads)} \qquad \text{... eq (1.43)}$$

$$CO_2 + CH_{3(ads)} \rightarrow CH_3COO_{\ (ads)} \qquad \text{... eq (1.44)}$$

$$CH_3COO_{(ads)} + H_{(ads)} \rightarrow CH_3COOH \qquad \text{... eq (1.45)}$$

Arandiyan and Parvari[78] studied the direct reaction of ethane with CO_2 in the presence of O_2 to synthesise acetic acid on LaMoV oxides catalysts at 450-850 ^oC, and 1-8 bar in a similar way to that used by Huang *et al*. [76]   with methane, CO_2 and O_2. Thermodynamically, the ethane reaction with CO_2 and O_2 is more favourable than the equivalent methane reaction (ΔG_{298k} = - 146.89 kJ/mol versus ΔG = - 703.61 kJ/mol) (equation 1.46) and these workers reported high conversion of ethane but only 2-4% selectivity to acetic acid. It appears that dry reforming to CO and H_2 competes.   The authors did not explain the mechanism of the acetic acid formation and the role of CO_2 and O_2.

$$2C_2H_6 + CO_2 + 2O_2 \rightarrow 5/2\ CH_3COOH + H_2O, \Delta G = -703.61 \text{ kJ/mol}\quad \text{eq. (1.46)}$$

One problem with acetic acid synthesis is the risk of acetic acid decomposing thermally if the reaction temperature is too high. Acetic acid can decompose at 450-600 °C and the main products are CO_2 and CH_4[88]. But over some catalysts it can resist decomposition at high temperature. For example, Fung and Wang [89] studied TPD of acetic acid on 50% w/w TiO_2-ZrO_2 from 224 °C to 520 °C. They concluded the basic sites on the surface stabilise the acetic acid, preventing decomposition.

1.5 Conclusions

1.5.1 Propane dehydrogenation by CO_2 to propene

The utilisation of CO_2 is a challenge in chemistry due to the stable structure of CO_2. This thesis focuses on CO_2 utilisation for the petrochemical field. To date oxidative catalysts based on Cr used for propane dehydrogenation have exhibited high propene selectivity but the low yields and poor catalyst stability. Previous work has shown that the choice of catalyst, and the nature of the support with supported catalysts, can influence activities.

Few non-oxidative catalysts have been reported for propane dehydrogenation by CO_2 and none of them has shown activity suitable for commercial use. A new approach is taken in the work reported here, where CO_2 is recognised as a possible participant in the RWGS reaction in which hydrogen atoms absorbed on the catalyst surface are abstracted by CO_2. Another aspect of this work is the recognition of CO_2 as a possibly important reagent in removing coke from the catalyst.

1.5.2 CO_2 insertion reaction

In general, those who have studied CO_2 insertion in CH_4 have all observed very low yields of acetic acid. In addition, dry reforming and the reverse water gas shift reactions are often favoured over insertion. Furthermore, the direct reaction between CO_2 and CH_4 on heterogeneous catalysts to form acetic acid has not been explained in terms a

suitable reaction mechanism so far. Due to the thermodynamic limitations of the conventional acetic acid formation reaction, a methyl surface species mechanism is possibly involved. This idea has been supported by DFT calculations which suggest that reaction between CO_2 and adsorbed CH_3 surface species is the most favourable reaction route.

Finally, the work reported here covers CO_2 insertion as a whole molecule not only in methane, but also ethane, ethene, acetylene and propane. Again, the difficulties of achieving activity in these reactions are compounded by competing reactions, particularly the reverse water gas shift and dry reforming processes.

References

1. J. Mascetti, F. Galan, and I. Pàpai, Coord. Chem. Rev., **190–192** (1999) 557–576.

2. H. Rogner and D. Zhou, Introduction. In Climate Change 2007: Mitigation, Contribution of Working Group III to the Fourth Assessment Report of the Intergovernmental Panel on Climate Change, https://www.ipcc.ch/pdf/assessment-report/ar4/wg3/ar4-wg3-chapter1.pdf (date: 7/21/2014).

3. U.S. Department of Commerce, National Oceanic & Atmospheric Administration, NOAA Research, http://www.esrl.noaa.gov/gmd/ccgg/trends/,(date: May 23, 2013).

4. J. Wang, C. Liu, Y. Zhang and B. Eliasson, Chem. Phys. Lett., **368** (2003) 313-318.

5. Parsons Brinckerhoff report: Accelerating the uptake of CCS: industrial use of captured carbon dioxide, (http://cdn.globalccsinstitute.com/sites/default/files/publications/14026/accelerating-uptake-ccs-industrial-use-captured-carbon-dioxide.pdf, (Date: March 2011)

6. T. Iijima and T. Yamaguchi, Appl. Catal. A, **345** (2008) 12–17.

7. X. B. Lu, J. H. Xiu, R. He, K. Jin, L. M. Luo and X. J. Feng, Appl. Catal. A, **275** (2004) 73–78.

8. Z. W. Z. Bu, T. Cao, T. Ren, L. Yang and W. Li, Polyhedron, **32** (2012) 86–89.

9. T. Zhao, Y. Han, Y. Sun, Fuel Process. Technol., **62** (2000) 187–194.

10. E. Leino, P. Mäki-Arvela, V. Eta, N. Kumar, F. Demoissond, A. Samikannu, A.R. Leinoc, A. Shchukarev, D. Y. Murzin and J.P. Mikkol, Catal. Today, Vol. **210** (2013) 47– 54.

11. S. Kaneco, H. Katsumata, T. Suzuki and K. Ohta, Electrochim. Acta, **51** (2006) 3316-3332.

12. C.S. Chen, W.H. Cheng and S.S. Lin, Appl. Catal. A, **238** (2003) 55–67.

13. G. Wu, K. Xie, Y. Wu, W. Yao and J. Zhou, J. Power Sources, **232** (2013) 187-192.

14. K. Takehira, Y. Ohishi, T. Shishido, T. Kawabata, K. Takaki, Q. Zhang and Y. Wang, *J. Catal.,* **224** (2004) 404–416.

15. S. Kaneco, H. Katsumata, T. Suzuki and K. Ohta, Electrochim. Acta, **51** (2006) 3316–3321.

16. M. Gattrell, N. Gupta and A. Co, J. Electroanal. Chem., **594** (2006) 1-19.

17. J. Gao, L.S. Jia, W.P. Fang, Q.B Li and H. Song, J. Fuel Chem Technol, , **37**, 5(2009), 573-577.

18. K. Hashimoto, H. Habazaki, M. Yamasaki, S. Meguro, T. Sasaki, H. Katagiri, T. Matsui, K. Fujimura, K. Izumiya, N. Kumagai and E. Akiyama, Mater. Sci. Eng. A, **88** (2001) 304–306.

19. H.J. Freund and M. W. Roberts, Surf. Sci. Rep., **25** (1996) 225-273.

20. J.G. Wang, C.J. Liu, Y.P. Zhang and B. Eliasson, Chem. Phys. Lett., **368** (2003) 313-318.

21. A. Markovits, A. Fahmi and C. Minot, J. Mol. Struct., **371** (1996) 219-235.

22. A. Behr, Angew. Chem., **100** (1988) 681-698.

23. J. R. Sohn and S. H. Lee, Appl. Catal. A, **321** (2007) 27-34.

24. M.E. Manríquez, T. López, R. Gómez and J. Navarrete, J. Mol. Catal. A., **220** (2004) 229–237.

25. R. Pérez-Hernández, D. Mendoza-Anaya, M.E. Fernández and A. Gómez-Cortés, J. Mol. Catal. A, **281** (2008) 200–206.

26. V. dos Santos, M. Zeni, J.M. Hohemberger and C.P. Bergmann, Rev. Adv. Mater. Sci., **24** (2010) 44-47.

27. B. Neppolian, Q. Wang, H. Yamashita and H. Choi, Appl. Catal. A., **333** (2007) 264–271.

28. V. Vishwanathan, H.S. Roh, J.W. Kim and K.W. Jun, Catal. Lett., **96** (2004) 23–28.

29. M. Suzuki and J. B. Moffat, Catal. Lett., **16**, 4 (1992) 389-398.

30. K. Murata, T. Hayakawa, S. Hamakawa and K. Suzuki, *Catal. Today,* **45** (1998) 41-5.

31. W. Jeon, J. Y. Lee, M. Lee, J. W. Choi, J. M. Ha, D. J. Suh and I. W. Kim, Appl. Catal. A, **464– 465** (2013) 68– 77.

32. B. M. Reddy and A. Khan, Catal. Rev. Sci. Eng., **47**, 2 (2005) 257-296.

33. J. Fung and I. Wang, J. Catal.,**164**, (1996) 166–172.

34. D. Das a, H.K. Mishraa, A.K. Dalai and K.M. Parida, Appl. Catal. A, **243** (2003) 271–284.

35. D. Mao, G. Lub and Q. Chen, Appl. Catal. A, **263** (2004) 83–89.

36. J. Ma, N. Sun, X. Zhang, N. Zhao, F. Xiao, W. Wei and Y. Sun, Catal. Today, **148** (2009) 221–231.

37. S. K. Hoekman, A. Broch, C. Robbins and R. Purcell, Int. J. Greenhouse Gas Control, **4**, 1, (2010) 44-50.

38. S. Wanga, D. Mao, X. Guo, G. Wu and G. Lu, Catal. Commun., **10** (2009) 1367–1370.

39. K. N. Raoa, B. M. Reddy, B. Abhishek, Y.H. Seo, N. Jiang and S. E. Park, Appl. Catal. B, **91** (2009) 649–656.

40. D. R. Burri, K. M. Choi, S. C. Han, A. Burri and S. E. Park, J. Mol. Catal. A., **269** (2007) 58–63.

41. A. Burri, N. Jiang and S. E. Park, Catal. Sci. Technol., **2** (2012) 514–520.

42. B. Xu, B. Zheng, W. Hua, Y. Yue and Z. Gao, *J. Catal.,* **239** (2006) 470–477.

43. G. Rajua, B. M. Reddy and S. E. Park, J. CO_2 Util., **5** (2014) 41–46.

44. S. Deng, H. Li, S. Li and Y. Zhang, J. Mol. Catal. A: Chem. **268** (2007) 169–175.

45. X. Zhang, Q. Ye, B. Xu and D. He, Catal. Lett., **117**, 3–4 (2007) 140–145.

46. X. Zhao, X. Wang, Catal. Commun.,**7** (2006) 633–638.

47. S. Wang, K. Murata, T. Hayakawa, S. Hamakawa and K. Suzuki, Appl. Catal. A, **196** (2000) 1–8.

48. P. Michorczyk, J. Ogonowski and K. Zeńczak, J. Mol. Catal. A: Chem., **349** (2011) 1–

12.

49.   P. Kuśtrowski, P. Michorczyk, L. Chmielarz, Z. Piwowarska, B. Dudek, J. Ogonowski and R. Dziembaj, Thermochim. Acta, **471** (2008) 26–32.

50.   F. M. Zhang, Y.C Yue, W. Hua and Z. Gao, Chin. J. Chem., **30** (2012) 929-934.

51.   Propene report number 06/07-3, Nexant Chem Systems PERP, 44 South Broadway, White Plains, New York, USA, issued date: January 2008.

52.   S. Ahmed, F. Rahman, A.M. J. Al-Amer, E. M. Al-Mutairi, U. Baduruthamal and K. Alam, Reac. Kinet. Mech. Cat., **105** (2012) 483–493.

53.   D. E. Resasco, Dehydrogenation by Heterogeneous Catalysts, School of Chemical Engineering and Materials Science, University of Oklahoma, January, 2000. http://www.ou.edu/catalysis/pubs/2003-1.pdf, (03/06/2014).

54.   K. Takehira, Y. Ohishi, T. Shishido, T. Kawabata, K. Takaki, Q. Zhang and Y. Wang, J. Catal., **224** (2004) 404–416.

55.   E.L. Lee, B. Kilos, I. Mbaraka and L. Luo, On-Purpose Propene Production via CO2 Facilitated Propane Dehydrogenation, extended abstract 22nd North American Catalysts society, 2011 (conference).

56.   M.M. Bhasin, J.H. McCain, B.V. Vora, T. Imai and P.R. Pujad, Appl. Catal. A, **221** (2001) 397–419.

57.   P. Michorczyk and J. Ogonowski and React. Kinet. Catal. Lett, **78** (2003) No. 1, 41-47.

58.   M.A. Botavina, C. Evangelisti, Yu.A. Agafonov, N.A. Gaidai, N. Panziera, A.L. Lapidus and G. Martra, J. Chem. Eng., **166** (2011) 1132–1138.

59.   T. Shishido, K. Shimamura, K. Teramura and T. Tanaka, Catal. *Today,* **185** (2012) 151– 156.

60.   H. Liu, Z. Zhang, H. Li and Q. Huang, J. Nat. Gas Chem., **20** (2011) 311–317.

61.   Q. Zhu, M. Takiguchi, T. Setoyama, T. Yokoi, J.N. Kondo and T. Tatsumi, Catal. Lett., **141** (2011) 670–677.

62.   F. Dury, M.A. Centeno, E.M. Gaigneaux and P. Ruiz, Catal. Today, **81** (2003) 95–105.

63.   M. Chen, J. Xu, Y. Cao, H.Y. He, K.N. Fan and J.H. Zhuang, J. Catal*.,* **272** (2010) 101–108.

64.   M. Chen, J. Xu, Y. M. Liu, Y. Cao, H.Y. He and J.H. Zhuang, Appl. Catal. A, **377** (2010) 35–41.

65.   M. Chen, J.L. Wu, Y.M. Liu, Y. Cao, L. Guo, H.Y.He and K.N. Fan, Appl. Catal. A, **407** (2011) 20– 28.

66.   Y. Ren, F. Zhang, W. Hua, Y. Yue and Z. Gao, Catal. Today, **148** (2009) 316–322.

67.   E.A. Pidko and R.A. van Santen, J. Phys. Chem. C, **111** (2007) 2643.

68.   B. Xu, B. Zheng, W. Hua, Y. Yue and Z. Gao, J. *Catal.,* **239** (2006) 470–477.

69.   F. T. Zangeneh, S. Sahebdelfar, and M. Bahmani, Chin. J. Chem. Eng., **21,** 7(2013), 730—735.

70.   X. Zhang, Q. Ye, B. Xu, and D. He, Catal. Lett., **117**, 3-4, (2007) 140–145.

71.   X. Longya , L. Jinxiang, X. Yide, Y. Hong, W. Qingxia and L. Liwu, Appl. Catal. A, **193**

(2000) 95–101.

72.   L. A. Palacio, A. Echavarría, L. Sierra and E.A. Lombardo, Catal. *Today,* **107–108** (2005) 338–345.

73.   E.M. Wilcox, G. W. Roberts and J. J. Spivey, Catal. Today, **88** (2003) 83–90.

74.   J.J. Spivey, E. M. Wilcox and G. W. Roberts, Catal. Commun., **9**, 5, (2008) 685-689.

75.   W. Huang, K.-C. Xie, J.-P. Wang, Z.-H. Gao, L.-H. Yin and Q.-M. Zhu, J. Nat. Gas Chem., **13** (2004) 113-115.

76.   W. Huang, C. Zhang, L. Yin and K. Xie, J. Nat. Gas Chem., **13** (2007) 113-115.

77.   Y.H. Ding, W. Huang and Y.G. Wang, Fuel Process. Technol., **88** (2007) 319–324.

78.   H. R. Arandiyan and M. Parvari, J. Nat. Gas Chem., **17** (2008) 213–224.

79.   X. Longya , L. Jinxiang, X. Yide, Y. Hong, W. Qingxia and L. Liwu, Appl. Catal. A, **193** (2000) 95–101.

80.   K. Otsuka and Y. Wang, Appl. Catal. A, **222** (2001) 145-161.

81.   G. Fu, X. Xu and H. Wan, *Catal. Today,* **117** (2006) 133-1037.

82.   A. Erdöhelyi, J. Cserényi and F. Solymosi, J. *Catal.,* **141**, (1993) 287-299.

83.   N. Yoneda, S. Kusano, M. Yasui, P. Pujado and S. Wilcher, Appl. Catal. A, **221** (2001) 253–265.

84.   K.X. Wang, H. F. Xu, W. S. Li and X. P. Zhou, J. Mol. Catal. A., **225** (2005) 65–69.

85.   M. Soliman, Y. Al-Zeghayer, A.S. Al-Awadi and S.Al-Mayman, Economics of Acetic Acid Production by Partial Oxidation of Ethane, APCBEE Procedia **3** (2012) 200-208.

86.   X. Li and E. Iglesia, Appl. Catal. A, **334** (2008) 339–347.

87.   R. Zhang, L. Song, H. Liu and B. Wang, Appl. Catal. A, **443– 444** (2012) 50– 58.

88.   J. W. Smith, R. Pallassew and L. S. K. Pang, Org. Geochem., **29**, I-3, (1998) 79-82.

89.   J. Fung l and I. Wang, Appl. Catal. A, **166** (1981) 327-334.

CHAPTER-2

CATALYST PREPARATION AND CHARACTERIZATION

Table of content

2.1 CATALYST PREPARATION

In this section, a number of binary oxides and ternary oxide heterogeneous catalysts, mainly based on TiO_2 and ZrO_2/TiO_2, were prepared. The two main catalyst preparation methods used in this study were:

- four cited methods for impregnated catalysts,
- four cited methods for co-precipitated catalysts.

2.1.1 Material

The chemicals and reagents that were used for heterogeneous catalysts preparation are listed in Table 2.1.

Table 2.1. List of chemical used for catalyst precursor

Chemical	Manufacture
Zirconium (IV) oxynitrate hydrate, $ZrO(NO_3)_2 .6H_2O$	Fisher Scientific
Aluminium nitrate, $Al(NO_3)_3.9H_2O$	Fisher Scientific
Zirconium (IV) hydroxide, $Zr(OH)_4$	Aldrich
Magnesium nitrate, $Mg(NO_3)_2.6H_2O$	Disons Analytical Reagent
Titanium (IV) chloride, $TiCl_4$	Sigma Aldrich
Titanium (IV) hydroxide, $Ti(OH)_4$	Sigma Aldrich
Titanium isopropoxide ($C_{12}H_{28}O_4Ti$)	Sigma Aldrich
Zirconium (IV) oxide, ZrO_2	Sigma Aldrich
Ferric (II) nitrate, $9H_2O$, $Fe(NO_3)_2$	Alfa Aesar
Titanium (IV) oxide, TiO_2	BASF
Cobalt (II) nitrate, $Co(NO_3)_2$	CHEM Service
Cupper (II) nitrate, $Cu(NO_3)_2. 3H_2O$	Fisher Scientific
Zirconylchloride octahydrate, $ZrOCl_2.8H_2O$	Sigma Aldrich
Platinum (III) chloride, $PtCl_3$	Sigma Aldrich
Chromium(III) nitrate, $Cr(NO_3)_3$	Fisher Scientific
Ammonium metavanadate, NH_4VO_3	Fisher Scientific
Gallium nitrate, $Ga(NO_3)_3.5H_2O$	Alfa Aesar
Potassium nitrate, KNO_3	Sigma Aldrich
Beryllium nitrate, $Be(NO_3)_2$	Fisher Scientific
Barium nitrate, $Ba(NO_3)_2$	Fisher Scientific
Niobium (V) chloride, $NbCl_5$	Alfa Aesar
Hafnium (IV) chloride, $HfCl_4$	Alfa Aesar
Thallium (III) nitrate, $Tl(NO_3)_3$	Alfa Aesar
Rhodium (III) nitrate, $RhNO_3$	Alfa Aesar
Uranyl nitrate	Alfa Aesar
Thorium nitrate	Alfa Aesar
Silica Gel SiO_2 80-120 mesh	Sigma Alderch
Aluminium oxide, Al_2O_3	Sigma Alderch
Zirconium oxide	Alfa Aesar
Nitric acid, HNO_3	Fisher Scientific
Ammonia hydroxide, NH_3OH, 30% in water	Sigma -Aldrich

2.1.2 Impregnation methods

Four incipient wetness impregnation methods were conducted. All catalysts are described with a percentage (%) of one oxide compared to the other(s). This percentage (%) is in fact the percentage weight/weight (% w/w) of the dopant metal related to the total metal content, for example, 5% ZrO_2/TiO_2 contains Zr and Ti in the weight ratio of 5 : 95 (the metals ratio calculation examples are shown in Appendix 2, Table A1 and A2). In each case the weights of the salt precursors needed are calculated from this. Following are representative examples of the use of the four methods.

2.1.2.1 Impregnation method-1

Impregnation method-1 is from Takahashi *et al.*[1]. The method used 0.5 g $ZrO(NO_3)_2.6H_2O$ dissolved in dilute nitric acid (0.2 N, 100 ml). 5 g TiO_2 in powder form was added for total mixing of 18 hours at room temperature. Then the centrifuge was applied to remove water. Then water washing with 200 ml of distilled water for 2-3 times was applied before drying at 100 °C for 18 hours. The calcination at static air via muffle furnace was applied at 700 °C.

In addition, six ternary oxide catalysts prepared by using impregnation method-1 and tested in **chapter-3**. The third metal oxide dopant was added to pre-calcined 5% Zr/Ti oxide. The method of impregnation was done by dissolving for example 0.30 g of $Cu(NO_3)_2$ in dilute nitric acid (0.2 N, 100 ml). Then the pre-calcined 5% Zr/Ti oxide in powder form was added for total mixing of 18 hours at room temperature. Then the centrifuge was applied to remove water. Then water washing with 200 ml of distilled water for 2-3 times was applied before drying at 100 °C for 18 hours. The calcination at static air via muffle furnace was applied at 700 °C.

2.1.2.2 Impregnation method-2

Impregnation method-2 is from Ruppert & Paryiczak [2]. The method used 0.5 g $ZrO(NO_3)_2.6H_2O$ dissolved in distilled water (100 ml). 5 g TiO_2 in powder form was added for total mixing of 18 hours at room temperature. Then the centrifuge was

applied to remove water. Then water washing with 200 ml distilled water 2-3 times was used before drying at 100 °C for 18 hours. The calcination at static air via muffle furnace was applied at 700 °C.

Four ternary oxide catalysts were prepared by using impregnation method-2 and tested in **chapter-4**. The method of impregnation was done by dissolving for example 0.35 g of $Al(NO_3)_3.9H_2O$ and 0.35g of $ZrO(NO_3)_2.6H_2O$ in dilute nitric acid (0.2 N, 100 ml). Then 3.0 g of TiO_2 support in powder form was added for total mixing of 18 hours at room temperature. Then the centrifuge was applied to remove water. Then water washing with 200 ml of distilled water for 2-3 times was applied before drying at 100 °C for 18 hours. The calcination at static air via muffle furnace was applied at 700 °C.

2.1.2.3 Impregnation method-3

Impregnation method-3 is from the Chepurna *et al.*[3] to make nano-ZrO_2 precursor. The method used 0.5 g $ZrO(NO_3)_2.6H_2O$ dissolved in ammonia solution (1 N, 50 ml) for 24 hours mixing at room temperature. 5 g TiO_2 in powder form was added for total mixing of 18 hours at room temperature. Then the centrifuge was applied to remove water. Then water washing with 200 ml of distilled water 2-3 times was applied before drying at 100 °C for 18 hours. The calcination at static air via muffle furnace was applied at 700 °C.

2.1.2.4 Impregnation method-4

Impregnation method-4 is from Laniecki and Ignacik [4] and this method used the metal chloride salts. The method used as an example 0.5 g $ZrCl_4$ dissolved in distilled water (50 ml). 5 g TiO_2 in powder form was added. During the stirring the pH level was adjusted by ammonia solution (1 N) to reach pH 8. The total mixing time was about 18 hours at room temperature. Then the centrifuge was also applied to remove water. Then water washing with 200 ml of distilled water for 4-5 times was used before drying at 100 °C for 18 hours. The calcination in static air via muffle furnace was applied at 700 °C.

The list of the prepared binary and ternary oxides catalysts is shown in Tables 2.2 and 2.3. The tables show two decimal places each catalyst preparation, chemical weight recipe, the impregnation method number applied and the chapter number in which the catalyst study is reported.

Table 2.2. Binary oxide catalysts prepared by the impregnation method

Catalyst by w/w%	Chemicals used for the synthesis	Salt weight	Impregnation method used	Tested in chapter
5% Zr/Ti oxide	$ZrO(NO_3)_2.6H_2O$	0.55 g	1, 2, and 3	**3 and 4**
	TiO_2 support	5.00 g		
8% ZrO_2/TiO_2	$ZrCl_4$	0.55 g	4	**4**
	TiO_2 support	3.00 g		
7.9% Hf/Ti oxide	$HfCl_4$	1.02 g	4	**3**
	TiO_2 support	12.0 g		
5.8% Al/Ti oxide	$Al(NO_3)_3.9H_2O$	1.20 g	1	**3**
	TiO_2 support	2.50 g		
6.9% Nb/Ti oxide	$NbCl_5$	1.15 g	4	**3**
	TiO_2 support	9.50 g		
10.5% Tl/Ti oxide	$Tl(NO_3)_3$	1.44 g	1	**3**
	TiO_2 support	12.0 g		
7.4% V/Ti oxide	NH_4VO_3	0.27 g	1	**3**
	TiO_2 support	2.90 g		
3.5% Ir/Ti oxide	$IrCl_3$	0.25 g	4	**3**
	TiO_2 support	6.00 g		
2% Pt/Ti oxide	$PtCl_3$	0.10 g	4	**3**
	TiO_2 support	3.00 g		
3.3% Rh/Ti oxide	$RhNO_3$	0.20 g	1	**3**
	TiO_2 support	5.00 g		
5% Th/Ti oxide	$Th(NO_3)_4$	0.20 g	1	**3**
	TiO_2 support	3.00 g		
5% U/Ti oxide	$UO_2(NO_3)_2$	0.20 g	1	**3**
	TiO_2 support	3.00 g		
5.8% Cr/Si oxide	Cr(III) nitrate	0.40 g	1	**3**
	SiO_2 support	4.00 g		
5.1% Ga/Al oxide	$Ga(NO_3)_3$	0.40 g	1	**3**
	Al_2O_3 support	4.00 g		

Table 2.3. Ternary oxides prepared by the impregnation method.

Catalyst synthesis by w/w%	Chemical used for the synthesis	Salt weight	Impregnation method used	Tested in chapter
2% Cu/5%Zr/Ti oxide	$Cu(NO_3)_2$	0.30 g	1	**3**
	5% ZrO_2/TiO_2 support	2.00 g		
2% Al/5%Zr/Ti oxide	$Al(NO_3)_3.9H_2O$	0.20 g	1	**3**
	5% ZrO_2/TiO_2 support	5.00 g		
2% Be/5% Zr /Ti oxide	$Be(NO_3)_2$	0.30 g	1	**3**
	5% ZrO_2/TiO_2 support	2.00 g		
2% Mg/5% Zr /Ti oxide	$Mg(NO_3)_2$	0.30 g	1	**3**
	5% ZrO_2/TiO_2 support	2.00 g		
1.3% Ba/5% Zr /Ti oxide	$Ba(NO_3)_2$	0.08 g	1	**3**
	5% ZrO_2/TiO_2 support	2.00 g		
2% Fe/5% Zr /Ti oxide	$Fe(NO_3)_3.9H_2O$	0.50 g	1	**3**
	5% ZrO_2/TiO_2 support	2.00 g		
2% Al/5% Zr/Ti oxide	$ZrO(NO_3)_2 .6H_2O$	0.35 g	2	**4**
	$Al(NO_3)_3. 9H_2O$	0.50 g		
	TiO_2 support	3.00 g		
3.6% Fe/ 5% Zr/Ti oxide	$ZrO(NO_3)_2 .6H_2O$	0.35 g	2	**4**
	$FrNO_3.9H_2O$	0.50 g		
	TiO_2 support	3.00 g		
3.4% Co/5% Zr/Ti oxide	$ZrO(NO_3)_2 .6H_2O$	0.35 g	2	**4**
	$Co(II)(NO_3)_2$	0.20 g		
	TiO_2 support	3.00 g		
4% Cu/5% Zr/Ti oxide	$ZrO(NO_3)_2 .6H_2O$	0.35 g	2	**4**
	$Cu(NO_3)_2. 3H_2O$	0.30 g		
	TiO_2 support	3.00 g		

2.1.3 Co-precipitation methods

Four co-precipitation methods were used in the preparation of catalysts to be used in the CO_2 direct reaction with methane described in **chapter-4**.

2.1.3.1 Co-precipitation method-1

The co-precipitation of Zr/Ti oxide catalyst was from Sohn and Lee [5]. The preparation was conducted by applying different weight ratios of $Zr(OH)_4$ and $TiCl_4$. (Table 2.4).

5.0 g TiCl$_4$ liquid was added dropwise to stirring water (100 ml) at room temperature. Then 5.0 g Zr(OH)$_4$ was added. Dilute ammonia solution (1 N) was added to adjust pH to 8-9 and stirred for 8 hours. Then the solution was centrifuged and washed with 200 ml of distilled water 5-8 times to remove Cl$^-$ ions from the solution. The washed water was tested by ion chromatography (IC). The precursor was dried at 100 ^{o}C for 18 hours and followed by calcination at a temperature 700 ^{o}C for 3 hours at static air via muffler furnace.

2.1.3.2 Co-precipitation method-2

The preparation was based on Sohn and Lee[6].   4.0 g TiCl$_4$ and 3.6 g ZrOCl$_2$ were dissolved in water (100 ml), then aqueous ammonia solution (2.7 N) was added dropwise to adjust to pH 8 at room temperature. The stirring was applied for 6-8 hours. Then the suspension was subjected to centrifuging and water washing with 200 ml of distilled water until the chloride was absent from the washing. The drying of precursor was made at 100 ^{o}C for 18 hours and the calcination was at 700 ^{o}C for 3 hours at static air via muffler furnace.

2.1.3.3 Co-precipitation method-3:

The method was based on Mao *et al*. [7]. 4.0 g TiCl$_4$ and 3.6 g ZrOCl$_2$ were dissolved in aqueous ammonia (100 ml, 1 N) and more diluted ammonia solution was added to adjust the pH to 7-8. Stirring was applied for 24 hours. The resultant precipitate was washed by 200 ml distilled water and centrifuged until chloride was absent in the washings. Then the salt was heated at 110 ^{o}C for 16 hours. The calcination was applied at 700 ^{o}C for 3 hours at static air via muffler furnace.

2.1.3.4 Co-precipitation method-4

The Machida *et al*.[8] co-precipitation method was based on 5.0 g titanium isopropoxide (C$_{12}$H$_{28}$O$_4$Ti) and 2.86 g ZrO(NO$_3$)$_2$, mixed in dilute ammonia (0.5 N, 100 ml). The mixture was stirred for 8 hours at room temperature. The precipitate was centrifuged and washed with 200 ml of distilled water three times. It was dried at 100 ^{o}C for 18 hours. Then it was calcined at 700 ^{o}C in static air via muffler furnace.

Table 2.4. The catalysts prepared by co-precipitation (**chapter 4**)

Catalyst synthesis by w/w%	Chemical used for the synthesis	Salt weight	Impregnation method used
2% w/w Ti/Zr oxide	$TiCl_4$	0.25 g	1
	$Zr(OH)_4$	5.00 g	
4% w/w Ti/Zr oxide	$TiCl_4$	0.50 g	1
	$Zr(OH)_4$	5.00 g	
8% w/w Ti/Zr oxide	$TiCl_4$	1.00 g	1
	$Zr(OH)_4$	5.00 g	
17% w/w Ti/Zr oxide	$TiCl_4$	2.00 g	1
	$Zr(OH)_4$	5.00 g	
44% w/w Ti/Zr oxide	$TiCl_4$	5.00 g	1
	$Zr(OH)_4$	5.00 g	
11% w/w Zr/Ti oxide	$TiCl_4$	5.00 g	1
	$Zr(OH)_4$	0.25 g	
50% w/w Zr/Ti oxide	$TiCl_4$	5.00 g	1
	$Zr(OH)_4$	2.00 g	
50% w/w Zr-Ti oxide	$TiCl_4$	4.00 g	2
	$ZrOCl_2$	3.60 g	
50% w/w Zr-Ti oxide	$TiCl_4$	4.00 g	3
	$ZrOCl_2$	3.60 g	
50% w/w Zr-Ti oxide	$C_{12}H_{28}O_4Ti$	5.00 g	4
	$ZrO(NO_3)_2$	2.86 g	

2.2 Method of catalyst characterization

The analytical techniques were used to characterize the catalyst were as follows.

- SEM and EDX
- pXRD
- Nitrogen adsorption
- NH_3-TPD
- TGA

2.2.1 SEM and EDX characterization

The SEM and EDX analytical techniques were used to characterize the surface morphology of selected ZrO_2 and TiO_2 based catalysts. The microscope (Figure 2.1) is an

environmental scanning electron microscope (ESEM) which has an advantage over a conventional SEM by examining non-conductive samples without coating. The ESEM is operated at 20 kV and at an overpressure of 0.23 torr. The objective of the ESEM measurement was to determine the homogeneity of catalysts, and the size and shape of particles. In addition, energy dispersive X-ray microanalysis (EDX) characterization was acquired from different parts of the catalyst surface to obtain semi-quantitative elemental composition data (Table 2.5). In addition, few samples were tested by using the SEM of King Fahd University of Petroleum and Minerals (KFUPM) as backup for surface morphology. The instrument is made from Tescan (VEGA 3 LMU) and several catalysts were coated by using carbon coater before testing.

Figure 2.1. ESEM instrument FEI Quanta 400

Table 2.5: EDX parameters for catalyst analysis by ESEM

Detector	EDX liquid-nitrogen cooled detector
Operating Voltage	20 kV
Spot Size	4 nm
Working Distance	10 mm
Acquisition Time	60 s
Amplification Time	26.5 µs
Counts per second	2500 CPS
Dead time	25%

2.2.2 Powder X-ray diffraction

Powder X-ray diffraction (p-XRD) was used to verify the crystal structures of catalysts and also used for fingerprinting the crystal structure formation. X-ray diffraction crystallography involves exposing a crystallite to a monochromatic collimated x-ray beam at an angle **θ**. As the X-ray source is scanned through a range of **θ** values, the intensity of a reflected beam at a reflected angle **θ** is measured. The diffractogram is a plot of intensity of the reflected beam against **2θ** (the angle through which the X-rays are deflected). Intense reflections are detected at angles at which there is constructive interference from X-rays reflected from series of adjacent of atomic planes. There are many sets of planes in any crystal that can cause reflection and each set is described by its Miller indices, **h**, **k** and **l**. The angle is related to the spacing **d** between the planes by Bragg's Law (equation 1):

$$n\lambda = 2d \sin \theta \qquad ..eq(1)$$

θ is the angle of the diffracted X-ray, **λ** is the wavelength of X-ray radiation, **d** is the spacing of atomic/crystal planes, and **n** is an integer (usually 1). The d-spacings of planes is related to their Miller indices so diffraction is detected at different angles for planes with different Miller Indices. The powder X-ray diffraction pattern of a particular salt therefore contains a series of maxima (lines) at angles that are characteristic of the material, and at a series of relative intensities that are also characteristic. The overall pattern can therefore be used as a fingerprint of a crystalline material. Crystallite size can be determined from the width of X-ray different peaks using the Scherrer equation (equation 2)

$$L_{2\theta} = \frac{K\lambda}{\beta cos\theta} \qquad ..eq(2)$$

Where **L** is the crystallite dimension, **β** the line width at half height, **θ** is the diffraction angle and **K** is a constant. In the work in this thesis, crystallite sizes were determined for TiO_2 using the major peak for planes with Miller Indices (1 0 1), before and after activity tests in the direct CO_2 reaction with methane and propane (result is discussed in **chapter 4**).

A Panalytical X'Pert PRO Diffractometer instrument was used for XRD analysis throughout this study. The XRD instrument is controlled by computer software (XRD Control System) to convert peak positions as 2θ values to **d**-spacings. The catalysts' XRD patterns are compared with the Powder Diffraction Files (PDF) of the International Centre for Diffraction Data (ICDD). The analysis was conducted from 4° to 80° degrees 2θ. The measurement parameters used for catalyst XRD characterization are shown in Table 2.6.

Table 2.6. XRD pattern measurement condition

Name	Description
Instrument	PANalytical X'PERT PRO MPD
Radiation	copper-anode tube operated at 40 kV and 100 mA Wavelength: = 1.5418 Å
Acquisition	Angular range in 2θ: 4° - 80° Step size: 0.04° and 0.4° Scanning step time: 9.7282 s

2.2.3 Nitrogen adsorption

The nitrogen adsorption analysis was conducted to determine porosities and surface areas. The calcined solid oxide catalysts were analysed using a Micromeritics ASAP 2420 instrument to measure the nitrogen adsorption/desorption isotherms at liquid nitrogen temperature (77 K). The surface area was calculated from the adsorption isotherm by using the B.E.T equation and the total volume of pores was determined from the amount of N_2 desorbed at STP. The pore size distribution was calculated using the Kelvin equation modified with the B.J.H method[1] [9]. A catalyst weight of 200-500 mg was introduced into the sample tube. The catalyst was heated to 150 ^{o}C for 1 hour at the degassing condition of vacuum at 10^{-4} Torr before measurement.

2.2.3.1 Type of isotherms:

There are six major isotherm types recognized by IUPAC for gas physisorption as seen in Figure 2.2. Solid oxide catalyst types are known to be mesoporous and normally exhibit type of IV isotherms with a hysteresis loops [10].

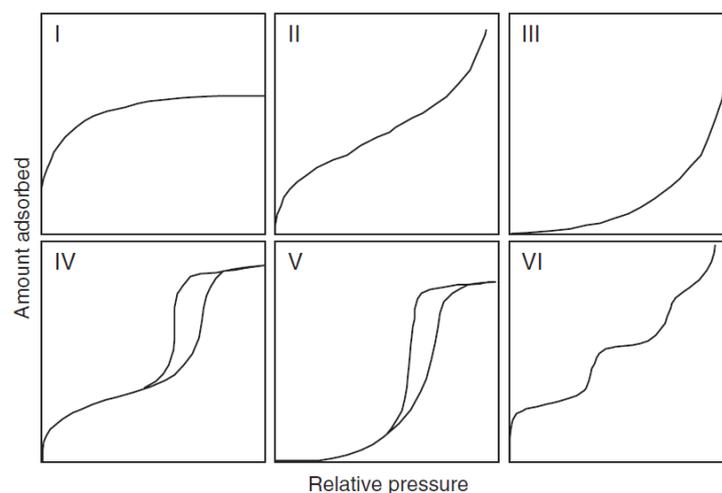---

[1] Barret-Joyner-Halenda (B.J.H)

Figure 2.2. Isotherms diagrams according to IUPAC classifications [10]

2.2.4 Temperature programmed desorption of ammonia (NH$_3$-TPD)

The temperature programmed desorption (TPD) analysis was conducted using a HIDEN CATLAB instrument. The instrument is equipped with a programmed furnace and quadrupole mass spectrometer (QMS) to detect desorbed NH$_3$ to study the acidic sites of catalysts. Solid oxide catalyst samples were exposed to NH$_3$ at 50 °C then heated to release the adsorbate from the catalyst surface.

The amount of NH$_3$ desorption is measured as the temperature is increased and a plot is made of amount of ammonia desorbing vs. temperature. On the basis that NH$_3$ is strongly held on acidic sites, generally stoichiometrically, this profile depends on both the concentration of acid sites and their strengths. The plot can be interpreted as a profile of the concentration of acid sites against acid site strength. Generally, ammonia that remains adsorbed to temperature of greater than 350 °C is consider to be bound to "strong acid sites"[11].

The NH$_3$-TPD was conducted on 100 mg sample, pre-heated at 650 °C and was on hold for 60 minutes under He (50 ml/min) prior the TPD testing. The catalyst was cooled to 50 °C and exposed to 1% NH$_3$ in He for 30 min (50 ml/min). Then the catalyst was purged helium for 60 min (50 ml/min) at 100 °C to remove weakly held ammonia. The furnace was then heated at 10 °C/min to the maximum temperature of 700 °C. The

desorbed NH_3 was measured using the QMS calibrated using the 1% NH_3 gas. The desorbed NH_3 concentration was then plotted against temperature to give the TPD profile [12].

Furthermore, NH_3 desorption was calculated. The HDEN-CATLAB was calibrated first by using known volume of NH_3 (10% NH_3 in He gas) injected at standard temperature and pressure (STB) by using gas syringe (1 ml). The gas injection was repeated for 9 times and average was taken in order to calculate reference factor (RF) as follow:

- The concentration of NH_3 10% in He used, and therefore, 1 ml injected was equal of 0.1 NH_3.
- Mole at STP = 22414.
- Peak area of 1 ml injected 10% NH_3 in He (0.1 ml of NH_3) was determined = 2.795×10^{-7} ion current [A] with CV of 5%.

$$RF = \frac{Moles\ of\ NH_3 at\ STP}{Peak\ area\ of\ Calibrated\ NH_3} = \frac{\frac{0.1}{22414}}{2.7950x10^{-7}} = 15.96 \ \frac{moles}{ion\ current\ [A]}$$

Then, the mole of NH_3 desorption of catalyst sample was calculated by taking peak area of sample as follow:

$$Total\ Adsorption\ of\ NH_3(moles) = Peak\ area\ of\ the\ analyzed\ sample \times RF$$

Them the μmole per catalyst sample weight was calculated as follow:

$$Total\ Adsorption\ of\ NH_3(\mu moles/g) = \frac{Total\ adsorption\ of\ NH_3(moles)}{Mass\ of\ the\ sample\ (g)} \times 1000000$$

2.2.5 Thermogravimetric analysis (TGA)

Thermogravimetric analysis (TGA) was conducted on the coked 5% ZrO_2/TiO_2 catalyst after the dehydrogenation of propane by CO_2 (**chapter-3**). The aim of the test was to determine the catalyst regeneration temperature profile and the extent of coke removal from the catalyst surface by air and CO_2.

The instrument TGA-Q50 from TA (Figure 2.3) was used under flowing air or CO_2 at heating rate of 10 ^{o}C/min and two methods was used as follow (Table 2.7):

Table 2.7. TGA methods used for coked 5% Zr/Ti oxide **(Chapter-3)**

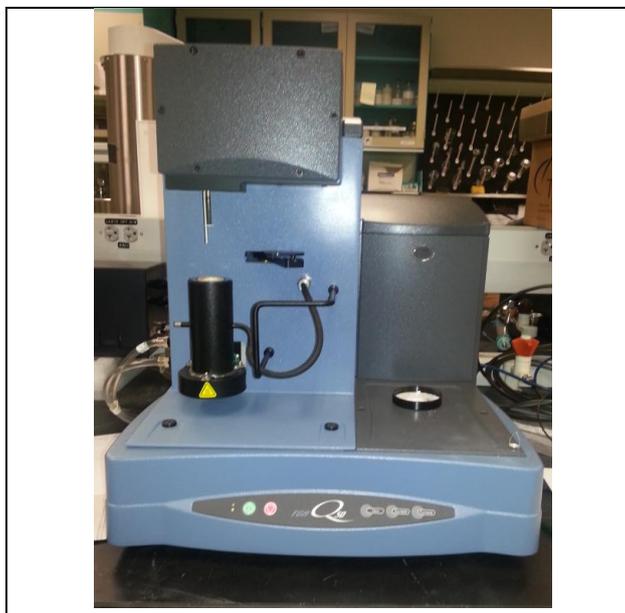| TGA method	Gas	1st sigma	2nd sigma
TGA by Air	Air	Heating rate: 10 °C/min Temperature: 25-200 °C, holding time: 45 min	Heating rate: 10 °C/min Temperature: 200-900 °C, holding time: 60 min
TGA by CO_2	99.5 % CO_2	Heating rate: 10 °C/min Temperature: 25-200 °C, holding time: 45 min	Heating rate: 10 °C/min Temperature: 200-600 °C, holding time: 360 min

Figure 2.3. TGA instruments applied to study the carbonic deposition of selected catalyst

2.3 CATALYST CHARACTERIZATION RESULTS

2.3.1 Scanning electron microscope (SEM)

The SEM was utilised to study topography of Zr/Ti oxide catalysts prepared by impregnation and co-precipitation methods and to determine the elemental composition using EDX. The SEM images of the singles oxide, TiO_2 and ZrO_2, are shown in Figures 2.4 and 2.5. Both single oxides show semi-round shapes and the size of particles were nano particles with diameters less than 1 µm.

Figure 2.4. SEM image of TiO_2: nano size of semi round shape particles around 30- 200 nm of TiO_2 as shown inside the bulb-shaped

Figure 2.5. SEM image of ZrO_2: nano size shape particles of ZrO_2

SEM images of the three Zr/Ti oxide catalysts prepared by impregnation methods -1, -3 and -4 are shown in Figures 2.6, 2.7 and 2.8. The impregnation catalysts also exhibit nano-scale particles with semi-rounded shapes.

SEM images of Zr/Ti oxide catalysts made by co-precipitation methods -1, -2, -3 and -4 at 50% w/w each Zr-Ti oxide were studied. Figures 2.9, 2.10, 2.11, and 2.12 were recorded by SEM instrument from King Fahd University of Petroleum and Minerals (KFUPM) and the figures show well distributed and semi-rounded nano particles with excellent homogeneity.

The first thing to note from the SEM images is a similarity of the topography between the Zr/Ti oxide catalysts prepared by co-precipitation and impregnation methods. The SEM images also are consistent with the SEM data for Zr/Ti oxide catalysts obtained by Rao *et al.* [13]. Finally, the study concludes that doping ZrO_2 with TiO_2 does not significantly change its morphology.

Figure 2.6. SEM image of 5% Zr/Ti oxide by impregnation method-1

Figure 2.7. SEM image of 5% Zr/Ti oxide by impregnation method-3

Figure 2.8. SEM image of 8% Zr/Ti oxide by impregnation method-4 studied by SEM instrument of KFUPM

Figure 2.9. SEM image of co-precipitation method-1 of 50% w/w Zr/Ti oxide

Figure 2.10. SEM image of co-precipitation method-2 of 50% w/w Zr/Ti oxide

Figure 2.11. SEM image of co-precipitation method-3 of 50% w/w Zr/Ti oxide

Figure 2.12. SEM image of co-precipitation method-4 of 50% w/w Zr/Ti oxide

In addition, EDX from SEM was applied to determine the metal contents of the prepared binary oxide and ternary oxides catalysts as shown in Tables 2.7 and 2.8. The EDS analysis is semi-quantitative was conducted 3-5 spots in order to determine the metal content. The metal contents of catalysts are similar to the values expected from the preparation formulations. Two Zr/Ti oxide catalysts made by co-precipitation differed in this respect from the formulation. This was due to difficulty using $TiCl_4$ liquid and it splashed on the beaker when it contacted ammonia solution during dropping. Other reasons are related to the complexity of the methods. In the work following, catalysts are named based on their nominal formulation, rather than on those determined by EDX.

Table 2.7. EDX results of catalysts prepared by co-precipitation method (confident level 95%)

Catalyst synthesis preparation recipe, metal ratio (w/w %)	Metal content detected by EDX (wt/wt %)	Co-precipitation method used	Chapter
2% w/w Ti/Zr oxide	1.3 % w/w Ti/Zr oxide (CV ± 13 %, CL ± 0.14)	1	4
4% w/w Ti/Zr oxide	4.5 % w/w Ti/Zr oxide (CV ± 7 %, CL ± 0.3)	1	4
17% w/w Ti/Zr oxide	14.4 % w/w Ti/Zr oxide (CV ± 24 %, CL ± 3.0)	1	4
44% w/w each Tr/Zr oxide	50 %/50% w/w Ti:Zr oxide (CV ± 8 %, CL ± 3.3)	1	4
50% each w/w Zr/Ti oxide	75 %/25% w/w Zr/Ti oxide (CV ± 8 %, CL ± 5.1)	1	4
50% w/w each Zr/Ti oxide	45 %/55% Zr:Ti oxide (CV ± 5 %, CL ± 2.3)	2	4
50% w/w each Zr/Ti oxide	60 %/40% w/w Zr:Ti oxide (CV ± 4 %, CL ± 2.0)	3	4
50% w/w each Zr:Ti oxide	25 %/80 % w/w Zr:Ti oxide (CV ± 36 %, CL ± 7.6)	4	4

* CV: coefficient of variation   ** CL: confident level of 95%

Table 2.8. EDX results catalysts prepared by impregnation methods (confident level 95%)

Catalyst synthesis preparation recipe, metal ratio, (wt/wt%)	Metal content detected by EDX (wt/wt%)	Chapter
2% Al/ 5% Zr/Ti oxide	1.8 % Al on 3.4 % Zr/Ti (CV ± 13 %, CL ± 0.3 of Al) (CV ± 19 %, CL ± 0.7 of Zr)	3
2% Cu/5%Zr/Ti oxide	2.0 % Cu on 6.6 % Zr/Ti (CV ± 12.0 %, CL ± 0.2 of Cu) (CV ± 18 %, CL ± 0.9 of Zr)	3
1.3% Ba/5% Zr /Ti oxide	Trace Ba on 3.7 % Zr /Ti (CV ± 9 %, CL ± 0.3 of Zr)	3
7.9% Hf/Ti oxide	13.5 % Hf/Ti (CV ± 36 %, CL ± 4.4 of Hf)	3
5.8% Al/Ti oxide	8.1 % Al/Ti (CV ± 3 %, CL ± 0.3 of Al)	3
6.9% Nb/Ti oxide	11.3 % Nb/Ti (CV ± 15 %, CL ± 1.3 of Nb)	3
10.5% Tl/Ti oxide	7.8 % Tl/Ti (CV ± 14 %, CL ± 1.0 of Tl)	3
7.4% V/Ti oxide	7.6 % V/Ti (CV ± 17 %, CL ± 1.1 of V)	3
2% Pt/Ti oxide	2.0 % Pt/Ti (CV ± 40 %, CL ± 0.7 of Pt)	3
5% Zr/Ti oxide by impregnation method-2	5.0 % Zr/Ti (CV ± 12 %, CL ± 0.5 of Zr)	3 and 4
8% Zr/Ti oxide by impregnation method-4	8.7 % Zr/Ti (CV ± 11 %, CL ± 0.9 of Zr)	4
5.8% Cr/Si oxide	5.0 % Zr/Ti (CV ± 12 %, CL ± 0.6 of Zr)	3
5.1% Ga/Al oxide	8.0 % Zr/Ti oxide (CV ± 9 %, CL ± 0.7 of Zr)	3

* CV: coefficient of variation   ** CL: confident level of 95%

2.3.2 X-ray diffraction (XRD)

Diffraction patterns are presented for Zr/Ti oxide catalysts prepared by both co-precipitation and impregnation as follows:

2.3.2.1 Zr-Ti oxide catalyst prepared by co-precipitation

The powder XRD pattern of ZrO_2 (from Alfa Aesar) calcined at 700 ^{o}C is shown in Figure 2.13. The sharp diffraction peaks were labelled according to International Centre for Diffraction Data (ICDD) numbers 01-080-2155 and 00-007-0343. The monoclinic phase and tetragonal phase were both detected for ZrO_2. It seems that the monoclinic phase is dominant.

Figure 2.13. XRD of ZrO_2 (Alfa Aesar) calcined at 700 ^{o}C [T] tetragonal phase [M] monoclinic phase

The TiO_2 calcined at 700 ^{o}C showed anatase sharp peaks and is labelled according to ICDD number 01-071-1166 reference as shown in Figure 2.14. In addition, Tables A3, A4, and A5 in **Appendix 2** show the reference data for the powder diffraction patterns from ICDD and Miller indices for 2θ of each TiO_2 and ZrO_2.

Figure 2.14. XRD graph of TiO_2 calcination at 700 °C showing mainly anatase phase

Figure 2.15 shows pXRD patterns for pure TiO_2, and TiO_2 containing 11%, 25% and 50% ZrO_2, prepared by the co-precipitation method-1. For the 11% ZrO_2 sample, there is almost no evidence of a separate ZrO_2 phase. But for the 25% and 50% ZrO_2 samples, reflections are visible that must be due to ZrO_2. Reflections at 50-51° and 60° are very similar to those seen for ZrO_2 in Figure 2.13. However, the intense reflections at 28° and 32° for monoclinic ZrO_2 are not seen for the Zr/Ti oxide mixture. In their place is a strong reflection at about 30° which increases in intensity as the ZrO_2 content is increased from 25 to 50% ZrO_2. This is assigned to tetragonal ZrO_2 and it appears that in these blends, tetragonal zirconia is more stable than monoclinic.

Figure 2.15. XRD patterns of Zr/Ti oxide catalysts of varying compositions, prepared by the co-precipitation method-1 and calcined at 700 °C : [A] anatase phase, [T] tetragonal phase [M] monoclinic phase.

On the other hand, when TiO_2 is loaded on ZrO_2, the 2% w/w Ti/Zr oxide (Figure 2.16) shows weak but clear diffraction peaks from the anatase phase at 25.3°. Increasing the loading to 8%, 17% and 44% of Ti, the anatase phase increases progressively.

Figure 2.16. XRD patterns of Ti/Zr oxide prepared by the co-precipitation method-1 and calcined at 700 °C: [A] anatase phase, [T] tetragonal phase and [M] monoclinic phase.

Figure 2.17 shows a comparison between catalysts prepared by co-precipitation methods 2, 3, and 4 (50% w/w each Zr/Ti oxide). XRD patterns show a mixture of diffraction peaks of tetragonal and monoclinic phases from ZrO_2 with anatase phases from TiO_2 peaks in all three cases.

Figure 2.17. XRD patterns of co-precipitation method-2, 3, and 4 of 50% w/w binary Zr/Ti oxide [A] anatase phase, [T] tetragonal phase [M] monoclinic phase (calcined at 700 °C) , XRD scanning conducted at step size 0.4 °

56

Now, turning back to Figure 2.15, it is possible to say how TiO_2 and ZrO_2 mix on preparation of TiO_2-rich catalysts. The 11% ZrO_2 catalyst shows virtually no free ZrO_2 so it can be concluded that at this low level ZrO_2 is incorporated completely in a solid solution (crystallized in the solid state) in TiO_2.   Furthermore, adding zirconia to titania at levels above the limit of solubility results in the free zirconia adopting the tetragonal phase and, in this respect, it differs from pure zirconia which exhibits the monoclinic phase on calcination at 700 ^{o}C.

In contrast, when TiO_2 is added to ZrO_2 (Figure 2.16), evidence of anatase is visible at loads down to 2% w/w TiO_2. This implies that the two solids are immiscible at these compositions.

2.3.2.2 Catalysts prepared by impregnation

The 5% w/w Zr/Ti oxide (calcined at 700 ^{o}C, impregnation method-2) was characterized. Figure 2.18 shows the diffraction pattern which, like the similar material prepared by co-precipitation, shows almost exclusively the anatase phase of TiO_2 and no X-ray diffraction of tetragonal or monoclinic of ZrO_2 was detected.

Similarly, several binary oxide catalysts: 5.8% Al, 10.5% Tl, 7.9% Hf, and 6.9% Nb doped on TiO_2 support prepared by impregnation methods -1 and -4 were tested by XRD. Figure 2.19 shows XRD patterns of the catalysts and it reveals that the anatase phase of TiO_2 is the dominant crystalline phase. The mixtures with niobium, hafnium and aluminium, show no reflections other than those due to anatase. For the catalyst 10.5% w/w Tl/Ti oxide, the pXRD also shows very weak peaks due to the cubic phase of Tl_2O_3 at 28-29° and 40-41° [14-15].

Figure 2.18. XRD pattern of 5% w/w Zr on Ti oxide (impregnation method-2).
[A] anatase phase, [T] tetragonal phase [M] monoclinic phase (calcined at 700 ºC)

Figure 2.19. 5.8% Al, 10.5% Tl, 7.9% Hf, and 6.9% Nb doped on TiO_2 support prepared by impregnation method 2. All catalysts calcined at 700 ºC except Al_2O_3-TiO_2 at 500 ºC.

2.3.3 Nitrogen adsorption analysis

Table 2.9 lists the surface areas, pore volumes and pore sizes for Zr/Ti oxides prepared by four co-precipitation methods, plus data for TiO_2 and ZrO_2. The data for similar catalysts prepared by the impregnation method along with the other mixed oxides prepared this way appears in Table 2.10. This table includes data for two ternary mixed oxides, which show relatively low surface areas and for the two catalysts prepared as benchmarks, 5% w/w Ga/Al oxide and 5.8% w/w Cr/Silica, which show relatively high surface areas in line with data by Nakagawa et *al.* [16] and Wang et *al.* [17].

In general, the mixed oxides show somewhat higher surface areas than the parent oxides but there are no significant trends and there are no major differences visible between catalysts made by the different methods. The data for Zr/Ti oxide catalysts is consistent with that reported for similar catalysts by Rao *et al.* [13].

Table 2.9. Surface area and porosity data for catalysts made by co-precipitation by increasing the loading of TiO_2 to ZrO_2 (calcined at 700 °C)

Catalyst	BET surface area, $m^2\ g^{-1}$	Pore volume cm^3g^{-1}	Average pore diameter, nm	Preparation method	Tested in chapter
TiO_2	11	0.10	38	-	3
ZrO_2	17.2	0.18	43	-	3
2% w/w Ti/Zr oxide	5.2	0.05	38	1	4
8% w/w Ti/Zr oxide	7.8	0.06	29	1	4
17% w/w Ti/Zr oxide	7.4	0.07	37	1	4
44% w/w Ti/Zr oxide	11.1	0.14	50	1	4
11% w/w Zr/Ti oxide	15.7	0.15	39	1	4
45% w/w Zr/Ti oxide	20.0	0.19	39	1	4
50% w/w each Zr/Ti oxide	15.3	0.11	29	1	4
50% w/w each Zr/Ti oxide	48.7	0.33	27	2	4
50% w/w each Zr/Ti oxide	31.5	0.30	38	3	4
50% w/w each Zr/Ti oxide	45.7	0.32	28	4	4

The pore volumes are shown and are, as expected, relatively low in line with the surface area data. Average pore diameters are shown but they, given the low pore volumes, are of limited significance (Table 2.10). The two literature-based catalysts Cr/Si and Ga/Al oxides exhibit larger pore volumes and pore diameter data which probably has more significance.

Table 2.10. Surface area and porosity data for three different impregnation methods of ZrO_2 doped on TiO_2 (calcination 700 ^oC)

Catalyst	BET surface area, $m^2 g^{-1}$	Pore volume $cm^3 g^{-1}$	Average pore diameter, nm	Preparation method used	Tested in chapter
TiO_2	11	0.10	38	-	3
5% w/w Zr/Ti oxide	26.5	0.22	34.0	1	3
5% w/w Zr/Ti oxide	19.2	0.14	28.1	2	3 and 4
5% w/w Zr/Ti oxide	23.9	0.19	29.9	3	4
2% w/w Pt/Ti oxide	18.1	0.15	33.6	4	3
7.9% w/w Hf/Ti oxide	33.7	0.23	248.7	4	3
6.9% w/w Nb/Ti oxide	28.1	0.21	302.6	4	3
5.8% w/w Al/Ti oxide	94.4	0.19	85.2	1	3
10.5% w/w Tl/Ti oxide	24.2	0.23	328.3	1	3
2% w/w Al, 5% Zr/Ti oxide	24.0	0.20	33.2	1	4
3.6% w/w Fe, 5% Zr/Ti oxide	10.9	0.10	35.5	1	4
3.4% w/w Co, 5% Zr/Ti oxide	5.1	0.05	45.7	1	4
4% w/w Cu, 5% Zr/Ti oxide	3.8	0.06	51.3	1	4
5.1% w/w Ga/Al oxide	147.2	0.48	133.7	1	3
5.8% w/w Cr/Si oxide	272.4	0.26	41.9	1	3

Figures A1 to A18 in **Appendix 1** show the isotherm plots for the binary and ternary oxides catalysts which are type IV isotherms according to IUPAC, with hysteresis loop associated with the most solid oxide catalysts. In general, they are all of a common type.

The isotherms shown in Figure A1 to A6 in **Appendix 1** are for ZrO_2 and TiO_2 and for 50% Zr/Ti oxide blends prepared by co-precipitation methods. Note that there are differences between the four isotherms associated with the four co-precipitation methods. It is not absolutely clear that these differences are reproducible but it is clear that there are ways in which the porosity and surface area can be controlled by synthesis conditions.

Figures A7 to A18 in **Appendix 1** show isotherms for the other catalysts. With the exceptions of the two literature catalysts (5.1% Ga/Al oxide and 5.8% Cr/Si oxide) the isotherms are all very similar. Nevertheless, there is no doubt that the control of

surface properties that are illustrated in Figure A7 (**Appendix 1**) could be applied to all the catalysts in this series.

Pore size distributions taken from the nitrogen desorption isotherms using the BJH method are shown in the following figures. In Figure 2.20, TiO_2 and ZrO_2 calcined at 700 ^oC are compared. In Figure 2.21, the distributions for 50% mixtures of these two prepared by the four different co-precipitation methods are shown, illustrating the differences in isotherms in Figure A3 and A6 (**Appendix 1**) described above.

Figure 2.20. BJH pore size distribution curves of single oxide of ZrO_2 and TiO_2

Figure 2.21. BJH pore size distribution curves of the four co-precipitation methods compared with impregnation method-2 of Zr/Ti oxide (**chapter -4**)

Equivalent distributions are shown for 5% ZrO_2/TiO_2 prepared by the impregnation methods in Figure 2.22. It is not possible to compare these data with those for co-

precipitated catalysts because the levels of doping are very different but it seems likely that porosity characteristics for materials prepared by the two methods would be a little different. Other distributions are shown in Figures 2.23 and 2.24, in general differences are minor.

Figure 2.22. BJH pore size distribution curves of the impregnation method-1, -2 -3 and 4 of 5% w/w Zr/Ti oxide (**chapter -4**)

Figure 2.25 shows pore size distribution for Cr/Si and Ga/Al oxides and these materials show much greater pore volumes and very different pore size distributions..

Figure 2.23. BJH pore volume distribution curves of ternary oxides catalysts based on Zr/Ti oxides (**chapter -4**)

Figure 2.24. BJH pore size distribution curves of the impregnation method-1, of binary oxides based on Ti support compared with 5% w/w Zr/Ti oxide (**chapter-3**)

Figure 2.25. BJH pore size distributions for 5%Ga/Al oxide and 5.8% Cr/Si oxide, calcined at 700 ^oC

2.3.4 Temperature programmed desorption (NH$_3$-TPD)

The selected catalysts were studied by NH$_3$-TPD to determine the acidity. Figure 2.26 shows low ammonia desorption for the single oxides, ZrO$_2$ and TiO$_2$. In contrast the mixed Zr/Ti oxide, exemplified by the 5% ZrO$_2$ mixture for which data is shown in the same figure, can show quite high ammonia desorption over the range 200-500 ^oC. The TPD profile shown for this catalyst in characteristic of a reasonable concentration of relatively strong acid sites, arising presumably as a result of the structural disruption associated with the mixtures – most likely the homogeneous phase containing the mixed oxides which was observed in the XRD patterns of the mixtures (see more discussion in **chapter 3**).

Higher ZrO_2 loadings resulted in more acid sites as measured by ammonia TPD (Figure 2.27 A & B), with some differences depending on the method used to prepare the catalyst. It is worth saying that the NH_3-TPD data for 50% w/w Zr-Ti oxide catalysts prepared by co-precipitation methods were in agreement with the data reported by Rao *et al.*[13] (see **chapter 4**).

Figure 2.26. NH_3-TPD comparison plot 5% w/w Zr/Ti oxide (impregnation method-1) and signal oxide of ZrO_2 and TiO_2

Figure 2.27A. Overlay plot of NH_3-TPD: comparison of impregnation methods of 5% w/w Zr/Ti oxide (**chapter-4**).

Figure 2.27B. NH$_3$-TPD a comparison between of co-precipitation method-2, -3 and -4 of 50% w/w each Zr-Ti oxide and the impregnation 5% w/w Zr/Ti oxide (**chapter-4**).

The 5% ZrO$_2$ mixture with TiO$_2$ was used as a basis for the series of three-oxide mixtures which were prepared by adding a third metal oxide at low concentration (typically 1-2 % metal content w/w). The ammonia TPD results for a number of these blends are shown in Figures 2.28 and 2.29. The effect on acidity is variable but in all cases the addition of the third component appears to reduce the concentration and/or the strength of the acid sites, based on the extent of ammonia desorption over the 200-500 ^{o}C range.

Figure 2.28. NH$_3$-TPD of 1.3% w/w Ba, 2% w/w Be and 2% w/w Mg were each impregnation on catalysts of 5% w/w Zr/Ti oxide (**chapter-3**).

Figure 2.29. NH$_3$-TPD plots of 2% w/w Cu/5% w/w Zr/Ti oxide and 2% w/w Fe/ 5% w/w Zr/Ti oxide compared with 5% w/w Zr/Ti oxide catalyst (**chapter-3**).

Alumina was used in place of zirconia in some materials and as a third oxide as above in others. TPD data is shown in Figure 2.30. The effect of aluminium appears to be to reduce acidity, although there does appear to be a relatively high concentration of weak sites (desorption at 250 °C) for the binary mixture contacting alumina.

Figure 2.30. NH$_3$-TPD 2% w/w Al /5% w/w Zr/Ti oxide and 5.8% w/w Al/Ti oxide compared with 5% w/w Zr/Ti oxide (**chapter-3**).

Figures 2.31 and 2.32 show NH$_3$-TPD temperature profiles for the other binary oxides catalysts prepared using TiO$_2$ as the base and the added oxide at less than 10% metal content by weight. Vanadium, niobium, iridium, and hafnium oxides as well as platinum all form mixtures of lower acid strengths than zirconia with titania (**chapter 3**).

Figure 2.31. NH$_3$-TPD plots 7.4% w/w V/Ti oxide, 6.9% w/w Nb/Ti oxide, 3.5% w/w Ir/Ti oxide and 3.3% w/w Rh/Ti oxide compared with 5% w/w Zr/Ti oxide

(**chapter-3**).

Figure 2.32. NH$_3$-TPD of 7.9% w/w Hf/Ti oxide and 2% w/w Pt/Ti oxide catalysts compared with 5% w/w Zr/Ti oxide (**chapter-3**).

In contrast to the results above, two metal oxides were found to generate higher acidity (as measured by ammonia TPD) than Zr/Ti oxide. These were the TiO$_2$ blends with thorium(IV) oxide and uranium(IV) oxide.   Data is shown in Figure 2.33 and the temperatures for maximum ammonia desorption are similar for these blends as for Zr/Ti oxide but the integrated areas of the desorption peaks are very much higher, suggesting that acid sites are of similar strengths but in considerably higher concentrations. (**chapter 3**).

Figure 2.33. NH$_3$-TPD of 5% w/w U/Ti oxide and 5% w/w Th/Ti oxide catalysts compared with 5% w/w Zr/Ti oxide (**chapter-3**)

TPD data for the Ga/Al oxide and Cr/Si oxide catalysts which have been used to benchmark the results in this thesis is shown in Figure 2.34. The data suggests that these catalysts exhibit relatively high concentrations of relatively weak acid sites when compared with Zr/Ti oxide.

Figure 2.34. NH$_3$-TPD comparison between bench mark catalysts of 5%Ga/Al oxide and 5.8% Cr/Si oxide compared with and 5% w/w Zr/Ti oxide catalysts (**chapter-3**)

The total ammonia adsorption of TPD was measured of single oxides, Zr-Ti mixed oxides and other binary oxides are shown in Table 2.11 and 2.12. The single oxides of ZrO$_2$ and TiO$_2$ have lower acidic strength compared to the mixed oxide of Zr-Ti. The Zr-Ti oxides prepared by impregnation and co-precipitation methods showed slightly different of total acidity between 215 to 396 µmoles/g . The binary oxide based TiO$_2$

support doped with second metal shows an increase of acidity ranged between 80-434 μmoles/g.

Table 2.11. Ammonia adsorption on TiO_2, ZrO_2, and ZrO_2-TiO_2 mixed oxides (calcined at 700 ºC)

Catalysts	NH₃ adsorbed, μmoles/g	Tested in chapter
TiO_4	45	3
ZrO_4	40	3
5% Zr/Ti oxide impregnation method-1	215.5	4
5% Zr/Ti oxide impregnation method-2	204.9	4
5% nano Zr/Ti oxide Impregnation method-3	274.3	4
50% w/w each Zr-Ti co-precipitation method-1	264.1	4
50% w/w each Zr-Ti co-precipitation method-3	274.1	4
50% w/w each Zr-Ti co-precipitation method-3	295.3	4
50% w/w each Zr-Ti co-precipitation method-4	396.9	4

Table 2.12. Ammonia adsorption of the binary oxide catalysts (calcined at 700 ºC)

Catalysts	Total acid, μmoles/g	Tested in chapter
3.3% Rh/Ti oxide	118.9	3
3.3% Th/Ti oxide	319.9	3
6.9% Nb/Ti oxide	79.9	3
10.5% Tl/Ti oxide	190.9	3
7.9% Hf/Ti oxide	434.4	3
5% U/Ti oxide	434.4	3
5.8% Al/Ti oxide	204.1	3
2% Al/5%Zr/Ti oxide	190.5	3
5.1% Ga_2O_3/Al_2O_3	366.2	3
5.8% CrO/SiO_2	155.3	3

In summary, a pronounced feature of the catalysts made by doping titania with zirconia is that they exhibit significant surface acidity compared to the component metal oxides. Compared to the catalysts against which new catalysts in this thesis are being benchmarked, that is Ga_2O_3/Al_2O_3 and CrO/SiO_2, they show stronger acid sites but possibly at lower concentrations. Almost all the other catalysts described here, where a third metal oxide has been added, show significantly reduced acidity compared. The overall expectation arising from this characterisation work is that, if surface acidity is

important in conferring activity to metal oxide catalysts, the simple blends in which TiO$_2$ is doped with ZrO$_2$ might be expected to show the highest activity of those tested.

The origin of the surface acidity is not clear, but when the observation that low concentrations of ZrO$_2$ do appear to dissolve in TiO$_2$ is taken into account, it seems likely that structural defects associated with the doping sites in the TiO$_2$ structure, are responsible.

2.3.5 Thermogravimetric analysis (TGA):

Thermogravimetric analysis (TGA) has been used in this work in certain areas. It was employed to study 5% w/w Zr/Ti oxide (impregnation method-1) catalysts which had been used in the dehydrogenation of propane by CO$_2$ for four days on the basis that these catalysts could well have been "coked" and this might be an explanation for their loss of activity (see **chapter 3**). The aim of the test was to determine whether the catalysts could be regenerated by heating. The used catalyst powder was black as shown in Figure 2.35, suggesting the presence of coke. The TGA test was conducted using heating rate of 10 ^{o}C/min. In addition, the TGA test was performed under air and CO$_2$. The idea was 1) to assess the prospect of regeneration of the catalysts and 2) to identify optimum conditions for regeneration.

Figure 2.35. The black colour of coke on 5% w/w Zr/Ti oxide

The results of TGA under air and CO_2 are illustrated in Figures 2.36 and 2.37. The TGA in air showed most of the coke weight lost was about 8.8 % before 580 °C. The total weight loss of carbonic coke was 9.2 %, and at temperature of 900 °C.

The TGA in CO_2 gas showed at 600 °C an effective removal of carbon deposition from Zr/Ti oxide catalyst surface via CO_2. The substantial removal of coke deposition was in the range of 8.2 % at isotherm of 8 hours from catalyst surface. The result indicates the catalyst of 5% ZrO_2/TiO_2 assists the coke gasification reaction[18] between CO_2 with carbon deposition as shown in equation (2.1) (**section 1.3.5**).

$$CO_2 + C_{(coke)} \rightarrow 2CO \qquad ..... \text{ Eq. (2.1)}[18]$$

Figure 2.36. TGA under Air of 5% w/w Zr/Ti oxide catalyst (9.2% weight loss at isotherm period of 1 hour), at 580 °C the most carbonic coke was removed at air oxidation

71

Figure 2.37. TGA by CO_2 gas of 5% Zr/Ti oxide catalyst (weight loss 8.2% at isotherm period of 8 hour)

2.4 Conclusions

TiO_2 can be doped with ZrO_2 and, at low concentrations, the two oxides are miscible in the solid phase and form a single phase with, essentially, the anatase structure. These blends exhibit significantly higher surface areas than the individual oxides from which they are made. These doped materials exhibit very much higher acidity than the component oxides, both in terms of acid site concentration and acid strength. It seems likely that defects in the anatase phase arising from the doping are responsible for these surface properties.

There is some dependence of the effectiveness of solid solution formation and the subsequent properties of the mixed oxides on the methods used to prepare these blends. Both co-precipitation and impregnation methods were investigated. It was found that co-precipitation of Zr/Ti oxide show slightly stronger acidic strength sites. On the other hand, the 5% Zr/Ti oxide catalysts prepared by impregnation methods have broader pore volume distribution than the catalysts Zr/Ti oxide made by co-precipitation method.

Incorporating a third metal oxide in these mixtures invariably resulted in lower acidities and, in general, the prospects for these three oxide blends to show activity were regarded as relatively low after this work. Comparison with other mixed oxide blends that have been cited as active catalysts in dehydrogenation of propane with CO_2 in the literature, notably Ga_2O_3/Al_2O_3 and CrO_x/SiO_2 was made. These two materials are obviously very different from those on which this thesis is based, but they were found to show surface acidity, although acid sites were somewhat weaker, if at higher concentration, that those found with ZrO_2/TiO_2 blends.

The final part of the chapter covered the facility with which used 5% Zr/Ti oxide catalysts could be regenerated. The evidence suggests that heating in CO_2 might be a very effective strategy for this, as it removes carbon by coke gasification reaction. .

References

1. N. Takahashi, A. Suda, I. Hachisuka, M. Sugiura, H. Sobukawa and H. Shinjoh, Appl. Catal. A, **72**, 1–2 (2007) 187-195.

2. A.M. Ruppert and T. Paryiczak, Appl. Catal. A, **320** (2007) 80-90.

3. I. Chepurna, R. Smortaev, C. Kanibolotsky and V. Strelko, J. Colloid Interface Sci., **356** (2011) 404-411.

4. M. Laniecki and M. Ignacik, Catal. Today, **116** (2006) 400–407.

5. J.R. Sohn and S. H. Lee, Appl. Catal. A, **321** (2007) 27-34.

6. J. R. Sohn and S. H. Lee, Appl. Catal. A, **266** (2004) 89–97.

7. D. Mao, G. Lu and Q. Chen, Appl. Catal. A, **263**, 1 (2004), 83-89.

8. M. Machida, S. Ikeda, D. Kurogi and T. Kijima, Appl. Catal. B, **35** (2001) 107–116.

9. E.P. Barrett, L.G. Joyner and P.P. Halenda, J. Am. Chem. Soc. **73** (1951) 373–380.

10. T. Horikawa, D.D. Do and D. Nicholson, Adv. Colloid Interface Sci., **169** (2011) 40–58.

11. M. AlSawalha, F. Roessner, L. Novikova and L. Bel'chinskaya, World Academy of Science, Eng. Technol., **5** (2011) 349-329.

12. D. R. Burri, K. M. Choi, S.C. Han, A. Burri and S. E. Park, J. Mol. Catal. A., **269** (2007) 58–63.

13. K. N. Rao, B. M. Reddy and S. E. Park, Appl. Catal. B, **100** (2010) 472–480.

14. M. S. Y. Parast, A. M. and P. Ebrahimpour, Dalton Trans., **41** (2012) 5848-5853.

15. M. Mohammadi, K. Akhbari, Y. Hanifehpour, A. Morsali, S. W. Joo, G. Bruno and H. A. Rudbari, J. Organomet. Chem., **733** (2013) 15-20.

16. K. Nakagawa, C. Kajita, K. Okumura, N. Ikenaga, M. Nishitani-Gamo, T. Ando, T. Kobayashi and T. Suzuki, *J. Catal.,* **203** (2001) 87–93.

17. S. Wang, K. Murata, T. Hayakawa, S. Hamakawa and K. Suzuki, Appl. Catal. A, **196** (2000) 1–8.

18. P. Kuśtrowski, P. Michorczyk, L. Chmielarz, Z. Piwowarska, B. Dudek, J. Ogonowski and R. Dziembaj, Thermochim. Acta, **471** (2008) 26–32.

CHAPTER-3

DEHYDROGENATION OF PROPANE USING CO$_2$

Table of content

3.1 Background and objectives

In this research, the dehydrogenation of propane by CO_2 is investigated. This research introduces a new non-chromium-based catalyst. Chromium-based catalysts are generally oxidative catalysts and are used on most propane dehydrogenation plants (in absence of CO_2). They exhibit high selectivity for propane to propene. However, chromium-based catalysts show low catalytic stability and are deactivated quickly (**chapter 2**). They require a recycling process to return chromium to the higher oxidation state after each period of use [1-5].

Recently, two non-oxidative catalysts (20% In_2O_3-Al_2O_3 and 5% ZnO/ZSM-5) were reported to give a propane conversion of 30 - 41% and propene yield >22.5 - 25.8% [6-9], and catalytic stability for 12 to 30 hours of propane conversion. Unfortunately the reactant gas composition required to observe this activity was too dilute in CO_2 and propane to be viable.

In this thesis, binary oxides of ZrO_2-TiO_2 have been studied because of their acidic and basic properties, tolerance to coke formation and thermal stabilities [10-12]. The individual oxides, ZrO_2 and TiO_2, have also been studied. There are reports in the literature of the binary oxide mixture ZrO_2-TiO_2 being used as a catalyst support, in the preparation of catalysts for propane dehydrogenation, as well as ethylbenzene, p-ethyltoluene and n-butane dehydrogenation, both with and without CO_2[13-17]. In this research, TiO_2 and ZrO_2-TiO_2 have been used as supports for other catalytic oxides, and metals for these reactions.

The objectives of the work described in this chapter were:

- To study binary and ternary metal oxide mixtures, based on TiO_2 and ZrO_2/TiO_2, as dehydrogenation catalysts using CO_2, and to establish the relationships between catalyst structure and catalytic properties, including activity, selectivity to propene and catalytic stability.

- To study the effects of reaction conditions on propane dehydrogenation, including the CO_2/propane reactant gas ratio, reactor temperature etc.

3.1.1 Equations for the dehydrogenation of propane by CO_2

The non-oxidative route for the dehydrogenation of propane by CO_2 is shown in equation (3.1). Kuśtrowski *et al.* [18] suggested the dehydrogenation proceeds in two steps. First, the coupling of propane occurs on the catalyst surface, losing H_2 as an adsorbed species as shown in equation (3.2). Then, CO_2 removes H_2 from the catalyst surface in a reverse water gas shift (RWGS) reaction as shown in equation (3.3) [19].

Overall dehydrogenation of propane by CO_2:	$C_3H_8 + CO_2 \rightarrow C_3H_6 + CO + H_2O$ .. Eq. (3.1)
Propane dehydrogenation on catalyst surface:	$C_3H_8 \rightarrow C_3H_6 + H_2{*}$ ..... Eq. (3.2)
Consumed H atoms by RWGS:	$CO_2 + H_2{*} \rightarrow CO + H_2O$ ..... Eq. (3.3)

CO_2 is thought to reduce coke deposition on the catalyst surface by coke gasification, producing CO as shown in equation (3.4) [18]. Other competing reactions, resulting in cracking of propane, can also occur on the catalyst surface, as shown in equations (3.5 A & B) and (3.6) [19].

Coke gasification by CO_2:	$CO_2 + C_{(coke)} \rightarrow 2CO$	Equation (3.4)
Cracking of propane to ethane and methane:	$C_3H_8 \xrightarrow{-H_2} C_3H_6$	Equation (3.5A)
	$C_3H_6 \xrightarrow{+H_2} C_2H_4 + CH_4$	Equation (3.5B)
Hydrogenation of ethene to ethane or methane:	$C_2H_4 \xrightarrow{+H_2} C_2H_6$ or $C_2H_4 \xrightarrow{+2H_2} 2CH_4$	Equation (3.6)

3.1.2 Thermodynamics of propane dehydrogenation by CO_2 and other reactions

The thermodynamic calculations and equations for propane dehydrogenation with CO_2 and without CO_2, dry reforming of propane, reverse water gas shift (RWGS), water gas shift (WGS) and propane cracking by H_2 are tabulated in **Appendix 2** (Tables B1, B2, B3, B4, B5, and B6) and summarised in equations 3.7, 3.8, 3.9, 3.10, 3.11, 3.12.

Propane dehydrogenation by CO_2 $C_3H_8 + CO_2 \rightarrow C_3H_6 + H_2O + CO$ Eq.(3.7)

Propane dehydrogenation without CO_2 $C_3H_8 \rightarrow C_3H_6 + H_2$ Eq. (3.8)

Dry reforming of propane $C_3H_8 + 3CO_2 \rightarrow 6CO + 4H_2$ Eq. (3.9)

RWGS $CO_2 + H_2 \rightarrow H_2O + CO$ Eq. (3.10)

WGS $CO + H_2O \rightarrow H_2 + CO_2$ Eq. (3.11)

Propane cracking by H_2 $C_3H_8 + H_2 \rightarrow C_2H_6 + CH_4$ Eq. (3.12)

The enthalpy (ΔH^o) and entropy (ΔS^o) of each reaction were obtained from the NIST database (http://cccbdb.nist.gov). The thermodynamic equations (3.13) and (3.14) have been applied to calculate the enthalpies and entropies of each reaction.

$$\Delta H^o = \sum \Delta H^o_{f\,products} - \sum \Delta H^o_{f\,reactants} \quad \text{Equation (3.13)}$$

$$\Delta S^o = \sum S^o_{products} - \sum S^o_{reactants} \quad \text{Equation (3.14)}$$

The Gibbs free energies (ΔG^o) and equilibrium constants (K) are calculated using equations (3.15) and (3.16). The Gibbs free energy and equilibrium constant of each reaction are calculated from 300 to 800 ^{o}C assuming (ΔH^o) and (ΔS^o) are temperature independent.

$$\Delta G^o = \Delta H^o - T\Delta S^o \quad \text{Equation (3.15)}$$

$$K = \exp\left(\frac{-\Delta G^o}{RT}\right) \quad \text{- - - Equation (3.16)}$$

(R = ideal gas constant = 8.314 J/mol K, T = temperature, Kelvin)

Table 3.1 shows that the propane dehydrogenation reactions with and without CO_2 are endothermic. The dry reforming reaction of propane by CO_2 is endothermic. However, the WGS reaction between CO and H_2O, and the H_2 cracking of propane, are exothermic and can provide extra heat to the catalyst surface. The Gibbs free energies and equilibrium constants for the six reactions are shown in Tables B1, B2, B3, B4, B5 and B6 of the **Appendix 2**.

Table 3.1. Thermodynamic values for six reactions.

Reaction	ΔH_{298}^o , kJ mol^{-1}	ΔS_{298}^o , JK^{-1} mol^{-1}
Propane dehydrogenation by CO_2: $C_3H_8 + CO_2 \rightarrow C_3H_6 + H_2O + CO$	127.0	169.1
Propane dehydrogenation without CO_2: $C_3H_8 \rightarrow C_3H_6 + H_2$	124.4	127.1
Dry reforming of propane: $C_3H_8 + 3CO_2 \rightarrow 6CO + 4H_2$	628.1	797
RWGS reaction: $CO_2 + H_2 \rightarrow H_2O + CO$	43.2	42
WGS reaction: $CO + H_2O \rightarrow H_2 + CO_2$	-43.17	-42
Propane cracking by H_2: $C_3H_8 + H_2 \rightarrow C_2H_6 + CH_4$	-53.9	14.5

It is useful to compare the thermodynamics of competing processes.

1) propane can react directly with CO_2 to form propene.

2) propane can dehydrogenate without CO_2, and CO_2 can react with the resultant H_2 in a reverse water gas shift process,

3) propane can react with CO_2 in a dry reforming reaction.

Figure 3.1 shows the Gibbs free energy (ΔG^o) vs. temperature for each of these reactions versus temperature. Note that the dry reforming reaction becomes the most favourable as the temperature is increased. However, as shown in Figure 3.2, if cracking occurs for any reason, then the dry reforming reaction of the products, ethane and methane, becomes considerably less favourable. (**Appendix 2** Tables B7 and B8).

Figure 3.1. Comparison of Gibbs free energy (ΔG^o) between propane dry reforming, RWGS and propane dehydrogenation with/without CO_2.

Figure 3.2. Gibbs free energy (ΔG) of dry reforming of each methane, ethane and propane.

3.1.3 Dissociation of propane on the catalyst surface

Propane dehydrogenation is an endothermic reaction and requires a high reactor temperature of > 670 ^{o}C in order to increase TΔS term to give a negative Gibbs free energy. Despite this, it has been reported that catalytic dehydrogenation of propane can be made to occur at lower temperatures (presumably involving a surface reaction) over certain metal oxides catalysts [20]. Although nominally the thermodynamics of the

reaction should limit the reaction, it is possible that very high local temperature on the catalysts surface might allow it to proceed.

In fact propane dissociation to propene on the catalyst surface is not fully understood. Some reports propose the dissociation of propane to propene over a non-oxidative catalyst surface as follows.

1- Over ZnO/ZSM-5 catalyst at 600 °C, it has been proposed that propane dissociates to C_3H_7* on $Zn^{(2+)}$ ($Zn^{(2+)}$-C_3H_7) and gives H* atom on $O^{(2-)}$ ($O^{(2-)}$-H) (chapter-1, Figure 1.2). This is followed by a one-step elimination of a second hydrogen atom and CO_2 then reacts with the adsorbed hydrogen atoms via RWGS [9],[21].

2- Propane dehydrogenation over GaO supported on Al_2O_3 in the absence and presence of CO_2 at 600 °C was studied by Xu *et al.*[5]. The XPS analysis suggested a heterolytic dissociation reaction on the gallium oxide surface forming a hydride and alkoxide species ($Ga^{(x+)}$-H^-) and ($O^{(2-)}$-C_3H_7)[5]. The alkoxide proceed further to the dehydrogenation to yield C_3H_6 and hydride ($O^{(2-)}$-H) (chapter-1, Figure 1.3).

3- The catalyst ZrO_2-TiO_2 has also been studied at 150 °C for the dehydrogenation of iso-propanol [11]. The paper suggested a (Zr-O-Ti) catalytic centre provides two reactive sites for reaction. They suggested that the Zr site forms (Zr-H). The O-Ti site then assists the reaction by attaching the hydrocarbon (hydrocarbon-O-Ti). The reaction then proceeds to form either H_2O and propene gas or H_2 and acetone.

3.1.4 The catalyst choice

The most wildly used catalysts for propane dehydrogenation are chromium-based which are not an environmentally ideal. Chromium-based catalysts are unstable and are

deactivated quickly. Other, experimental, non-oxidative catalysts are reported and exhibit improved stability but tend to have lower catalytic activity [10-12].

In the work described in this thesis, several catalysts based on TiO_2 and ZrO_2/TiO_2 supports have been synthesised and tested in order to increase the yield and selectivity to propene to superior to the industrial catalysts. The catalysts were studied in a series of experiments as follows:

1. **Baseline propane dehydrogenation:** a) experiment without catalyst (quartz wool) and b) using single oxides TiO_2 and ZrO_2. In these experiments a CO_2/propane ratio of 16.9 – 20.9:1 and reactor temperature 600 °C were used

2. **Binary mixed oxides: 5% ZrO_2/TiO_2:** experiment over a range of CO_2/propane gas ratios at temperature 600 °C.

3. **Ternary mixed oxides catalysts based on 5% ZrO_2/TiO_2:** several catalysts were investigated with the following additional metals, chosen to influence and control acidic/ basic properties (CO_2/propane ratio ~20:1 and reactor temperature 600 °C): Be, Mg, Ba, Cu, Fe, Al.

4. **Other metal oxides and metals were added to TiO_2, on the basis of literature reports of catalytic activities:** Pt, Ir, Hf, Tl, Nb, Rh, Th, U, V, Al, tested at CO_2/propane ratio ~20:1 and reactor temperature 600 °C.

5. **Two cited catalysts as benchmarks:** two catalysts were prepared as examples of new catalysts that have been reported as active in propane dehydrogenation as follows: 5% Cr oxide supported on SiO_2 [22] and 5% Ga oxide supported on Al_2O_3 [5] at CO_2/propane ratio ~20:1 and reactor temperature 600 °C.

6. **The effect of reactor temperature and reactant compositions** have been also studied.

3.2 Experimental method

3.2.1 Material

The binary and ternary metal oxide mixtures to be used as catalysts were prepared by the impregnation methods 1 [23] and 4 [24] as described in detail in **sections** (**2.1. 2.1**) and (**2.1. 2.4**). The impregnation method-1 used for example 0.5 g of $ZrO(NO_3)_2.6H_2O$ dissolved in diluted 100 ml 0.2 N nitric acid for 2 hours with mixing. Then 5 g TiO_2 in powder form was added and the mixture stirred for 18 hours at room temperature. The precursor was then centrifuged to remove water, and washed with distilled water three times before drying at 100 °C for 18 hours. The calcination at static air was applied at 700 °C. In addition, six catalysts of ternary oxide used the impregnation method-1. The third metal oxide dopant was added to the pre-calcined 5% Zr/Ti oxide as described in detail in **section** (**2.1.2.1**).

Impregnation method-4 was used to prepare metal chloride salts. The preparation is described in **chapter 2**. The impregnation method-2 used for example 1.02 g of $HfCl_4$ dissolved in distilled water (50 ml) for 2 hours with mixing. Then 12 g TiO_2 in powder form was added and during the stirring (18 hours) the pH level was adjusted by ammonia solution (1N) to reach pH 8. The precursor was then centrifuged to remove water, and washed with distilled water five times before drying at 100 °C for 18 hours. The calcination at static air was applied at 700 °C. The list of binary and ternary oxides catalysts are also tabulated in **Chapter-2** (Tables 2.3 and 2.4).

3.2.2 Catalyst characterization

In this thesis, several catalyst characterisation techniques were used as follows: SEM and EDX, pXRD, Nitrogen adsorption, NH_3-TPD and TGA. The characterisation of catalysts of the binary and ternary oxide are discussed in detail at **Chapter 2**.

3.2.3 Catalyst activity test

Catalytic activity testing was conducted in a stainless steel bed reactor as shown in Figures 3.3 and 3.4. The length of the reactor was 700 mm with external diameter of

6.35 mm (0.25 inch) and a tube furnace from Thermo was used. A weight of 0.3 g catalyst was placed to the middle of reactor and held in place with quartz wool at both sides. The inside reactor temperature was monitored by inserting a thermocouple contacted to the catalyst bed. The gas inlet was controlled by a needle valve for pre-adjustment of the flow rate of gas reactant feed. In addition, the outlet of the fixed bed reactor was connected to a GC-TCD for gas analysis. The reaction conditions for dehydrogenation of propane by CO_2 are tabulated in Table 3.2.

The catalyst bed was activated under nitrogen gas at 500 ^{o}C for four hours before introducing the reactant gas. Then it was cooled to 200 ^{o}C. The CO_2/propane gas was introduced at 200 ^{o}C for 2 hours. Then the reactor temperature was increased gradually by 50 ^{o}C per hour to 500-600 ^{o}C to test propane dehydrogenation. The testing of dehydrogenation was conducted over a prolonged time to observe the catalyst performance during the reaction. The spent catalyst containing coke was de-coked in an air flow of 50 ml/min for 8 hours at 700 ^{o}C. The catalyst was then re-tested for propane dehydrogenation.

Figure 3.3. Stainless steel fixed bed and tube furnace.

Figure 3.4. Diagram of the fixed bed for propane dehydrogenation by CO_2.

Table 3.2. The reaction conditions for the dehydrogenation of propane.

Condition	Propane dehydrogenation by CO_2
Reactant feed flow	0.2 ml/min
Temperature condition	550-600 ^oC
Volume of catalysts sample	1.25 cm^{-3}
GSVH	9.6 h^{-1}

3.2.4 Gas analysis by GC-TCD

A gas chromatography instrument equipped with a thermal conductivity detector (GC-TCD) was used to study the outlet gases. The initial temperature of the GC oven was 45 ^oC, ramped to 250 ^oC at 10 ^oC/min where the temperature was held for 10 min. The oven contained two columns: Haysep Q (length: 3 ft. for hydrocarbon separation) and Porapak Q (length: 6 ft. for CO_2, CO, O_2, N_2, H_2 separation). The gas produced from the reactor was connected directly to the gas inlet via a gas loop of volume 0.5 µl in order to provide continuous measurement of gas from the reactor to GC.

GC-TCD data was calibrated with a certified gas standard in mol% using response factors (RF) and confident level of 95% [25]. The certified gas samples from gas cylinders were analysed several times as tabulated in Table 3.3. The coefficient of variation (CV)

of peak areas indicates a high precision. The response factor for each gas was used to quantify the gases produced from the CO_2 dehydrogenation of propane and ethane. The quantification of water was not carried out in this process.

Table 3.3. GC-TCD analysis of the certified gas standard in mol% (confident level of 95%).

Gas ID	Conc. mol%	Test-1 Peak area	Test-2 Peak area	Test-3 Peak area	Test-4 Peak area	Test-5 Peak area	Test-6 Peak area	peak area mean	Peak area s[*]	Peak area CV%[**]	CL [***] 95%	RF[****]
H_2	67.8	7789.7	7799.7	7905.6	7909.6	8168.0	8300.8	7979	208.5	2.6 %	± 166.8	8.497×10^{-3}
CO	5	6555.8	6422.1	6351.8	6502	N.T[*****]	N.T	6458	89.6	1.61%	± 87.8	7.74×10^{-3}
CH_4	4.03	6697	6663	6775	6821	7098	7096	6859	193.0	2.8 %	± 154.4	5.876×10^{-4}
CO_2	50	154387	154523	163716	163925	N.T	N.T	159138	5408	3.4 %	± 5299.8	3.142×10^{-4}
C_2H_4	2.03	4786	4748	4832.7	4893.1	4930	5091	4880	123.1	2.5 %	± 98.5	4.159×10^{-4}
C_2H_6	5.31	13796	13773	14075	14080	14638	14632	14166	386.3	2.7 %	± 309.1	3.748×10^{-4}
C_3H_6	3	7571	7419	7512	7650	7687	7654	7582	102.4	1.35%	± 81.9	3.96×10^{-3}
C_3H_8	3.99	13641.3	13572	14108	13859	14098	14360	13940	303.5	2.2 %	± 242.9	2.862×10^{-4}

*s: standard deviation   ** CV: coefficient of variation   *** CL: confident level 95%

****RF: response factors   *****N.T: not tested

3.2.5 Data treatment and calculation

The GC-TCD output was integrated and converted to mol% for H_2, CO, CO_2, methane, ethene, ethane, propene and propane. Conversion (equation 3.17), selectivity (equation 3.18) and yield (equation 3.19) were calculated according to Chen *et al.* [6] and Xu *et al.*[5].

$$C_3H_8 \text{ conversion (mol\%)} = \frac{C_3H_{8\,in} - C_3H_{8\,out}}{C_3H_{8\,in}} \times 100\% \quad \dots \text{Equation (3.17)}$$

$$CO_2 \text{ conversion (mol\%)} = \frac{CO_{2\,in} - CO_{2\,out}}{CO_{2\,in}} \times 100\% \quad \dots \text{Equation (3.17)}$$

$$C_3H_6 \text{ Selectivity (mol\%)} = \frac{C_3H_{6\,out}}{C_3H_{8\,in} - C_3H_{8\,out}} \times 100\% \quad \dots \text{Equation (3.18)}$$

$$CO \text{ Selectivity (mol\%)} = \frac{CO_{out}}{CO_{2\,in} - CO_{2\,out}} \times 100\% \quad \dots \text{Equation (3.18)}$$

$$\text{Yield \%} = \text{Conversion } C_3H_8 \; X \; \text{Selectivity } C_3H_6 \; \dots \text{Equation (3.19)}$$

3.3 Results and discussion

3.3.1 Reaction without catalyst and with single oxides: TiO_2 and ZrO_2

Figure 3.5 shows the conversion of CO_2 vs the conversion of propane made without catalyst (quartz wool) and with the single oxides TiO_2 and ZrO_2 at 600 °C at CO_2/propane ratios 20.4:1, 16.9:1 and 20.9:1 respectively. The single oxide of TiO_2 shows the highest conversion of CO_2, more than 25%, and propane conversion >90%. ZrO_2 shows propane conversion of 63-64% but lower CO_2 conversion of 13-14%. The reactor without catalyst (quartz wool) shows the lowest conversion of propane at 20-21%. Tables B9, B10, B11, B12, B13 and B14 in **Appendix 2** tabulate the results of GC data of gas concentrations, conversions, selectivities and yields of propene. The single oxides of ZrO_2 and TiO_2produced significant amounts of CO, H_2 and methane, indicating some dry reforming and even propane cracking.

Figure 3.5. Conversion of propane and CO_2 without catalysts and with TiO_2 and ZrO_2 (600 °C).

Figure 3.6 shows selectivity to propene vs. propane conversion for reaction without catalysts (quartz wool) and with the single oxides. Propane conversion without catalysts was low (<210%) but propene selectivity was 32-47%, which is higher than for the single oxides. TiO_2 gave propane conversion of 90 % with poor selectivity to propene of 4 %. ZrO_2 achieved a lower conversion of propane of 63-64 % and, again,

poor propene selectivity of 4 %. Figure 3.7 shows propane yield vs. ethene yield for the same three systems. Yields of both propene and ethene were low both with and without TiO_2 and ZrO_2 catalysts.

In conclusion, there is very little reaction of any kind between CO_2 and propane in the absence of catalyst. With ZrO_2 and with TiO_2 propane conversion takes place at a significant level, but through either dry reforming or cracking, and not through the desired dehydrogenation reaction.

Figure 3.6. Propene selectivity vs. propane conversion: comparison between single oxides ZrO_2 and TiO_2 (600 ^oC).

Figure 3.7. Propene yield vs. ethene yield: comparison between single oxides ZrO_2 and TiO_2 (600 ^oC).

3.3.2 Binary oxides 5% ZrO_2/TiO_2 - effect CO_2/propane gas ratios

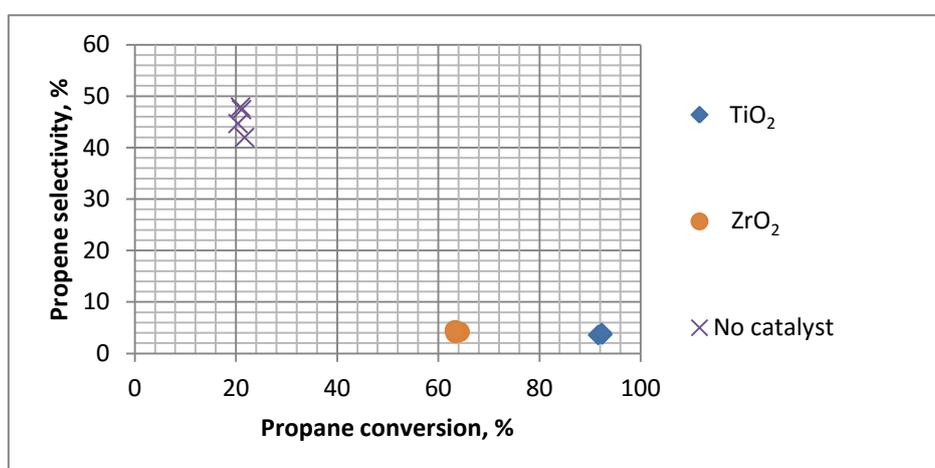## **3.3.2.1 CO_2/propane ratio 0:1**

The catalyst 5% ZrO_2/TiO_2 was tested for propane dehydrogenation without CO_2 at a space velocity of 9.6 h^{-1} for 98 hours. Tables B15 and B16 in the **Appendix 2** show the GC data for the products of this reaction.

Figure 3.8 shows propane conversion, propene selectivity, ethene selectivity, all vs. reaction time. The propane conversion was 63% and decreased a little to 59% over time while propene selectivity was constant at 24%. This represents very much greater activity in the dehydrogenation reaction than is exhibited by the individual oxides. Ethene selectivity was 11% and increased to 13%. Figure 3.9 shows the olefins yield. That is the sum of ethene and propene yield about 22%. The propene/ethene ratio from this experiment was 2.2 to 1.8. In summary, the catalyst showed stable propane conversion but selectivity to propene was low compared to that typically observed for commercial chromium-based catalyst (85-90%) [26].

Figure 3.8. Catalytic stability of the conversion of propane without CO_2 over 5% ZrO_2/TiO_2 at 600 ^{o}C.

Figure 3.9. Yields of propene and ethene over 98 hours at 600 °C with 5% ZrO_2/TiO_2 in absence of CO_2.

3.3.2.2 CO_2/propane ratio 1:1.4

Propane dehydrogenation by CO_2 was conducted on 5% ZrO_2/TiO_2 at a gas ratio of CO_2/propane 1:1.4 for 61 hours. Figure 3.10 shows propane conversion, propene selectivity, and ethene selectivity, all vs. reaction time. Propane conversion increased with time, but overall olefin yield decreased slightly. The propene/ethene ratio was 2.2 initially and decreased to 2.0 at the end of the reaction.

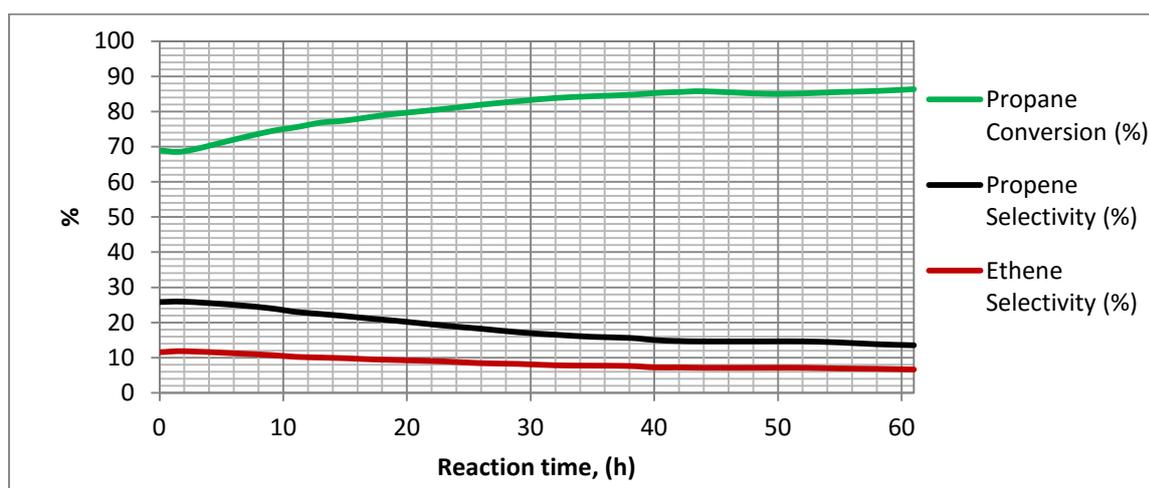Figure 3.10. Catalytic stability of the conversion of propane over 5% ZrO_2/TiO_2 at CO_2/propane gas ratio 1:1.4 (600 °C).

A comparison between propane conversion and propene selectivity with and without CO_2 is shown in Figure 3.11. The presence of CO_2 results in a lowering the selectivity to propene but higher overall conversion of propane. This suggests that CO_2 prompts undesired reactions, possibly dry reforming of propane and possibly further propane cracking to smaller compounds. Full GC results appear in Tables B17 and B18 in the **Appendix 2**.

Figure 3.11.Propene selectivity vs propane conversion without CO_2 and with CO_2 (CO_2/propane 1:1.4) on 5% ZrO_2/TiO_2 at 600 ^oC.

The differences in activity exhibited by the mixed oxides compared to the individual oxides are not obvious. X-ray diffraction studies reported in **Chapter 2** show that the titania exists as anatase throughout. Surface area and porosity measurements show only minor differences between the individual oxides and the mixture (Table 3.4 and Figure 3.12). The major differentiating measurement is through ammonia TPD, which shows that the mixed oxides are significantly more acidic than the component oxides alone (Figure 3.13). The preliminary conclusion is that it is this acidity that gives rise to the activity in the desired reaction. The origin of the acidity is unclear, but it seems very likely that it is linked to structural defects that arise from incorporation of the zirconium ion in the titania structure.

In the presence of CO_2 at this level (1:1.4 with propane) where selectivity to propene is poor, more CH_4, H_2 and CO, is formed than in its absence (Tables B17 in the **Appendix**

2), suggesting, in other words, at 600 °C and with this ratio of CO_2 to propane, there is significant C-C bond breaking over the catalyst.

Table 3.4. Texture proprieties of single oxides and 5% ZrO_2/TiO_2.

Catalyst	BET surface Area, m^2/g	Pore volume cm^3/g	Average pore size, nm
TiO_2	55.8	0.14	9.8
5% w/w Zr/Ti oxides	29.0	0.18	20.7
ZrO_2	17.2	0.18	42.6

Figure 3.12. BJH pore volume distribution curves of single oxides and 5% ZrO_2/TiO_2.

Figure 3.13. NH_3-TPD of 5% ZrO_2/TiO_2 and single oxides.

93

3.3.2.3 CO_2/Propane gas ratio 1:3.1

It seemed possible that the extent of dry reforming might be linked to the level of CO_2 in the feed and the objective of this experiment was to decrease the extent of dry reforming by lowering the CO_2 gas content to a CO_2/propane ratio of 1:3.1. Full GC results appear in Tables B19 and B20 in **Appendix 2**. Figure 3.14 shows summary data as propane conversion and olefin selectivity with time. Propane conversion increased to 47-65% over 72 hours but propane selectivity fell from 23% to 30%. The propene/ethene ratio was low at about 1.8.

Figure 3.14. Catalytic stability of the conversion of propane over 5% ZrO_2/TiO_2 at CO_2/propane gas ratio 1:3.1 (600 ^{o}C).

Figure 3.15 shows a comparison between total olefin yield (total yield of propene + ethene) and propane conversion over 5% ZrO_2/TiO_2 at 600 ^{o}C using gas feed with a CO_2 content from zero to 1:3.1 and 1:1.4 CO_2/propane ratio. The propane without CO_2 shows the most stable conversion/yield with time. Adding CO_2 to the reaction does not improve the catalytic selectivity although it does increase propane conversion and therefore yield of propene.

Figure 3.15. Total olefins yield and propene conversion: Comparison between CO_2/propane ratios of 0:1, 1:1.4 and 1:3.1 of 5% ZrO_2/TiO_2 at 600 °C.

3.3.2.4 CO_2/Propane gas ratio 2.6:1

The objective of this experiment was to use a higher CO_2/propane ratio of 2.6:1, hoping to increase the reaction of CO_2 with hydrogen via RWGS (equation 3.10). By doing this it was hoped that the prevalence of side reactions such as dry reforming might be reduced. The reaction was carried out for a longer time than earlier experiments, 257 hours. Results are shown in Figure 3.16 and Tables B21 and B22 in the **Appendix 2**. The results do not follow the trend established with lower CO_2 concentration. In this case, overall conversion is lower than before but the olefin yield is increased as illustrated in Figure 3.17. Note that the catalyst exhibited high stability over a long reaction time. In addition, the ratio of the propene/ethene ratio was 2.3 which was higher than in previous tests.
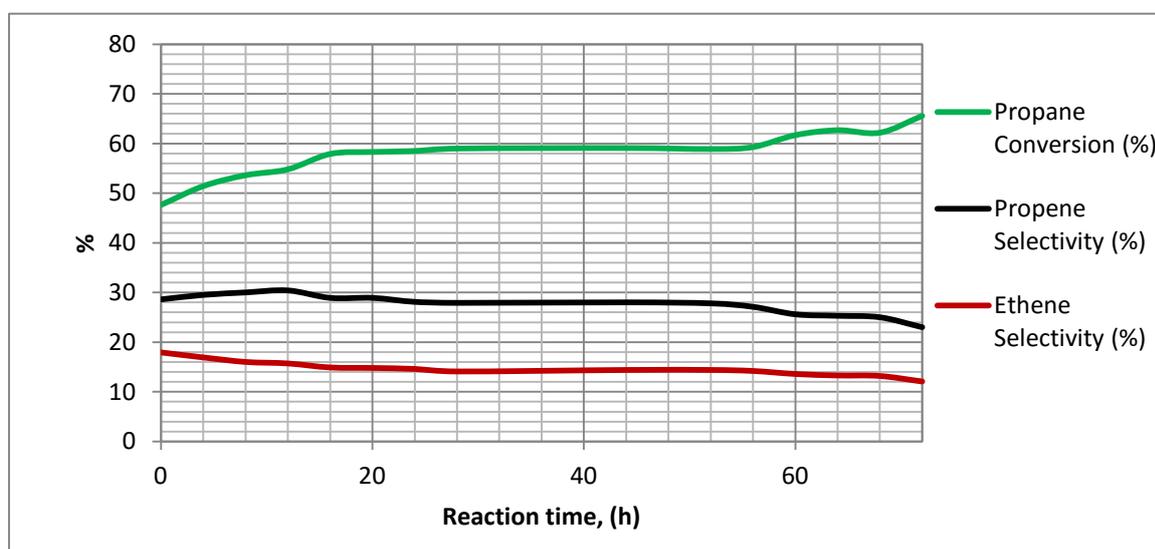
Figure 3.16. Catalytic stability of the conversion of propane over 5% ZrO_2/TiO_2 at CO_2/propane gas ratio 2.6:1 (600 °C).

Figure 3.17. Total olefins yield and propene conversion: comparison between CO_2/propane gas ratios of 0:1, 1:1.4, 1:3.1 and 2.6:1 of 5% ZrO_2/TiO_2 at 600 °C.

The higher CO_2 content seems to result in more RWGS than dry reforming or propane cracking, and results show a reduction in H_2. The reduction of H_2 could mean a reduction in the H_2 cracking reaction. This is an exothermic reaction so it is conceivable that the associated reduction in available heat might impede the desired, endothermic propane dehydrogenation.

Figure 3.18 shows an overall comparison of propene and ethene yields at four different gas ratios. The simple observation is that the highest CO_2 concentration results in the highest olefin yields.

Figure 3.18. Propene and ethene yield comparison for CO_2/propane gas ratios of 0:1, 1:1.4, 1:3.1 and 2.6:1 with 5% ZrO_2/TiO_2 at 600 ºC.

3.3.2.5 CO_2/Propane gas ratio 12.2:1

Further increasing CO_2 content to CO_2/propane 12.2:1 shows propane conversion was slightly reduced but propene selectivity increased to63.3% as shown in Figure 3.19. The ethene selectivity was increased to 22.7%. Detailed data appears in Tables B23 and B24 in **Appendix 2**.
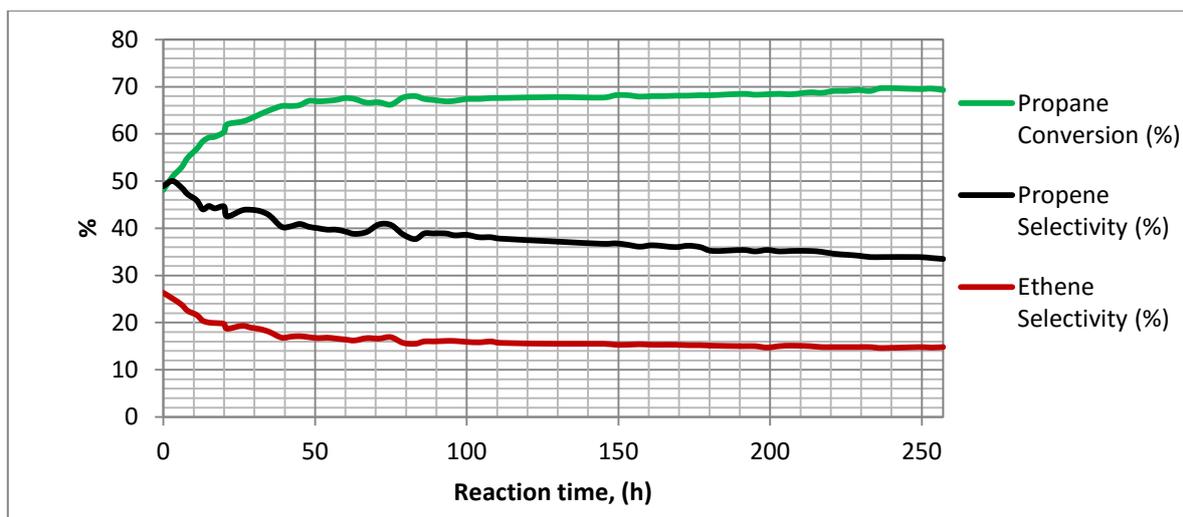
Figure 3.19. Catalytic stability of the conversion of propane over 5% ZrO_2/TiO_2 at CO_2/propane gas ratio 12.2:1 (600 ^oC).

Figures 3.20 shows the total olefins yield maintained at 40-45% but propane conversion at 40-45%. Figure 3.21 shows that the propane yield is slightly higher for CO_2/propane 12.2:1 then for other CO_2/propane ratios. The propene/ethene ratio is about 2.8. Selectivity to propene over ethene is improved at this relatively high CO_2 level.
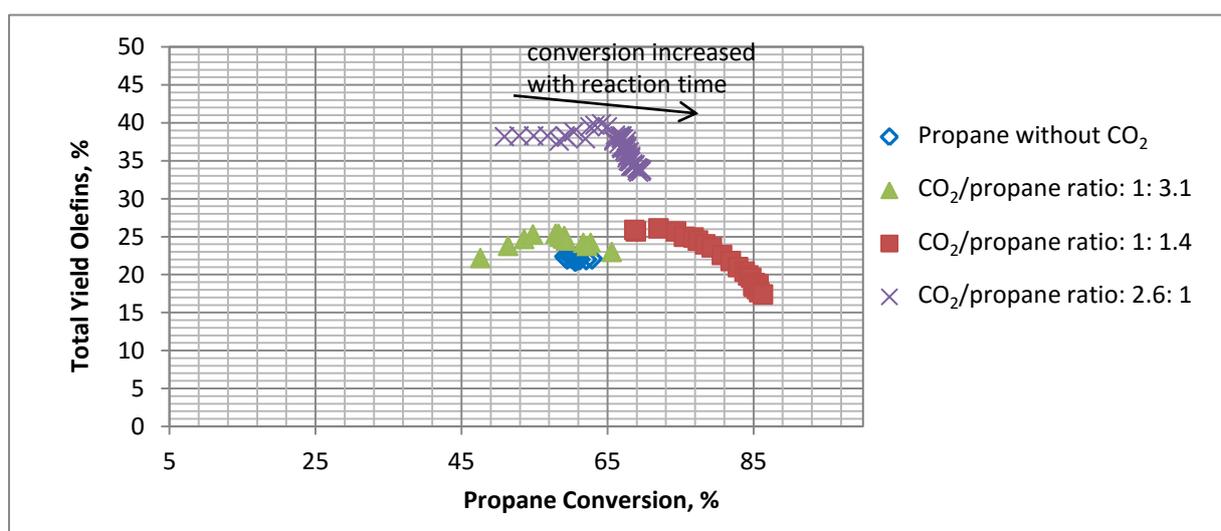

Figure 3.20. Total olefins yield and propene conversion: comparison between CO_2/propane ratios of 0:1, 1:1.4, 1:3.1, 2.6:1 and 12.2:1 of 5% ZrO_2/TiO_2 (600 ^oC).

Figure 3.21. Propene and ethene yields: comparison between CO_2/propane ratios of 0:1, 1:1.4, 1:3.1, 2.6:1 and 12.2:1 of 5% ZrO_2/TiO_2 at 600 °C.

3.3.2.6 CO_2/Propane gas ratio 24.2:1 and 34.3:1

The results are shown in Figures 3.22 and 3.23 in summary form and in detail in Tables B25, B26, B27 and B28 in the **Appendix 2**. The propene/ethene ratio appears to increase with increasing CO_2 concentration, indicative of increasing selectivity to dehydrogenation over cracking. Although propane conversion is relatively low with these CO_2 levels, the increasing selectivity to propene means that propene yield increases with CO_2 level. Furthermore, the catalysts seem to retain activity over long reaction times.

Figure 3.22. Catalytic stability of the conversion of propane over 5% ZrO_2/TiO_2 at CO_2/propane gas ratio 24.2:1 (600 °C).

Figure 3.23. Catalytic stability of the conversion of propane over 5% ZrO_2/TiO_2 at CO_2/propane gas ratio 34.3:1 (600 °C).

Figure 3.24 shows the overall comparison of the total olefins yield vs. propane conversion for all seven gas ratios of CO_2/propane. At CO_2/propane of 2.6:1 to 34.3:1 the total olefin yield was maintained at about 40% while the conversion of propane decreased with the increase of the gas ratio. Figure 3.25 shows propene vs. ethene yield, as the CO_2/propane ratio is increased. Note the increase in relative propene yield suggests that C-C bond breaking is becoming less favoured as CO_2 concentration is increased.

Figure 3.24. Total olefins yield and propene conversion: comparison between CO_2/propane gas ratios of 0:1, 1:1.4, 1:3.1, 2.6:1, 12.2:1, 24.2:1 and 34.3:1 of 5% ZrO_2/TiO_2 at 600 °C.

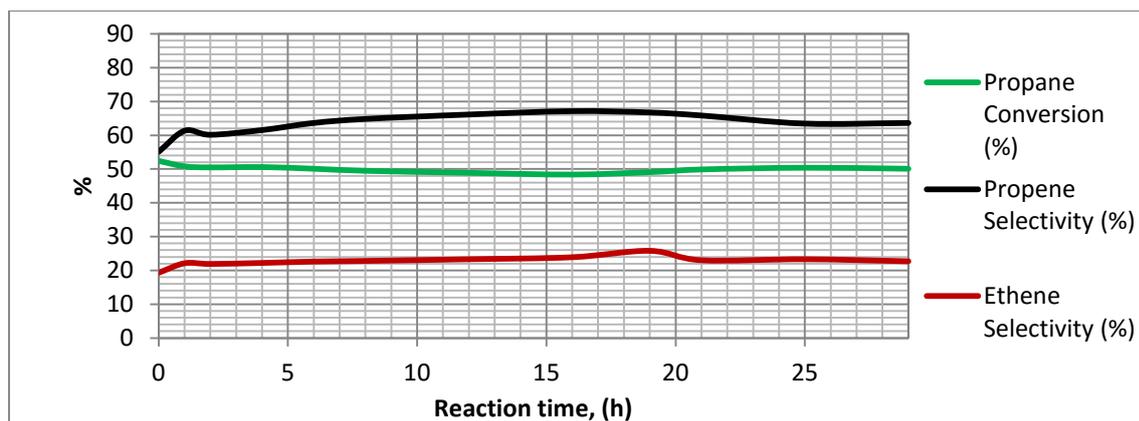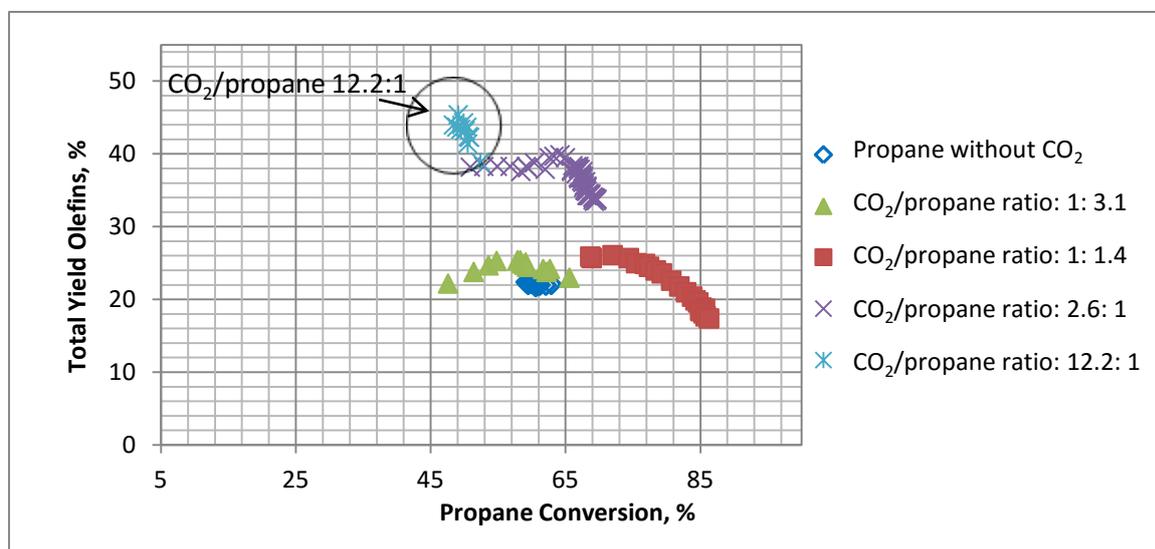Figure 3.25. Propene and ethene yield: comparison between CO_2/propane gas ratios of 0:1, 1:1.4, 1:3.1, 2.6:1, 12.2:1, 24.2:1 and 34.3:1 of 5% ZrO_2/TiO_2 at 600 °C.

Overall, the results suggest that catalytic activity is improved by increasing CO_2/propane ratio. It seems likely that the fall in propane conversion that accompanies an increase in propene yield as CO_2 concentration is increased might be due to a simultaneous reduction in activity towards dry reforming.

The increased selectivity to propene over ethene suggests C-C bond breaking becomes less favoured as CO_2 concentration is increased. The fall in H_2 yield (Table B29, **Appendix 2**) with increasing CO/H ratio suggests that CO_2 may be taking part in the Reverse Water Gas Shift reaction.

3.3.3 Ternary mixed oxide catalysts based on 5% ZrO_2/TiO_2

The propane dehydrogenation by CO_2 experiments with the mixtures of three metal oxides were conducted at 600 °C and a CO_2/propane ratio of ~20:1.

3.3.3.1 The effect of basic metal oxide doped on 5% ZrO_2/TiO_2:

In this research, several modifications of 5% ZrO_2/TiO_2 catalyst were performed by adding a third metal oxide. This was done in the hope that the surface acidity would be modified and that this might influence catalytic performance. The following mixtures (%w/w based on the metals only, not the oxides, as described above) of metal oxides were used: 1.3%BaO/5%ZrO_2/TiO_2, 2%BeO/5%ZrO_2/TiO_2 and 2%MgO/5%ZrO_2/TiO_2. NH_3 TPD data is shown in Figure 3.26. It can be seen that the catalyst incorporating the basic metal oxide MgO in 5%ZrO_2/TiO_2 shows almost no ammonia desorption and so exhibits very little if any surface acidity. The other basic metal oxides showed a reduction also, particularly in the amount of ammonia desorbed above 350 °C, indicative of a loss of the stronger acid sites.

Figure 3.26. NH_3-TPD of 1.3% BaO, 2% BeO and 2% MgO were each impregnated on catalysts of 5%ZrO_2/TiO_2.

Detailed data appears in Tables B30 and B31 in **Appendix 2**, and summary data in Figures 3.27 and 3.28. In all cases, the propene yield is lower than for 5% ZrO_2/TiO_2 (Figure 3.27). In the case of 2%BeO/5%ZrO_2/TiO_2 a slightly higher propane conversion is detected than for 5% ZrO_2/TiO_2 (Figure 3.28). The propene/ethene ratios for the three ternary oxides were low at 0.5-1, compared to 3.2 for 5% ZrO_2/TiO_2.   This implies that these more basic oxide catalysts promote C-C breakage more extensively than the parent 5% ZrO_2/TiO_2 catalysts which, as already noted, is significantly acidic.

Figure 3.27. Propene and ethene yields of ternary oxide catalysts: 1.3%BaO/5% ZrO_2/TiO_2, 2% BeO/5% ZrO_2/TiO_2 and 2% MgO/5% ZrO_2/TiO_2 compared with 5% ZrO_2/TiO_2 (CO_2/propane ratio ~20:1 at 600 ºC).

Figure 3.28. Propene selectivity and propane conversion over the ternary mixed metal oxide catalysts: 1.3%BaO/5% ZrO_2/TiO_2, 2% BeO/5% ZrO_2/TiO_2 and 2% MgO/5% ZrO_2/TiO_2 compared with 5% ZrO_2/TiO_2 (CO_2/propane ratio ~20:1 at 600 ºC).

3.3.3.2 Alumina containing catalyst: 2%Al_2O_3/5%ZrO_2/TiO_2 and 5.8% Al_2O_3/TiO_2

In the previous section, the basic metal oxide dopants lowered the catalytic activities of 5% ZrO_2/TiO_2. The study was extended to increase the acidity by doping 2% Al_2O_3 on 5% ZrO_2/TiO_2. In addition, 5.8% Al_2O_3 impregnated on TiO_2 alone was synthesized. The NH_3-TPD data for both these showed higher concentrations of low and medium of strength acidic sites (adsorption sites that desorb NH_3 at less than 380 ^oC) compared with 5% ZrO_2/TiO_2 (Figure 3.29).

Figure 3.29. NH_3-TPD 2%Al_2O_3/5%ZrO_2/TiO_2 and 5% Al_2O_3/TiO_2.

Detailed catalytic data is given in Tables B32 and B33 in **Appendix 2**. Summary data is shown in Figures 3.30 and 3.31. Propane conversions were similar to 5% ZrO_2/TiO_2. The ethene yields were also similar but propene yields were lower at 5-9 % compared to 30% with 5% ZrO_2/TiO_2 (Figure 3.31).

Figure 3.30. Propene selectivity vs. propane conversion of ternary oxides catalysts for 2% Al_2O_3/5% ZrO_2/TiO_2 and 5.8% Al_2O_3/TiO_2 compared with 5% ZrO_2/TiO_2 (CO_2/propane ratio ∼20:1 at 600 ºC).

Figure 3.31. Propene and ethene yields results of 2%Al_2O_3/5%ZrO_2/TiO_2 and 5.8% Al_2O_3/TiO_2 compared with 5% ZrO_2/TiO_2 (CO_2/propane ratio 20: 1 at 600 ºC).

3.3.3.3 CuO and FeO dopants on 5%ZrO_2/TiO_2

Both CuO and FeO were also added to modify acid/base properties. They evidently reduce the concentration of strong acid sites as measured by NH_3-TPD (Figure 3.32). Detailed catalytic results are in Tables B34 and B35 in **Appendix 2.** Summary data appear in Figures 3.33. The dopant of 2% FeO on 5% ZrO_2/TiO_2 shows almost complete conversion of propane, but selectivity to propene is almost zero (Figure 3.33). Yields of H_2 and CO are relatively high, suggesting dry reforming of propane on iron oxide

ternary oxides. The 2% CuO doped on 5% ZrO_2/TiO_2 shows a conversion of propane of >68% but very much lower selectivity to propene than ZrO_2/TiO_2 (Figure 3.33). Overall, neither catalyst is advantageous for the dehydrogenation of propane.

Figure 3.32. NH_3-TPD 2% CuO /5% ZrO_2/TiO_2 and 2% FeO/ 5% ZrO_2/TiO_2.

Figure 3.33. Propene selectivity vs. propane conversion via the ternary oxides catalysts of 2%CuO/5%ZrO_2/TiO_2 and 2%FeO/5%ZrO_2/TiO_2 compared with 5%ZrO_2/TiO_2 (CO_2/propane ratio ~20:1 at 600 °C).

3.3.4 Other titania-based catalysts

The propane dehydrogenation by CO_2 experiments using these mixed metal oxides were conduct at 600 °C and CO_2/propane ratio of ~20:1.

3.3.4.1 7.4% VO/TiO$_2$, 6.9% NbO$_2$/TiO$_2$, 3.5% IrO$_2$/TiO$_2$ and 3.3% RhO$_2$/TiO$_2$

Four metals from group VB and VIII (V, Nb, Ir, and Rh) were used in binary oxide mixtures based of TiO_2. Detailed catalytic results appear in Tables B36 and B37 in **Appendix 2** with summary data in Figure 3.34 below. Propane conversion is generally higher than for 5% ZrO_2/TiO_2, but propene selectivity was very low again compared to 5% ZrO_2/TiO_2.

Figure 3.34. Propene selectivity vs. propane conversion via binary oxides catalysts of 7.4%VO/TiO_2, 6.9%NbO$_2$/TiO_2, and 3.5%IrO$_2$/TiO_2 compared with 5% ZrO_2/TiO_2.

3.3.4.2 7.9% HfO$_2$/TiO$_2$ and 2% PtO/TiO$_2$, 5% UO$_3$/TiO$_2$ and 5% ThO$_2$/TiO$_2$

A further series of catalytically important metal oxides together with platinum metal were supported on TiO_2 and tested in the propane dehydrogenation by CO_2 reaction. NH_3-TPD data for this series was described in **chapter 2**. Generally, all these mixed materials showed lower acidity than 5% ZrO_2/TiO_2. Detailed catalytic data appears in Tables B38 and B39 in **Appendix 2.** Propene selectivities and propane conversions are shown for all the catalysts in Figure 3.35. Disappointingly, although propane conversion are comparable with 5% ZrO_2/TiO_2, selectivities to propene are all very low.

Figure 3.35. Propene selectivity vs. propane conversion of binary oxides catalysts of 7.9% HfO_2/TiO_2 and 2% PtO/TiO_2, 5% UO_3/TiO_2 and 5% ThO_2/TiO_2 compared with 5% ZrO_2/TiO_2 (CO_2/propane ratio ~20:1 at 600 °C).

3.3.4.3 10.5% Tl_2O_3/TiO_2

One catalyst of those examined showed results worthy of separate discussion. The 10.5% Tl_2O_3/TiO_2 showed reasonable propane conversion, along with quite high selectivity to ethene (rather than propene). The data is presented showing time dependence of these values in Figure 3.36, with detailed catalytic data in Tables B40 and B41 in **Appendix 2**. The catalytic data can be compared with NH_3-TPD and surface area/porosity data in Table 3.5, and it is clear that Tl_2O_3 does not impart any acidity to the catalyst. Despite this lack of acidity, the catalyst clearly promotes C-C bond breaking (to form ethene). The average pore size on Tl_2O_3/TiO_2 is surprisingly large, given that the surface area is about the same as that of ZrO_2/TiO_2. Whether this is significant is unclear.

Figure 3.36. 10.5% Tl_2O_3/TiO_2 propane conversion and olefin selectivity over 10 hours, 600 °C CO_2/propane ratio 20.1:1.

Figure 3.37. NH_3-TPD comparison between 10.5% Tl_2O_3/TiO_2 and 5% ZrO_2/TiO_2 catalysts.

Table 3.5. Texture proprieties of TiO_2 support, 5% ZrO_2/TiO_2 and 10.5% Tl_2O_3/TiO_2.

Catalysts	BET surface area m^2/g	Pore volume cm^3/g	Average pore size nm
TiO_2	55.8	0.14	10
5% ZrO_2/TiO_2	26.5	0.22	34
Tl_2O_3/TiO_2	24.2	0.23	328

3.3.5 CrO/SiO$_2$ and Ga$_2$O$_3$/Al$_2$O$_3$

Two catalysts, 5.8% CrO/SiO_2 and 5.1% Ga_2O_3/Al_2O_3, prepared by impregnation were tested for catalytic activity in propane dehydrogenation. These catalysts have been reported to give high conversion of propane to propene for a short time stability [1],[3].

The results from the work reported in this thesis show that these catalyst behave in away similar to many already described, giving high propane conversion but very low selectivity to propene (Figure 3.39). Detailed data appear in Tables B42 and B43 in

Appendix 2. It is worth noting that NH_3-TPD experiments showed that these catalysts exhibit some surface acidity.

The results obtained here differ from those reported in the literature for silica supported chromium oxide(s) and alumina supported gallium oxide, for which higher propene yields were found. It seems likely that the reason for these differences, other than the fact that different supports were used, might be related to the very different reactant gas compositions used in the reported work. In this work, for consistency, the same ~20:1 CO_2:propane ratio was maintained throughout.

Figure 3.38. NH_3-TPD comparison between 5%Ga_2O_3/TiO_2 CrO/SiO_2 compared with and 5% ZrO_2/TiO_2 catalysts.

Table 3.6. Texture proprieties of 8% CrO/SiO_2 and 5.1% Ga_2O_3/Al_2O_3, and 5% ZrO_2/TiO_2.

Catalysts	BET surface area m^2/g	Pore volume cm^3/g	Average pore Size nm
5% ZrO_2/TiO_2	26.5	0.22	34
8% Ga_2O_3/Al_2O_3	147	0.48	134
5.1% CrO/SiO_2	272	0.26	42

Figure 3.39. Propene selectivity vs. propane conversion of ternary oxides catalysts of 7.8% CrO/SiO₂ and 5.1% Ga₂O₃/Al₂O₃ compared with 5% ZrO₂/TiO₂ (CO₂/propane ratio ~20:1 at 600 °C).

3.3.6 Effect of reactor temperature on propane dehydrogenation by CO₂

So far, all data reported were taken at a reaction temperature of 600 °C. For the four most active catalysts in the dehydrogenation reaction, 5% ZrO₂/TiO₂, 7.9% HfO₂/TiO₂, 5.8% Al₂O₃/TiO₂, and 2% PtO/TiO₂, experiments were also performed at 550 to 600 °C. Summary results appear in Figures 3.40A, 3.41A, 3.42A and 3.43A.   In all cases, the propane conversion increases with increasing reaction temperature but, also in all cases, selectivity to propene decreases as reaction temperature is increased. Clearly, there is a balance between activity towards propane reactions generally, and activity specifically towards propene formation by dehydrogenation, and in designing a catalyst for this reaction, relative activities towards the desired and towards other reactions has to be taken into account (more discussion in **section 3.3.9**).

The propane dehydrogenation is endothermic ($\Delta \mathbf{H}^{o}_{298}$128 kJmol^{-1}). The activation energy of propane dehydrogenation for four catalysts was calculated assuming the reaction is first order. The natural log of the Arrhenius equation is rearranged in the equation 3.20.

$$\ln(r) = -\frac{Ea}{R}\left(\frac{1}{T}\right) + \ln A \ \text{-----} \ \text{Eq. (3.20)}$$

The activation energy (Ea) is determined directly by calculating the slope of curve of $1/T$ vs. $\ln(r)$ (Figures 3.40B, 3.41B, 3.42B and 3.43B). Table 3.7 shows small difference of the activation energy of the propane conversion of four catalysts. The activation energy may reflect on the differences in the dissociation energy of the H-C bond over catalysts and may correlate with propane selectivity. The catalyst of 5% ZrO_2/TiO_2 showed an activation energy 81.4 $kJmol^{-1}$ higher than 7.9% HfO_2/TiO_2 and 5.8% Al_2O_3/TiO_2 catalysts but it showed higher selectivity of propene. The catalyst of 2% PtO/TiO_2 showed higher activation energy catalysts but it showed a dry reforming of propane than propane dehydrogenation to propene.

Figure 3.40A. CO_2 dehydrogenation of propane between 550, 575 and 600 ºC tested on catalyst 5% ZrO_2/TiO_2 (CO_2/propane 24.2:1).

Figure 3.40B. Temperature versus natural logarithm of rate conversion of propane over 5% ZrO_2/TiO_2

Figure 3.41A. CO_2 dehydrogenation of propane between 550 and 600 ^{o}C tested on catalyst 7.9% HfO_2/TiO_2 (CO_2/propane 20.5:1).

Figure 3.41B. Temperature versus natural logarithm of rate conversion of propane over 7.9% HfO_2/TiO_2

Figure 3.42A. CO_2 dehydrogenation of propane between 526, 560 and 600 ^{o}C tested on catalyst 5.8% Al_2O_3/TiO_2 (CO_2/propane 21.3:1).

Figure 3.42B. Temperature versus natural logarithm of rate conversion of propane over 5.8% Al_2O_3/TiO_2

Figure 3.43A. CO_2 dehydrogenation of propane between 550 and 600 ^{o}C tested on catalyst 2% Pt/TiO_2 (CO_2/propane 22.9:1).

Figure 3.43B. Temperature versus natural logarithm of rate conversion of propane over 2% PtO/TiO_2

Table 3.7. Activation energy of propane dehydrogenation of 4 catalysts

Catalyst	CO_2/Propane ratio	Activation energy
5% ZrO_2/TiO_2	24.2:1	81.4 kJ mol^{-1}
7.9% HfO_2/TiO_2	20.5:1	44.2 kJ mol^{-1}
5.8% Al_2O_3/TiO_2	21.3:1	42.0 kJ mol^{-1}
2% PtO/TiO_2	22.9:1	137.8 kJ mol^{-1}

3.3.7 CO/H_2 and propene/ethane ratios

There are clear differences between the reactions that occur in a propane steam cracker and those that occur in the controlled propane dehydrogenation reactions described here. None of the previous studies of propane dehydrogenation by CO_2 (mainly by the oxidative route using chromium-based catalysts) have reported propene/ethene ratios or CO/H_2 ratios, and so conclusions about the relative activity of the catalysts towards C-C and C-H bond breaking have not been made, and the relative importance of reforming reactions and the reverse water gas shift reaction (RWGS) has not been determined. In the work reported in this thesis, these measures have been reported so it is possible to comment on competing reactions in much more detail than hitherto.

Figures 3.44 and 3.45 show the produced H_2 and CO from propane and CO_2 were correlated with propene selectivity. By increasing CO_2/propane ratio the concentration of H_2 and CO were reduced. This reduction of H_2 and CO concentrations have positive effect on propane dehydrogenation reaction and more propene selectivity generated from C-H bond breaking of propane. The higher yield of H_2 and CO was resulted of more C-C breaking of propane and dry reforming over catalyst than propane dehydrogenation to propene.

Figure 3.44. Comparison of H_2 concentration vs. propene selectivity at different CO_2/propane ratio.

Figure 3.45. Comparison of CO concentration vs. propene selectivity at different CO_2/propane ratio.

Table 3.8 shows ratios of CO/H_2 and propene/ethene for 5% ZrO_2/TiO_2 catalysed reactions at different gas ratios at reactor temperature 600 °C. The table shows the CO/H_2 ratio increased from 1.1 to 7.0 when the CO_2/propane gas ratio was increased from 1:1.4 to 34.3:1. The CO/H_2 ratio is an important indicator. Both gases are produced in the reforming reaction; hydrogen is consumed and CO produced in the RWGS reaction. At low CO_2 levels, the ratio of CO to H_2 would be expected to be low since there are few sources of CO and H_2 would be produced by direct dehydrogenation

of propane on the catalyst surface. As CO_2 levels are increased, CO can be produced by CO_2 dehydrogenation of propane (via a dehydrogenation step followed by the reverse water gas shift reaction between CO_2 and H_2 on the catalyst surface). Hydrogen, on the other hand, can only be produced by the reforming reaction between propane and CO_2. So the observation that this ratio increases with increasing CO_2 concentration implies that the, undesired, reforming reactions become less important at higher CO_2 levels and the dehydrogenation reaction takes over.

The parallel observation that the propene to ethane ratio increases as CO_2 is increased is also a reason to use high levels of CO_2 in this reaction. An interpretation is that high levels of CO_2 result in fast removal of adsorbed hydrogen atoms on the catalyst surface, promoting the formation of propene rather than the C-C bond breaking processes that are needed for ethane formation.

Table 3.8. The ratios of CO/H_2 and propene/ethene of 5% ZrO_2/TiO_2 at different ratios of CO_2/propane at 600 ^{o}C.

CO_2/propane ratio	CO/H_2 ratio	propene/ethene ratio
gas ratio 1:1.4	1.1	2.1
gas ratio 2.6:1	1.1	2.3
gas ratio 12.2:1	4.6	2.8
gas ratio 24.2:1	7.3	3.2
gas ratio 34.3:1	7	3.3

Table 3.9 shows the propene/ethene ratio produced over the other binary and ternary oxides catalysts. In general these ratios are lower than from 5% ZrO_2/TiO_2. It suggests that the metal oxide catalysts tend to promote cracking reaction (C-C bond breaking) of propane to ethene over dehydrogenation of propane to propene. The catalysts 7.4% VO/TiO_2 and 3.5% Ir/TiO_2 show the highest propene/ethene ratios of 4.7 and 6.1, but these data are of limited significance because of very low propene and ethene yields, and both catalysts favoured dry reforming as discussed in **section (3.3.3.1)**. The binary oxides catalyst 10.5% Tl_2O_3/TiO_2 showed the lowest propene/ethene ratio of 0.2, suggesting propane cracking via a C-C bond breaking pathway is more important than the propane coupling to propene as discussed in the **section (3.3.3.3)**.

Table 3.9. The ratios of propene/ethene formed with catalysts at 600 ^{o}C and CO_2/propane ~20:1.

Catalysts	propene / ethene ratio
TiO_2	1.0
ZrO_2	1.5
2% PtO/TiO_2	0.7
7.4% VO/TiO_2	4.7
7.9% HfO_2/TiO_2	1.2
10.5% Tl_2O_3-TiO_2	0.2
5% Al_2O_3/TiO_2	0.7
3.5% IrO_2/TiO_2	6.1
6.9% NbO_2/TiO_2	1.2
5.8% CrO/SiO_2	0.4
1.3% BaO/5% ZrO_2/TiO_2	0.6
2% BeO/5% ZrO_2-TiO_2	0.7
2% MgO/5% ZrO_2/TiO_2	0.6
2% Al_2O_3/5% ZrO_2/TiO_2	0.7
2% CuO/5% ZrO_2/TiO_2	0.7

3.3.8 CO_2 conversion compared to propane dehydrogenation

None of the reported studies of propane dehydrogenation emphasised the amount of CO_2 utilised for this reaction. In this research, we have evaluated the most active catalyst 5% ZrO_2/TiO_2 at 600 ^{o}C in terms of CO_2 consumption with a range of CO_2/propane ratios.

Figure 3.46 shows conversion of propane vs. conversion of CO_2 at six CO_2/propane ratios. Unsurprisingly, the highest conversions of CO_2 were detected at low CO_2 ratio levels, and CO_2/propane ratios of 1:3.1 and 1:1.4, at ~45-65% and ~30-75%, respectively. Propane conversions under these reactant compositions were high at 45% to 88%. These encouraging results are tempered by the fact that selectivity to propene in both cases is low at 30%, suggesting that CO_2 was consumed mainly via propane cracking and dry reforming.

Interestingly, at higher CO_2/propane ratios, the conversion of CO_2 is obviously reduced, but the reduction to less than 10% consumption even when the CO_2/propane ratio was only 13.1:1 is surprising. Against this, selectivity to propene is increases sharply under these high CO_2 conditions as shown in Figure 3.47.

Figure 3.46. Propane conversion vs. CO_2 conversion of different CO_2/propane gas ratios on the catalyst 5% ZrO_2/TiO_2 at 600 ºC.

Figure 3.47. Propene selectivity vs. CO_2 conversion of different CO_2/propane gas ratios on the catalyst 5% ZrO_2/TiO_2 at 600 ºC.

Figure 3.48 shows Propene selectivity vs CO_2 conversion for the wider range of binary and ternary metal oxides catalyst at a CO_2/propane ratio of ~20. The binary oxide of 5% ZrO_2/TiO_2 shows the highest activate propene selectivity but with low CO_2 conversions of less than 10% as discussed above. The other catalysts showed higher CO_2 conversions, but relatively low propene selectivities.

Figure 3.48. Propene selectivity vs. CO_2 conversion of CO_2/propane gas ratio 10:1 at 600 ^oC for binary and ternary oxides catalysts.

3.3.9 Summary of catalytic activity results

There are clear differences between the single oxides, ZrO_2 and TiO_2, and the same oxides mixed, exemplified by 5% ZrO_2/TiO_2, for propane dehydrogenation by CO_2. The single oxides showed bond breaking of propane to produce H_2, CO and methane through dry reforming combined with propane cracking. Table 3.10 summaries the overall product data for propane dehydrogenation by CO_2 over 5% ZrO_2/TiO_2, including the effect of CO_2:propane ratio.

Table 3.10. The effect of CO_2/propane ratio on yields, conversion and selectivities over 5% ZrO_2/TiO_2 at 600 ºC.

gas ratio of CO_2 / propane	propene/ethene ratio	Ratio of CO/H_2	Propene Selectivity (%)	Propane Conversion (%)	Propene Yield (%)	CO_2 conversion (%)
0 : 1	2	-	24.3	60.7	14.7	
1 : 1.4	2.1	1.1	18.6	80.6	14.7	46.2
1 : 3.1	1.9	0.5	27.6	58	16	45.6
2.6 : 1	2.3	1.1	38.8	66	25.5	24.4
12.2 : 1	2.8	4.6	63.3	50.1	31.6	9.3
24.2 : 1	3.2	7.3	57.1	55.4	31.6	5.6
34.3 : 1	3.3	7	57.8	50	28.9	2

As discussed above, there are clear trends in this data, all of which can be seen in the Table. Propane conversion occurs even without CO_2, but reaches a maximum value of 80% when the CO_2 at ratio 1:1.4 with the propane, as would be required of the dehydrogenation reaction.   The propene yield is always less than the propane conversion however, showing that selectivity to propene varies. In fact, propene yield gradually increases as the CO_2 level is increased, such that when the CO_2/propane ratio is 12.2:1 or higher, the yield of propene from propane is about 30%. This value is close to that reported on commercial propane to propene plants and, crucially, this value remains stable with this catalyst over an extended reaction period.   And propene selectivity improves also with CO_2 level, reaching 57-63% when there is a large excess of CO_2.

CO_2 conversions are always lower than would be expected were propane reacting stoichiometrically with CO_2 and there are obviously cracking reactions occurring that do not involve CO_2. There may also be water gas shift reactions occurring to produce CO_2.

The CO/H_2 ratio increases with CO_2, and this indicates that dry reforming becomes a less important competing reaction as CO_2 concentration is increased. This has been discussed above, alongside the observation that the propene/ethane ratio increases with CO_2, suggesting that high CO_2 levels favour C-H over C-C bond breaking reactions. There does appear to be a relationship between the propene selectivity over ethane and the reduction in the dry reforming reaction (manifested by a high CO/H_2 ratio). These are plotted against each other in Figure 3.49 for the gas ratios studied.

Figure 3.49. Comparison between CO/H_2 ratios with selectivity of propene/ethene yield ratio, at 600 °C.

One other catalyst made from two metal oxides showed some activity, and that was 10.5% Tl_2O_3/TiO_2. However, the catalytic results using this catalyst were very different to those from 5%ZrO_2/TiO_2 suggesting that a different catalytic route might be responsible for its activity. The results under a reactant mixture with CO_2/propane of 10 are shown in Table 3.1. Firstly, propane conversion with the thallium oxide catalyst are much lower, suggesting lower activity overall. But the propene/ethane and for CO/H_2 ratios are out of line with those seen for ZrO_2/TiO_2. With this catalyst, selectivity to propene over ethene is very low, but the CO/H_2 ratio is very much higher than any observed for 5% ZrO_2/TiO_2.

Data from the **Appendix** is shown in Figure 3.50 and Table 3.11. From this it can be seen that methane and hydrogen levels from the two catalysts are similar, but CO is

generated in much greater concentration using 10.5% Tl_2O_3/TiO_2. And propane conversion is much lower using this catalyst. Olefin selectivities for the two catalysts are similar but with 10.5% Tl_2O_3/TiO_2 ethene is the preferred olefin whereas propene is preferred over 5% ZrO_2/TiO_2

Methane and hydrogen are produced by reforming so it appears that dry reforming occurs to a similar extent over the two catalysts. CO is generated from both the dehydrogenation process and from RWGS, but the latter consumes hydrogen and the fact that detected hydrogen levels are similar suggests that possible differences in the selectivity towards the RWGS reaction is not responsible for the high CO level. It seems more likely that it is due to differences in selectivity towards dehydrogenation with CO_2, over thallium oxide, for a reason that is unclear, dehydrogenation occurs to produce CO and the process evidently goes on to include C-C bond breaking to yield ethene.

Table 3.11. Comparison between CO_2 dehydrogenation of propane between 5% ZrO_2/TiO_2 and 10.5% Tl_2O_3/TiO_2 (CO_2/propane 10:1, 600 ^{o}C)

Catalyst	Propene Selectivity (%)	Ethene Selectivity (%)	Propane Conversion (%)	Propene Yield (%)	Ethene Yield (%)	Total olefins Yield, (%)	Propene/ ethene ratio	CO/H_2 ratio
5% ZrO_2/TiO_2	57.1	17.5	55.4	31.6	9.7	40.9	3.3	7.3
10.5% Tl_2O_3/TiO_2	12.2	55.7	46.2	5.6	25.7	31.3	0.2	15.4

Figure 3.50. Comparison between 5% ZrO_2/TiO_2 (CO_2/propane 24.1:1)and 10.5% Tl_2O_3/TiO_2 (CO_2/propane 20.1:1, 600 ^{o}C) [A] H_2 mol% vs. CO mol%, [B] H_2 mol% vs. methane mol%,
[C] CO_2 conversion vs. CO yield, [D] propane conversion vs. CO_2 conversion

In general, the other catalysts that were studied gave poorer yields of propene than 5% ZrO_2/TiO_2 often, like Tl_2O_3/TiO_2, catalysing dehydrogenation but forming ethene rather than propene (Figures B1 and B2 **Appendix 2**). Another factor that evidently leads to increasing selectivity to ethene over propene is reaction temperature, and experiments with 5% ZrO_2/TiO_2 showed that raising reaction temperature from 550 to 600 ^{o}C reduced the propene/ethene ratio, increased the selectivity towards the reforming reaction, but at the same time increased overall conversion of propane and propene yield.

Another important feature of these results is the relative stability of the catalytic activities of 5% ZrO_2/TiO_2 with time on stream. This is almost certainly linked to the observation in **chapter 2** in which CO_2 was shown to aid in the removal of coke deposits from the catalyst and it is the prevention of coke build up, combined with the retention of structural integrity of the catalysts, that appears to be responsible for this desirable property of the catalysts.

The radical mechanism of propane dehydrogenation via non-oxidative catalyst is suggested [5][9][20-21]. The result tables in **Appendix 2** listed the formation of propene, ethene, ethane, methane, CO and H_2 as result from C-H and C-C, C-O bond breaking from propane and CO_2 reaction on 5% ZrO_2/TiO_2. The adsorption of C_3H_6 on catalyst surface together with two hydrogen atoms to formulate propene and followed by RWGS as follows:

1. Propane dehydrogenation to propene via C-H bond breaking:

   Adsorption of C_3H_6 to propene:

   $CH_3CH_2CH_3$ (g) $\rightarrow$ $CH_3CH_2CH_2$ (ads) + $H_{(ads)}$

   $CH_3CH_2CH_2$ (ads) $\rightarrow$ $CH_3CH=CH_2$ (ads) + $H_{(ads)}$

   $CH_3CH=CH_2$ (ads) $\rightarrow$ $CH_3CH=CH_2$ (g)

   RWGS reaction:

   $2H_{(ads)}$ + $CO_{2(g)}$ $\rightarrow$ CO (g) + H_2O (g)

   H_2 gas yield:

   $2H_{(ads)}$ $\rightarrow$ H_2 (g)

The propane is also cracked by C-C bond breaking to produce ethene, ethane and methane as follows:

2. Propane cracking to ethene via C-C bond breaking:

   C-C bond breaking:

   $CH_3CH_2CH_3$ (g) $\rightarrow$ CH_3CH_2 (ads) + $CH_{3(ads)}$

   CH_3CH_2 (ads) $\rightarrow$ $CH_2=CH_2$ (ads) + $H_{(ads)}$

   $CH_2=CH_2$ (ads) $\rightarrow$ $CH_2=CH_2$ (g)

RWGS breaking:

$2H_{(ads)} + CO_2 \rightarrow CO_{(g)} + H_2O_{(g)}$

Hydrogenation of methyl and ethyl surface species:

$H_{(ads)} + CH_{3(ads)} \rightarrow CH_{4(g)}$

$CH_3CH_{2\,(ads)} + H_{(ads)} \rightarrow CH_3CH_{3\,(g)}$

H_2 gas yield:

$2H_{(ads)} \rightarrow H_{2\,(g)}$

3.4.10 Comparison between ZrO_2/TiO_2 catalysts and other catalysts reported in the literature

The most active reported catalysts for propane dehydrogenation by CO_2 in the literature are: 20% In_2O_3-Al_2O_3 [6-8] and 5% ZnO/ZSM-5 [9]. Commercially, CrO/Al_2O_3 is used but without CO_2. Table 3.12 lists the catalyst stability, propane conversion, propene selectivity and propene yield with and without CO_2 for these three from the literature, in comparison with ZrO_2/TiO_2. The comparison is limited by relatively few literature reports and data taken under non-identical reaction conditions. No data is available on propene/ethene or CO/H_2 ratios.

As a benchmark, the commercial plant catalyst of CrO/Al_2O without CO_2 provides a propene yield 30-35% but only for half an hour or less, after which it requires oxidative regeneration [26]. The catalyst of 5% ZrO_2/TiO_2 gives propene yields of 29-30% and the catalytic stability over 22-37 hours for CO_2/propane ratios of 12.2:1, 24.2:1 and 34.3:1 with higher space velocity (9.6 h^{-1}) compared the low catalytic stability and low space velocity of the commercial plant catalyst of CrO/Al_2O. The cited catalysts of 20% In_2O_3-Al_2O_3 and 5% ZnO/ZSM-5 showed propene yields 22.5 to 25.8% lower propene yield than 5% ZrO_2/TiO_2 and those catalysts were tested at low dilution of propane ratios (N_2/CO_2/propane 18:1:1 and 35:4:1)[6-9].

Table 3.12. Comparisons of propane to propene by different catalyst and methods

Catalysts	Method of dehydrogenation	Propene selectivity	Propane conversion	Propene yield	Catalytic stability
10-20% CrO/Al_2O_3	Commercial plant without CO_2	85-90 %	35-40 %	30% -35 %	0.5 hour
5% ZrO_2/TiO_2	Without CO_2	24.3%	60.7%	14.7%	98 hour
5% ZrO_2/TiO_2	CO_2/propane ratio 3.1:1	35.8%	66.0%	25.5%	257 hour
5% ZrO_2/TiO_2	CO_2/propane ratio 12.2:1	63.3%	50.1%	31.6%	29 hour
5% ZrO_2/TiO_2	CO_2/propane ratio 24.2:1	57.1%	55.4%	31.6%	37 hour
5% ZrO_2/TiO_2	CO_2/propane ratio 34.3:1	57.8%	50.0%	28.9%	22 hour
Cited catalyst: 20% In_2O_3-Al_2O_3 [6-8]	CO_2/ N_2/propane Mixing ratio: 4:35:1	75 %	30 %	22.5 %	12 hour
Cited catalyst: 5% ZnO/ZSM-5 [9]	CO_2/ N_2/propane Mixing ratio 1:18:1	65-75 %	40 %	25.8 %	30 hour

3.5 Conclusions

This study addresses propane dehydrogenation to propene via a non-oxidative route, for the first time. Propane dehydrogenation is thermodynamically limited but this study demonstrates that if the reaction takes place on the surface of a suitable catalyst, probably by a radical mechanism, then local concentrations can be such that the reaction may proceed.

The best catalyst identified in this work is ZrO_2 supported on TiO_2 at a level where the ZrO_2 is intimately mixed with the support so that it does not exist as a discrete phase. The catalyst on which most of the work is based contains Zr and Ti in a weight ratio of

5:95. The titania structure (as determined by powder XRD) remains unaltered by the presence of dissolved zirconia and is anatase. Measurements show that this mixed oxide catalyst exhibits significant surface acidity, almost certainly Lewis acidity, and almost certainly generated at defect sites in the anatase structure through the incorporation of the supported oxide.

The activity of this catalyst and selectivity for propene formation from propane depends very much on the composition of the CO_2/propane blend used in the reaction, with an excess of CO_2 being necessary to suppress competing reforming reactions. Gratifyingly, and in contrast to many of the other catalysts studied here, there is relatively little tendency towards cracking of the propane or propene, and ethene, for example, is formed in relatively small amounts. The overall mechanism is thought to involve the adsorption of C_3H_6 on the catalyst surface together with two hydrogen atoms. CO_2 then reacts with the hydrogen atoms in a reverse water gas shift reaction to give CO and water.

Another highly desirable property of the 5% ZrO_2/TiO_2 catalyst is its stability over time on stream. In this respect is greatly superior to other catalysts which have been investigated for this reaction. One reason for this appears to the ease with which coke can be oxidised (and removed) by CO_2. In this work stability over 257 hours has been demonstrated, at 600 ^{o}C, and using CO_2/propane mixtures with no diluent. This lifetime (and the catalyst could have been used for much longer) compares with the 30 minute time which is allowed between regeneration steps for the commercial chromium-based commercial plant catalyst.

References

1. K. Takehira, Y. Ohishi, T. Shishido, T. Kawabata, K. Takaki, Q. Zhang, and Y. Wang, J. Catal., **224** (2004) 404–416.

2. E. L. Lee, B. Kilos, I. Mbaraka and L. Luo, Abstract 22nd North American Catalysts society conference (June, 5-10, 2011)

3. P. Michorczyk and J. Ogonowski, React. Kinet. Catal. Lett., **78**, 1 (2003), 41-47.

4. T. Shishido, K. Shimamura, K. Teramura and T. Tanaka, Catal. Today, **185** (2012) 151– 156.

5. B. Xu, B. Zheng, W. Hua, Y. Yue and Z. Gao, J. Catal., **239** (2006) 470–477.

6. M. Chen, J. Xu, Y. Cao, H. Y. He, K.N. Fan and J.H Zhuang, J. Catal., **272** (2010) 101-108.

7. M. Chen, J. Xu, Y. M. Liu, Y. Cao, H. Y. He and J. H. Zhuang, Appl. Catal. A., **377** (2010) 35–41.

8. M. Chen, J. L. Wu, Y. M. Liu, Y. Cao, Li Guo, H.Y. He and K. N. Fan, Appl. Catal. A, **407** (2011) 20– 28

9. Y. Ren, F. Zhang, W. Hua, Y. Yue and Z. Gao, Catal. Today **148** (2009) 316–322.

10. J. R. Sohn and S. H. Lee, Appl. Catal. A Gene., **321** (2007) 27-34.

11. M.E. Manríquez, T. López, R. Gómez and J. Navarrete, J. Mol. Catal. A - Chemical **220** (2004) 229–237.

12. R. Pérez-Hernández, D. Mendoza-Anaya, M.E. Fernández, A. Gómez-Cort J. Mol. Catal. A – Chemical, **281** (2008) 200–206.

13. S. Deng, H. Li, S. Li and Y. Zhang, J. Mol. Catal. A – Chemical, **268** (2007) 169-175.

14. S. Wang, K. Murata, T. Hayakawa, S. Hamakawa and K. Suzuki, Appl. Catal. A, **196** (2000) 1-8.

15. K. N. Raoa, B. M. Reddy, B. Abhishek, Y. H. Seo, N. Jiang and S. E. Park, Appl. Catal. B, **91** (2009) 649–656.

16. D. R. Burri, K. M. Choi, S. C. Han, A. Burri, S. E. Park, J. Mol. Catal. A – Chemical, **269** (2007) 58–63.

17. A. Burri, N. Jiang and S. E. Park, Catal. Sci. Technol., **2** (2012) 514–520.

18. P. Kuśtrowski, P. Michorczyk, L. Chmielarz, Z. Piwowarska, B. Dudek, J. Ogonowski, R. Dziembaj, Thermochim. Acta, **471** (2008) 26–32.

19.   P. Michorczyk, J. Ogonowski and K. Zeńczak, J. Mol. Catal. A – Chemical, **349** (2011) 1–12.

20.   D. E. Resasco, Dehydrogenation by Heterogeneous Catalysts, Encyclopaedia of Catalysis, School of Chemical Engineering and Materials Science, University of Oklahoma, January 2000.

21.   F. Z.hang, C. Miao, Y. Yue, W. Hua and Z. Gao, Chin. J. Chem., **30** (2012) 929-934.

22.   M.A. Botavina, C. Evangelisti, Y. A. Agafonov, N.A. Gaidai, N. Panziera, A.L. Lapidus and G. Martra, Chem. Eng., **166** (2011) 1132–1138.

23.   N. Takahashi, A. Suda, I. Hachisuka, M. Sugiura, H. Sobukawa, H. Shinjoh, Appl. Catal. B, Volume **72**, 1–2 (2007) 187-195.

24.   M. Laniecki and M. Ignacik, Catal. Today, **116** (2006) 400–407.

25.   N. Laosiripojana and S. Assabumrungrat, Appl. Catal. B, **60**, 1–2 (2005) 107–116.

26.   Propene report number 06/07-3, Nexant Chem Systems PERP, 44 South Broadway, White Plains, New York, USA, issued date: January 2008.

CHAPTER 4

DIRECT REACTION OF CO$_2$

Table of content

4.1 Introduction

This chapter is aimed to study the insertion reaction of CO_2 with methane, ethane, ethane, acetylene and propane in order to formulate carboxylic acids such as acetic acid. The experiments were carried out on heterogeneous binary and ternary oxide catalysts based on the ZrO_2-TiO_2 catalysts.

The direct reaction of CO_2 and CH_4 is considered a new research area for both CO_2 and CH_4 utilisation. Challenges were expected to determine the reaction conditions and the catalyst system, and how the reaction could be performed by a direct reaction route.

Previous workers reported, as described in **Chapter 1**, the possibility of direct reaction of CO_2 as a whole molecule with methane over selected heterogeneous catalysts to synthesise acetic acid but did not really provide clear conclusions on the mechanism. In this thesis, binary oxides of Zr-Ti have been used because of their two catalytic sites of acidic/basic bifunctional catalytic properties, tolerance to coke formation and thermal stabilities [1-3]. In addition, the catalysts based on ZrO_2 and TiO_2 have been reported to perform methane coupling to formulate ethane and ethylene [4-6]. It was therefore hoped that these catalysts would show high activity in the possible CO_2 reaction with these hydrocarbons.

If the reaction proceeds via CH_4 activation to produce radicals such as CH_3*, CH_2* and $CH*$ (* indicates a surface site or surface species), then there is always the possibility that any reaction with CO_2 could be accompanied by the formation of ethane, ethylene and even larger alkanes and alkenes

Erdöhelyi *et al.*[7] has shown how CH_4 decomposed to CH_3* and CH_2* surface species quite readily over Rh catalysts at 150 °C and Moya *et al.* [8] has shown similar processes over Pd/Al_2O_3 at slightly higher temperatures as seen in equations (4.1), (4.2) and (4.3). In both cases, ethane and ethylene were detected despite the presence of CO_2 in the reaction mixture.

$$CH_4 \rightarrow CH_{3(ads)} + H_{(ads)} \qquad\qquad \text{eq. (4.1)}$$

$$CH_{3(ads)} \rightarrow CH_{2(ads)} + H_{(ads)} \qquad \text{eq. (4.2)}$$

$$CH_{2(ads)} \rightarrow CH_{(ads)} + H_{(ads)} \qquad \text{eq. (4.3)}$$

In general, CO_2 reaction seems likely to take place as follows. The carbon center of CO_2 has a positive shell charge (δ^+) compared with the negative shell charge (δ^-) of the carbon centers of CH_4. The negative shell charge on the carbon center increases with hydrocarbon number. The suggested overall direct reaction of CO_2 is shown by the equation (4.4) to form acetic acid from the reaction of CO_2 and methane. Equation (4.5) is about the formation of propanoic acid from the direct reaction of CO_2 with ethane. Equation (4.6) is about the formation of butanoic acid from the direct reaction of CO_2 with propane.

Acetic acid   ... eq (4.4)

Propanoic acid   ... eq (4.5)

Butanoic acid   .... eq (4.6)

Huang *et al.* [9] and Zhang *et al.* [10] suggested a two-step reaction sequence for the insertion reaction in which CH_4 was activated to form a CH_x surface species on Cu/Co oxide catalysts followed by hydrogenation in order to form acetic acid as shown in equations (4.7, 4.8 and 4.9). In 2012, a CH_3 radical mechanism was proposed and studied by density functional theory (DFT) calculations (**Chapter 1**). CO_2 insertion into the CH_3-Cu surface species to form CH_3COO-Cu was found to be the most favourable reaction pathway followed by H atom interaction with $CH_3COO(Cu)$ to form CH_3COOH [9-10].

$$CH_4 \rightarrow CH_{3\ ads} + H_{ads} \qquad \text{eq. (4.7)}$$

$$CH_{3\,ads} + CO_2 \rightarrow CH_3COO_{ads} \qquad \text{eq. (4.8)}$$

$$CH_3COO_{ads} + H_{ads} \rightarrow CH_3COOH \qquad \text{eq. (4.9)}$$

4.1.2 Thermodynamics of CO_2 reaction

Chapter 3 discussed the thermodynamic calculation of propane dehydrogenation by CO_2. In this chapter, the thermodynamic calculation is extended to the reaction of CO_2 with CH_4. The calculation shows the formation of acetic acid from CO_2 and CH_4 is an endothermic reaction and thermodynamically unfavourable (equation 4.10).

$$CO_{2(g)} + CH_{4(g)} \rightarrow CH_3COOH_{(g)} \qquad .. \text{ eq. (4.10)}$$
ΔH_{298} 37.8 kJ mol^{-1}, ΔS_{298} -116.7 JK^{-1} mol^{-1}, ΔG_{298} 72.5 kJ mol^{-1}

However, other reactions could have a direct effect on the insertion reaction as follows which may, under certain circumstances, by shifting chemical equilibria sufficiently, bring the overall reaction closer to being possible.

1. **Dry reforming:** the reaction is an endothermic reaction which produces H_2 and CO as shown in equation (4.11).

$$CO_{2(g)} + CH_{4\,(g)} \rightarrow 2CO_{(g)} + 2H_{2(g)} \quad .. \text{ eq. (4.11)}$$
ΔH_{298} 249 kJ mol^{-1}, ΔS_{298} 256.5 JK^{-1} mol^{-1}, ΔG_{298} 172.6 kJmol^{-1}

2. **Reverse water gas shift (RWGS):** the reaction between CO_2 and H_2 (produced from dry reforming of CH_4) produces H_2O and CO as the main products. The reaction is endothermic as shown in equation (4.12). An important route that this reaction could take is via reaction between CO_2 and a hydrogen atom adsorbed on the catalyst surface rather than gas phase H_2 and this could influence the progress of an insertion reaction between CO_2 and surface-adsorbed surface species.

$$CO_{2(g)} + H_{2(g)} \rightarrow CO_{(g)} + H_2O_{(g)} \quad ... \text{ eq. (4.12)}$$
ΔH_{298} 43.2 kJ mol^{-1}, ΔS_{298} 42 JK^{-1} mol^{-1}, ΔG_{298} 30.6 kJ mol^{-1}

3. **Water gas shift (WGS):** the reaction is exothermic and CO (produced from dry reforming) reacts with H$_2$O and the reaction will produce CO$_2$ and H$_2$ as illustrated by equation (4.13). The main point is that this reaction, if it proceeds, generates heat and could affect other reactions that are important.

$$CO_{(g)} + H_2O_{(g)} \rightarrow CO_{2(g)} + H_{2(g)} \quad \dots \text{ eq. (4.13)}$$

ΔH$_{298}$ -43.1 kJ mol^{-1}, ΔS$_{298}$ -42 JK^{-1} mol^{-1}, ΔG$_{298}$ -30.6 kJ mol^{-1}

4. **Decomposition of acetic acid: chapter-1** discusses acetic acid stability on several catalyst surfaces. Several reports highlighted acetic acid decomposition at different temperatures and reaction conditions. Acetic acid cracking is exothermic and the Gibbs free energy is favourable at 298K as seen in equation (4.14). Despite this, Fung and Wang [11] have shown that acetic acid can remain intact on the surface of a 50% w/w TiO$_2$-ZrO$_2$ catalyst up to 520 °C. This is one reason why catalysts based on this pair of oxides are the focus of work described in this thesis.

$$CH_3COOH \rightarrow CO_2 + CH_4 \quad .. \text{ eq. (4.14)}$$

ΔH$_{298}$ -37.8 kJ mol^{-1}, ΔS$_{298}$ 116.7 JK^{-1} mol^{-1}, ΔG$_{298}$ -72.6 kJ mol^{-1}

In contrast to the above, the reaction of CO$_2$ with methyl surface species followed by dehydrogenation has a high negative Gibbs free energy as shown in equation (4.15). So if a radical mechanism can be established, then it might offer a catalytic route to preparing acetic acid from methane and CO$_2$. This is the role the catalyst must take, to stabilise these surface species on its surface and, at the same time, allow reaction between adsorbed surface species and CO$_2$.

$$CO_2 + CH_3{}^* + H^* \rightarrow CH_3COOH \quad .. \text{ eq. (4.15)}$$

ΔH$_{298}$ -339.5 kJ mol^{-1}, ΔS$_{298}$ -239 JK^{-1} mol^{-1}, ΔG$_{298}$ -262.5 kJ mol^{-1}

4.2 Experimental

4.2.1 Material

The binary oxide and ternary oxide mixture catalysts based on Zr and Ti oxides were prepared by the co-precipitation and impregnation methods described in detail in sections (**2.1.2**) and (**2.1.3**). The four co-precipitation methods were studied based on zirconium(IV) and titanium(IV) salts as described in cited methods [1],[12-14]. Catalysts prepared by four incipient wetness impregnation methods were studied. Three of these routes were based on zirconium(IV) oxynitrate hydrate [15-17]. The fourth binary oxide was made from zirconium(IV) chloride doped on titanium(IV) oxide [18]. All catalysts were calcined at 700 °C to produce binary or ternary oxides based on ZrO_2/TiO_2 (section **2.1.2**).

4.2.2 Catalyst characterization

In this thesis, the catalysts characterisation techniques were used as follows: SEM, EDX, *p*XRD, nitrogen adsorption, NH_3-TPD. The characteristics of the binary and ternary oxide catalysts are discussed in detail in **Chapter 2**.

4.2.3 Catalyst activity test

The micro-reactor from HIDEN (CATLAB model) was used to study the insertion reaction of CO_2 to methane, ethane, ethylene, acetylene and propane. The micro-reactor instrument consisted of two modules as seen in Figure 4.1. The first is the furnace, described as a micro-reactor, which consists of a quartz tubular fixed bed. The furnace temperature ramps from 20 °C to 1000 °C. The inner glass reactor has I.D. 7 mm x length 300 mm. Quartz wool is placed at the bottom, followed by the weighed catalyst. The thermocouple is placed on the top of catalyst bed to monitor the temperature inside the reactor.

The CATLAB was equipped with four gas flow controllers and high-purity (99.9%) gases were used in this study. The gases used were: He, CO_2, methane, ethane, ethylene, acetylene, and propane, obtained from Saudi-Linde Gas. The CATLAB reactor is connected to a quadrupole mass spectrometer (QMS) by heated silica capillary column at 100 ^{o}C for on-line and the real-time analysis of products from the micro-reactor. The reaction conditions were set for the direct reaction of CO_2 at the selected gas ratios as shown in Table 4.1. The catalyst activation was done by taking around 0.30 g of catalyst in glass reactor. The catalyst was activated at 600 ^{o}C for 2 hours in helium gas and cooled to 100 ^{o}C before the reaction started.

The second module is the on-line quadrupole mass spectrometer (QMS) QIC-20 from HIDEN with two detectors. The QIC-20 is equipped with electron impact ionisation (EI) via thermionic emission from a hot filament with typical vacuum of $1x10^{-6}$ torr. Then the ions enter the quadrupole field and are extracted into the mass filter. The first detector is a Faraday cup detector and it measures mass ion concentration to the minimum of $5 x 10^{-11}$ torr that corresponds to 1 ppm of gas. The second detector is a secondary electron multiplier (SEM) channeltron detector that detects low concentrations of 0.001 ppm that corresponds to a QMS vacuum of $2 x 10^{-14}$ torr.

Table 4.1. The experiment parameters conducted by the micro-reactor

Parameter	Description
Pressure	Atmospheric pressure
Total gas flow	2 ml/min of reactant gas
Temperature ranged for catalysts testing	$\sim$ 100 to 800 ^{o}C
Certified gas mixture tested	CO_2/CH_4 1:1 CO_2/CH_4 1:9 CO_2/CH_4 9:1 CO_2/ethane 1:1 CO_2/propane 1:1 CO_2/ethylene 1:1 CO_2/acetylene 9:1
Catalyst volume	0.85 cm^3
GSVH	140 hr^{-1}

Figure 4.1. The Micro-reactor of HIDEN CATLAB consists
of two modules

Both detectors were calibrated by standard gases at 95% confident level so they could be used for determination of reactant and product concentrations. Conversion (equation 4.15), selectivity (equation 4.16) and yield (equation 4.17) were calculated according to Chen *et al.* [19] and Xu *et al.* [20].

$$\text{Feed conversion (mol\%)} = \frac{\text{Methane (in)} - \text{Methane (out)}}{\text{Methane (in)}} \, x100\% \quad \ldots \text{eq. (4.15)}$$

$$\text{Product Selectivity (mol\%)} = \frac{\text{Acetic acid}}{\text{Methane (in)} - \text{Methane (out)}} \, x100\% \quad \ldots \text{eq. (4.16)}$$

$$\text{Product Yield \%} = \text{feed conversion } X \text{ product selectivity} \ldots \text{eq. (4.17)}$$

A gas chromatography instrument equipped with thermal conductivity detector (GC-TCD) was used to study CO_2 insertion to methane, ethane and propane. The initial temperature of the GC oven was 45 °C and ramped to 250 °C at 10 °C/min where the temperature was held for 10 min. The oven contained two columns: Haysep Q (length: 3 ft. for hydrocarbon separation) and Porapak Q (length: 6 ft. for CO_2, CO, O_2, N_2, H_2 separation). The gas produced from the HIDEN CATLAB reactor was connected directly to the gas inlet to gas loop volume of 0.5 μl in order to provide continuous flow from the reactor. The calculation and data treatment (confident level of 95%) are discussed in **Chapter-3**.

4.2.4 The catalyst and reaction condition choice

The research studied the reactions of CO$_2$ by using binary oxides of ZrO$_2$/TiO$_2$ catalyst in order to determine the catalytic activity for direct reaction of CO$_2$ with CH$_4$. Catalysts prepared by the following routes, together with the variables described were studied:

- The co-precipitation route for catalyst preparation at CO$_2$/CH$_4$ ratio 1:1.
- The impregnation route for catalyst preparation at CO$_2$/CH$_4$ ratio 1:1.
- The ternary oxides based on ZrO$_2$/TiO$_2$ at CO$_2$/CH$_4$ ratio 1:1.
- The effect of CO$_2$/CH$_4$ gas ratios.
- Direct reaction of CO$_2$ with ethane, ethylene, acetylene and propane.

Also studied were:
- Catalyst stability.
- Catalyst selectivity of CO$_2$ reaction with methane, ethane and propane to determine the C-H bond breaking of methane and the C-C bond breaking of each ethane and propane.

4.2.5 Hydrogen-temperature programmed reduction (H$_2$-TPR)

The temperature programmed reduction (TPR) method was studied to determine the reduction behaviour of binary oxides based on Zr/Ti oxide at the temperatures used in the reaction between CO$_2$ and CH$_4$. It was thought that the TPR study might show differences between mixed metal oxide catalysts (Zr/Ti oxides) prepared in different ways (i.e. co-precipitation and impregnation).

Temperature programmed reduction (TPR) experiment was carried out on a Micromeritics Autochem 2910 instrument. In the experiment, 100 mg of catalyst sample was placed in U-shaped quartz sample tube. Prior to the TPR experiment, the catalyst sample was first pre-heated in helium, 50 ml/min at 300 ^{o}C for one hour. After pre-

treatment, the sample was cooled to 35 °C and 10% hydrogen balanced by argon at 50 ml/min was allowed to pass over the sample and the temperature was raised from 35 °C to 900 °C at rate of 10 °C/min. The hydrogen concentration in the effluent stream was monitored by a thermal conductivity detector (TCD). The peak area was integrated in order to measure the H_2 uptake of each catalyst [21]. The H_2-TPR proceeds by reaction between metal oxide and H_2 and the result of the reduction is water and reduced metal.

4.3 Results and Discussion

Results are distributed between this chapter and **Appendix 3**.

4.3.1 Direct reaction of CO_2 with CH_4 over binary oxides ZrO_2/TiO_2

Catalysts made by four co-precipitation and four impregnation methods described in **Chapter-2** (sections **2.1.2** and **2.1.3**) were studied in the CO_2/CH_4 reaction as seen in Table 4.2.

Table 4.2. The cited methods for impregnation and co-precipitation precursors used for preparation ZrO_2/TiO_2 catalyst.

Method number	Authors
Co-precipitation method-1	Sohn and Lee [1]
Co-precipitation method-2	Sohn and Lee [12]
Co-precipitation method-3	Mao *et al*. [13]
Co-precipitation method-4	Machida *et al*. [14]
Impregnation method-1	Takahashi *et al.* [15]
Impregnation method-2	Ruppert & Paryiczak *et al.*[16]
Impregnation method-3	Chepurna *et al.* [17]
Impregnation method-4	Laniecki and Ignacik [18]

4.3.1.1 Catalytic activities of Zr-Ti oxide catalysts prepared by the co-precipitation route

Eight binary oxide catalysts were prepared by the co-precipitation method-1[1] at different ratios of Zr to Ti. The experiments were carried out at gas feed ratio of CH_4/CO_2 1:1. The activity test was conducted from 100 to 800 °C. However, only two catalysts showed acetic acid formation during the activity tests as summarized in Table 4.3:

Table 4.3. Performance of Zr/Ti oxides prepared by four co-precipitation method-1[1] at gas feed of CH_4/CO_2 1:1.

% Zr/Ti oxide Catalyst *	Temperature range over which acetic acid formation was detected	Temperature for maximum acetic acid yield	Maximum concentration of acetic acid detected
TiO$_2$	ND**	ND**	ND**
2% w/w Ti/Zr oxide	560 - 680 °C	560 °C	80 ppm
4% w/w Ti/Zr oxide	ND**	ND**	ND**
8% w/w Ti/Zr oxide	580 - 680 °C	595, 620 °C	8-9 ppm
17% w/w Ti/Zr oxide	ND**	ND**	ND**
44% w/w Ti/Zr oxide	ND**	ND**	ND**
11% w/w Zr/Ti oxide	ND**	ND**	ND**
45% w/w Zr/Ti oxide	ND**	ND**	ND**
50% w/w each Zr/Ti oxide	ND**	ND**	ND**
ZrO$_2$	ND**	ND**	ND**

    * metal ratio (w/w%)   **ND: Not detection of acetic acid

Catalyst 2% w/w Ti/Zr oxide showed some reaction between CO_2 with CH_4 and acetic acid was detected at reaction temperatures 560 °C to 670 °C as shown in Figure 4.2. Two maximum peaks were detected and the estimated maximum concentration of acetic acid was 80 ppm at 560 °C. **Appendix-3** Figures C1 (A), (B) and (C) show the plots of CO_2, CH_4, CO, and H_2 vs. temperature. The formation of some CO implies RWGS reaction with H_2 formed from methane. Catalyst of 8% w/w Ti/Zr oxide showed some acetic acid as shown in Figure 4.3. Two very small peaks were observed at 580-670 °C. In this study no ethane or ethylene from methane activation as detected.

Figure 4.2. Acetic acid yield as reaction temperature was increased. Catalyst: 2% w/w Ti/Zr oxide prepared by co-precipitation method-1. CO_2/CH_4 1:1.

Figure 4.3. Acetic acid yield as reaction temperature was increased. Catalyst: 8% w/w Ti/Zr oxide prepared by co-precipitation method-1. CO_2/CH_4 1:1.

The activity test results for 50% w/w Zr/Ti oxides prepared by co-precipitation methods-1, -2, -3 and -4 are summarised in Table 4.4. The acetic acid from the co-precipitation method-2 was detected at 8 ppm at 550 °C with a wide peak from 600 to 700 °C. The catalysts prepared by co-precipitation methods-3 and -4 showed only a trace of acetic acid at 1-6 ppm as shown in **Appendix-3** Figures C2, C3 and C4.

Table 4.4. Performance of three catalysts prepared by co-precipitation methods-2, 3 and 4.

% Zr/Ti oxide Catalyst *	Catalysts method	Temperature range over which acetic acid formation was detected	Temperature for maximum acetic acid yield	Maximum concentration of acetic acid detected
50% w/w Zr/Ti oxide	co-precipitation method-1[1]	ND**	ND**	ND**
50% w/w Zr/Ti oxide	co-precipitation method-2[12]	600-700 °C	500 °C	8 ppm
50% w/w Zr/Ti oxide	co-precipitation method-3 [13]	550-700 °C	670 °C	6 ppm
50% w/w Zr/Ti oxide	co-precipitation method-4 [14]	ND**	ND**	ND**

* metal ratio (w/w%)   ** ND: not detection of acetic acid

In summary, the four co-precipitation methods resulted in Zr/Ti oxide catalysts that showed poor direct reactions of CO_2 with CH_4 and made only traces of acetic acid. The catalysts prepared by the four co-precipitation methods showed some dry reforming of methane. Because dry reforming requires C-H bond breaking, this implies that a methyl surface species might form on the catalyst surface. In addition, there was no H_2 detected but some CO was seen. Taken together, this suggests that the RWGS reaction might also have been occurring.

4.3.1.2 Catalytic activities of Zr/Ti oxide catalysts prepared by the impregnation route

Four preparation impregnation methods using different pH precursor solutions were used to synthesis five catalysts of binary oxides of Zr/Ti to study the direct reaction of CO_2 with CH_4.

4.3.1.2.1 Impregnation method-1

The activity test of impregnation catalysts of 1% and 5% Zr/Ti oxide showed some formation of acetic acid as shown in Table 4.5. Data for 1% Zr/Ti oxide appears in Figure 4.4 [A]. A wide acetic acid peak was detected from 525 to 750 °C and the

estimated maximum concentration of acetic acid was 600 ppm at 555 ^{o}C. In addition, ethane and ethylene were produced at similar temperatures to acetic acid which possibly suggests methane coupling on the catalyst surface. Ethane was detected at 200 ppm and the concentration increased as the reactor temperature was increased. The observation of ethane and ethylene suggests that methane was adsorbed in surface species form, so it seems likely that the reaction of CO_2 and CH_4 to form acetic acid occurred via a surface species route.

Figure 4.4 [A]. Acetic acid, ethane and ethylene yield with increasing reactor temperature over 1% w/w Zr/Ti oxide (CO_2/CH_4 1:1).

Figure 4.4 [B] and [C]. CO_2 and methane reduction and increase of hydrogen and CO with increasing reactor temperature over 1% w/w Zr/Ti oxide (CO_2/CH_4 1:1).

Data for the 5% Zr/Ti oxide catalyst made by the impregnation method-1 appears in Figure 4.5 and Table 4.5. This showed a wider peak of acetic acid from 522 to 750 °C. The estimated maximum concentration of acetic acid was 800 ppm at 575 °C which was higher than for 1% Zr/Ti oxides. In addition, ethane and ethylene were also detected at the same temperature as acetic acid formation. The ethane was detected at 300 ppm, and the concentration increased gradually with reactor temperature as acetic acid yield fell.

Figure 4.5. Acetic acid, ethane and ethylene formation with increasing reactor temperature over 5% w/w Zr/Ti oxide (CO_2/CH_4 1:1).

In the appendix to this chapter it can be seen that the two catalysts also showed CO and H_2 formation started below 600 °C then increased to 800 °C, at which temperature the yields of these were similar at >20 mol% (Figure 4.4 [B] and [C]). This implies dry reforming is occurring (**Appendix-3** Figures C5 and C6 (A, B, and C)). At the lower temperature of about 525 °C, close to the temperature where acetic acid formation began, CO was also detected, but without accompanying H_2 at anything like the same concentration. This implies that the reverse water gas shift reaction was occurring at this lower temperature.

So, in summary, it seems that acetic acid formation starts at about 520 °C, and that this is accompanied by formation of CO by the RWGS reaction. As the temperature was increased to over 600 °C, acetic acid yield drops and dry reforming takes over from the RWGS reaction, presumably meaning CO_2 reacts with CH_4 before it can adsorb as a

surface species on the catalyst surface. Formation of ethane and ethylene increases continuously with temperature alongside the dry reforming, suggesting that any methane that does adsorb as a surface species on the catalyst surface reacts rapidly with other methane molecules or other adsorbed surface species, rather than with gas phase CO_2.

The acetic acid formation for the two catalysts is compared in Figure 4.6 and Table 4.5. The binary oxides of 5% Zr/Ti oxides generated slightly higher acetic acid yield but the temperature dependence of the activity was largely the same.

Table 4.5. Performance of impregnation method-1 of Zr/Ti oxide (CO_2/CH_4 1:1).

Catalyst	Temperature for maximum acetic acid yield	Maximum concentration of acetic acid detected ppm	Maximum concentration of ethane detected ppm	Maximum concentration of ethylene detected ppm
1% Zr/Ti oxide	550 ºC	560	560	200
5% Zr/Ti oxide	550 ºC	800	200-2000	18

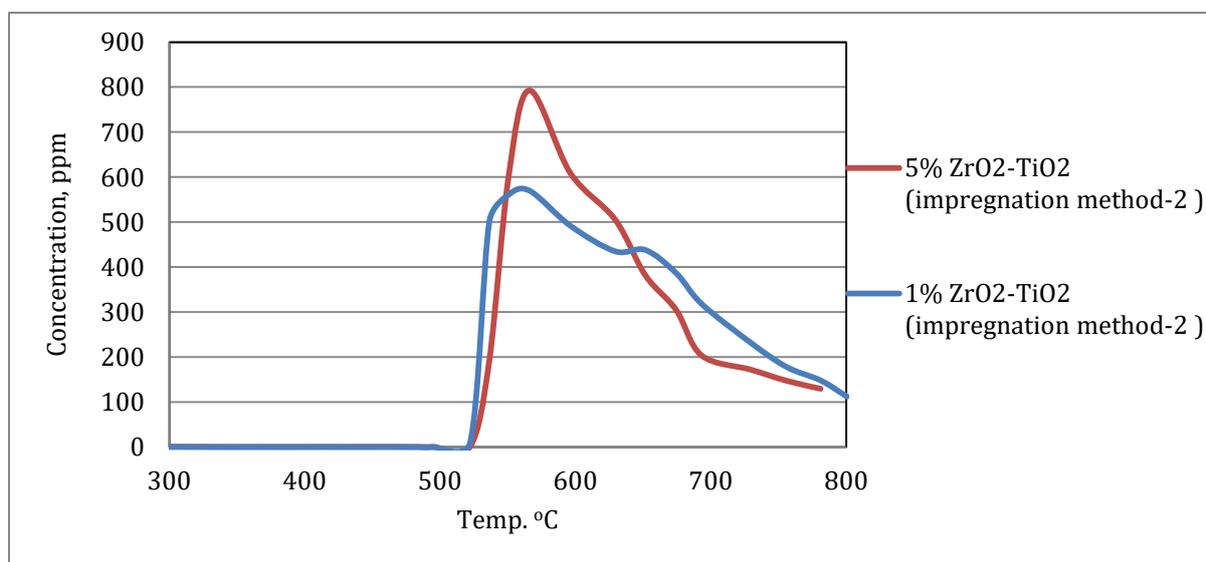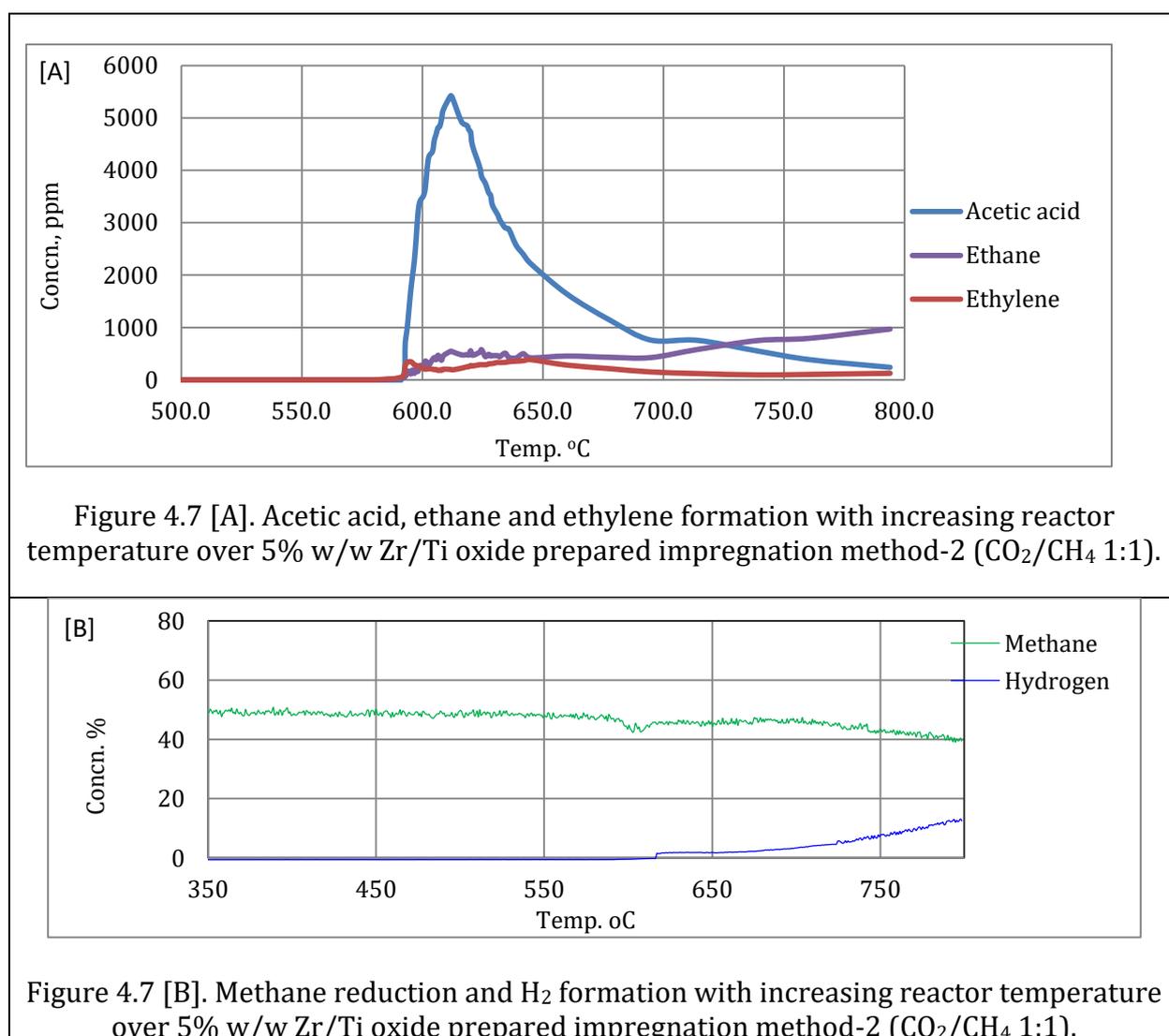Figure 4.6. The comparison acetic acid formation over catalysts of 1% and 5% Zr/Ti oxide (CO_2/CH_4 1:1).

4.3.1.2.2 Impregnation method-2

The catalyst 5% w/w Zr/Ti oxides prepared by impregnation method-2 resulted in more acetic acid formation, starting at 588 °C with a broad peak to 800 °C. The estimated maximum concentration was 5,400 ppm at 609 °C as seen in Figure 4.7 [A]. The yield of acetic acid was almost six times higher than with the last catalyst. Ethane and ethylene formation were also detected at the same temperature as acetic acid formation and ethane concentration was 600 ppm. This again suggested that methyl and methylene surface species (CH_3^* and CH_2^*) generated from methane were coupling on the catalyst surface. The general trend was the same as for the first catalyst. The plots of CH_4 and H_2 vs. temperature in Figure 4.7 [B] and **Appendix-3** Figure C7 (A and B) shows methane reduction and peak of H_2 at same temperature of acetic formation.

Figure 4.7 [A]. Acetic acid, ethane and ethylene formation with increasing reactor temperature over 5% w/w Zr/Ti oxide prepared impregnation method-2 (CO_2/CH_4 1:1).

Figure 4.7 [B]. Methane reduction and H_2 formation with increasing reactor temperature over 5% w/w Zr/Ti oxide prepared impregnation method-2 (CO_2/CH_4 1:1).

4.3.1.2.3 Impregnation method-3

The 5% w/w Zr/Ti oxides catalyst prepared by impregnation method-3 was cited by Chepurna *et al.* [17] in order to obtain nano sized particles of ZrO_2 doped on TiO_2 support. In this work, the catalyst resulted in acetic acid formation as a sharp peak at 670-720 °C. The estimated concentration at the maximum was above 7,200 ppm as shown in Figure 4.8 [A]. Ethane was also detected at about 2,000 ppm which indicated again the possibility of reaction of methyl surface species on the catalyst. Higher yields of ethane were detected than from similar catalysts prepared using the other impregnation methods. Figure 4.8 [B] shows CH_4 and CO_2 peaks decreased at the same temperature at which acetic acid formation occurred.
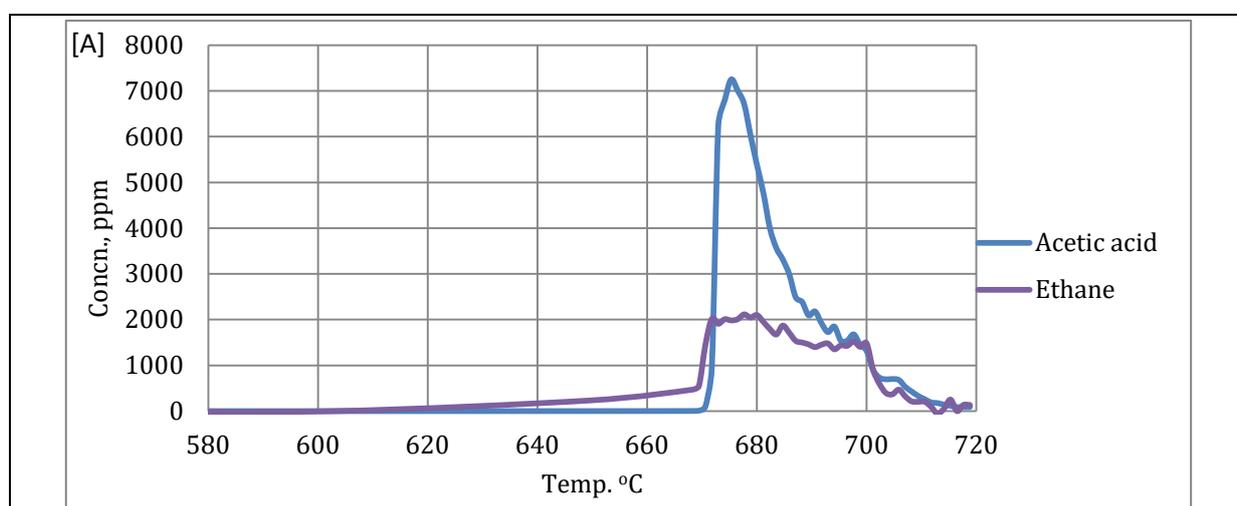

Figure 4.8 [A]. Acetic acid and ethane formation with increasing reactor temperature over 5% w/w Zr/Ti oxide prepared impregnation method-3 (CO_2/CH_4 1:1).
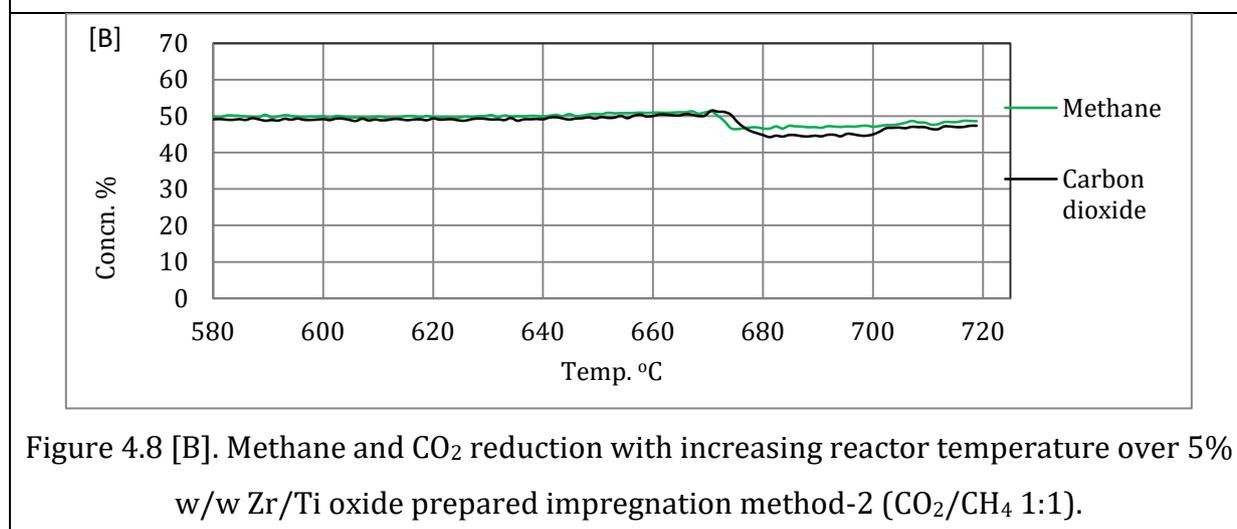

Figure 4.8 [B]. Methane and CO_2 reduction with increasing reactor temperature over 5% w/w Zr/Ti oxide prepared impregnation method-2 (CO_2/CH_4 1:1).

4.3.1.2.4 Impregnation method-4

The catalyst prepared by impregnation method-4 was applied by using $ZrCl_4$ salt doped on TiO_2 support to synthesise the 8% Zr/Ti oxides catalyst. Using this catalyst, acetic acid was detected at 525 °C and ended at 630 °C. The estimated concentration was 520 ppm at the maximum peak as shown in Figure 4.9. Ethane and ethylene were also detected and the ethane concentration was estimated at 75 ppm. The profile in Figure 4.9 is similar to that detected with the equivalent catalyst made using impregnation method 1.

Figure 4.9. Acetic acid, ethane and ethylene formation with increasing reactor temperature over 8% w/w Zr/Ti oxide prepared impregnation method-4 (CO_2/CH_4 1:1).

4.3.1.2.5 Methane activation without CO_2 over 5% Zr/Ti oxide

Figure 4.10 shows results of reacting methane over Zr/Ti oxide catalyst without CO_2. In this case, 5% w/w Zr/Ti oxide catalyst (impregnation method 2 was used). Ethane was formed, as it was in the presence of CO_2 (section 4.3.1.2.2), but at a concentration of about ten times that detected with CO_2. This result appears to show that methyl surface species form on the catalyst surface which can form acetic acid with CO_2, or can combine to form ethane.
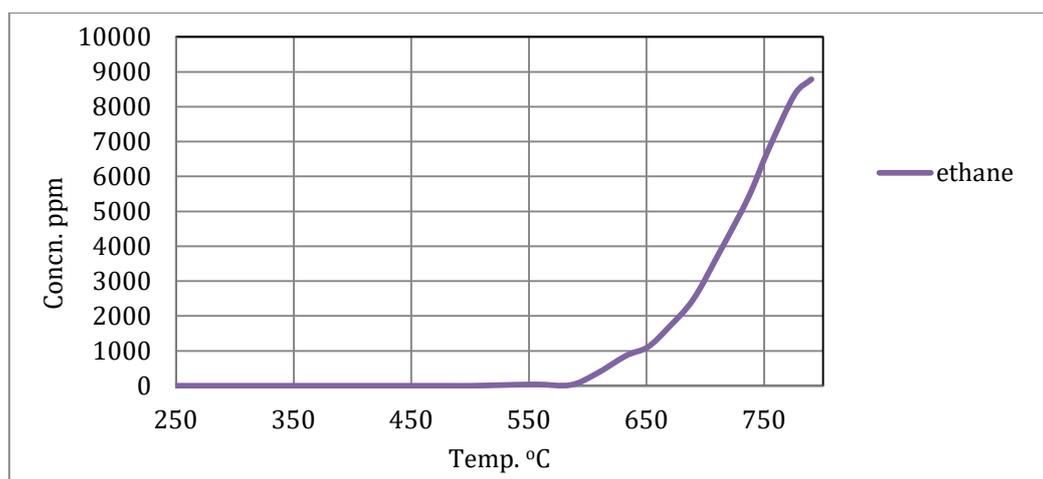
Figure 4.10. Ethane formation from methane (without CO_2) with increasing reactor temperature over 5% w/w Zr/Ti oxide prepared impregnation method-2.

4.3.1.2.6 Overall performance of the catalysts made by the impregnation methods

Table 4.6 summarizes the results for acetic acid formation over Zr/Ti oxide catalysts made by the impregnation methods. The different preparation methods had a direct effect on the acetic acid yield. Figure 4.11 shows the concentrations of acetic acid vs temperature over each of the catalysts.

Acetic acid concentrations were highest for catalysts made using methods 2 and 3. These also yielded higher ethane concentrations, but at relatively high temperatures where acetic acid formation had ceased. The other catalysts resulted in less acetic acid,

Catalysts prepared by methods -1 and -4 resulted in lower yields of acetic acid but, surprisingly, acetic acid was formed at lower temperatures than over the other two catalysts. The two pairs of catalysts were that, for these two (1 and 4), formation of acetic acid was also accompanied by ethane and ethylene formation. This suggests that methane coupling takes place over these catalysts at lower temperatures.

The ratio of the generated acetic acid yield to the sum of ethane and ethylene yields over catalysts prepared by the impregnation methods varied from 2.5 to 8.7. The catalyst prepared by the impregnation method-2 showed the highest ratio. This

151

suggests that CO$_2$ insertion to a methyl surface species occurs more readily than methyl surface species dimerization to ethane on this catalyst.

Figure 4.11. Overall yield of acetic acid formation with increasing reactor temperature from five Zr/Ti oxide catalysts prepared by different impregnation methods (using a CO$_2$:CH$_4$ ratio of 1:1).

Differences in the preparation methods of the four catalysts detailed in Figure 4.11 are assumed to be responsible for differences in catalyst performance. NH$_3$-TPD data for the four were very similar (**chapter 2, Figure 2.27A**), suggesting that their acidities were effectively the same. Data from N$_2$ adsorption shows differences in porosities amongst the four catalysts as shown in Figure 4.12, with the two most active catalysts (methods 2 and 3) showing much larger pore volumes, especially in the mesopore range, than the others Whether this is associated with differences in activities is uncertain although the differences are certainly significant.

Table 4.6. Activity data for Zr/Ti oxides prepared by the four methods of impregnation (CO_2/CH_4 1:1)

(standard gases calibrated at confident level 95%).

Catalyst and preparation method	Gas feed ratio	Temp. for max. acetic acid yield T_{max}	CO_2 in	CO_2 out	CH_4 in	CH_4 out	Acetic acid at T_{max}	Ethane at T_{max}	Ethylene at T_{max}	Ratio of acetic acid / ethane + ethylene	H_2 at T_{max}	Conv.* CO_2 at T_{max}	Conv.* Methane at T_{max}	Acetic acid selec.** at T_{max}	ethane selec.** at T_{max}	Ethylene selec.** at T_{max}	H_2 selec.** at T_{max}	Acetic acid yield at T_{max}
		°C	%	%	%	%	%	%	%	-	%	%	%	%	%	%	%	%
1% ZrO_2/TiO_2 Impreg-1(i)	CO_2 50%, CH_4 50%	550	49.3	49.8	50.7	50.2	0.056	0.015	0.002	3.4	0.10	1.38	0.99	11.2	3.0	0.3	20.0	0.11
5% ZrO_2/TiO_2 Impreg-1(i)	CO_2 50%, CH_4 50%	550	49.4	48.1	50.6	49.9	0.080	0.030	0.002	2.5	ND ***	2.83	1.38	11.4	4.3	0.3	ND ***	0.16
5% ZrO_2/TiO_2 Impreg-2(ii)	CO_2 50%, CH_4 50%	610	50.5	48.6	49.5	45.9	0.54	0.040	0.022	8.7	0.037	2.61	7.23	15.1	1.1	0.6	10.3	1.09
5% nano ZrO_2/TiO_2 Impreg-3(iii)	CO_2 50%, CH_4 50%	675	49.8	49.2	50.2	46.3	0.72	0.19	ND ***	3.8	0.99	2.57	7.71	18.6	4.9	ND***	25.6	1.44
8% ZrO_2/TiO_2 Impreg-4(iv)	CO_2 50%, CH_4 50%	550	49.1	49.5	50.9	48.8	0.052	0.007	0.0001	7.3	0.415	2.69	4.11	2.5	0.3	0.0	2.0	0.10

(i): Impregnated method-1, (ii): Impregnated method-2, (iii): Impregnated method-3, (iv): Impregnated method-4,

* Conv. = Conversion   ** Selec. = selectivity   ***ND = not determined
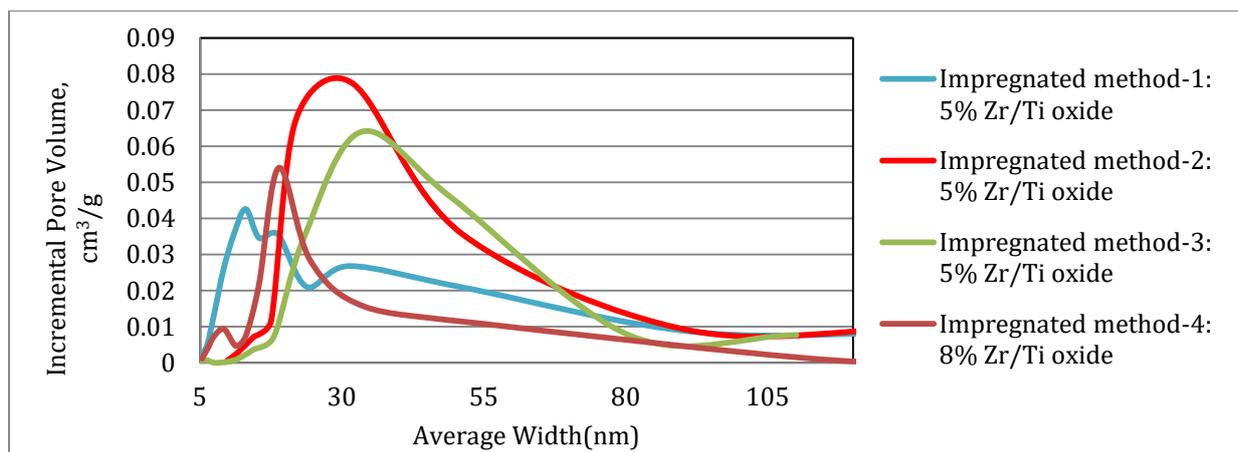
Figure 4.12. BJH pore volume distribution curves of impregnation methods of Zr/Ti oxides.

In summary, when comparing the catalysts made by the four impregnation routes, there are some significant observations and differences that can be noted. Firstly, it does seem that high acetic acid yields are detected alongside high ethane yields. The simple fact of ethane formation suggests that the catalysts promote methyl surface species coupling. The fact that high acetic acid yields correspond to high ethane yields suggests that both products are formed by a methyl surface species route. Differences in yields and differences in the temperatures at which the products are formed on the different catalysts are difficult to interpret but the differences observed do suggest that there is scope to improve further and optimise Zr/Ti oxide catalysts prepared by the methods used here.

In general, as can be seen from Table 4.6, the H_2 is made when CO_2 and CH_4 are passed over these catalysts as acetic acid is produced. This suggests that acetic acid formation involves a hydrogenation step to execute the reaction.

4.3.2 Direct reaction of CO_2 with CH_4 using ternary metal oxide catalysts

On the basis that binary metal oxide catalysts prepared by impregnation method 2 showed the highest activity of those tested above, the impregnation method 2 was used for all the ternary metal oxide catalysts used. In the method used, the third metal was added as a metal salt of Al, Co, Cu or Fe to the zirconium oxynitrate, and the mixture was

added to the TiO_2 support as described in section **2.1.1.2**. The following were studied. (Note that %w/w of the metals based on the formulations used in synthesis, not the oxides, as described earlier in section **2.1.2.2**):

1- 2.0% w/w Al, 5% w/w Zr / 93 % Ti oxide

2- 3.4% w/w Co, 5% w/w Zr /Ti 91.6% oxide

3- 4.0% w/w Cu, 5% w/w Zr /Ti 91% oxide

4- 3.6% w/w Fe, 5% w/w Zr /Ti 91.4% oxide

The first catalyst, 2% w/w Al, 5% w/w Zr /Ti, yielded high acetic acid concentration at 600 °C of 8,700 ppm as shown in Figure 4.13 [A]. Although not shown here, CH_4 concentration dropped off at the same temperature, as expected, and the H_2 yield increased as shown in Figure 4.13 [B] and **Appendix-3** Figures C8). Ethane and ethylene were also formed, as shown.
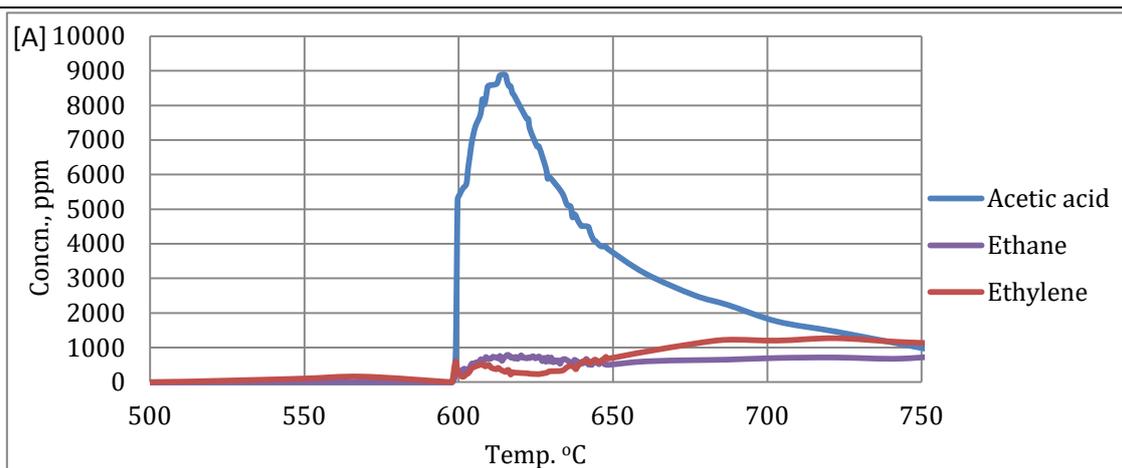

Figure 4.13 [A]. Acetic acid, ethane and ethylene formation with increasing reactor temperature over 2% w/w Al/ 5% w/w Zr/Ti oxide prepared by impregnation method-2 (CO_2/CH_4 1:1).
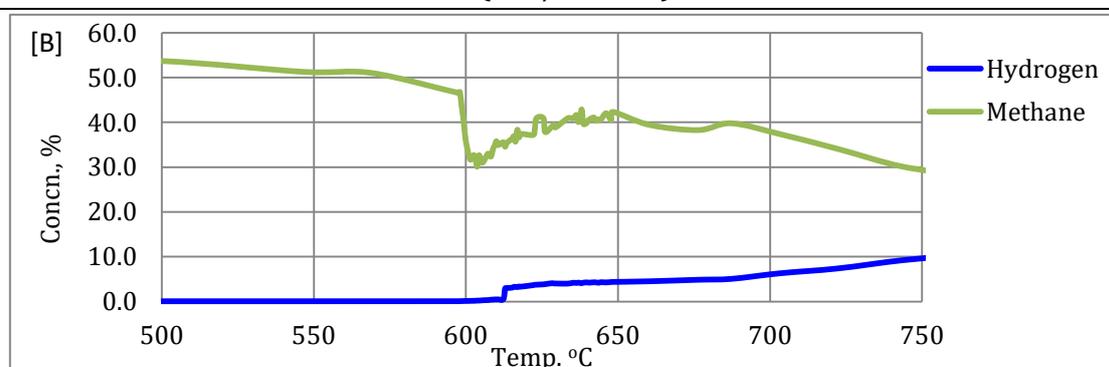

Figure 4.13 [B]. Reduction of methane and raise of hydrogen formation with increasing reactor temperature over 2% w/w Al/ 5% w/w Zr/Ti oxide prepared by impregnation method-2 (CO_2/CH_4 1:1).

The activity test of 3.4% w/w Co, 5% w/w Zr /Ti catalyst resulted in acetic acid at lower temperature (560 ^{o}C) with a maximum concentration of 2,500 ppm at 600 ^{o}C as seen in Figure 4.14. This catalyst showed more dry reforming of CO_2 and CH_4 as seen in plots of CH_4, CO_2, CO and H_2 in **Appendix-3** Figure C9. In addition, at the same temperature of acetic acid formation, ethane and ethylene were detected in much higher concentrations than when using the aluminium-containing catalyst described above.   Ethane yield showed a maximum of 1200 ppm at 560 ^{o}C, and then followed a path largely reciprocating the formation of acetic acid.

Figure 4.14. Acetic acid, ethane and ethylene formation with increasing reactor temperature over 3.4% w/w Co / 5% w/w Zr/Ti oxide prepared by impregnation method-2 (CO_2/CH_4 1:1).

The ternary oxide of 4% w/w Cu, 5% w/w Zr/Ti showed the formation of acetic acid at much higher concentration (maximum 3400 ppm) at higher temperature (630 ^{o}C). Ethane and ethylene again showed a reciprocal yield pattern but at much lower concentrations this time (Figure 4.15). The plot of acetic acid and H_2 yield vs. temperature in **Appendix-3** Figure C10 shows the formation of H_2 at the same temperature as acetic acid formation.

Figure 4.15. Acetic acid, ethane and ethylene formation with increasing reactor temperature over 4% w/w Cu / 5% w/w Zr/Ti oxide prepared by impregnation method-2 (CO$_2$/CH$_4$ 1:1).

The ternary oxide of 3.6% w/w Fe 5% w/w Zr /Ti showed acetic acid formation at the lower temperature of 510 ^{o}C (Figure 4.16), with maximum concentration of 2,500 ppm. Ethane and ethylene were again formed at the same time, with yields following the opposite pattern to acetic acid. An unusual feature was that ethylene yields were higher than ethane yields.
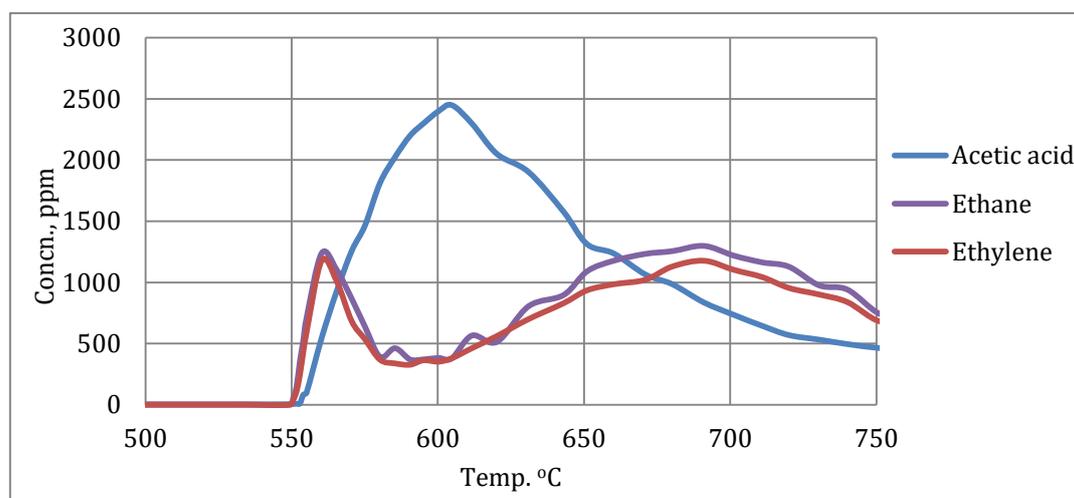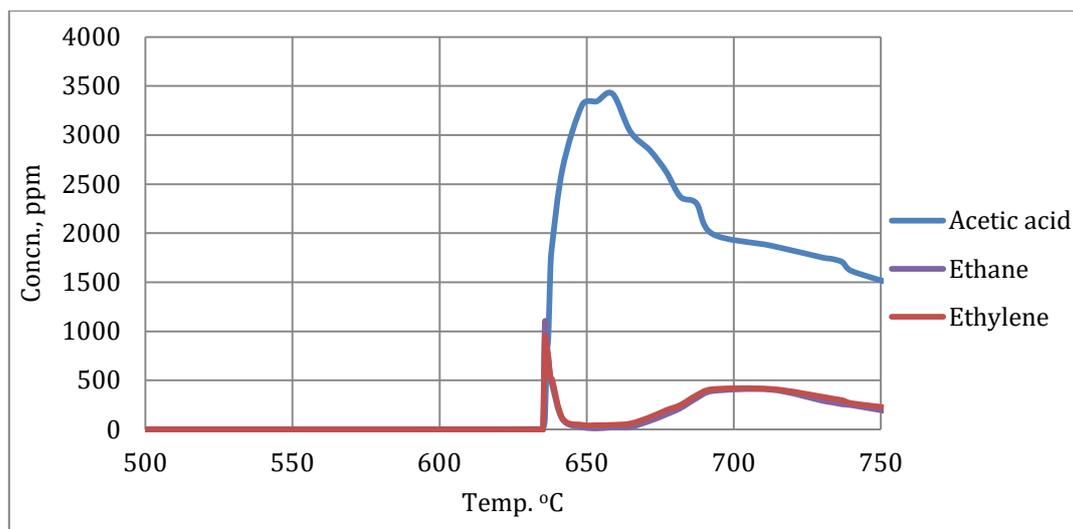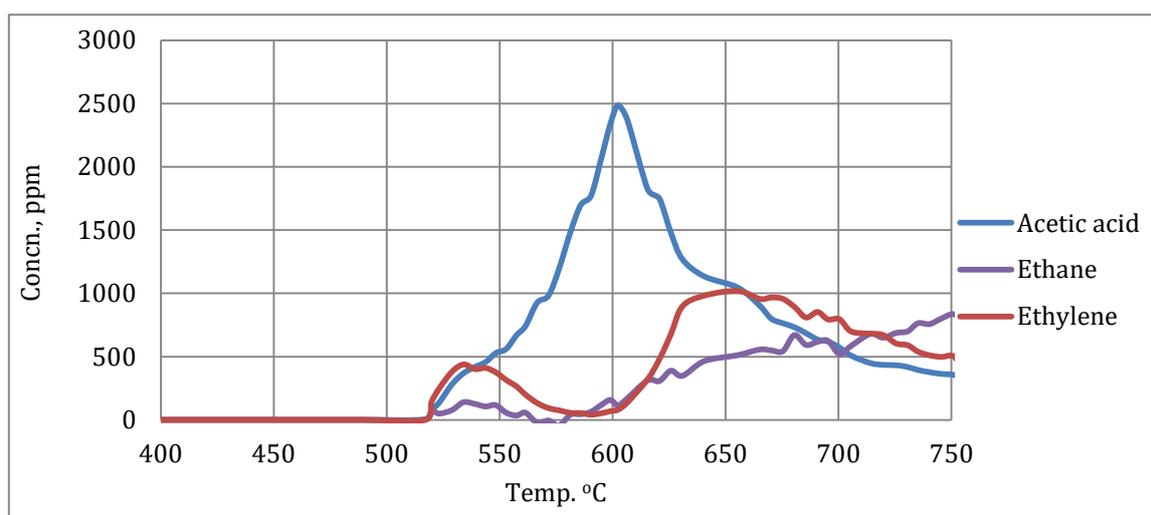

Figure 4.16. Acetic acid, ethane and ethylene formation with increasing reactor temperature over 3.6% w/w Fe / 5% w/w Zr/Ti oxide prepared by impregnation method-2 (CO$_2$/CH$_4$ 1:1).

So, in summary, the already quite high catalytic activity of 5% ZrO_2/TiO_2 (made by impregnation method (2) can be modified by the addition of a third metal oxide. Yields of acetic acid are different for the four catalysts described above. It is very clear that there is a balance between formation of acetic acid and formation of ethane and ethylene, and it seems that the third metal affects the relative balance between these two product types, the carboxylic acid and the alkane/alkene. The Al-containing catalyst seems to be the catalyst for which this balance is tipped most noticeably towards the acid.

The TPD-NH_3 data as shown in **Chapter 2**, (Figure 4.17) suggests that the 2% Al oxide dopant on ZrO_2/TiO_2 has a significant effect on acidity. The large peak in the desorption profile at 180-280 °C possibly means that it exhibits a larger concentration of acid sites than the other catalysts, although they do appear to be relatively weak. It is possible therefore that "weak" acid sites are needed to show selectivity to acetic acid in this reaction.

Furthermore, nitrogen adsorption data show that the Al-containing catalyst does appear to retain relatively high porosity in the mesopore region when compared to the catalysts containing Fe, Co and Cu (Figure 4.18 and Table 4.8).
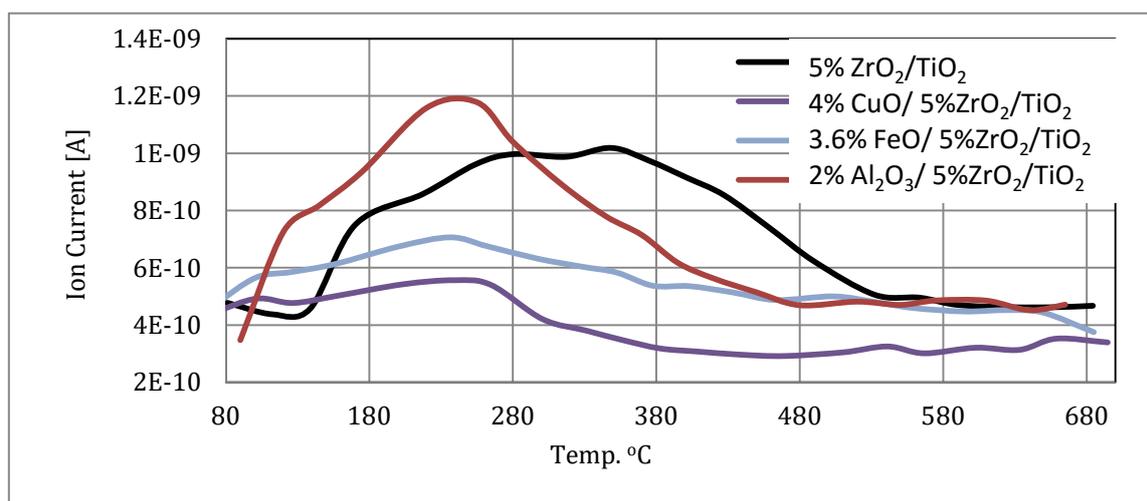

Figure 4.17. NH_3-TPD profiles for the ternary oxide catalysts based on 5% Zr/Ti oxide.

Table 4.8. Textural properties of ternary oxide catalysts based on Zr/Ti oxide prepared by impregnation method 2.

Catalysts	BET surface area m^2/g	Pore volume cm^3/g	Average pore size nm
TiO_2 support	56	0.14	10
5% w/w Zr/Ti oxides	29	0.18	21
2.0% w/w Al, 5% w/w Zr /Ti oxides	24	0.20	33
3.6% w/w Fe, 5% w/w Zr /Ti oxides	11	0.10	36
3.4% w/w Co, 5% w/w Zr /Ti oxides	5	0.05	46
4.0% w/w Cu, 5% w/w Zr /Ti oxides	4	0.06	51

Figure 4.18. BJH pore volume distribution curves from nitrogen adsorption/desorption isotherms for ternary oxide catalysts based on 5% Zr/Ti oxide.

Table 4.9 lists the activities of the four ternary oxides catalysts compared with binary oxide Zr/Ti catalyst, all prepared by the same impregnation method 2.

Although not shown in the earlier data, it is worth saying that overall methane conversion over the ternary oxides catalysts was in the range 36% – 84%, which was a much higher methane conversion than that over the binary oxide catalyst of 5% Zr/Ti. And, as discussed above, acetic acid yields were broadly similar for the binary and the ternary catalysts. This means that the ternary catalysts were particularly active towards alternative reactions, particularly dry reforming of methane.

The most important comparison between 5% ZrO_2/TiO_2 and the same catalyst with added Al, Cu, Co and Fe, is shown in Figure 4.19, where the dramatic differences in acetic acid yields are visible. The observation that the $Al_2O_3/ZrO_2/TiO_2$ catalyst is the most active must be seen alongside the observations that 1) selectivity to acetic acid over sum of ethane and ethylene is also very high and 2) the catalyst is also very active towards dry reforming of methane. The important properties of this catalyst that result in this activity profile have not been clearly identified but it seems possible that they are related to surface acidity, combined with the surface area/porosiy characteristics.
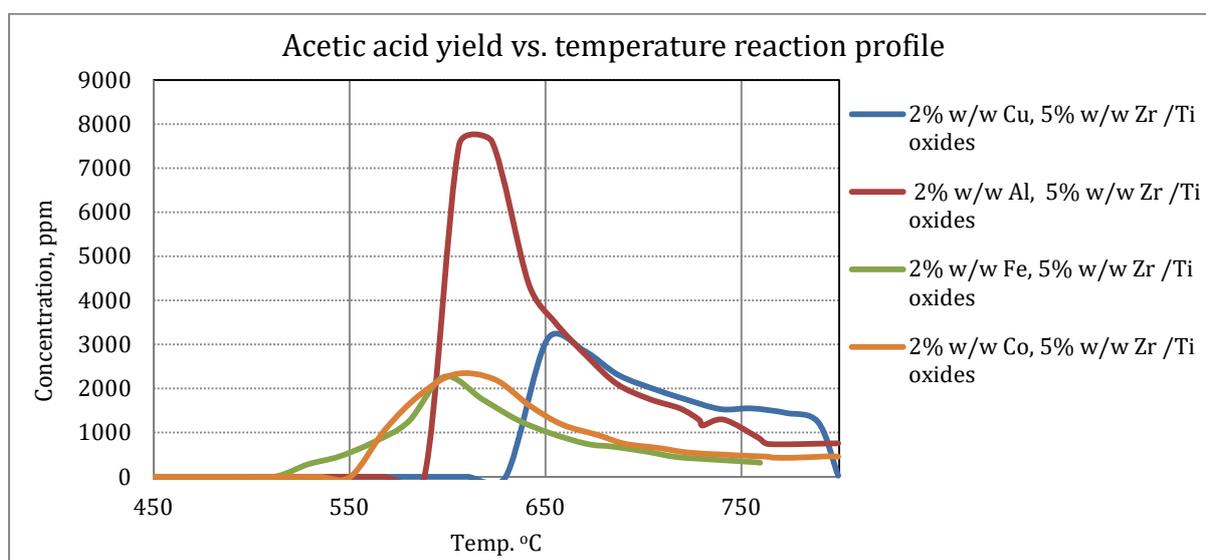

Figure 4.19. Acetic acid formation with increasing reactor temperature from ternary oxide catalysts based on Zr/Ti oxide ($CO_2:CH_4$ 1:1).

Table 4.9. Activities of ternary oxide catalysts based on Zr/Ti catalyst prepared by impregnation method-2 (CO_2/CH_4 1:1).

(standard gases calibrated at confident level 95%).

Catalyst and preparation method	Gas feed ratio	Temp. for max. acetic acid yield T_{max}	CO_2 in	CO_2 out	CH_4 in	CH_4 out	Acetic acid at T_{max}	Ethane at T_{max}	Ethylene at T_{max}	Ratio of acetic acid / ethane + ethylene	H_2 at T_{max}	Conv.* CO_2 at T_{max}	Conv.* Methane at T_{max}	Acetic acid selec.** at T_{max}	ethane selec.** at T_{max}	Ethylene selec.** at T_{max}	H_2 selec.** at T_{max}	Acetic acid yield at T_{max}
		^{o}C	%	%	%	%	%	%	%	-	%	%	%	%	%	%	%	%
5% ZrO_2/TiO_2 Impreg-2[(i)]	CO_2 50%, CH_4 50%	610	50.5	46.3	49.5	45.9	0.54	0.040	0.022	8.7	0.04	2.61	7.23	15.1	1.1	0.6	10.3	1.09
Al_2O_3/5%ZrO_2/TiO_2	CO_2 50%, CH_4 50%	614	44.4	46.3	55.6	35.3	0.87	0.070	0.040	7.9	1.75	8.31	36.51	4.3	0.3	0.2	8.6	1.56
CoO/5% ZrO_2/TiO_2	CO_2 50%, CH_4 50%	610	50.8	40.1	49.2	30.2	0.25	0.056	0.046	2.5	2.19	32.70	38.62	1.3	0.3	0.2	11.5	0.51
CuO/5% ZrO_2/TiO_2	CO_2 50%, CH_4 50%	650	50	35	50	8	0.34	0.005	0.005	34.0	0.34	29.42	84.00	0.8	0.01	0.01	0.8	0.68
FeO/5% ZrO_2/TiO_2	CO_2 50%, CH_4 50%	600	51.7	42.2	48.3	24.1	0.25	0.008	0.005	19.2	2.46	16.44	50.10	1.0	0.03	0.02	10.1	0.52

(i): Impregnated method-2,   * Conv. = Conversion   ** selec. = selectivity

4.3.3 Effect of CO_2/CH_4 ratios

The effect of gas ratio of CO_2 and CH_4 was studied by using the binary oxide 5% w/w Zr/Ti catalyst prepared by impregnation method-2. The aim of the study was to optimise the CO_2/CH_4 ratio for acetic acid formation.

The summary of the activity test results for three gas ratios are shown in Figure 4.20. The activity test of gas ratio CO_2/CH_4 1:9 formulates acetic acid at 620 °C with a broad peak from 620 °C to 800 °C and maximum acetic acid concentration of 1,600 ppm.

The gas ratio CO_2/CH_4 1:1 showed acetic acid was made at lower temperature, starting at 588 °C with a broad peak and higher acetic acid concentration (5,400 ppm). The gas ratio CO_2/CH_4 9:1 showed the highest concentration of acetic acid of 9,300 ppm and the formation started at 670 °C.

Figure 4.20. Overlay plot of acetic acid yields at three different gas ratios of CO_2 and CH_4 over 5% w/w Zr/Ti oxide prepared by impregnation method-2.

Ethane and ethylene yields largely followed the acetic acid yields as shown in Table 4.10 and in **Appendix-3** Figures C11 and C12. That suggested the concentration of methyl surface species made from methane was affected by the CO_2/methane ratios in the same way as acetic acid yield. The yield of acetic acid was increased when the CO_2/CH_4 gas ratio was decreased (in Table 4.10).

Table 4.10. Activities of Zr/Ti oxide catalyst using different gas ratios of CO_2 to CH_4.

(standard gases calibrated at confident level 95%).

Catalyst and preparation method	Gas feed ratio	Temp. for max. acetic acid yield T_{max}	CO_2 in	CO_2 out	CH_4 in	CH_4 out	Acetic acid at T_{max}	Ethane at T_{max}	Ethylene at T_{max}	Ratio of acetic acid / ethane + ethylene	H_2 at T_{max}	Conv.* CO_2 at T_{max}	Conv.* Methane at T_{max}	Acetic acid selec.** at T_{max}	ethane selec.** at T_{max}	Ethylene selec.** at T_{max}	H_2 selec.** at T_{max}	Acetic acid yield at T_{max}
		°C	%	%	%	%	%	%	%	-	%	%	%	%	%	%	%	%
5% ZrO₂/TiO₂ Impreg-2[(i)]	CO_2/CH_4 1:9	641	9.6	4.2	90.4	87.4	0.16	0.0025	0.003	32.0	2.10	58.95	3.32	5.3	0.1	0.1	70.0	0.18
5% ZrO₂/TiO₂ Impreg-2[(i)]	CO_2/CH_4 1:1	610	50.5	48.6	49.5	45.9	0.54	0.040	0.022	8.7	0.37	2.61	7.23	15.1	1.1	0.6	10.3	1.09
5% ZrO₂/TiO₂ Impreg-2[(i)]	CO_2/CH_4 9:1	714	89.6	78.4	10.4	4.4	0.93	0.0750	0.011	10.8	0.064	12.79	57.69	15.5	1.3	0.2	1.1	8.94

(i): Impregnated method-2,　* Conv. = Conversion　　** selec. = selectivity

4.3.4 Direct reaction of CO_2 with ethane and propane

The direct reaction was extended to study the CO_2 insertion in ethane and propane. The activity test was conducted on one catalyst, the binary 5% Zr/Ti oxide mixture prepared by impregnation method-2.

It was anticipated that CO_2 would react with ethane to produce propanoic acid (CH_3CH_2-COOH) as shown in equation (4.5). However, no propanoic acid was detected at any reaction temperature with a CO_2/ethane mixture in the ratio 1:1 (**Appendix-3**, Figure C15). Instead, acetic acid was formed as shown in Figure 4.21, at up to 2000 ppm. In addition, methane and H_2 at high concentrations (15000 ppm) were detected [**Appendix-3** (Figure C14)] indicating that cracking of the C-C bond of ethane was a major process over this catalyst.

Figure 4.21 Acetic acid from the activity test reaction between CO_2 and ethane (CO_2/ethane ratio 1:1).

When propane was used with CO_2 (CO_2:propane = 1:1), the direct product of CO_2 insertion in propane, butanoic acid ($CH_3CH_2CH_2$-COOH), was not detected (**Appendix-3** Figure C15). However, acetic acid and propanoic acid were detected (Figure 4.22). Acetic acid formation peaked at only 500 °C and 1700 ppm, and propanoic acid formed at higher temperature, peaking at 685 °C, but at a very low concentration, 44 ppm (Figure 4.23).

Figure 4.22. Acetic acid concentration vs. temperature from the reaction between CO_2 and propane (CO_2/propane 1:1).

Figure 4.23. Propanoic acid (CH_3CH_2COOH) concentration vs. temperature from the reaction between CO_2 and propane (CO_2/propane 1:1).

This data is summarised in Table 4.11. In Figure 4.24 the concentration of acetic acid vs temperature is shown for the three starting alkanes with CO_2, methane, ethane and propane. The trend is clear, with acetic acid forming at lower temperature as the chain length of the hydrocarbon is increased. If, as seems certain, acetic acid is formed by a radical mechanism in which methyl surface species are active on the catalyst surface, this implies that the formation of methyl surface species from C-C bond breaking becomes easier as the precursor chain length is increased, compared to simply C-H bond breaking.

The cracking process that is required to produce methyl surface species from ethane and propane evidently occurs readily and, unfortunately, selectivity to the cracking products methane and hydrogen is very high for the ZrO_2/TiO_2 catalyst, and the alternative product that could arise from the cracking products, acetic acid, is formed in very low concentration Table 4.11 tabulates the acetic acid yields from ethane and propane.
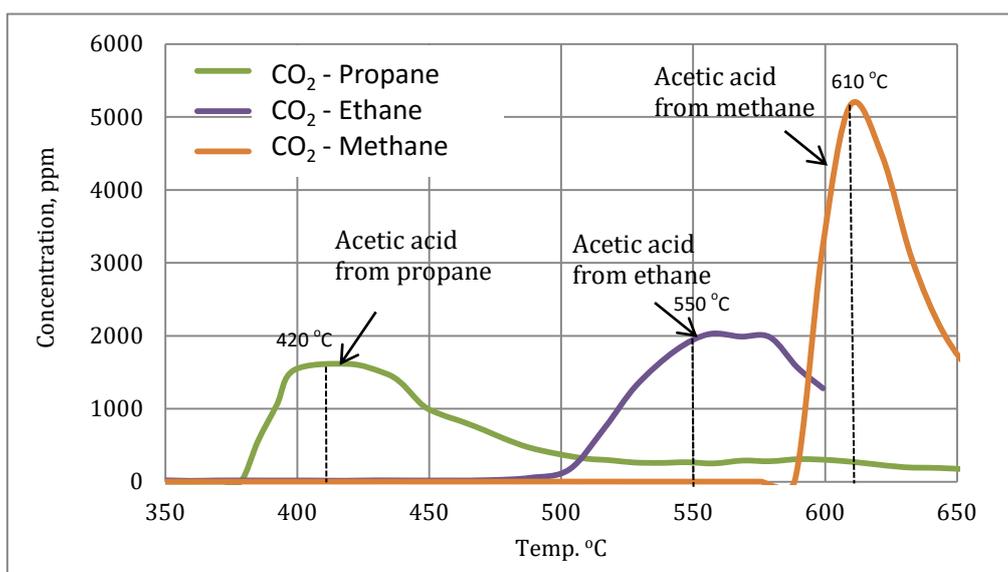

Figure 4.24. Acetic acid formation profile from reaction of CO_2 with methane, ethane, and propane.

Table 4.11. Performance of the activity test of CO$_2$ reaction with each of methane, ethane, propane, ethylene and acetylene on binary oxide of 5% Zr/Ti, (standard gases calibrated at confident level 95%).

Catalyst and preparation method	Gas feed ratio	Temp. for max. acetic acid yield T$_{max}$	CO$_2$ in	CO$_2$ out	HC gas feed in	HC gas feed out	Acetic acid at T$_{max}$	Ethane at T$_{max}$	Ethylene at T$_{max}$	Ratio of acetic acid / ethane + ethylene	H$_2$ at T$_{max}$	Conv.* CO$_2$ at T$_{max}$	Conv.* Methane at T$_{max}$	Acetic acid selec.** at T$_{max}$	ethane selec.** at T$_{max}$	Ethylene selec.** at T$_{max}$	H$_2$ selec.** at T$_{max}$	Acetic acid yield at T$_{max}$
		°C	%	%	%	%	%	%	%	-	%	%	%	%	%	%	%	%
5% ZrO$_2$/TiO$_2$ Impreg-2$^{(i)}$	CO$_2$/ methane 1:1	610	49.9	48.6	49.5	45.9	0.54	0.04	0.022	8.7	0.37	2.61	7.23	15.1	1.1	0.6	10.3	1.1
5% ZrO$_2$/TiO$_2$ Impreg-2$^{(i)}$	CO$_2$/ ethane 1:1	550	50.5	43.7	49.6	44.0	0.20	ND **	ND **	ND **	1.56	13.47	11.29	3.6	ND **	ND **	27.8	0.4
5% ZrO$_2$/TiO$_2$ Impreg-2$^{(i)}$	CO$_2$/ propane 1:1	420	50.3	49.7	49.7	49.4	0.17	ND **	ND **	ND **	0.13	1.19	0.60	56.7	ND **	ND **	43.3	0.3
5% ZrO$_2$/TiO$_2$ Impreg-2$^{(i)}$	CO$_2$/ ethylene 1:1	560	50.4	43.0	49.6	41.9	0.30	ND **	ND **	ND **	40.0	14.68	15.52	3.9	ND **	ND **	51.9	0.6
5% ZrO$_2$/TiO$_2$ Impreg-2$^{(i)}$	CO$_2$/ acetylene 9:1	624	90.7	ND **	9.3	ND **	0.30	ND **	ND **	ND **	ND **	ND **	ND **	ND **	ND **	ND **	ND **	ND **

(i): Impregnated method-2,   * Conv. = Conversion   ** selec. = selectivity   *** ND = not determined

4.3.5 The direct reaction of CO_2 with alkenes and alkynes

The direct reaction of CO_2 with ethylene and acetylene were studied over the 5% Zr/Ti binary oxide catalyst prepared by impregnation method-2, [16] anticipating the direct insertion products, acrylic acid ($CH_2=CHCOOH$) from ethylene and propiolic acid ($CH\equiv C\text{-}COOH$) from acetylene.

The CO_2 reaction with ethylene showed traces of acrylic acid but propiolic acid was formed at higher concentration (50 ppm). Reaction occurred at the relatively low temperatures of 175-425 ^{o}C (Figure 4.25). The main insertion product was acetic acid (3000 ppm). This formed at higher temperature than acrylic acid but, significantly, at a lower temperature than acetic acid was formed with the other starting materials, methane and even ethane (Figure 4.26).   The temperature profile of acetic acid formation from ethylene was much broader than with the alkanes.

Figure 4.25. Concentrations of acrylic and propiolic acids vs temperature for reaction of CO_2 with ethylene (CO_2/ethylene 1:1).

Figure 4.26. Acetic acid concentration vs temperature from direct reaction of CO_2 with ethylene (CO_2/ethylene 1:1).

The reaction of acetylene with CO_2 also formed propiolic acid, at higher concentration than with ethylene (1300 ppm vs 50 ppm). Reaction occurred from 350 ^{o}C to 550 ^{o}C as shown in Figure 4.27.

Propiolic acid is a product of CO_2 insertion to acetylene after losing an H atom.   The results here are consistent with those of Zhang *et al.* [22] who proposed the direct reaction between acetylene with CO_2, via C-H bond activation.

As with ethylene, acetic acid was also detected as a product of CO_2 insertion in acetylene, below 400 ^{o}C, with yield increasing above this temperature, to 3000 ppm as shown in Figure 4.26.

Figure 4.27. Products from direct reaction of CO_2 with acetylene (CO_2/acetylene 9:1).

A summary of the results of CO$_2$ insertion into ethylene and acetylene is given in Table 4.11. What is not shown here is the evidence for substantial dry reforming that went on alongside the insertion reactions. This dry reforming reaction is known to be very much more thermodynamically favourable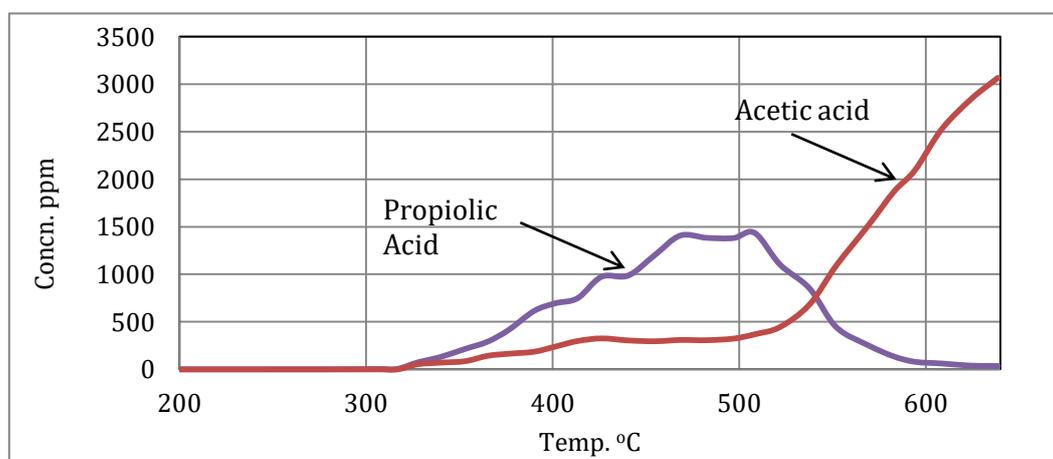 for acetylene than for ethylene, and for ethylene than ethane in the presence of CO$_2$ (Figure 4.29). In fact, the temperatures at which the Gibbs Free Energy change for the dry reforming reaction become negative are about 150 ^{o}C for acetylene, 450 ^{o}C for ethylene and 550 ^{o}C for ethane.

An explanation for the formation of the smaller carboxylic acids than were expected from C$_2$ and larger hydrocarbons might be that the Zr/Ti catalyst assists C-C bond breaking of, for instance, ethylene and acetylene. Methylene and possibly methylidyne surface species, CH$_2$* and CH*, are probably the result of bond activation on the catalyst surface. On the other hand, the formation of propiolic acid must be linked to C-H bond activation on ethylene and acetylene prior to direct reaction with CO$_2$.
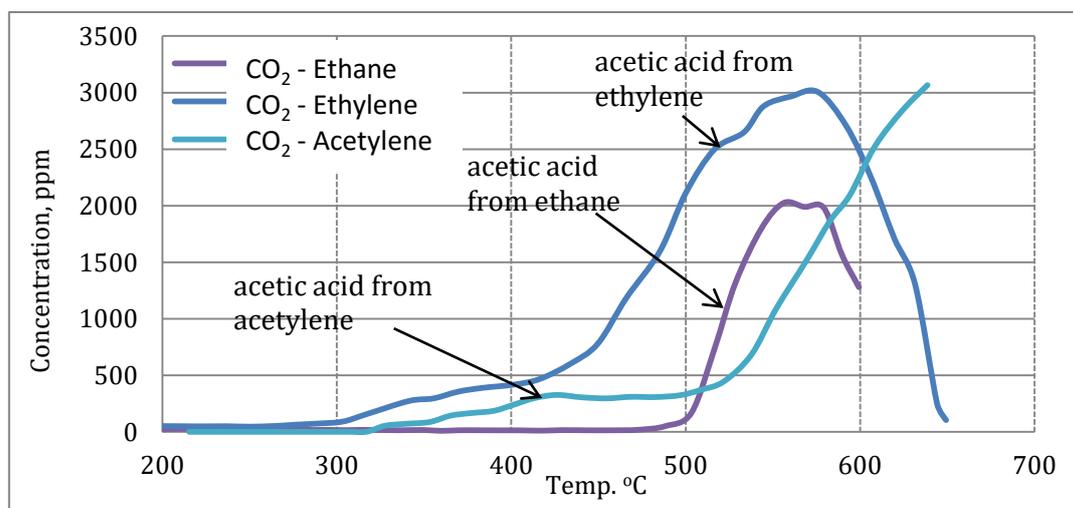

Figure 4.28. Acetic acid formation from different activity test of CO$_2$ with ethane, ethylene and acetylene.
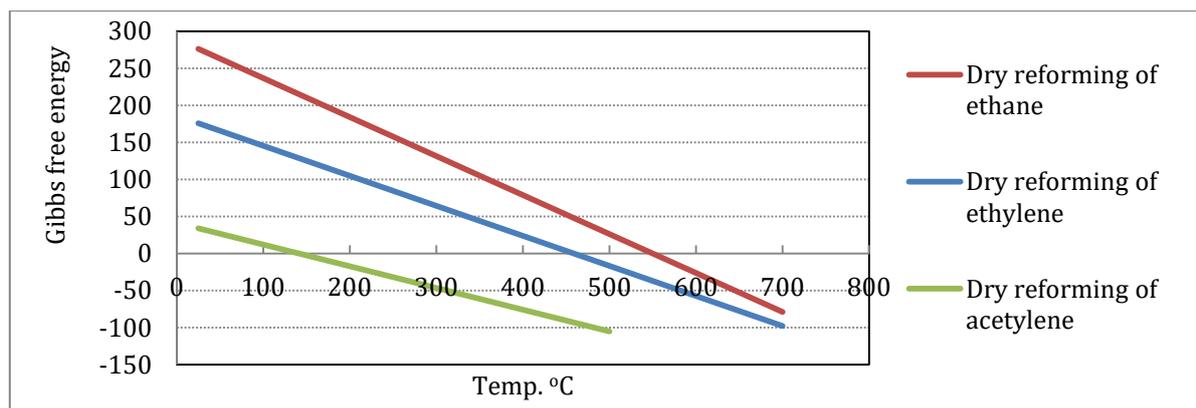
Figure 4.29. The Gibbs Free Energy Change associated with dry reforming of ethane, ethylene and acetylene vs. reaction temperature.

4.3.6 Catalytic stability

The aim of the study was to investigate the stability of Zr/Ti oxide catalysts prepared by impregnation method-2[16] to form acetic acid from CO_2 and methane at 620 °C, and from CO_2 and propane at 390 °C.

Figures 4.30-4.32 show the product yields of the CO_2 reaction with CH_4 over time. The initial rise in product peaks in the figures corresponds to the reactor reaching the reaction temperature of 620 °C. Although acetic acid is formed in high yield (8200 ppm) initially, it rapidly falls off after 2-3 hours. Ethylene is produced in parallel with acetic acid. CO is formed as acetic acid yield decreases, but CO yield also decreases eventually.

A possible explanation is that a C-H bond breaking process occurs on the catalyst surface, providing methyl surface species and hydrogen atoms, which go on to react with CO_2 to produce acetic acid.   There is some reaction between pairs of methyl surface species, or between methyl surface species and methane, to produce ethylene. However, it seems likely that the reverse water gas shift reaction takes over from these processes quite quickly (as shown in Figure 4.32), with the hydrogen reacting directly with CO_2 to produce water and CO, although it is not clear why.   Whatever the exact mechanism is for this sequence of processes, it is clear that catalyst stability is relatively low for the surface species -based reactions that are proposed.
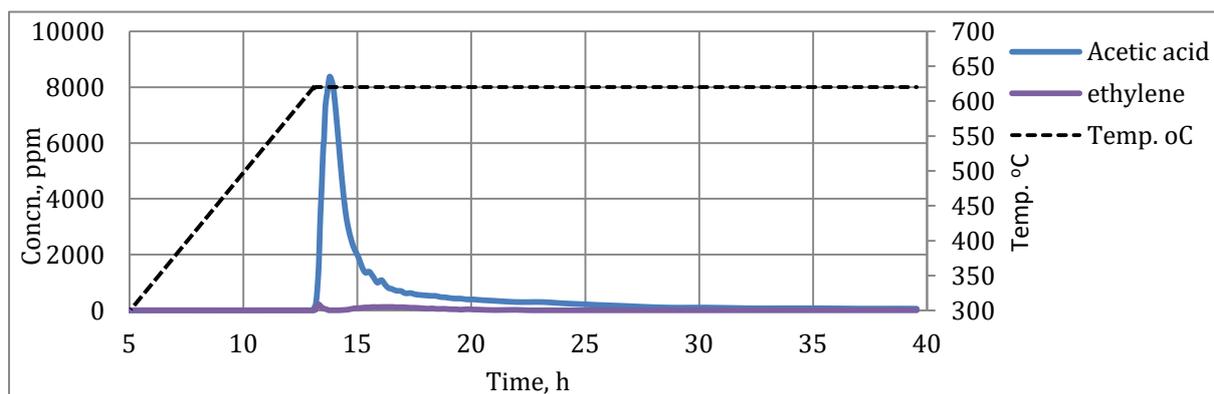
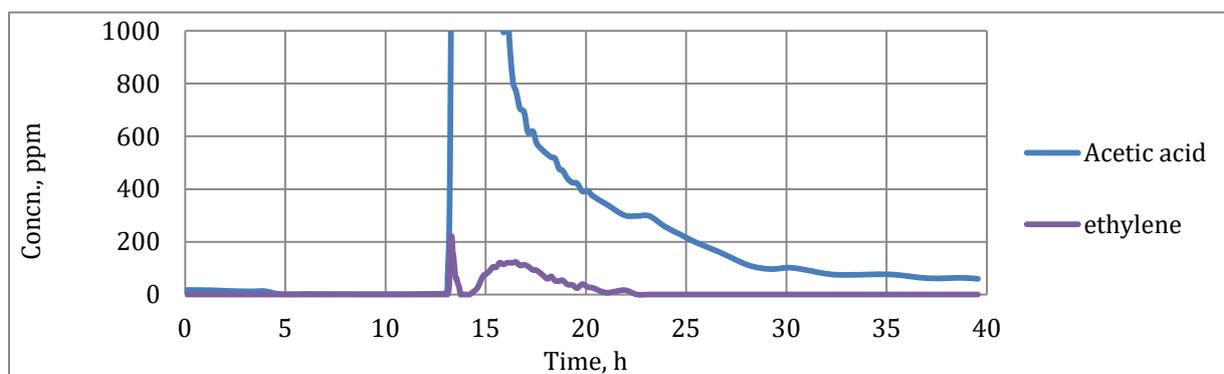Figure 4.30. Catalytic stability test of 5% w/w Zr/Ti oxide catalyst at 620 ^{o}C (CO$_2$/CH$_4$ 1:1).

Figure 4.31. Zoom in plot of concentration between 0-500 ppm of the catalytic stability test of 5% w/w Zr/Ti oxide catalyst at 620 ^{o}C (CO$_2$/CH$_4$ 1:1).
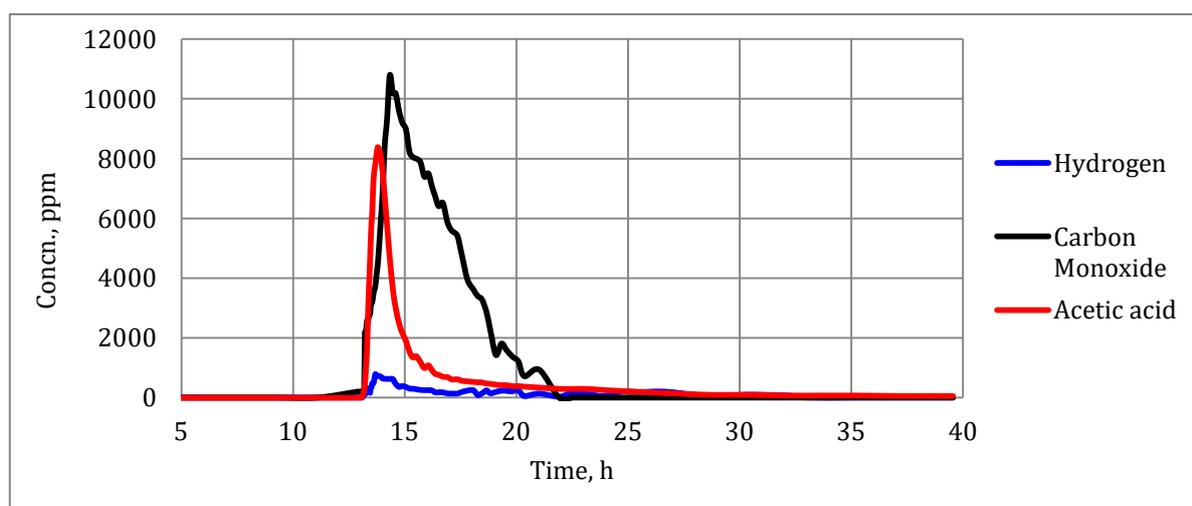

Figure 4.32. Catalytic stability test of 5% w/w Zr/Ti oxide catalyst at 620 ^{o}C (CO$_2$/CH$_4$ ratio 1:1).

The results for the second reaction, that of CO_2 with propane are shown in Figure 4.33. Again, the reactor temperature of 390 °C was selected due to substantial acetic acid yield, after the experiment began, at about 4 h on the figure. Acetic acid was formed (480 ppm) but, as before, fell away quite quickly.

In this experiment, the catalyst was regenerated with air at 700 °C after about 19 h (data collection was stopped and re-started). Significantly, only a very limited recovery in acetic acid yield was seen after this step (yield 20-50 ppm) which may well be within experimental error given the disturbance to the system.

To explain the loss in activity is difficult. Results given in **Chapter 2** for the powder X-ray diffraction patterns for the Zr/Ti oxide catalysts showed that the X-ray patterns were effectively the same before and after this reaction, in which reflections from anatase were dominant. A slight fall in crystallite size was detected (253 nm to 230 nm – Table 4.13) through slight line broadening but this is unlikely to be significant.

It is not clear why the catalyst deactivates as it does. There is no change in catalyst structure as the catalyst is used, and the fact that high temperature air treatment at 700 °C has no effect signifies that coking is not the reason. Nevertheless, since no structural changes were detected on the catalyst, it seems likely that catalyst poisoning, perhaps by reaction products is responsible, and that removing the poison is difficult.
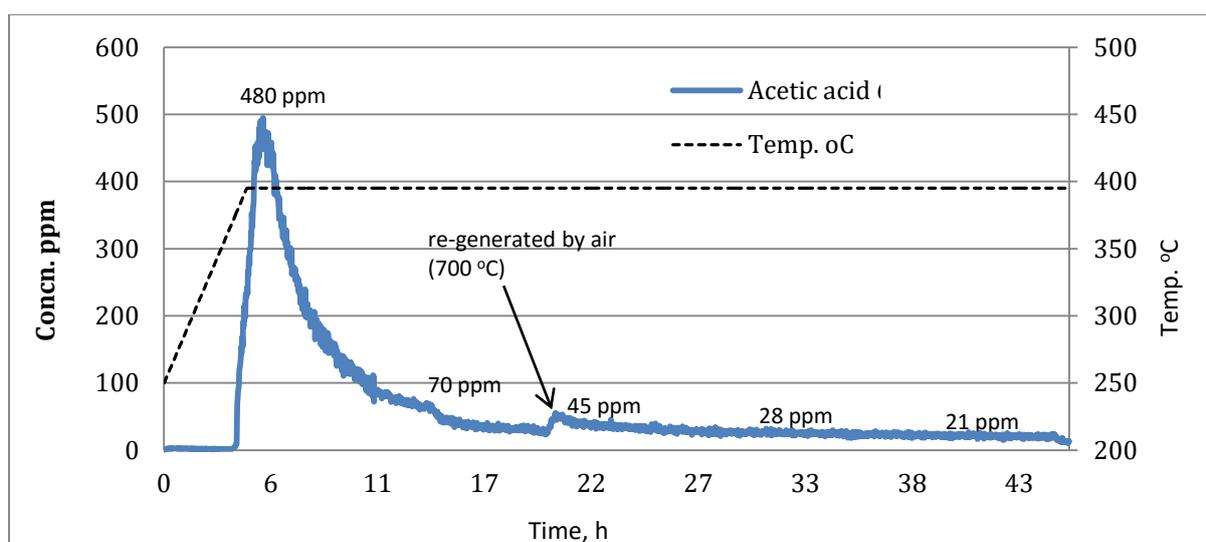

Figure 4.33. Acetic acid yield from the catalytic stability test of 5% w/w Zr/Ti oxide catalyst at reaction temperature 390 °C (CO_2/propane ratio 1:1)

Table 4.13. Anatase crystallite size of binary oxides Zr/Ti after the stability test.

Catalyst	Crystallite size (Å)
Binary oxides Zr/Ti (fresh)	253
Binary oxides Zr/Ti after catalyst stability of CO_2/propane reaction at 390 °C	231
Binary oxides Zr/Ti after catalyst stability of CO_2/methane reaction at 620 °C	225

4.3.7 Hydrogen-temperature programmed reduction (H_2-TPR)

The oxidation state of the catalysts was studied relatively late in the project and the results of this are presented here and not alongside the other characterisation data which is presented in **chapter 2**. Figures 4.34 and 4.35 show H_2 temperature programmed reduction profiles of pure ZrO_2 and pure TiO_2 used as reference. The amount of H_2 consumption is tabulated in Table 4.14. It is clear that pure TiO_2 used as support shows two reduction peaks. The T_{max} peak at 600-820 °C might be attributed to reduction of Ti^{4+} to Ti^{3+} and the T_{max} peak >820 °C might be attributed to further reduction of Ti^{3+}[23]. At the T_{max} 600-820 °C, H_2 uptake by Ti is significantly lower than amount Ti presence in sample, therefore it could mean only the external Ti atom in particle would reduce.

The pure ZrO_2 shows a lower reduction temperature than TiO_2 as two broad peaks at T_{max} of 508 °C and 800 °C. The data suggests that reduction of ZrO_2 was relatively difficult or that only a small proportion of the oxide could be reduced because H_2 consumption was low.

Table 4.14. H_2 uptake of single oxide of ZrO_2 and TiO_2

Sample	Method of preparation	H_2 uptake mmol^{-1}g STP	T_{max} (°C)
ZrO_2	commercially available	0.05	508
TiO_2	Commercially available	1.4 *	784

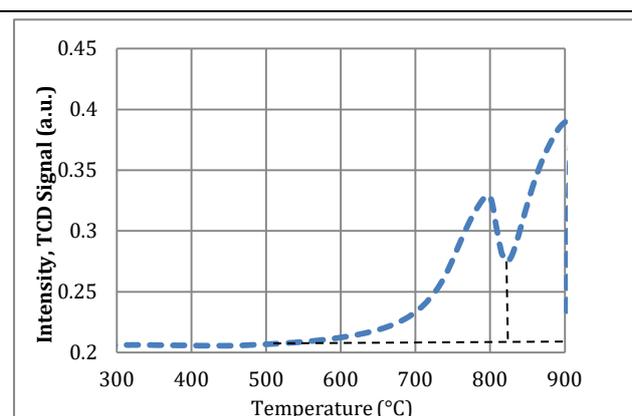* H_2 uptake at the peak of T_{max} 784 °C

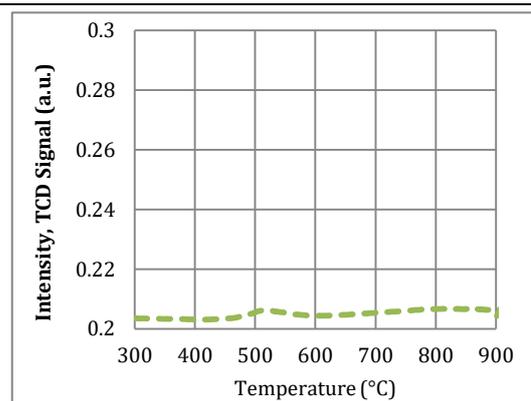Figure 4.34. H_2-TPR profile of pure TiO_2 support

Figure 4.35. H_2-TPR profile of pure ZrO_2

Different ratios of mixed oxide of Zr/Ti prepared by co-precipitation methods 1, 2, 3 and 4 were tested by H_2-TPR. The result show very little reduction as seen in Figures 4.36 and 4.37. The catalysts of Zr/Ti oxide prepared in 1:1 ratio by the co-precipitation methods also shows little reduction, implying very stable mixed oxides, similar to the observation by Raju *et al.* [24] and Rao *et al.* [25]. Table 4.15 shows data for a range of mixture compositions. H_2 consumption is generally low but, significantly, catalysts made by co-precipitation methods 2 and 3 show much high H_2 uptake than the others.

Table 4.15. H_2 uptake by binary oxide Zr/Ti oxide catalysts prepared by the co-precipitation route.

Sample	Method of preparation	H_2 uptake mmol^{-1}g STP
2% w/w Ti/Zr oxide	co-precipitation method -1	0.08
8% w/w Ti to Zr oxide	co-precipitation method -1	0.12
17% w/w Ti to Zr oxide	co-precipitation method -1	0.02
68% w/w Ti to Zr oxide	co-precipitation method -1	0.12
11% w/w Zr/Ti oxide	co-precipitation method -1	0.08
45% w/w Zr/Ti oxide	co-precipitation method -1	0.07
1:1 w/w Ti to Zr oxide	co-precipitation method -1	0.09
1:1 w/w Ti to Zr oxide	co-precipitation method -2	0.28
1:1 w/w Ti to Zr oxide	co-precipitation method -3	0.31
1:1 w/w Ti to Zr oxide	co-precipitation method -4	0.10

Figure 4.36. H$_2$-TPR of co-precipitation method -1 binary oxide catalysts of Zr-Ti.

Figure 4.37. H$_2$-TPR of four co-precipitation methods of binary oxide of Zr-Ti.

The binary Zr/Ti oxide catalysts made by impregnation methods 1, 2 and 3 show more extensive reduction compared to the catalysts made by co-precipitation methods (Table 4.16). The different results for catalysts in which ZrO$_2$ is supported on TiO$_2$ made by the different impregnation methods possibly suggests that the form of the zirconium oxide differs, depending on the preparative method. It is possible that different Zr metal oxide species grow on TiO$_2$ and this may account for differences in T$_{max.}$ (for the Ti^{4+} to Ti^{3+} process) as shown in Figure 4.38. The H$_2$-TPR analysis of the samples, as shown in Figure 4.39, clearly reveals the effect of the different Zr addition methods on the reduction temperature of the TiO$_2$.

There are clear differences of H$_2$ uptake between catalysts prepared by the impregnation and co-precipitation methods. The H$_2$ uptake and therefore extent of reduction of Zr/Ti oxides prepared by impregnation methods is much higher than for the Zr/Ti oxides prepared by co-precipitation. That may possibly be related to the lower activities of catalysts prepared by the co-precipitation routes. It is possible here that the Zr addition by co-precipitation did not result in the generation of reducible and active Ti sites under hydrogen atmosphere.

The materials prepared by the impregnation methods 1, 2 and 3 exhibited a hydrogen reductive behaviour, as noted by their higher hydrogen uptake (over 5% Zr/Ti), also showed significant C-H bond activation of methane and reaction with CO$_2$. On the other hand, catalysts made by co-precipitation methods that exhibited poor reductive behaviour also showed poor C-H activation.

Table 4.16. H$_2$ computation measured by H$_2$-TPR of three impregnation methods of 5% Zr/Ti oxide

Catalyst Sample	Method of preparation	H$_2$ uptake * mmol^{-1}g STP	T$_{max}$ (^{o}C)
TiO$_2$	Support	1.40	784
5% ZrO$_2$-TiO$_2$	Impregnation Method-2, precursor made via wetness by water	0.65	714
5% ZrO$_2$-TiO$_2$	Impregnation Method-1, precursor made via diluted nitric acid	1.26	760
5% ZrO$_2$-TiO$_2$	Impregnation Method-3, precursor made via ammonia solution	0.80	688

* H$_2$ uptake at the peak of T$_{max}$

Figure 4.38. H$_2$-TPR of three impregnation methods of 5% Zr/Ti oxide show different bulk reduction profiles

Figure 4.39. Overall H$_2$-TPR plot of impregnation methods of 5% Zr/Ti oxide and reference samples of ZrO$_2$ and TiO$_2$

4.3.8 Competing reactions

In further work, the product yields from reactions were measured at reactor temperatures of 300 to 700 °C. This section is included to clarify the nature of competing reactions, and the following is largely based on the results from one of the catalysts – 5% Zr/Ti oxide prepared by impregnation method.   The idea was to study competing reactions such as the reverse water gas shift (RWGS) reaction over 5% Zr/Ti oxide catalyst. These experiments were performed with methane, ethane and propane in the presence of CO$_2$. The product yields are shown in Tables 4.17, 4.18 and 4.19.

The reaction of CO_2 and methane was tested using Zr/Ti oxide catalyst prepared by the impregnation method-1[15] which showed low temperature of C-H bond activation of methane in presence of CO_2. It can be seen from Table 4.17 and Figure 4.40 that H_2 and CO formation started at 490 °C, indicating C-H and C-O bond breaking from methane and CO_2 to form CO and H_2 by dry reforming (eq. 4.18).

Dry reforming reaction: $CH_4 + CO_2 \rightarrow 2CO + 2H_2$ (eq. 4.18)

This reaction would lead to equal amounts of CO and H_2 but Table 4.17 shows that CO is always in excess. This may be explained if the hydrogen produced is going on to react with CO_2 in the RWGS reaction (eq. 4.19) as follows.

RWGS reaction: $CO_2 + H_2 \rightarrow H_2O + CO$ (eq. 4.19)

The ratio of CO to H_2 falls a little as the temperature is increased. An explanation for this might be an increase relative rate of dry reforming. At temperatures from 550 to 580 °C acetic acid (equation 4.20) is formed (Figure 4.5). The yield of CO and H_2 increased as the reactor temperature was increased further. This implies that both the dry reforming reaction and the RWGS reaction occur more extensively as the temperature is increased.
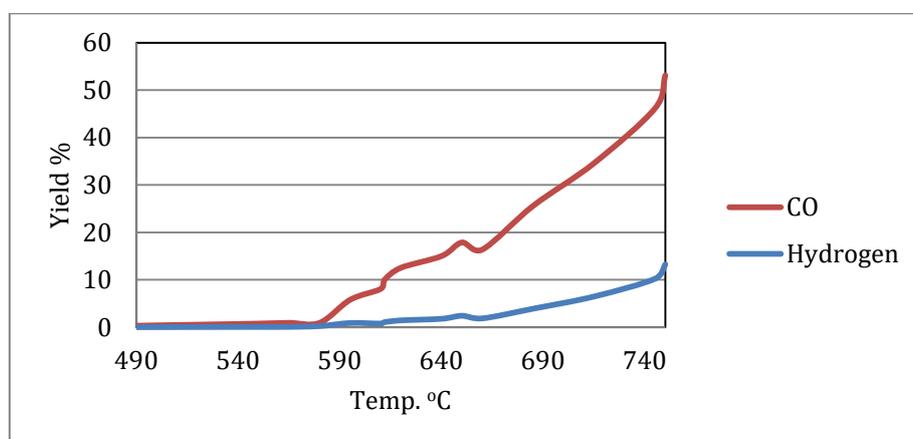
Acetic acid formation: $CH_4 + CO_2 \rightarrow CH_3COOH$ (eq. 4.20)

Figure 4.40. Yield of CO and H_2 from the activity test of CO_2 with CH_4

Table 4.17. Product yields for reaction between of CO_2 with methane (ratio 1:1) over 5% Zr/Ti oxide prepared by impregnation (standard gases calibrated at confident level 95%).

Temperature °C	CH_4 Conversion %	CO_2 Conversion %	H_2 yield %	CO yield %	Yield of Acetic acid (QMS)** %	CO/H_2 ratio
300	0.00	0.00	0.00	0.00	0	0
400	0.00	0.00	0.00	0.00	0	0
430	0.00	0.00	0.00	0.00	0	0
460	0.00	0.00	0.00	0.00	0	0
490	0.10	0.10	0.02	0.34	0	17.0
520	0.32	0.26	0.05	0.56	0.01	11.2
550	0.65	0.28	0.07	0.79	0.08	11.3
565	2.35	1.69	0.08	0.95	0.08	11.3
580	4.00	3.20	0.25	0.95	0.07	3.8
595	4.04	4.26	0.89	5.81	0.07	6.5
610	3.50	6.12	0.78	8.10	0.06	10.4
612	3.76	7.38	1.09	10.07	0.06	9.3
620	4.52	9.22	1.45	12.56	0.06	8.7
640	5.19	10.94	1.79	15.03	0.05	8.4
650	6.07	12.80	2.42	17.89	0.04	7.4
660	5.54	11.86	1.87	16.39	0.04	8.8
685	9.00	17.89	3.91	25.61	0.03	6.6
715	14.30	25.62	6.48	34.62	0.02	5.3
745	20.17	34.13	10.23	46.19	0.02	4.5
750	24.1	39.5	13.23	53.10	0.02	4.0

** Acetic acid concentration obtained from Figure 4.5 (impregnation method -1)

Table 4.18 and Figure 4.41 show the products of the ethane and CO_2 reaction over binary 5% Zr/Ti oxide catalyst prepared by impregnation method-1 as the reaction temperature is progressively increased as in the experiments described above. The first thing to note is that reaction starts at 400 °C, a significantly lower temperature than that at which reaction started with methane. Hydrogen, carbon monoxide, and ethylene are formed. Ethane dehydrogenation may be occurring (eq. 4.21) followed by RWGS (see equation 4.19).

Ethane dehydrogenation: $C_2H_6 \rightarrow C_2H_4 + H_2$ (eq. 4.21)

RWGS: $CO_2 + H_2 \rightarrow H_2O + CO$ (eq. 4.19)

At 450 °C, methane was also detected, implying some C-C bond breaking followed by hydrogenation of the methyl surface species to form methane gas as shown in equation (4.22). CO is in large excess to start with but then the relative yield falls back as the

temperature is increased, Other trends are difficult to identify as there are fluctuations in the yields of all products as temperature is increased that may not be significant. At around 475 °C acetic acid is detected, again with yield increasing with temperature but falling above 600 °C (equation 4.23). The fact that the acetic acid yield does not appear to increase at the expense of methane yield suggests that acetic acid is probably made as a direct product of reaction between CO_2 and ethane.

Partial ethane cracking to methane in presence of CO_2:

$$C_2H_6 + CO_2 \rightarrow CH_4 + 2CO + H_2 \text{ (eq. 4.22)}$$

Formation of acetic acid from partial ethane breaking at presence of CO_2:

$$C_2H_6 + 2CO_2 \rightarrow CH_3COOH + 2CO + H_2 \text{ (eq. 4.23)}$$

Acetic acid yield is higher than methane yield at 450-475 °C. But the yield of methane increased over 500-625 °C. This suggests that C-C bond breaking is occurring and the resultant surface species are reacting with hydrogen to form methane rather than acetic acid. At higher reaction temperature, the dry reforming of ethane increased (equation 4.24). However, the CO/H_2 ratio is low, possibly indicative of the of water gas shift reaction (WGS) (equation 4.25) which consumes CO and produces H_2.

Dry reforming of ethane $C_2H_6 + 2CO_2 \rightarrow 4CO + 3H_2 \text{ (eq. 4.24)}$

Water gas shift (WGS) $CO + H_2O \rightarrow CO_2 + H_2 \text{ (eq. 4.25)}$

Table 4.18. Product yields for reaction between of CO_2 with ethane (ratio 1:1) over 5% Zr/Ti oxide (standard gases calibrated at confident level 95%).

Temperature °C	Ethane conv* %	CO_2 conv* %	Methane Yield %	Ethylene Yield %	H_2 Yield %	CO Yield %	Acetic acid** (detected by QMS) Yield %	CO/H_2 yield
250	0.00	0.00	0.00	0.00	0.00	0.00	0	0.0
350	0.00	0.00	0.00	0.00	0.00	0.00	0	0.0
400	2.77	1.19	0.00	0.06	0.03	0.68	0	20.7
450	3.58	2.08	0.04	0.58	0.29	1.37	0.18	4.7
475	3.89	1.61	0.12	0.48	0.29	1.75	0.36	6.0
500	7.4	10.9	1.72	0.52	3.79	10.9	0.51	2.9
575	13.8	14.2	1.65	0.75	5.66	16.4	0.50	2.9
600	17.2	14.4	2.27	0.92	5.30	9.60	0.51	1.8
625	33.7	11.4	6.18	1.19	12.9	5.04	0.39	0.4
650	50.6	12.5	14.7	1.22	21.3	2.18	0.24	0.1

* Conversion   ** 5% Zr/Ti oxide catalyst was made by impregnation method -2 from Figure 4.21
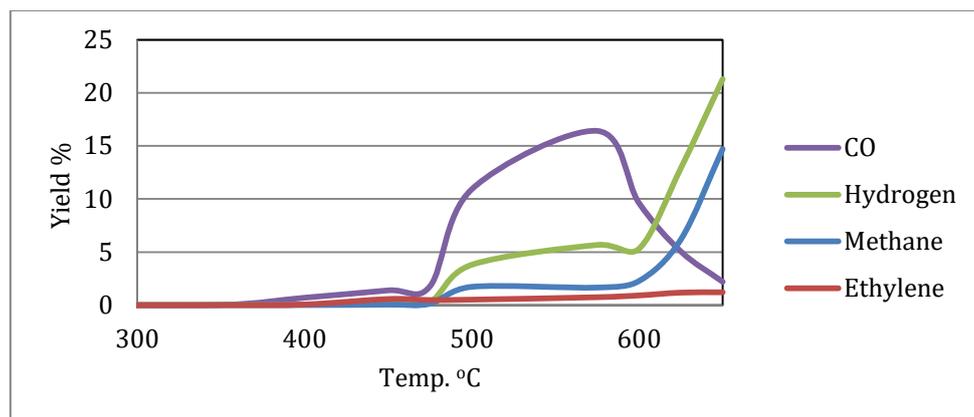
Figure 4.41. Yield of CO, H$_2$, methane and ethylene from the activity test of CO$_2$ with ethane

Table 4.19 and Figure 4.42 show the products of the propane and CO$_2$ reaction over binary 5% Zr/Ti oxide catalyst prepared by impregnation method-1 as the reaction temperature is progressively increased as in the experiments described above. The first thing to note is that reaction starts at 400 ^{o}C, a significantly lower temperature than that at which reaction started with hydrogen, carbon monoxide, methane and ethylene are formed. C-C bond breaking may be occurring (eq. 4.26 and 4.27). The acetic acid yield was detected by QMS at 400-450 ^{o}C and the possible reaction of breaking propane to the methyl surface species before reaction with CO$_2$.

At 475 to 550 ^{o}C, the increased yields of methane, ethane, ethylene, propylene along with H$_2$ and CO may be explained by further partial bond breaking of propane and CO$_2$. In addition, hydrogenation reaction observed as result from methyl and ethyl surface species to produce more yield of methane and ethane also consume H$_2$.

Partial propane cracking $C_3H_8 + 2CO_2 \rightarrow CH_4 + 4CO + 2H_2$ (eq. 4.26)
in presence of CO$_2$:

Further propane cracking to $C_3H_8 \rightarrow CH_4 + C_2H_4$ (eq. 4.27)
methane and ethane:

182

Table 4.19. Product yields for reaction between of CO_2 with propane (ratio 1:1) over 5% Zr/Ti oxide (standard gases calibrated at confident level 95%).

Temp. ^oC	Propane Conv* %	CO_2 Conv* %	H_2 Yield %	CO Yield %	C1 Yield %	C2 Yield %	Ethylene Yield %	Propylene Yield %	Acetic acid** (detected by QMS) Yield (%)	CO/H_2 ratio
400	0.68	3.09	0.23	1.17	0.12	0.00	0.04	0.00	0.30	5.1
450	1.87	3.17	0.42	2.42	0.20	0.01	0.04	0.01	0.22	5.8
475	3.18	7.08	1.14	6.46	0.69	0.03	0.14	0.01	0.12	5.7
500	8.69	11.83	3.08	14.34	2.43	0.16	0.72	0.02	0.08	4.7
525	20.78	22.55	7.18	21.73	6.23	2.31	2.30	0.73	0.07	3.0
550	33.58	29.02	14.57	30.49	12.05	3.06	3.56	3.05	0.05	2.1

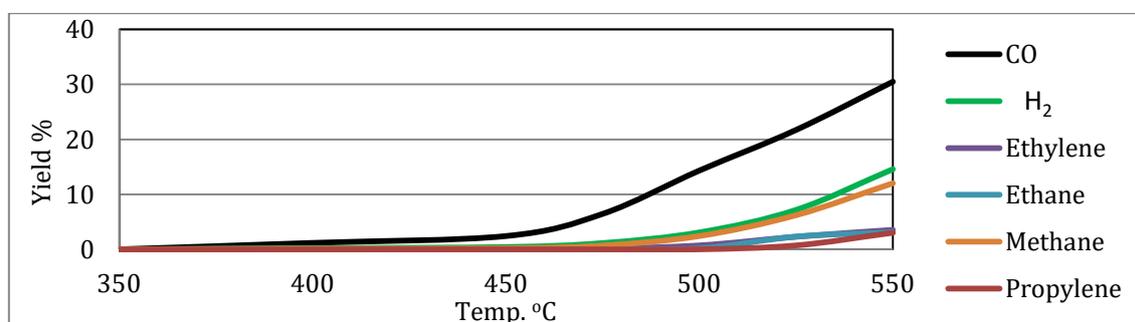* Conversion,   ** 5% Zr/Ti oxide catalyst was made by impregnation method -2 from Figure 4.22

Figure 4.42. Yield of CO, H_2, methane, ethane, ethylene and propylene from the activity test of CO_2 with propane

To summarise the data for this detailed (variable temperature) study of CO_2 reaction with methane, ethane and propane, the following important conclusions/observations can be reported.

1. The partial cracking of methane, ethane and propane to smaller compounds were detected over Zr/Ti oxide catalyst but each reaction showed significantly different yields of by-products. These differences can indicate several things. For instance, high CO/H_2 ratios indicate an active RWGS reaction on the catalyst surface.

2. Comparing yields of CO from RWGS to acetic acid from C-C direct reaction, the RWGS consumes H_2 and CO_2 higher and it is competing reaction of acetic acid.

4.4 Mechanism of CO_2 direct reaction as a whole molecule

In the work described above in this chapter, the direct reaction of CO_2 as a whole molecule was investigated during the reactions of CO_2 with CH_4, C_2H_6, C_2H_4, C_2H_2 and C_3H_8 on binary oxides of Zr/Ti as follow:

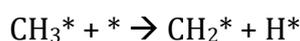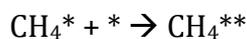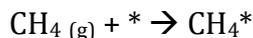### 4.4.1 Proposed mechanism of direct reaction CO_2 to CH_4

Although others have proposed an Eley–Rideal (E–R) mechanism for the reaction of CO_2 with CH_4 over copper-cobalt catalyst [9-10]. The results of the work presented in this thesis for the reaction with CO_2 with methane over Zr/Ti oxide tend to support the alternative Langmuir-Hinshelwood model in which both reactants are adsorbed on the catalyst surface and the rate-determing reaction step occurs on the catalyst surface. The following observations are combined to allow conclusions to be drawn about the mechanism of the CO_2 insertion reaction.

- Prior to acetic acid formation, CO_2 and CH_4 react on catalyst surface and produce CO and H_2.

- High yields of CO and of H_2 must arise from C-O and C-H bond breaking steps as part of the overall reaction mechanism. The fact that CO yields are invariably considerably higher than H_2 yields might be explained by involvement of the RWGS reaction which consumes H_2 and produces CO.

- The appearance of H_2 suggests that C-H bond breaking occurs on the catalyst surface. In turn this implies that methyl or methylene surface species are also produced on the catalyst surface. This further suggests that these surface species are responsible for reaction with CO_2 to produce acetic acid.

- Further strong evidence for methyl and methylene surface species formation on the catalysts is the detection of ethane and ethylene, which can only reasonably be formed from dimerisation of such surface species.

The direct reaction of CO_2 to CH_4 is provisional mechanism based on the reaction observation. The suggested reaction pathway of direct reaction is as follow:
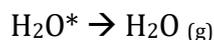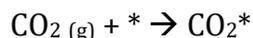
4.4.1.1 CH₄ dissociation

Methane dissociates[26-27] over catalyst to form intermediate methyl and methylene surface species prior to producing hydrogen gas as follow:
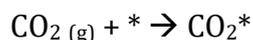
$$CH_{4\,(g)} + * \rightarrow CH_4*$$

$$CH_4* + * \rightarrow CH_4**$$

$$CH_4** \rightarrow CH_3* + H*$$

$$CH_3* + * \rightarrow CH_2* + H*$$

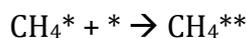$$H* + H* \rightarrow H_{2(g)} + 2*$$

(* indicates a surface site or surface species)

4.4.1.2 RWGS reaction

Prior acetic acid formation, CO is formed as result from C-O bond breaking in CO_2 and reacts with H_2 made from methane dissociation as proposed by McGuire *et al.* [26-27]. The RWGS reaction is proceed as follow:

$$CO_{2\,(g)} + * \rightarrow CO_2*$$

$$CO_2* + 2H* \rightarrow CO* + H_2O* + *$$

$$CO* \rightarrow CO_{(g)} + *$$

$$H_2O* \rightarrow H_2O_{(g)}$$

4.4.1.3 Direct reaction of CO₂ with methyl surface species followed by hydrogenation of acetic acid

The direct reaction of methyl surface species generated from methane reacts with CO_2 over catalyst to form acetic acid as follow:

$$CH_{4\,(g)} + * \rightarrow CH_4*$$

$$CH_4* + * \rightarrow CH_4**$$

$$CH_4** \rightarrow CH_3* + H*$$

$$CO_{2\,(g)} + * \rightarrow CO_2*$$

$$CH_3* + CO_2* \rightarrow CH_3COO* + *$$

$$CH_3COO* + H* \rightarrow CH_3COOH* + *$$

$$CH_3COOH* \rightarrow CH_3COOH_{(g)} + *$$

4.4.1.4 Dimerization of methyl surface species to ethane and ethylene

At same temperature of acetic acid formation the dimerization reaction was observed. The detected yield of ethane and ethylene and resulted from dimerization of methyl and methylene surface species over catalyst as follow:

$$CH_3* + CH_3* \rightarrow C_2H_6* + *$$
$$C_2H_6* \rightarrow C_2H_{6\ (g)} + *$$
$$CH_2* + CH_2* \rightarrow C_2H_4* + *$$
$$C_2H_4* \rightarrow C_2H_{4\ (g)} + *$$

4.4.2 Direct reaction of a whole molecule CO$_2$ with ethane

In the reaction of CO$_2$ with ethane, acetic acid was formed and none of the expected product, propanoic acid was observed. The equations below show the possible CO$_2$ reaction with methyl surface species generated from C-C bond breaking on Zr/Ti oxide catalyst. In addition, the evidence suggests that the reaction followed a Langmuir–Hinshelwood mechanism.

The detection of methane is evidence of C-C bond breakage. This is almost certainly due to reforming of the ethane with CO$_2$. It does however provide evidence for methyl or methylene surface species formation on the catalyst surface. The detection of CO is consistent with this, again forming via CO$_2$ adsorption on the surface. This dry reforming process occurs at relatively low temperature. Acetic acid is formed at higher temperature but it would seem likely that it is formed from the same surface-adsorbed surface species, as adsorbed CO$_2$ reacts with adsorbed methyl surface species and then with adsorbed hydrogen from ethane. The suggested reaction pathway is as follow:

4.4.2.1 Ethane dissociation

Ethane dissociates over the catalyst to produce methane, ethylene and hydrogen. The C-C and C-H bond breaking of ethane leads to intermediate products of methyl and methylene surface species as follow:

$$C_2H_{6\ (g)} + * \rightarrow C_2H_6*$$
$$C_2H_6* + * \rightarrow C_2H_6**$$
$$C_2H_6** \rightarrow C_2H_5* + H*$$

$$H^* + H^* \rightarrow H_2^* + ^*$$

$$H_2^* \rightarrow H_{2\ (g)} + ^*$$

$$C_2H_5^* + ^* \rightarrow CH_3^* + CH_2^*$$

$$CH_3^* + H^* \rightarrow CH_4^* + ^*$$

$$CH_4^* \rightarrow CH_{4\ (g)} + ^*$$
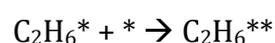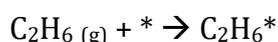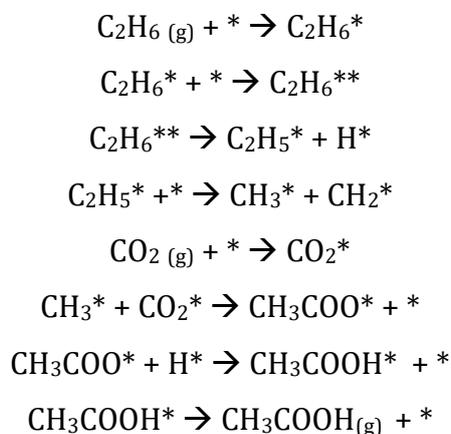
$$CH_2^* + CH_2^* \rightarrow C_2H_4^* + ^*$$

$$C_2H_4^* \rightarrow C_2H_{4\ (g)} + ^*$$

4.4.2.2 Direct reaction of CO_2 with methyl surface species followed by hydrogenation of acetic acid:

$$C_2H_{6\ (g)} + ^* \rightarrow C_2H_6^*$$

$$C_2H_6^* + ^* \rightarrow C_2H_6^{**}$$

$$C_2H_6^{**} \rightarrow C_2H_5^* + H^*$$

$$C_2H_5^* + ^* \rightarrow CH_3^* + CH_2^*$$

$$CO_{2\ (g)} + ^* \rightarrow CO_2^*$$

$$CH_3^* + CO_2^* \rightarrow CH_3COO^* + ^*$$

$$CH_3COO^* + H^* \rightarrow CH_3COOH^* + ^*$$

$$CH_3COOH^* \rightarrow CH_3COOH_{(g)} + ^*$$

4.4.3 Proposed mechanism of insertion CO_2 with ethylene

The reaction of CO_2 with ethylene and acetylene showed formation of acetic acid and some propiolic acid. A possible mechanism is as follows. Again, the reaction involves the adsorption of reactants and the reaction of two adsorbed surface species in the rate determining step, in line with a Langmuir-Hinshelwood mechanism.

4.4.3.1 Ethylene dissociation

The ethylene dissociation over catalyst is suggested as follow:

$$C_2H_{4\ (g)} + ^* \rightarrow C_2H_4^*$$

$$C_2H_4^* + ^* \rightarrow C_2H_4^{**}$$

$$C_2H_4^{**} \rightarrow C_2H_3^* + H^*$$

$$C_2H_4^* + H^* \rightarrow CH_3^* + CH_2^*$$

$$CH_2^* + H^* \rightarrow CH_3^* + ^*$$

$$H^* + H^* \rightarrow H_2^* + *$$

$$H_2^* \rightarrow H_{2\ (g)} + *$$

4.4.3.2 Direct reaction CO_2 with ethylene surface species followed by hydrogenation to form propiolic acid

The ethylene dissociates to hydrogen over the catalyst prior direct reaction with CO_2 is suggested as follow:

$$CO_{2\ (g)} + * \rightarrow CO_2^*$$

$$C_2H_4 + * \rightarrow C_2H_3^* + H^*$$

$$C_2H_3^* + * \rightarrow C_2H_2^* + H^*$$

$$C_2H_2^* + * \rightarrow C_2H^* + H^*$$

$$C_2H^* + CO_2^* \rightarrow C_2HCOO^* + *$$

$$C_2HCOO^* + H^* \rightarrow C_2HCOOH^* + *$$

$$C_2HCOOH^* \rightarrow C_2HCOOH_{(g)} + *$$

4.4.3.3 Direct reaction CO_2 with methyl surface species followed by hydrogenation for acetic acid formation

$$CH_3^* + CO_2^* \rightarrow CH_3COO^* + *$$
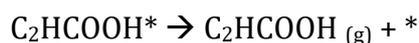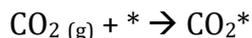
$$CH_3COO^* + H^* \rightarrow CH_3COOH^* + *$$

$$CH_3COOH^* \rightarrow CH_3COOH_{(g)} + *$$

4.4.4 Proposed mechanism for reaction of CO_2 with propane

The reaction of CO_2 with propane resulted in acetic acid and propanoic acid. The following mechanism, based on similar principles to those above, is proposed.

4.4.4.1 Dissociation of propane

$$C_3H_{8\ (g)} + * \rightarrow C_3H_8^*$$

$$C_3H_8^* + * \rightarrow C_3H_8^{**}$$

$$C_3H_8^{**} \rightarrow C_3H_7^* + H^*$$

$$C_3H_7^* + * \rightarrow CH_2^* + C_2H_5^*$$

$$\text{or } C_3H_7^* + * \rightarrow CH_3^* + C_2H_4^*$$

$$CH_2^* + H^* \rightarrow CH_3^* + *$$

$$CH_3^* + H^* \rightarrow CH_4^* + *$$

$$CH_4^* \rightarrow CH_{4\,(g)} + *$$

$$C_2H_5^* + H^* \rightarrow C_2H_6^* + *$$

$$C_2H_6^* \rightarrow C_2H_{6\,(g)} + *$$

$$C_2H_4^* \rightarrow C_2H_{4\,(g)} + *$$

$$H^* + H^* \rightarrow H_2^* + *$$
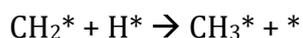
$$H_2^* \rightarrow H_{2\,(g)} + *$$

4.4.4.2 Direct reaction of CO$_2$ with methyl surface species followed by hydrogenation to acetic acid

$$CH_3^* + CO_2^* \rightarrow CH_3COO^* + *$$

$$CH_3COO^* + H^* \rightarrow CH_3COOH^* + *$$

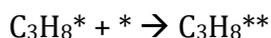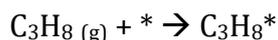$$CH_3COOH^* \rightarrow CH_3COOH_{(g)} + *$$

4.4.4.3 Direct reaction CO$_2$ with ethyl surface species followed by hydrogenation to form propanoic acid

$$C_2H_5^* + CO_2^* \rightarrow C_2H_5CO_2^* + *$$

$$C_2H_5CO_2^* + H^* \rightarrow C_2H_5COOH^* + *$$

$$C_2H_5COOH^* + H^* \rightarrow C_2H_5COOH_{(g)} + *$$

4.5 Conclusions

The reaction between CO$_2$ and CH$_4$ shows a clear differences when carried out over Zr/Ti oxide catalysts prepared by the various routes used here. These differences may be due to differences in catalyst surface areas and porosities, or may be due to electronic effects which are revealed through H$_2$-TPR experiments, which show that the binary oxides prepared by the impregnation routes are easily reduced and this seems to be associated with higher reaction activity of methane with CO$_2$.

The key objective of this chapter is to investigate the direct reaction of CO$_2$ and CH$_4$. The results demonstrate the importance of C-H bond breaking of methane, allowing

adsorption of hydrogen on the catalyst surface prior to direct reaction with CO_2. The results suggest that a Langmuir-Hinshelwood model, in which the rate-determining reaction step occurs on the catalyst surface, best explains the results of direct reaction of CO_2 to methane. In the absence of CO_2 the methyl surface species dimerise to produce ethane gas. In contrast, in the presence of CO_2, acetic acid forms as result of the direct reaction of CO_2 with methyl surface species followed by hydrogenation.

The most active catalysts for this reaction is TiO_2 promoted by ZrO_2 prepared by the impregnation route. Additional metal dopants (a third metal) lowers the catalytic activity for acetic acid formation, generally by increasing the rate of the Reverse Water Gas Shift reaction and dry reforming reactions, forming CO. Despite their good activities, the Zr/Ti oxide catalysts prepared by the impregnation method suffer from catalytic activity loss after a few hours of acetic acid formation, presumably due to poisoning of active sites.

These Zr/Ti oxide catalysts have also proved active for reaction between CO_2 and the larger alkanes, ethane and propane. However, the expected simple insertion products, propanoic and butanoic acid, were not formed in significant amounts, but acetic acid is the main insertion product in both cases. In fact, acetic acid is formed at lower temperatures from these starting alkanes than from methane. This implies that C-C bond breaking in ethane and propane is more important for direct reaction of CO_2. In fact, low concentrations of propanoic acid were detected from direct reaction of CO_2 with propane (alongside the major, acetic acid, product) indicating that ethyl surface species generated from C-C bond breaking in propane can go on to react with CO_2.

With the alkene, ethylene and alkyne, acetylene, the study suggests that the Zr/Ti oxide catalysts favour C-H bond activation with both reactants, which then allows CO_2 insertion to synthesise propiolic acid. Secondly, acetic acid is formed from both reactants, suggesting C-C bond fission and formation of methyl surface species which can react with CO_2 to form acetic acid.

It should be noted that, in all cases, the Reverse Water Gas Shift (RWGS) reaction competes with the CO_2 insertion reactions and a vital property of any catalyst developed

for these insertion reactions is the extent to which it is selective for insertion over the RWGS process. Overall, the Zr/Ti oxide catalyst identified in this work as the most active also shows relatively high selectivity for CO_2 insertion. Finally, the concept level of the study demonstrates that three carboxylic acids can be produced from direct insertion of CO_2 into small alkanes, alkenes and alkynes, using new Zr/Ti oxide catalysts. Key to these reactions is a radical mechanism that generates hydrogen that is dissociatively adsorbed on the catalyst surface in a highly reactive form.

4.6 References

1. J. R. Sohn and S. H. Lee, Appl. Catal. A, **321** (2007) 27-34.

2. M.E. Manríquez, T. López, R. Gómez and J. Navarrete, J. Mol. Catal. A., **220** (2004) 229–237.

3. R. Pérez-Hernández, D. Mendoza-Anaya, M.E. Fernández and A. Gómez-Cort , J. Mol. Catal. A., **281** (2008) 200–206.

4. K. Suzuki and J. B. Moffat, Catal. Lett., **16**, 4 (1992) 389-398.

5. K. Murata, T. Hayakawa, S. Hamakawa and K. Suzuki, Catal. Today, **45** (1998) 41-5.

6. W. Jeon, J. Y. Lee, M. Lee, J. W. Choi, J.M. Ha, D. J. Suh and I. W. Kim, Appl. Catal. A, **464–465** (2013) 68–77.

7. A. Erdöhelyi, J. Cserényi, and F. Solymosi, J. Catal., **141**, (1993) 287-299.

8. S. F. Moya, R. L. Martins, A. Ota, E. L. Kunkes, M. Behrens and M. Schmal, Appl. Catal. A, **411–412** (2012) 105–113.

9. W. Huang, K.C. Xie, J.P. Wang, Z.H. Gao, L.H. Yin and Q.M. Zhu, J. Nat. Gas Chem., **13** (2004) 113-115.

10. R. Zhang, L. Song, H. Liu and B. Wang, Appl. Catal. A, **443–444** (2012) 50–58.

11. J. Fung l and I. Wang, Appl. Catal., A 166 (1981) 327-334, Appl. Catal. A, **166** (1981) 327-334.

12. J. R. Sohn and S. H. Lee, Appl. Catal. A, **266** (2004) 89–97.

13.   D. Mao, G. Lu and Q. Chen, Appl. Catal. A, **263**, 1 (2004), 83-89.

14   M. Machida. S. Ikeda, D. Kurogi and T. Kijima, Appl. Catal. B, **35** (2001) 107–116.

15.   N. Takahashi, A. Suda, I. Hachisuka, M. Sugiura, H. Sobukawa and H. Shinjoh, Appl. Catal. A, **72**, 1–2, 8 (2007), 187-195.

16.   A.M. Ruppert and T. Paryiczak, Appl. Catal. A, **320** (2007) 80-90.

17.   I. Chepurna, R. Smortaev, C. Kanibolotsky and V. Strelko, J. Colloid Interface Sci., **356** (2011) 404-411.

18.   M. Laniecki and M. Ignacik, Catal. Today, **116** (2006) 400–407.

19.   M. Chen, J. Xu, Y. Cao, H.Y. He, K.N. Fan and J.H. Zhuang, J. Catal., **272** (2010) 101–108.

20.   B. Xu, B. Zheng, W. Hua, Y. Yue and Z. Gao, J. Catal., **239** (2006) 470–477.

21   V. P. Kumar, Y. Harikrishna, N. Jagaraju and K. V.R. Chary, Indian J. Chem., **53A** (2014) 516-523.

22.   Y. Zhang, D. Yu, S. N. Riduan, and J. Y. Ying, AIChE Annual Meeting (conference), San Francesco, USA, November 1, 2012.

23.   Z. Gu, L. Luo and S. Shen, Indian J. Chem., **16** (2009) 175-180.

24.   G. Raju, B. M. Reddy and S.E. Park, Indian J. Chem., **51**, (2012) 1315-1324.

25.   K. N. Rao, B. M. Reddy, B. Abhishek, Y.H. Seo, N. Jiang and S.E. Park, Appl. Catal. B, **91** (2009) 649–656.

26.   N. E. McGuire, N. P. Sullivan, O. Deutschmann, H. Zhu and R. J. Kee, Appl. Catal. A, **394** (2011) 257–265.

27.   M. Hartmann, L. Maier, H.D. Minh and O. Deutschmann, Combust Flame, **157** (2010) 1771–1782.

CHAPTER 5

OVERALL CONCLUSIONS AND FUTURE WORK

5.1 Conclusions

In this work, the total of eight co-precipitation and impregnation methods were used to synthesise binary Zr/Ti oxide catalysts for CO_2 utilisation and reaction. The catalysts were shown to exhibit similar levels of surface acidity and relatively low surface areas. However, the catalysts prepared by the impregnation methods showed significantly higher pore volumes in the mesopore range and easily reduced as revealed through H_2-TPR than the catalysts prepared by the co-precipitation method. The overall conclusions of this research relative to the objectives stated in chapter 1 are as follows.

5.1.1 Dehydrogenation of propane by CO_2

The first study in this thesis was of propane dehydrogenation to propene using CO_2 over Zr/Ti oxide catalysts. The propane dehydrogenation is thermodynamically limited and the study emphasized the role of a radical mechanism on the catalyst surface which, presumably, involves surface concentrations high enough to compensate for the unfavourable equilibrium constants controlling the reaction. The results showed that with high CO_2 to propane ratios (5:1 and 15:1) propene yields and reaction selectivities comparable to those achieved with the industrial chromium based catalyst were possible. The results clearly demonstrate the role of the Zr/Ti oxide catalysts in promoting C-H bond dissociation and loss of H_2, so that hydrogen atoms are formed on the catalyst surface, and the essential role of CO_2 in removing hydrogen from the catalyst surface by the reverse water gas shift reaction. It is clear that these mixed metal oxide catalysts are selective to C-H bond dissociation over C-C bond dissociation, witnessed by the selectivity exhibited to propene formation over ethene.

Although most of the work has been based on binary Zr/Ti oxide catalysts, parts of the study are based on other metal oxides. However, the most active catalysts examined in this work were found to be the Zr/Ti oxides, and the composition of the most active was that labelled as 5%, where this refers to the mass/mass % of Zr based on total metal content. Third metal oxides were added to this base mixture, using a wide range of potentially catalytic metals at relatively low % compositions, but they all showed lower

activities than the binary mixture. Other binary mixtures were prepared based on titania. These binary oxides showed lower activities than 5% Zr/Ti oxide catalyst. All these catalysts showed both lower conversions of propane than 5% Zr/Ti oxide and lower selectivities to propene over ethene.

The 5% Zr/Ti oxide catalyst prepared by one of the impregnation methods in particular was the most active of all catalysts, although it was not possible to identify any physical or structural properties of the catalyst that could be directly linked with its higher activity. It is possible that the surface acidity of the catalyst is a requirement for the activity, simply on the basis that acidic sites on solid surfaces are quite likely to activate reactant molecules. However, it is difficult to say precisely how such sites might be involved in the reaction mechanism, since the catalytic mechanism is thought to involve surface species formation on the catalyst surface.

It is worth noting that this 5% Zr/Ti oxide catalyst also showed superior stability in use and permitted higher space velocities than are generally accepted as available from the commercial catalysts based on chromium for propene dehydrogenation. Studies of coke removal in this thesis show that gasification of coke held in the catalyst by reaction with CO_2 is facile over 5% Zr/Ti oxide, and this may account for the high stability of this catalyst.

5.1.2 Direct reaction of CO_2 with methane, ethane, ethene, acetylene and propane

Catalysts for the reaction of CO_2 with small alkanes to produce acetic acid were studied. Reaction with methane yielded acetic acid in low yield, increasing with increasing CO_2 concentration, plus ethane and ethene. The most active catalysts were again 5% Zr/Ti oxide mixtures and there was some correlation amongst these catalysts (made by the various routes) between activity towards acetic acid formation and volume in mesopores. The presence of C_2 products clearly points to radical mechanisms on the catalyst surface. It is significant that some C_2 products were detected from methane even in the absence of CO_2. This strongly suggests that methane undergoes C-H bond

scission on the surface of Zr/Ti oxide catalysts. All the other catalysts studied, including those containing three metal oxides, gave lower acetic acid yields, in line with the results for propane dehydrogenation above.

Reaction of CO_2 with ethane and propane over 5% Zr/Ti oxide catalysts was expected to yield propanoic acid and butanoic acid but, instead, gave acetic acid as the major insertion reaction product in both cases. A small amount of propanoic acid was seen from the propane reaction (but no butanoic acid).   Interestingly, lower reaction temperatures were needed than with methane – despite the apparent fact that these reactions involved C-C as well as C-H bond dissociation.

Unsaturated compounds, ethylene and acetylene, were also studied for direct reaction with CO_2 over the same catalyst.   In these cases, propiolic acid ($CH{\equiv}C\text{-}COOH$) was formed (alongside some acetic acid), again suggesting that alkene C-H bond dissociation occurs on the catalyst surface prior to reaction with CO_2.

A striking observation was that, in all experiments with the catalysts made in this thesis, acetic acid formation under flow conditions persisted for a relatively short time. In all cases, as acetic acid yield fell, the yield of other products rose. It appears that the reverse water gas shift reaction becomes more important as acetic acid yield falls, consuming the hydrogen that presumably is adsorbed on the catalyst surface.

5.2 Future work

This work has shown that CO_2 can be usefully used in dehydrogenation reactions and in direct insertion reactions, over mixed oxide catalysts based on zirconia and titania. There are subtle dependences of activity and selectivity on the nature of the catalysts and on the way in which the catalysts are prepared. However, the catalyst characterisation work described in this thesis has not offered a complete explanation of the reasons for the observed activities and selectivities. Broad conclusions based on the acidities of the catalysts and the porosities of the catalysts, and even of the crystal sizes of the catalysts, have been suggested but these are very speculative. The key further work needed is thorough catalyst characterisation to identify the physical and structural features of the catalyst that are responsible for the catalytic performance. Only with this information will new strategies be possible to design catalysts that may have activities of practical use.

Detailed surface techniques such as X-ray photoelectron spectroscopy (XPS) could usefully be used to investigate the nature of metal species on the surface of the catalysts, both before and after reaction. Adsorption isotherms could usefully be measured for reactants and products in the reactions of interest, to shed light on reaction mechanisms. Surface Raman and infrared spectroscopies could be used to study surface species on the catalyst on exposure to reactants. Other high vacuum techniques could be used for similar experiments. Electron spin resonance spectroscopy would be used to identify and stable surface species formed. Basicity as well as acidity could be assessed by suitable experiments.

Further work is needed to explore in-depth the CO_2 dehydrogenation of propane through Zr/Ti oxide catalyst. Observations that require further investigation include the way propene selectivity and propane conversion depend on the CO_2/propane ratio. The following approach is suggested for further work.

- Study the methods of catalyst preparation of Zr/Ti oxide aiming to increase the conversion of propane to exceed the commercial catalyst but at the same

time maintaining high propene selectivity. The objective should be to maintain this catalyst performance as the CO_2/propane ratio is lowered.

- It would be useful to examine the scaling up the catalytic reaction in order to determine in-depth the dependence of catalyst performance on the space velocity, reaction temperature and time on-stream. Catalyst regeneration should also be studied.

Future work to study the insertion of CO_2 to hydrocarbons based on Zr/Ti oxides may involve the following:

It would be of interest to study the effect of the reactant gas pressures on the direct reaction of CO_2, in the hope that this may influence yield and possibly selectivities, and so provide information on the reaction mechanisms. Varying the CO_2 to hydrocarbon ratios might also be informative. It would be useful to examine liquid hydrocarbons (pentane, hexane or heptane) to generate surface species for direct reaction of CO_2.

Further work is needed to improve the reaction stability and catalyst reusability. One approach might be to incorporate rare earth or noble metals in the Zr/Ti oxide catalysts to assist the catalysts stability.

Appendix 1

Additional Results for Chapter-2

Table A1. Example of calculating 5% Zr/Ti oxide

Chemical	Weight of salt	g of Zr (FW 91)
$ZrO(NO_3)_2.6H_2O$ (FW 339)	0.5 g	0.134 g
Chemical	Weight of salt	g of Ti (FW 48)
TiO_2 (support) (FW 80)	5.0 g	3.00 g
Zr: Ti ratio	0.045 : 1	

Table A2. Example of calculating 2% Al 5% Zr/Ti oxide

Chemical	Weight of salt	g of Al (FW 27)
$Al(NO_3)_3. 9H_2O$ (FW 375)	0.5 g	0.036 g
Chemical	Weight of salt	g of Zr (FW 91)
$ZrO(NO_3)_2.6H_2O$ (FW 339)	0.3 g	0.0804 g
Chemical	Weight of salt	g of Ti (FW 48)
TiO_2 (support) (FW 80)	3.0 g	1.80 g
Al : Zr: Ti ratio	0.02 : 0.045 : 1	

Appendix 1

Table A3. Tetragonal zirconium oxide of Powder Diffraction Files (ICDD[1]) 01-080-2155, (Fixed Slit Intensity Cu K1, 1.54056Å).

2θ	d(Å)	Intensity	Miller indices		
			h	k	l
30.2692	2.95028	999	1	0	1
34.9588	2.5645	87	0	0	2
35.1595	2.55032	134	1	1	0
43.2524	2.09003	3	1	0	2
50.4229	1.80834	303	1	1	2
50.5722	1.80335	313	2	0	0
53.8431	1.70126	1	2	0	1
59.8147	1.54489	106	1	0	3
60.0813	1.53867	207	2	1	1
62.9564	1.47514	50	2	0	2
68.6878	1.36536	1	2	1	2
73.8437	1.28225	14	0	0	4
74.3232	1.27516	35	2	2	0
79.2201	1.20817	1	1	0	4
82.0732	1.17324	63	2	1	3
82.306	1.17051	62	3	0	1
84.5022	1.1456	22	1	1	4
84.8491	1.1418	22	2	2	2
84.9649	1.14054	19	3	1	0
90.0832	1.08855	1	3	0	2
94.9704	1.04501	25	2	0	4
95.3176	1.04212	63	3	1	2
100.2451	1.00373	1	2	1	4
102.6471	0.986669	17	1	0	5
103.1201	0.983428	19	3	0	3
103.3569	0.98182	34	3	2	1
111.4903	0.931931	1	3	2	2
116.8419	0.904171	16	2	2	4
117.3599	0.901675	15	4	0	0
122.8712	0.877032	1	3	0	4
125.721	0.865582	24	2	1	5
126.291	0.863391	37	3	2	3
126.5775	0.862302	26	4	1	1
128.603	0.854833	3	0	0	6
129.3442	0.852198	20	3	1	4
129.793	0.850628	11	4	0	2
129.9431	0.850107	15	3	3	0
135.6548	0.83179	1	1	0	6
136.9903	0.827914	1	4	1	2
143.7426	0.810514	13	1	1	6
145.3317	0.806928	19	3	3	2
145.5348	0.806483	19	4	2	0

---

[1] International Centre for Diffraction Data

Appendix 1

Table A4. Monoclinic zirconium oxide of Powder Diffraction Files (ICDD) 00-007-0343, (Fixed Slit Intensity Cu K1, 1.54056Å)

2θ	d(Å)	Intensity	Miller indices		
			h	k	l
17.5472	5.05	5	1	0	0
24.098	3.69	15	0	1	1
24.5024	3.63	12	1	1	0
28.2171	3.16	100	1	1	1
31.4744	2.84	65	-1	1	1
34.1952	2.62	20	0	0	2
34.4664	2.6	12	0	2	0
35.307	2.54	15	2	0	0
35.891	2.5	3	1	0	2
38.6095	2.33	5	0	2	1
40.7964	2.21	10	2	1	1
41.1858	2.19	5	-1	0	2
41.3834	2.18	5	1	2	1
44.8318	2.02	7	-1	1	2
45.5453	1.99	7	2	0	2
49.3247	1.846	15	0	2	2
50.1659	1.817	20	2	2	0
50.6127	1.802	12	1	2	2
51.2525	1.781	5	2	2	1
54.1272	1.693	10	-2	0	2
55.4756	1.655	12	0	1	3
55.9532	1.642	7	1	3	0
57.2053	1.609	5	3	1	0
57.9134	1.591	5	1	3	1
58.3148	1.581	5	2	2	2
59.9382	1.542	10	-1	3	1
61.4337	1.508	5	-1	1	3
62.0267	1.495	5	2	1	3
62.8681	1.477	10	-3	1	1
64.2265	1.449	3	0	2	3
65.7013	1.42	7	-2	2	2
68.9967	1.36	2	-1	3	2
71.2761	1.322	5	1	0	4
75.2317	1.262	5	0	4	1
76.3699	1.246	2	4	1	1
78.843	1.213	2	-1	4	1

Appendix 1

Table A5. Anatase Titanium dioxide of Powder Diffraction Files (ICDD) 01-071-1166, (Fixed Slit Intensity Cu K1, 1.54056Å).

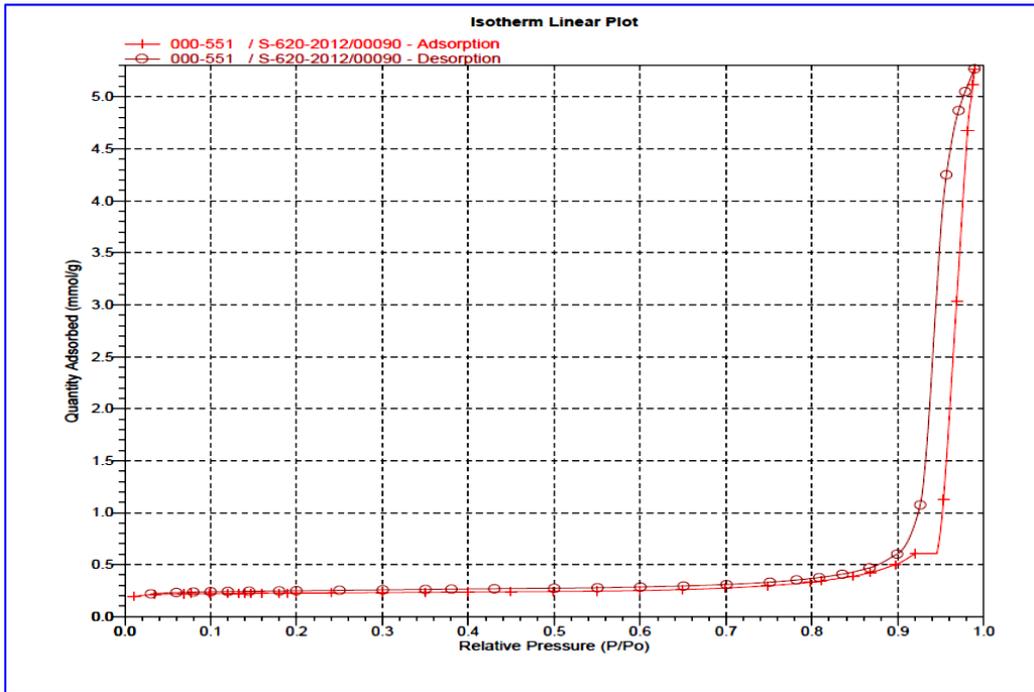| 2θ	d(Å)	Intensity	Miller indices		
			h	k	l
25.3077	3.51629	999	1	0	1
36.9502	2.43073	61	1	0	3
37.7895	2.37865	186	0	0	4
38.5712	2.33222	70	1	1	2
48.046	1.8921	242	2	0	0
53.8839	1.70007	150	1	0	5
55.0713	1.66619	148	2	1	1
62.1153	1.49308	26	2	1	3
62.6903	1.48076	110	2	0	4
68.7544	1.3642	47	1	1	6
70.3015	1.33792	51	2	2	0
74.0485	1.27921	5	1	0	7
75.051	1.26459	77	2	1	5
76.0488	1.25046	21	3	0	1
80.7306	1.18933	4	0	0	8
82.1702	1.1721	5	3	0	3
82.6845	1.16611	38	2	2	4
83.171	1.16052	16	3	1	2
93.2472	1.05974	5	2	1	7
94.2159	1.05138	17	3	0	5
95.1851	1.04322	20	3	2	1
98.3165	1.01819	13	1	0	9
99.8115	1.00692	8	2	0	8
101.2587	0.996406	6	3	2	3
107.4914	0.955208	24	3	1	6
109.0179	0.94605	13	4	0	0
112.8366	0.924597	2	3	0	7
113.8894	0.91903	23	3	2	5
114.9507	0.913563	14	4	1	1
118.4611	0.896474	38m	2	1	9
118.4611	0.896474	m	1	1	10
120.1233	0.888891	7	2	2	8
121.7832	0.881629	5	4	1	3
122.3844	0.879073	17	4	0	4
122.9585	0.876669	11	3	3	2
131.0965	0.846173	21	4	2	0
131.8819	0.843564	11	3	1	8
131.9876	0.843217	5	1	0	11
136.019	0.830718	4	3	2	7
137.4287	0.826674	20	4	1	5
142.9172	0.812451	1	4	0	6
143.8594	0.810244	9	3	0	9

Figure A1. Isotherm linear plot of adsorption and desorption of single oxide of ZrO_2
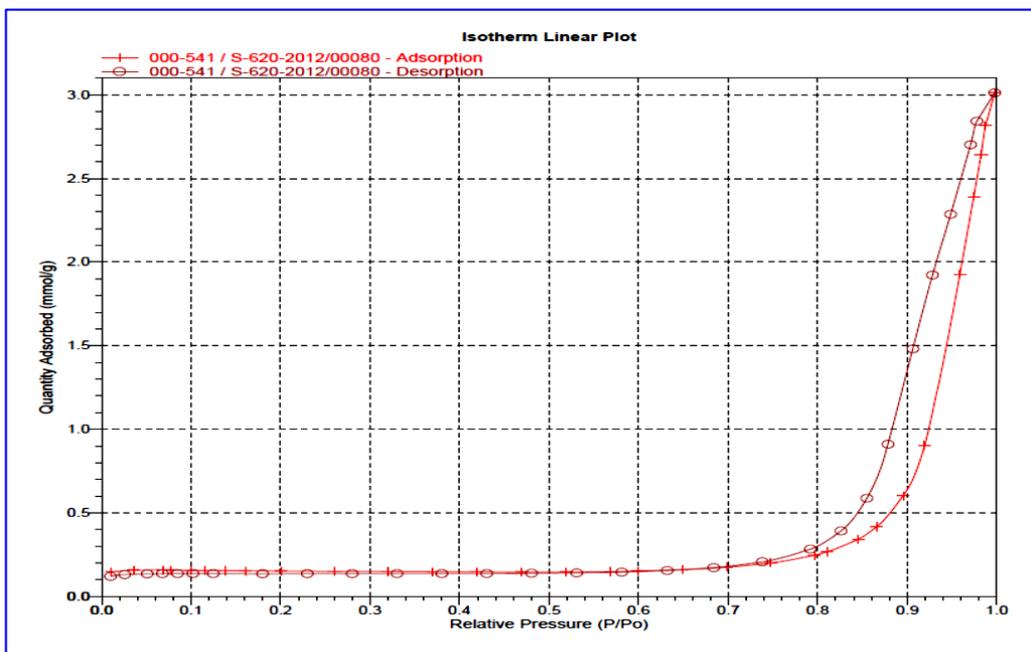

Figure A2. Isotherm linear plot of adsorption and desorption of single oxide of TiO_2
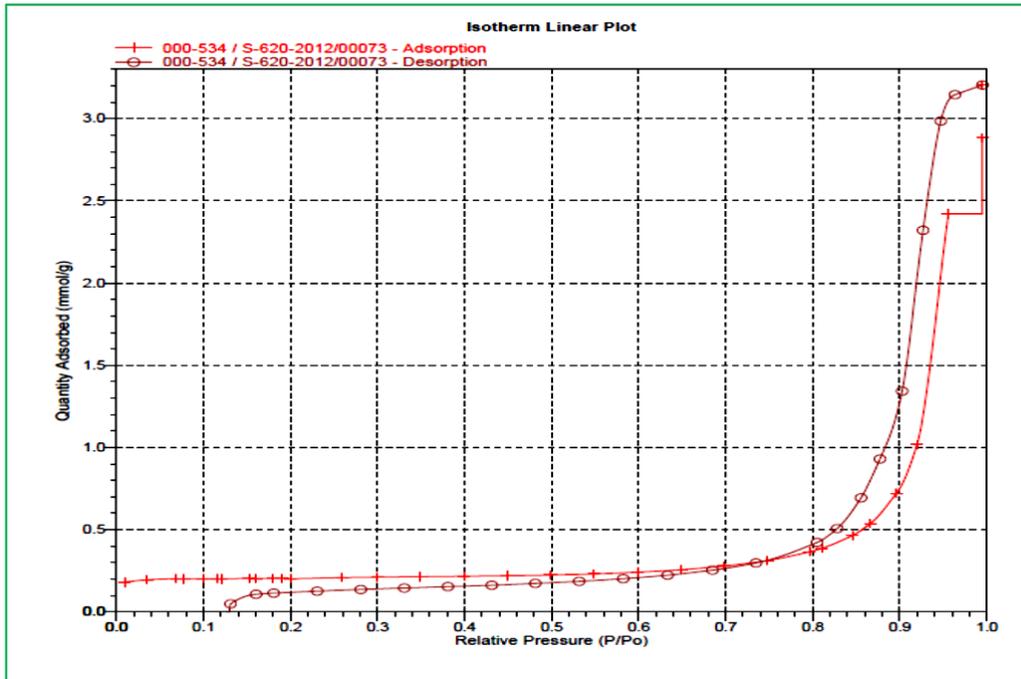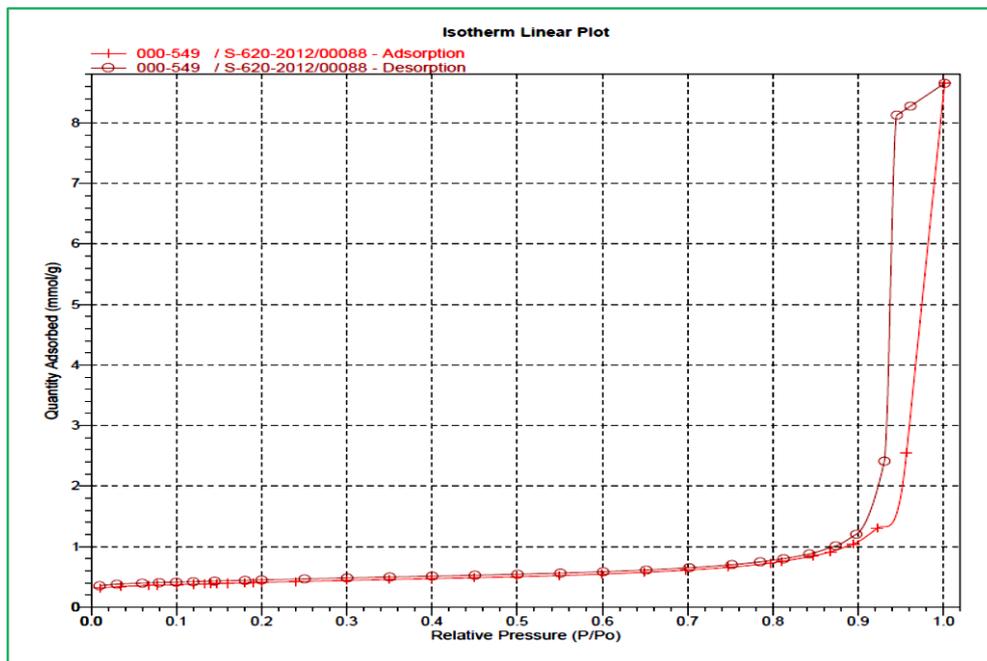
Figure A3. Isotherm linear plot of adsorption and desorption of 50% w/w each Zr-Ti co-precipitation method-1, (**chapter-4**)

Figure A4. Isotherm linear plot of adsorption and desorption of 50% w/w each Zr-Ti co-precipitation method-2, (**chapter-4**)
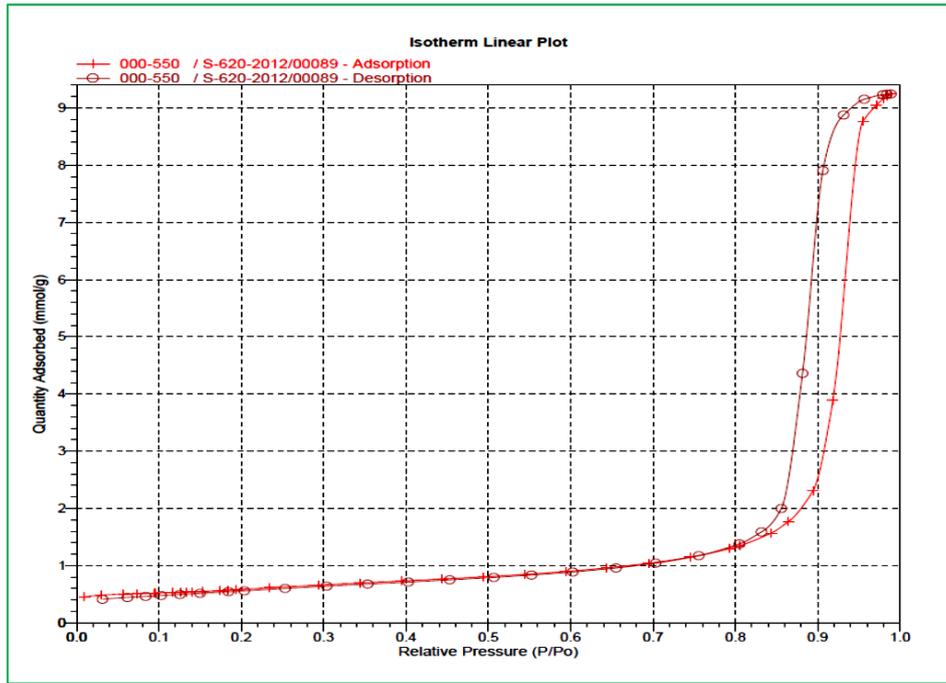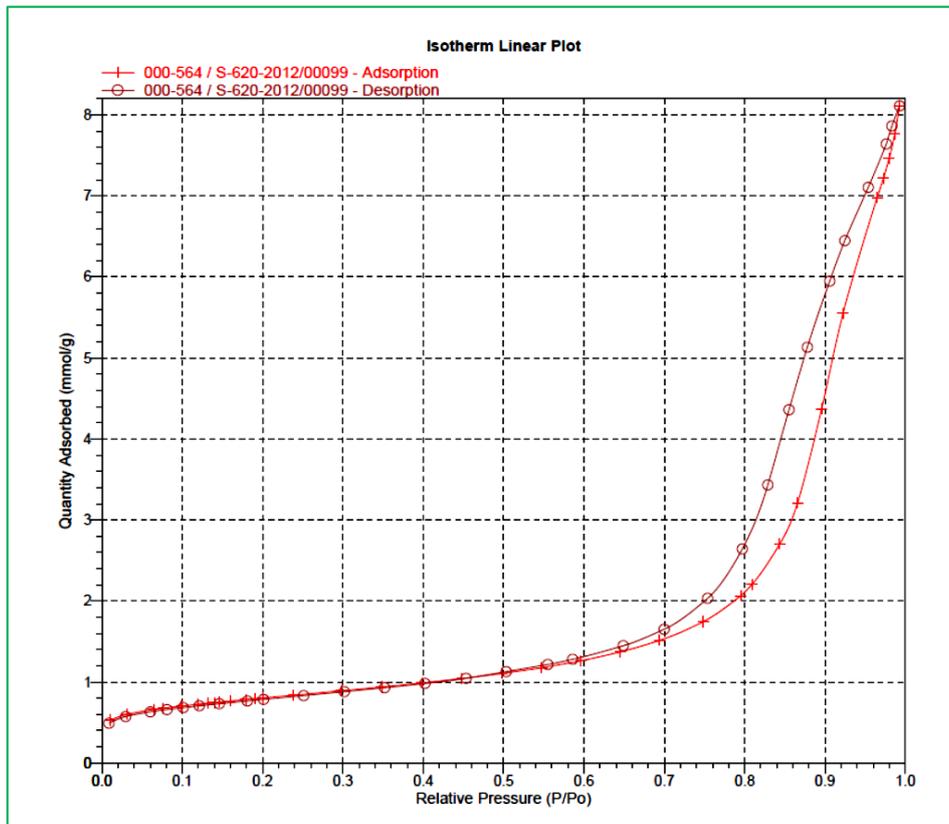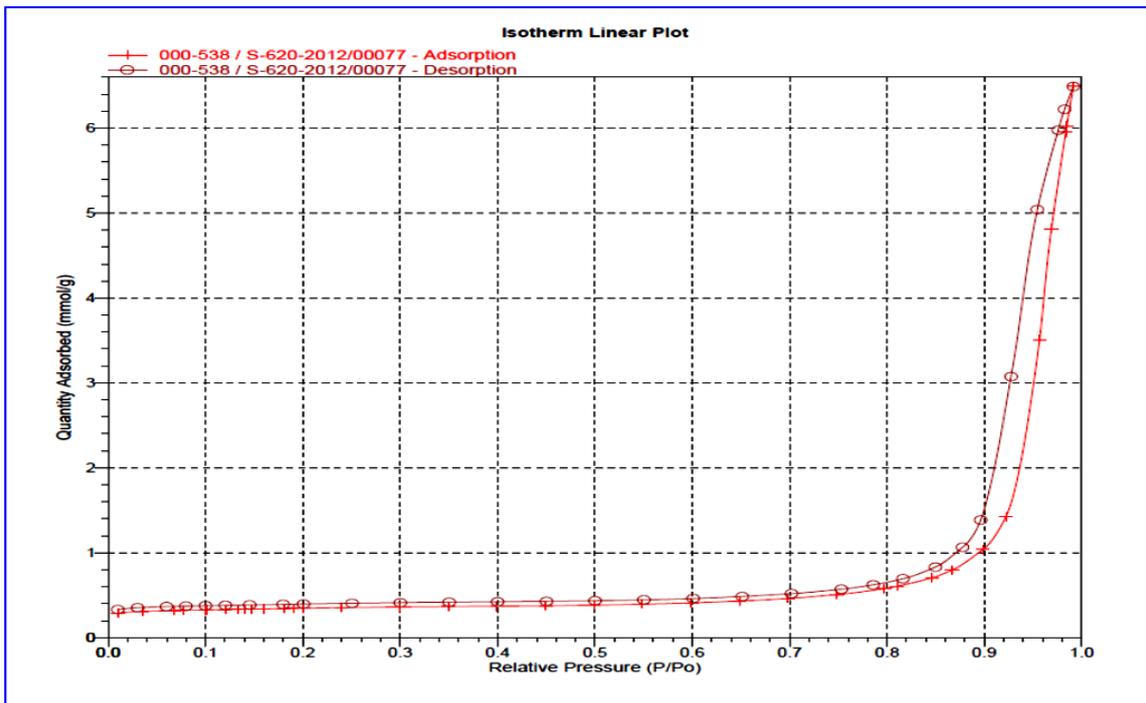
Figure A5. Isotherm linear plot of adsorption and desorption of 50% w/w each Zr-Ti co-precipitation method-3, (**chapter-4**)

Figure A6. Isotherm linear plot of adsorption and desorption of 50% w/w each Zr-Ti co-precipitation method-4, (**chapter-4**)

Figure A7. Isotherm linear plot of adsorption and desorption of impregnation method-2: 5% w/w Zr/Ti oxide   (**chapter-3** and **4**)
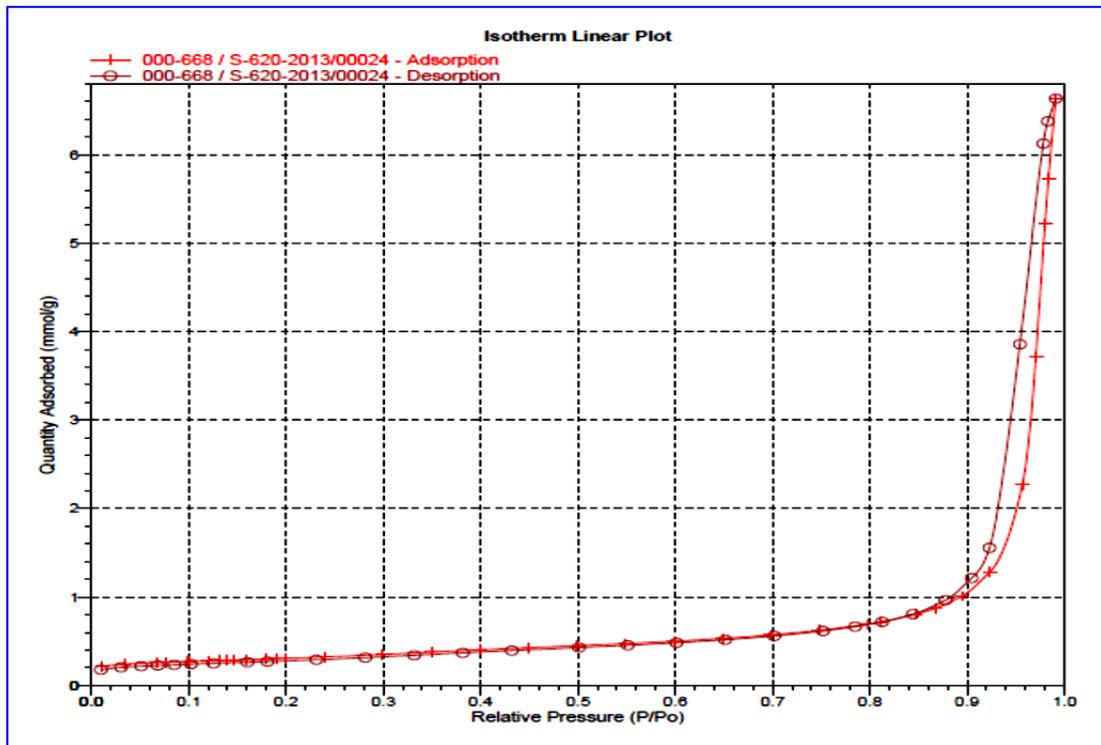

Figure A8. Isotherm linear plot of adsorption and desorption of impregnation method-3: 5% w/w Zr/Ti oxide (**chapter-4**)

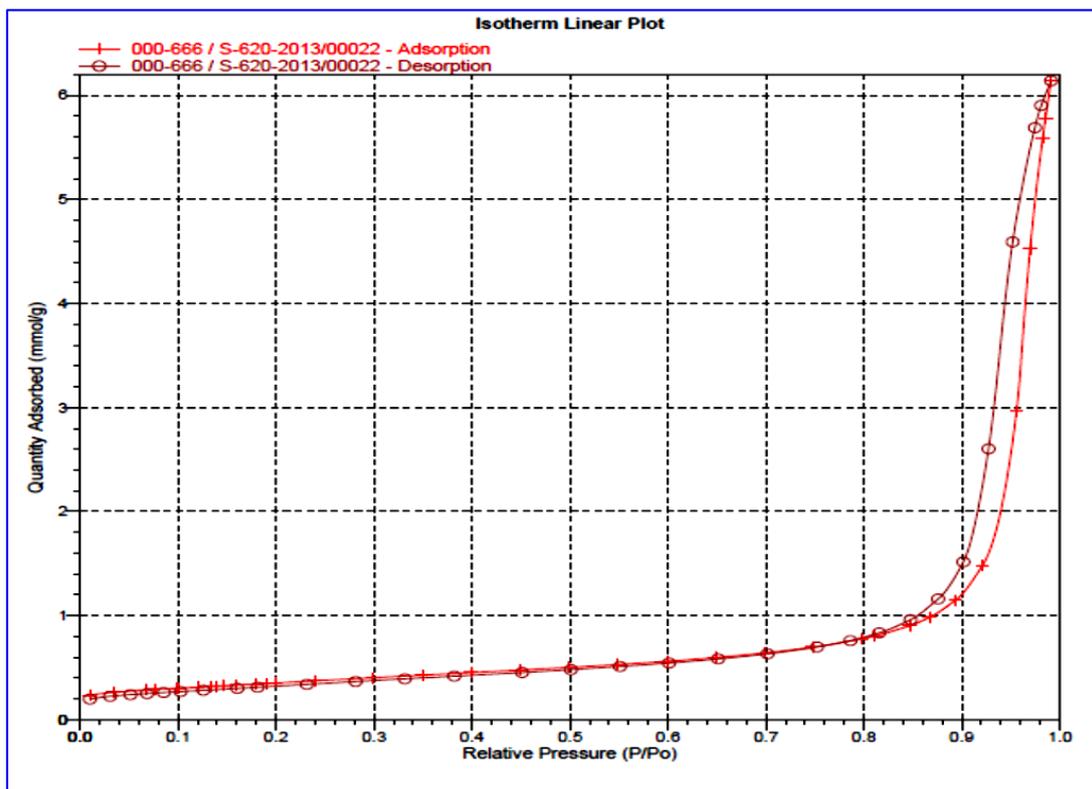Figure A9. Isotherm linear plot of adsorption and desorption of 10.5% w/w Tl/Ti oxide (**chapter-3**)

Figure A10. Isotherm linear plot of adsorption and desorption of 6. 9% w/w Nb/Ti oxide (**chapter-3**)
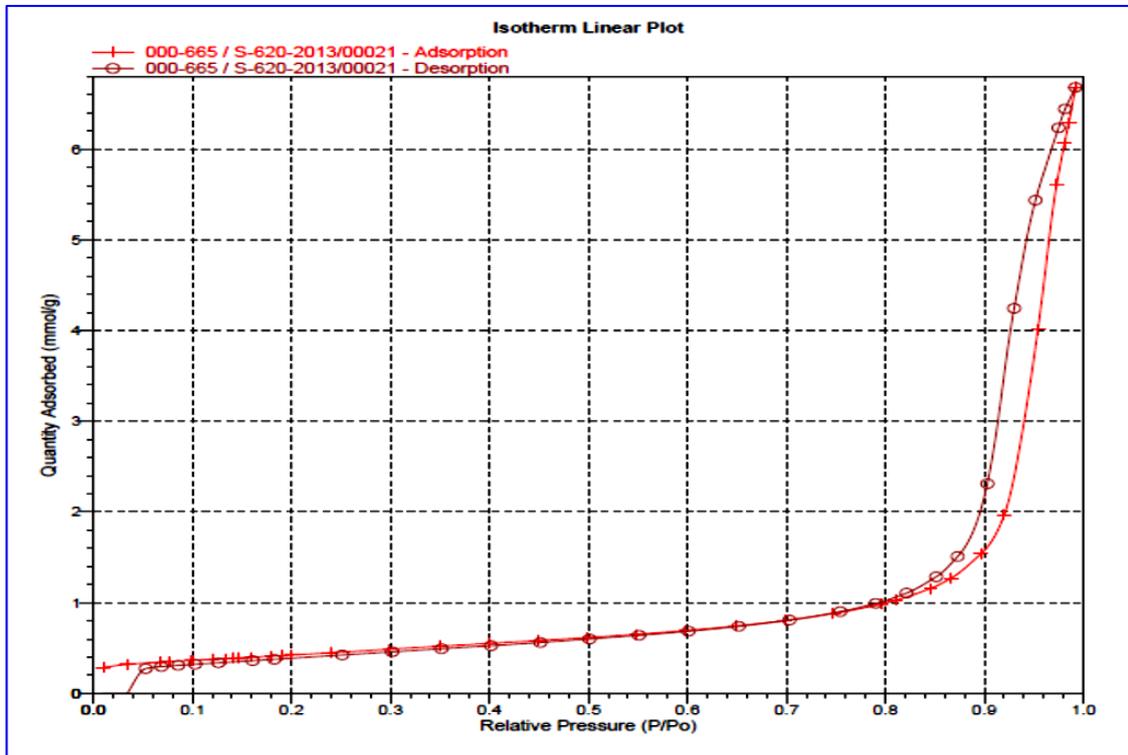

Figure A11. Isotherm linear plot of adsorption and desorption of 7. 9% w/w Hf/Ti oxide (**chapter-3**)
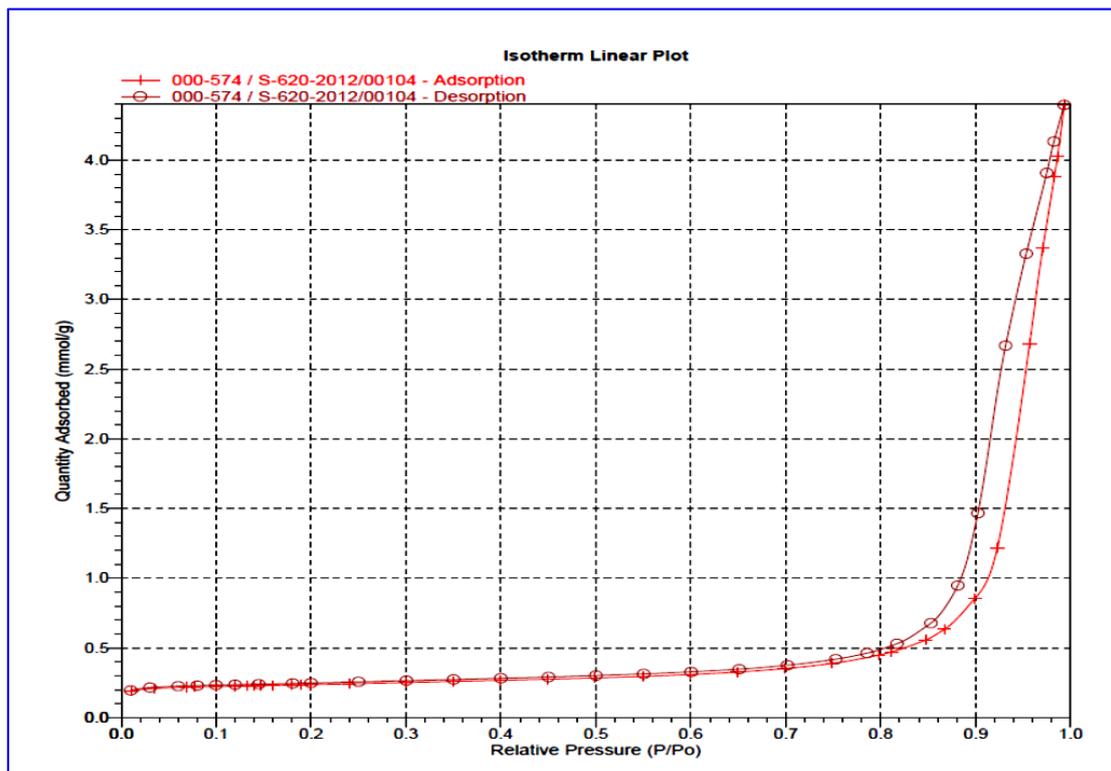
Figure A12. Isotherm linear plot of adsorption and desorption of 2% Pt impregnation on TiO$_2$ (**chapter-3**)
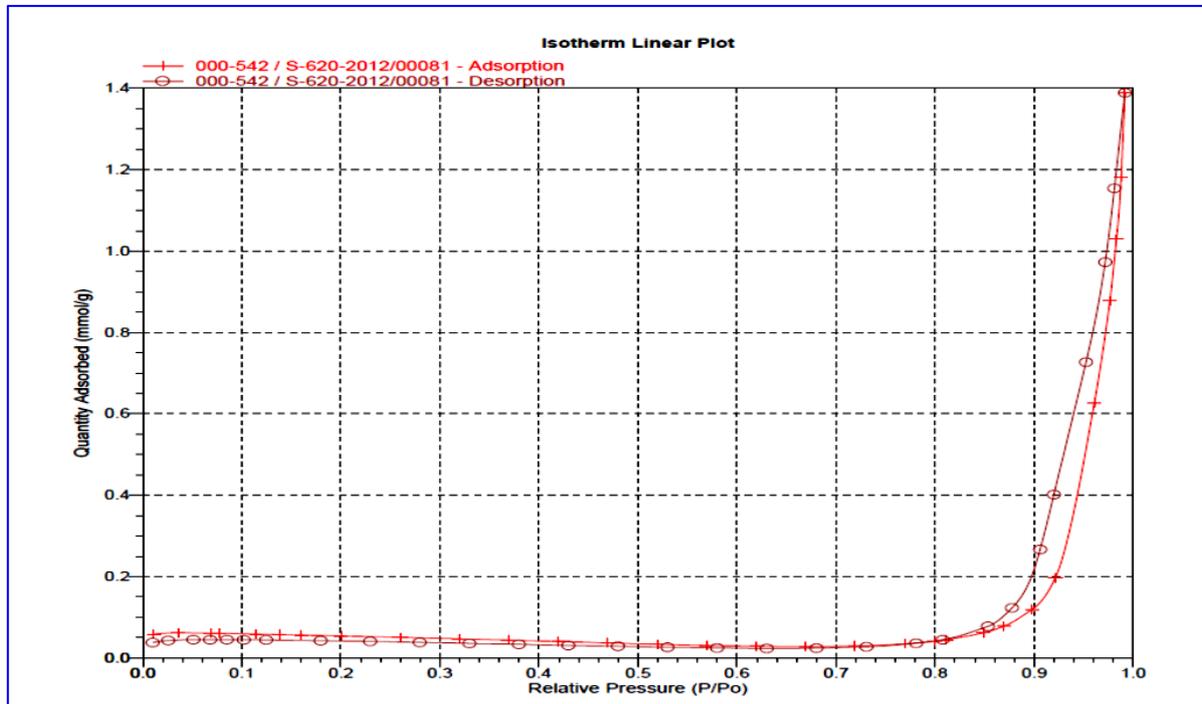

Figure A13. Isotherm linear plot of adsorption and desorption of 4% w/w Cu, 5% Zr/Ti oxide (**chapter-4**)
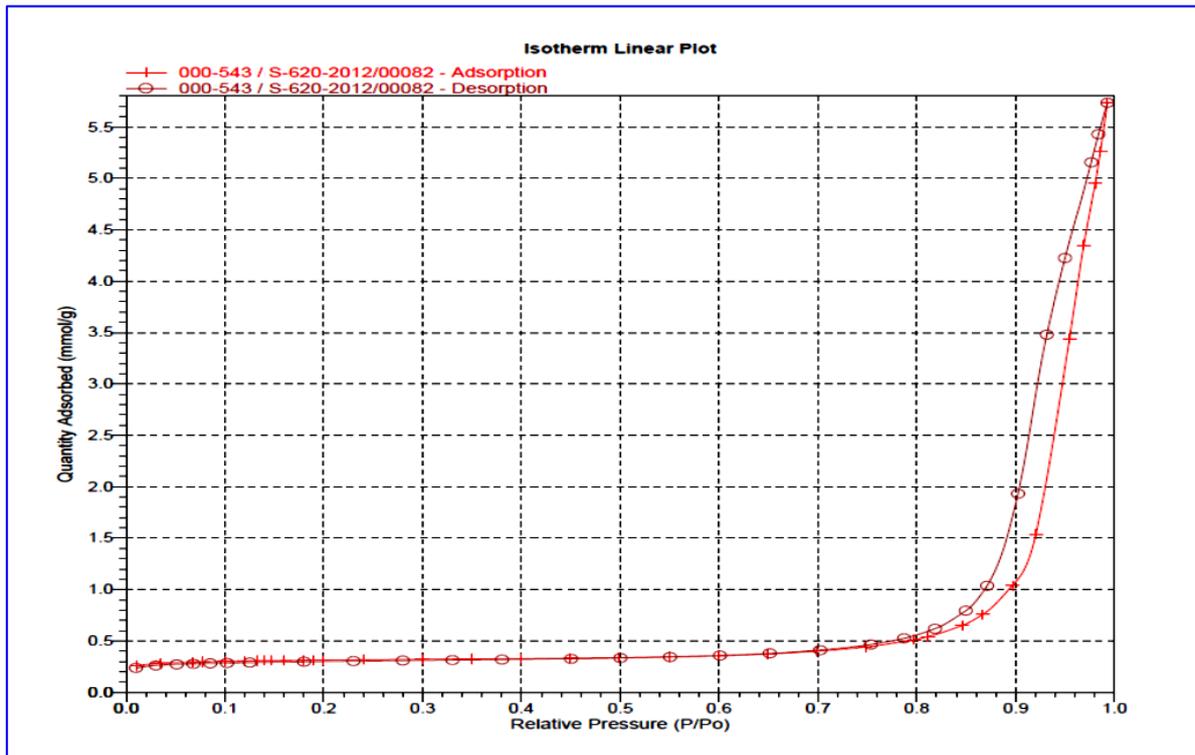
Figure A14. Isotherm linear plot of adsorption and desorption of 2% w/w Al, 5% Zr/Ti oxide (**chapter-4**)
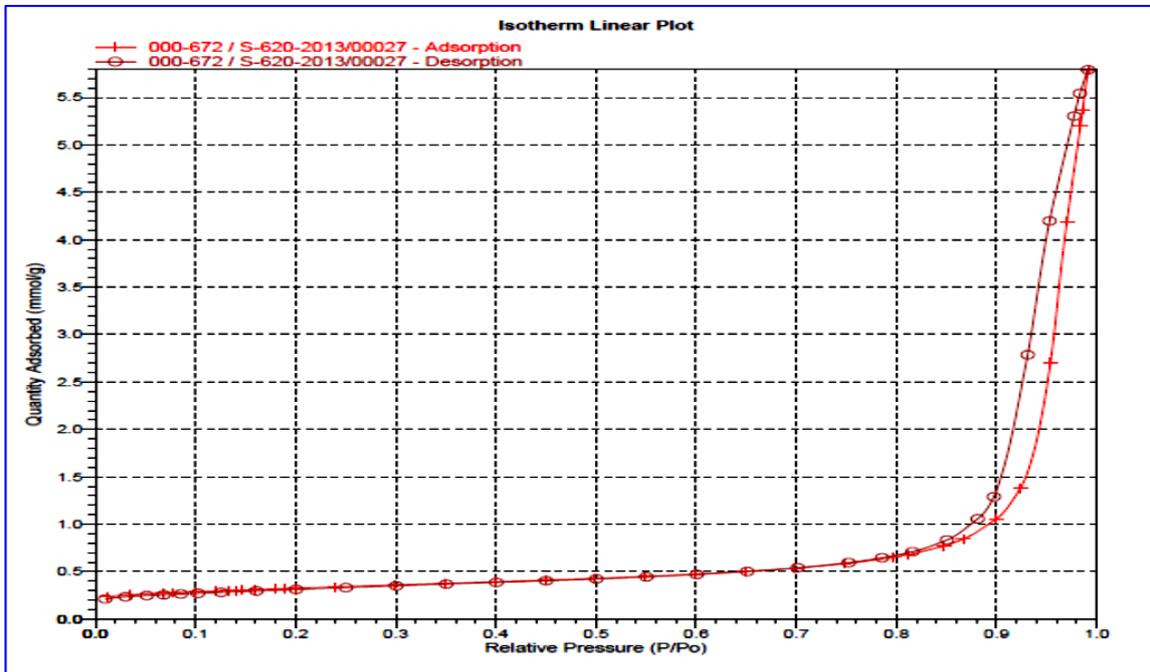

Figure A15. Isotherm linear plot of adsorption and desorption of 2% w/w Ba/5% Zr/Ti oxide (**chapter-3**)
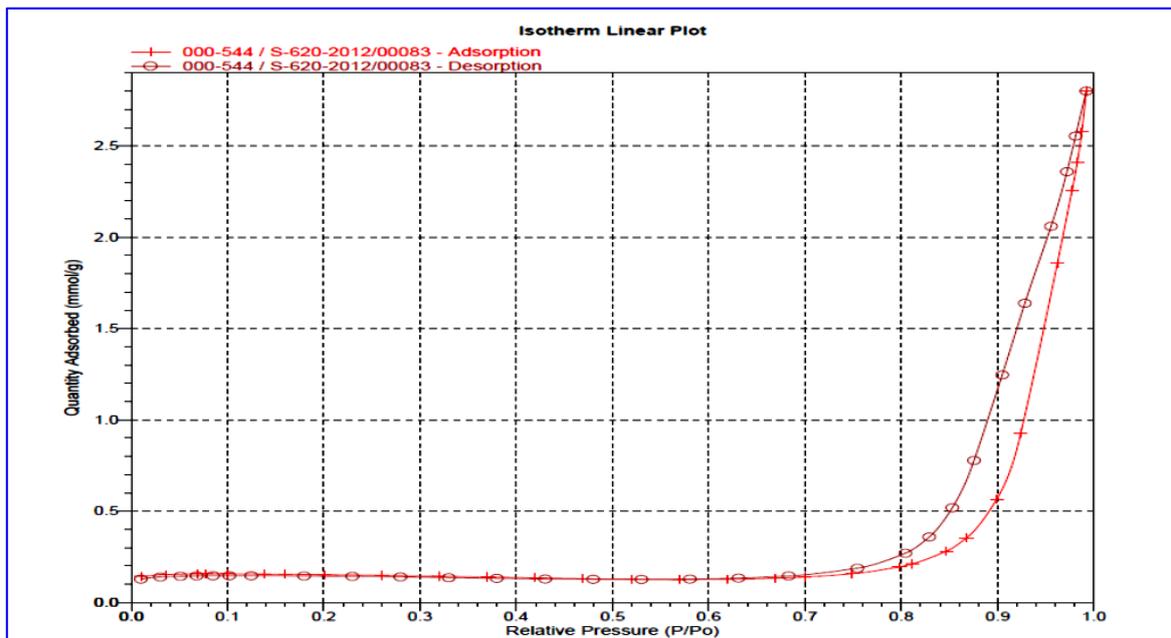

Figure A16. Isotherm linear plot of adsorption and desorption of 3.6% w/w Fe, 5% Zr/Ti oxide (**chapter-4**)
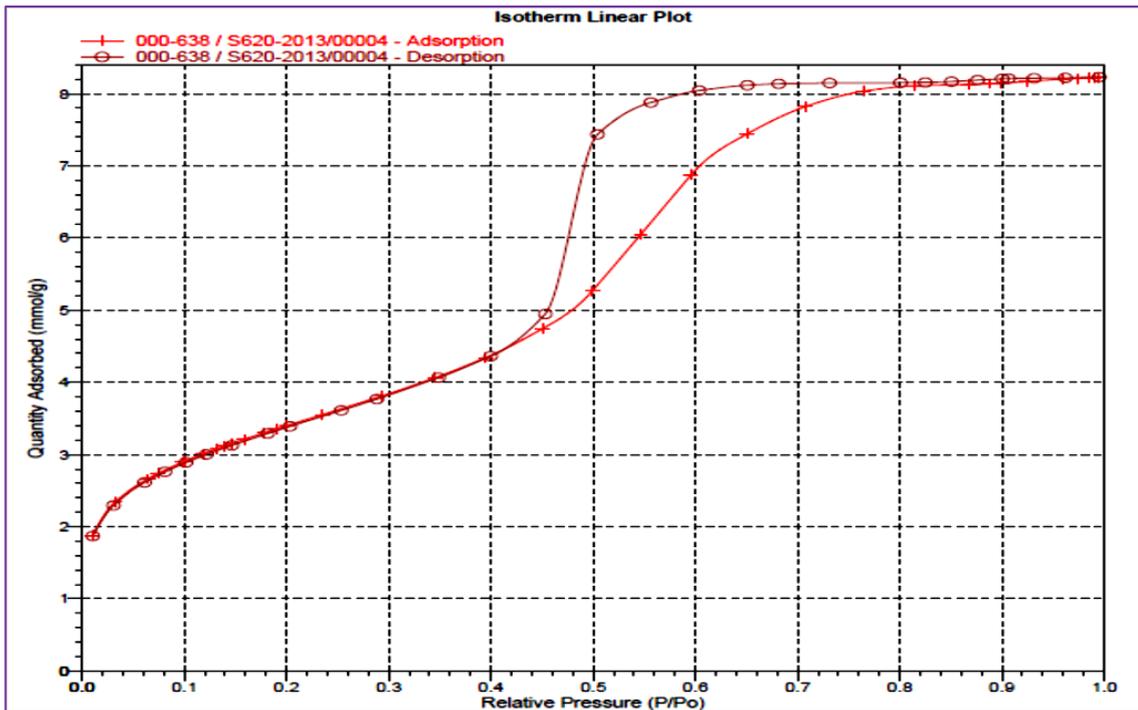
Figure A17. Isotherm linear plot of adsorption and desorption of 5.8% Cr/Si oxide
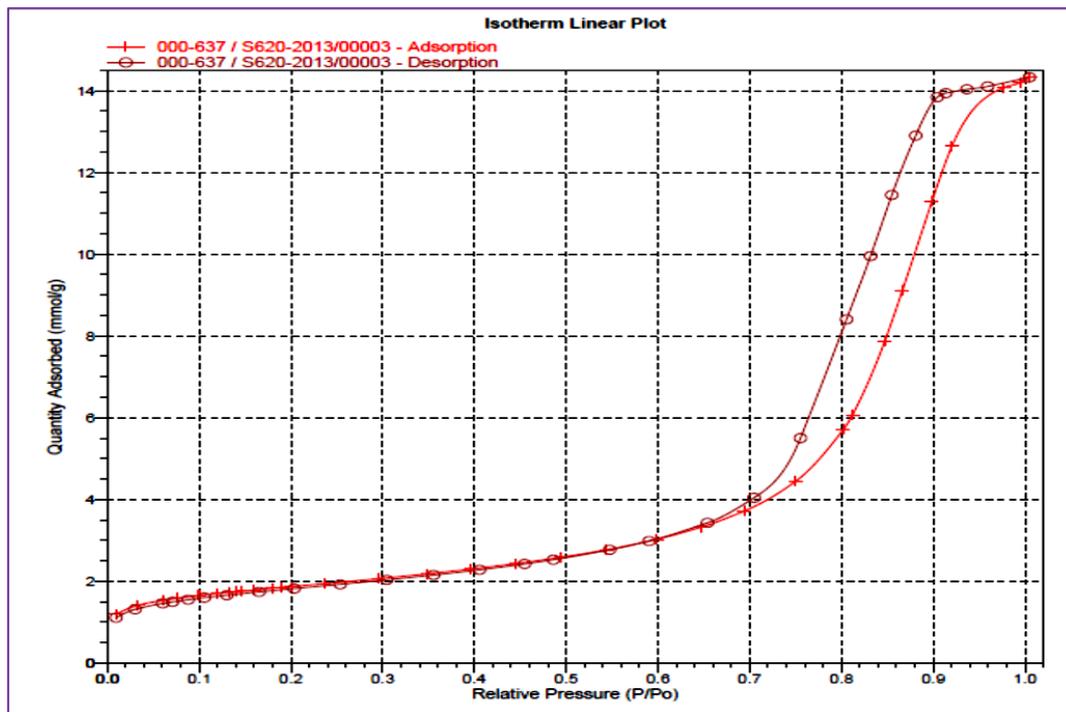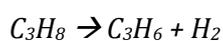(**chapter-3**)

Figure A18. Isotherm linear plot of adsorption and desorption of 5.1% Ga/Al oxide
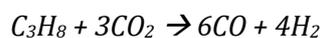(**chapter-3**)

Appendix 2

Additional Results for Chapter-3

Table B1. Thermodynamic *propane dehydrogenation by CO_2:*

$$C_3H_8 + CO_2 \rightarrow C_3H_6 + H_2O + CO$$

Temp. °C	Enthalpy ΔH, kJ	Entropy ΔS, $JK^{-1}mol^{-1}$	Free energy ΔG, kJ/mol	Equilibrium Constants (K)
300	127	169.1	70.65	3.53×10^{-7}
400	127	169.1	53.75	6.63×10^{-5}
500	127	169.1	36.83	0.003212
600	127	169.1	19.92	0.0638
700	127	169.1	3.01	0.689
800	127	169.1	-13.91	4.765

Table B2. Thermodynamic *propane dehydrogenation without CO_2:*

$$C_3H_8 \rightarrow C_3H_6 + H_2$$

Temp. °C	Enthalpy ΔH, kJ	Entropy ΔS, $JK^{-1}mol^{-1}$	Free energy ΔG, kJ/mol	Equilibrium Constants (K)
300	124.4	127.1	51.57	1.95×10^{-5}
400	124.4	127.1	38.86	0.00095
500	124.4	127.1	26.15	0.0169
600	124.4	127.1	13.44	0.1564
700	124.4	127.1	0.73	0.9133
800	124.4	127.1	-11.97	3.838

Table B3. Thermodynamic *dry reforming of propane:*

$$C_3H_8 + 3CO_2 \rightarrow 6CO + 4H_2$$

Temp. °C	Enthalpy ΔH, kJ	Entropy ΔS, $JK^{-1}mol^{-1}$	Free energy ΔG, kJ/mol	Equilibrium Constants (K)
300	628.1	797	171.4	2.25×10^{-16}
400	628.1	797	91.7	7.48×10^{-08}
500	628.1	797	12	0.16
600	628.1	797	-67.7	1.15×10^4
700	628.1	797	-147.5	8.49×10^7
800	628.1	797	-227.2	1.19×10^{11}

Appendix 2

Table B4. Thermodynamic *RWGS:*

$$CO_2 + H_2 \rightarrow H_2O + CO$$

Temp. °C	Enthalpy ΔH, kJ	Entropy ΔS, JK^{-1}mol^{-1}	Free energy ΔG, kJ/mol	Equilibrium Constants (K)
300	43.2	42	19.1	0.0118
400	43.2	42	14.9	0.069
500	43.2	42	10.7	0.19
600	43.2	42	6.5	0.41
700	43.2	42	2.27	0.75
800	43.2	42	-1.91	1.24

Table B5. Thermodynamic *WGS:*

$$CO + H_2O \rightarrow H_2 + CO_2$$

Temp. °C	Enthalpy ΔH, kJ	Entropy ΔS, JK^{-1}mol^{-1}	Free energy ΔG, kJ/mol	Equilibrium Constants (K)
300	-43.17	-42	-19	55.33
400	-43.17	-42	-14.9	14.36
500	-43.17	-42	-10.68	5.28
600	-43.17	-42	-6.47	2.44
700	-43.17	-42	-2.27	1.33
800	-43.17	-42	1.928	0.805

Table B6. Thermodynamic *propane cracking by H$_2$:*

$$C_3H_8 + H_2 \rightarrow C_2H_6 + CH_4$$

Temp. °C	Enthalpy ΔH, kJ	Entropy ΔS, JK^{-1}mol^{-1}	Free energy ΔG, kJ/mol	Equilibrium Constants (K)
300	-53.9	14.5	-62.2	4.81E+05
400	-53.9	14.5	-63.7	8.94E+04
500	-53.9	14.5	-65.1	2.56E+04
600	-53.9	14.5	-66.6	9.80E+04
700	-53.9	14.5	-68	4.57E+04
800	-53.9	14.5	-69.5	2.45E+04

Appendix 2

Table B7. Thermodyamic *dry reforming of ethane:*

$$C_2H_6 + 2CO_2 \rightarrow 4CO + 3H_2$$

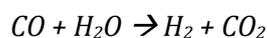| Temp. °C	Enthalpy ΔH, kJ	Entropy ΔS, J/K	Free energy ΔG, kJ/mol	Equilibrium Constants (K)
300	432.9	525.9	131.5	9.75×10^{-11}
400	432.9	525.9	78.9	7.29×10^{-7}
500	432.9	525.9	26.3	0.02
600	432.9	525.9	-26.3	37.45
700	432.9	525.9	-78.8	1.74×10^4
800	432.9	525.9	-131.4	2.57×10^8

Table B8. Thermodyamic *dry reforming of methane:*

$$CH_4 + CO_2 \rightarrow 2CO + 2H_2$$

Temp. °C	Enthalpy ΔH, kJ	Entropy ΔS, J/K	Free energy ΔG, kJ/mol	Equilibrium Constants (K)
300	249	256.5	102	4.79×10^{-10}
400	249	256.5	76.4	1.15×10^{-6}
500	249	256.5	50.7	3.67×10^{-3}
600	249	256.5	25.1	0.03
700	249	256.5	-0.5	1.07
800	249	256.5	-26.2	18.90

Table B9. Single oxide of TiO_2: Gas concentrations produced from propane dehydrogenation by CO_2 (CO_2/propane ratio: 16.9:1, 600 ^oC)

Time hours	H_2 mol%	CO mol%	methane mol%	CO_2 mol%	ethene mol%	ethane mol%	propene mol%	propane mol%
C_o				94.7				5.6
0	4.58	26.54	3.31	68.87	0.20	0.18	0.19	0.47
9	4.51	24.47	3.03	64.45	0.17	0.17	0.19	0.42
10	4.56	25.54	3.19	67.93	0.22	0.18	0.20	0.43

Table B10. Single oxide of TiO_2: Conversion, selectivity and yield from dehydrogenation of propane by CO_2 (CO_2/propane ratio: 16.9:1, 600 ^oC)

Reaction Time (h)	Propene Selectivity (%)	Ethene Selectivity (%)	Propane Conversion (%)	Propene Yield (%)	Ethene Yield (%)	Total olefins Yield (%)	CO Yield %	CO_2 Conversion (%)
0	3.6	3.9	91.6	3.3	3.6	6.9	28.0	27.3
9	3.7	3.4	92.4	3.4	3.1	6.5	25.8	31.9
10	4.0	4.2	92.3	3.6	3.9	7.5	27.0	28.3

Table B11. Single oxide of ZrO_2: Gas concentrations produced from the CO_2 dehydrogenation of propane (CO_2/propane ratio: 20.9:1, 600 ^oC)

Time hours	H_2 mol%	CO mol%	methane mol%	CO_2 mol%	ethene mol%	ethane mol%	propene mol%	propane mol%
C_o				96.2				4.6
0	1.05	13.03	3.82	82.29	0.08	0.08	0.12	1.65
2	1.13	13.51	3.63	82.05	0.08	0.07	0.12	1.68
3	1.33	13.57	3.49	82.11	0.08	0.07	0.13	1.69

Table B12. Single oxide of ZrO_2: Conversion, selectivity and yield from dehydrogenation of propane by CO_2 (CO_2/propane ratio: 20.9:1, 600 ^oC)

Reaction Time (h)	Propene Selectivity (%)	Ethene Selectivity (%)	Propane Conversion (%)	Propene Yield (%)	Ethene Yield (%)	Total olefins Yield (%)	CO Yield %	CO_2 Conversion (%)
0	4.2	2.7	64.2	2.7	1.7	4.4	93.6	13.5
2	4.0	2.8	63.4	2.6	1.8	4.4	95.5	14.0
3	4.5	2.8	63.3	2.8	1.8	4.6	96.3	14.1

Appendix 2

Table B13. Without catalysts: Gas concentrations produced from the CO_2 dehydrogenation of propane (CO_2/propane ratio: 20.4:1, 600 °C)

Time hours	H_2 mol%	CO mol%	methane mol%	CO_2 mol%	ethene mol%	ethane mol%	propene mol%	propane mol%
C_o				93.7				4.6
0	0.07	0.72	0.21	91.71	0.23	0.12	0.42	3.60
1	0.08	0.76	0.22	91.46	0.25	0.11	0.46	3.63
2	0.07	0.75	0.21	91.58	0.24	0.12	0.42	3.66
4	0.09	0.76	0.21	92.98	0.25	0.11	0.46	3.64

Table B14. Without catalysts: Conversion, selectivity and yield from dehydrogenation of propane by CO_2 (CO_2/propane ratio: 20.4 :1, 600 °C)

Reaction Time (h)	Propene Selectivity (%)	Ethene Selectivity (%)	Propane Conversion (%)	Propene Yield (%)	Ethene Yield (%)	Total olefins Yield (%)	CO Yield %	CO_2 Conversion (%)
0	42.0	23.0	21.7	9.1	5.0	14.1	0.8	2.1
1	47.4	25.8	21.1	10.0	5.4	15.4	0.8	2.4
2	44.7	25.5	20.4	9.1	5.2	14.3	0.8	2.3
4	47.9	26.0	20.9	10.0	5.4	15.4	0.8	0.8

Appendix 2

Table B15. 5% ZrO_2/TiO_2: Gas concentrations produced from propane
dehydrogenation without CO_2 at 600 °C gas space velocity of 9.6 h^{-1}

Time hours	H2 mol%	CO mol%	methane mol%	ethene mol%	CO2 mol%	ethane mol%	propene mol%	propane mol%
C_o					0			98.0
0	16.04	0.18	21.89	6.67	0.02	7.80	14.95	36.33
14	17.88	0.12	22.60	6.78	0.02	8.10	14.75	37.13
38	15.52	0.10	23.32	7.07	0.00	8.21	14.52	38.04
44	14.90	0.07	23.24	7.11	0.00	8.16	14.41	38.30
50	14.62	0.09	23.32	7.25	0.00	8.14	14.42	38.49
56	14.49	0.12	23.18	7.21	0.00	8.06	14.20	38.59
62	14.69	0.09	23.42	7.29	0.00	8.13	14.74	38.18
68	15.31	0.03	23.39	7.40	0.00	8.18	14.42	38.66
74	13.95	0.09	23.15	7.37	0.00	8.01	14.40	39.12
80	14.01	0.08	23.09	7.35	0.00	7.97	14.45	38.86
86	13.43	0.11	22.83	7.61	0.01	7.66	14.01	39.68
92	13.48	0.09	22.75	7.47	0.00	7.70	14.32	39.76
98	13.96	0.05	22.63	7.65	0.00	7.77	14.31	39.94

Table B16. 5% ZrO_2/TiO_2: conversion, propene selectivity and yield from
propane dehydrogenation without CO_2 (600 °C)

Reaction Time (h)	Propene Selectivity (%)	Ethene Selectivity (%)	Propane Conversion (%)	Propene Yield (%)	Ethene Yield (%)	Total olefins Yield (%)	propene / ethene ratio
0	24.2	10.8	62.9	15.3	6.8	22.1	2.2
14	24.2	11.1	62.1	15.1	6.9	22.0	2.2
38	24.2	11.8	61.2	14.8	7.2	22.0	2.1
44	24.1	11.9	60.9	14.7	7.3	22.0	2.0
50	24.2	12.2	60.7	14.7	7.4	22.1	2.0
56	23.9	12.1	60.6	14.5	7.4	21.8	2.0
62	24.6	12.2	61.0	15.0	7.4	22.5	2.0
68	24.3	12.5	60.6	14.7	7.6	22.3	1.9
74	24.5	12.5	60.1	14.7	7.5	22.2	2.0
80	24.4	12.4	60.3	14.7	7.5	22.2	2.0
86	24.0	13.0	59.5	14.3	7.8	22.1	1.8
92	24.6	12.8	59.4	14.6	7.6	22.2	1.9
98	24.7	13.2	59.2	14.6	7.8	22.4	1.9

Appendix 2

Table B17. 5% ZrO_2/TiO_2: Gas concentrations produced from the
dehydrogenation of propane by CO_2 600 °C at CO_2/propane gas ratio 1:1.4

Time hours	H_2 mol%	CO mol%	methane mol%	CO_2 mol%	ethene mol%	ethane mol%	propene mol%	propane mol%
C_o				44.3				62.0
0	6.61	9.79	15.33	32.31	4.92	4.29	11.04	19.27
2	8.28	10.99	19.22	29.70	5.04	5.56	11.02	19.41
6	9.16	10.73	21.65	27.89	5.02	6.58	11.15	17.33
9	9.06	10.53	23.01	26.90	4.91	7.15	11.05	15.89
11	9.10	10.40	23.87	26.54	4.76	7.33	10.74	15.21
13	9.53	10.25	24.71	26.18	4.76	7.63	10.67	14.41
15	8.82	10.19	25.31	25.75	4.70	7.81	10.48	14.00
17	9.38	10.11	25.82	25.39	4.63	7.98	10.24	13.37
19	9.85	9.87	26.35	25.03	4.55	8.07	10.06	12.85
23	9.47	9.99	27.92	24.52	4.46	8.49	9.54	11.98
26	9.36	10.01	28.87	23.81	4.27	8.75	9.26	11.22
29	8.27	9.86	29.68	23.17	4.20	8.77	8.84	10.60
32	9.18	9.60	30.34	22.60	4.07	8.85	8.55	10.06
35	8.78	9.68	30.67	22.15	4.00	8.84	8.33	9.76
38	8.26	9.60	31.60	21.80	3.99	9.00	8.19	9.49
40	8.80	9.48	31.65	21.31	3.82	8.97	7.92	9.15
42	8.30	9.54	32.06	20.98	3.81	8.96	7.77	8.98
44	8.84	9.24	32.78	20.90	3.78	9.06	7.78	8.85
49	9.53	8.94	33.69	20.92	3.74	9.30	7.71	9.31
52	9.38	8.80	33.60	20.58	3.73	9.34	7.68	9.24
55	9.21	8.55	34.02	20.19	3.67	9.39	7.56	8.98
58	9.18	8.52	34.50	19.87	3.63	9.42	7.36	8.79
61	8.89	8.54	34.94	19.46	3.55	9.37	7.21	8.52

Appendix 2

Table B18. 5% ZrO_2/TiO_2: Conversion, propene selectivity and yield of propane dehydrogenation by CO_2 (600 ^oC at CO_2/propane gas ratio 1:1.4)

Reaction Time (h)	Propene Selectivity (%)	Ethene Selectivity (%)	Propane Conversion (%)	Propene Yield (%)	Ethene Yield (%)	Total olefins Yield (%)	propene / ethene ratio	CO Yield (%)	CO_2 Conversion (%)
0	25.8	11.5	68.9	17.8	7.9	25.7	2.2	22.1	27.0
2	25.9	11.8	68.7	17.8	8.1	25.9	2.2	24.8	32.9
6	25.0	11.2	72.0	18.0	8.1	26.1	2.2	24.2	37.0
9	24.0	10.7	74.4	17.8	7.9	25.7	2.2	23.8	39.2
11	23.0	10.2	75.5	17.3	7.7	25.0	2.3	23.5	40.0
13	22.4	10.0	76.8	17.2	7.7	24.9	2.2	23.2	40.8
15	21.8	9.8	77.4	16.9	7.6	24.5	2.2	23.0	41.8
17	21.1	9.5	78.4	16.5	7.5	24.0	2.2	22.9	42.6
19	20.5	9.3	79.3	16.2	7.3	23.6	2.2	22.3	43.4
23	19.1	8.9	80.7	15.4	7.2	22.6	2.1	22.6	44.6
26	18.2	8.4	81.9	14.9	6.9	21.8	2.2	22.6	46.2
29	17.2	8.2	82.9	14.3	6.8	21.0	2.1	22.3	47.7
32	16.5	7.8	83.8	13.8	6.6	20.4	2.1	21.7	48.9
35	15.9	7.7	84.3	13.4	6.4	19.9	2.1	21.9	49.9
38	15.6	7.6	84.7	13.2	6.4	19.6	2.1	21.7	50.7
40	15.0	7.2	85.2	12.8	6.2	18.9	2.1	21.4	51.9
42	14.7	7.2	85.5	12.5	6.1	18.7	2.0	21.6	52.6
44	14.6	7.1	85.7	12.5	6.1	18.7	2.1	20.9	52.8
49	14.6	7.1	85.0	12.4	6.0	18.5	2.1	20.2	52.7
52	14.6	7.1	85.1	12.4	6.0	18.4	2.1	19.9	53.5
55	14.3	6.9	85.5	12.2	5.9	18.1	2.1	19.3	54.4
58	13.8	6.8	85.8	11.9	5.9	17.7	2.0	19.2	55.1
61	13.5	6.6	86.3	11.6	5.7	17.4	2.0	19.3	56.0

Table B19. 5% ZrO_2/TiO_2: Gas concentrations produced from the propane dehydrogenation by CO_2 at CO_2/propane ratio 1:3.1 (600 °C)

Time hours	H_2 mol%	CO mol%	methane mol%	CO_2 mol%	ethene mol%	ethane mol%	propene mol%	propane mol%
C_o				25.0				77.5
0	12.30	10.31	18.49	11.38	6.59	5.45	10.58	40.57
4	11.52	8.25	21.14	12.43	6.72	6.69	11.75	37.68
8	11.36	6.87	22.20	13.12	6.66	7.36	12.47	35.92
12	11.34	6.30	22.74	13.58	6.67	7.83	12.90	35.02
16	10.84	6.46	23.30	13.41	6.69	8.09	12.98	32.61
20	10.55	5.92	23.38	13.63	6.67	8.20	13.04	32.32
24	10.81	5.52	23.72	13.78	6.62	8.32	12.73	32.14
28	10.78	5.35	23.79	13.87	6.45	8.44	12.75	31.80
44	10.93	5.09	23.98	14.07	6.59	8.42	12.83	31.66
52	11.05	4.78	24.05	14.24	6.56	8.45	12.68	31.81
56	11.34	4.66	24.11	14.27	6.54	8.52	12.44	31.53
60	11.79	4.20	25.52	14.22	6.50	8.99	12.27	29.65
64	11.22	3.96	25.78	14.20	6.44	9.08	12.31	28.90
68	11.34	3.82	25.64	14.19	6.36	9.10	12.05	29.30
72	10.81	4.10	27.52	13.64	6.16	9.86	11.68	26.65

Table B20. 5% ZrO_2/TiO_2: Conversion, propene selectivity and yield of propane dehydrogenation by CO_2 at CO_2/propane ratio 1:3.1 (600 °C)

Reaction Time (h)	Propene Selectivity (%)	Ethene Selectivity (%)	Propane Conversion (%)	Propene Yield (%)	Ethene Yield (%)	Total olefins Yield (%)	CO Yield %	CO_2 Conversion (%)
0	28.6	17.9	47.6	13.6	8.5	22.2	41.3	54.5
4	29.5	16.9	51.4	15.2	8.7	23.8	33.0	50.3
8	30.0	16.0	53.6	16.1	8.6	24.7	27.5	47.5
12	30.4	15.7	54.8	16.6	8.6	25.3	25.2	45.7
16	28.9	14.9	57.9	16.8	8.6	25.4	25.8	46.4
20	28.9	14.8	58.3	16.8	8.6	25.4	23.7	45.5
24	28.1	14.6	58.5	16.4	8.5	25.0	22.1	44.9
28	27.9	14.1	59.0	16.5	8.3	24.8	21.4	44.5
44	28.0	14.4	59.1	16.6	8.5	25.1	20.4	43.7
52	27.8	14.4	58.9	16.4	8.5	24.8	19.1	43.0
56	27.1	14.2	59.3	16.1	8.4	24.5	18.6	42.9
60	25.6	13.6	61.7	15.8	8.4	24.2	16.8	43.1
64	25.3	13.3	62.7	15.9	8.3	24.2	15.8	43.2
68	25.0	13.2	62.2	15.5	8.2	23.8	15.3	43.3
72	23.0	12.1	65.6	15.1	8.0	23.0	16.4	45.5

Table B21. 5% ZrO_2/TiO_2: Gas concentrations produced from propane

dehydrogenation by CO_2 (600 °C at CO_2/propane ratios of 2.6:1)

Time hours	H_2 mol%	CO mol%	methane mol%	CO_2 mol%	ethene mol%	ethane mol%	propene mol%	propane mol%
C_o				71.0				27.6
0	4.62	15.14	10.04	52.35	3.49	2.27	6.49	14.31
3	6.96	13.31	10.85	53.39	3.53	2.49	7.01	13.54
6	4.19	12.60	11.62	53.93	3.48	2.66	7.09	12.97
8	4.41	12.08	11.93	53.71	3.41	2.78	7.14	12.43
11	4.46	11.91	12.50	54.01	3.38	3.00	7.18	11.92
13	4.91	11.37	12.59	53.18	3.28	3.03	7.07	11.48
15	4.98	10.89	12.78	53.29	3.26	3.11	7.29	11.25
17	5.55	9.89	12.94	53.27	3.26	3.21	7.24	11.20
20	5.54	10.09	13.57	53.35	3.28	3.44	7.43	10.93
21	5.49	9.85	13.38	51.73	3.20	3.41	7.25	10.48
26	5.65	10.34	14.65	52.87	3.33	3.83	7.56	10.30
29	5.74	10.44	14.94	52.89	3.29	3.92	7.66	10.11
32	5.87	10.29	15.13	53.14	3.29	4.02	7.72	9.86
35	5.94	10.23	15.25	53.26	3.23	4.04	7.66	9.64
39	5.06	10.03	14.22	51.36	3.05	3.85	7.32	9.39
42	5.77	9.45	14.20	51.29	3.08	3.88	7.34	9.39
45	5.55	9.65	14.75	51.64	3.12	3.98	7.46	9.34
48	5.44	9.88	15.17	51.18	3.12	4.17	7.44	9.10
51	6.14	9.83	15.26	51.25	3.08	4.23	7.38	9.12
54	5.87	9.70	15.43	51.50	3.10	4.24	7.34	9.11
57	5.67	9.76	15.56	52.02	3.09	4.29	7.36	9.03
60	6.14	9.04	15.29	51.78	3.05	4.23	7.32	8.92
63	6.26	8.50	14.96	51.25	3.00	4.12	7.21	8.99
67	6.77	8.46	15.31	52.37	3.07	4.30	7.21	9.21
71	6.42	8.81	15.36	53.49	3.05	4.25	7.50	9.18
75	6.34	8.45	14.77	54.80	3.07	4.09	7.42	9.33
79	5.84	8.13	14.29	54.68	2.94	3.92	7.23	8.91
83	6.05	7.97	14.21	54.47	2.91	3.90	7.07	8.81
86	6.50	7.96	14.50	55.61	2.98	3.97	7.22	8.98
89	6.61	7.64	14.39	55.57	2.96	3.97	7.20	9.05
93	6.63	7.46	14.56	55.59	2.97	4.03	7.17	9.13
96	6.44	7.40	14.73	55.31	2.98	4.09	7.12	9.09
100	6.41	7.31	14.92	55.07	2.96	4.13	7.16	9.00
104	6.67	7.20	15.07	54.94	2.93	4.15	7.07	8.99
108	6.68	7.20	15.16	54.90	2.98	4.20	7.10	8.93
111	6.54	6.95	15.09	54.60	2.92	4.18	7.03	8.94
129	6.89	6.55	15.22	54.58	2.90	4.22	6.95	8.87
145	6.87	6.20	15.48	54.84	2.90	4.31	6.86	8.90
149	7.15	6.22	15.59	54.84	2.89	4.34	6.93	8.75
153	7.27	6.04	15.60	54.84	2.88	4.34	6.87	8.76
157	6.89	6.07	15.65	54.92	2.87	4.35	6.76	8.85
161	7.19	5.78	15.57	54.83	2.87	4.32	6.82	8.83
165	7.25	5.79	15.62	54.68	2.87	4.39	6.78	8.83
169	6.96	5.86	15.75	54.63	2.87	4.38	6.75	8.80
173	7.38	5.76	15.76	54.51	2.86	4.40	6.82	8.79

177	7.19	5.66	15.79	54.49	2.86	4.40	6.77	8.76
181	7.05	5.58	15.83	54.62	2.84	4.43	6.62	8.78
191	7.37	5.45	15.81	54.52	2.84	4.42	6.69	8.69
195	6.89	5.47	15.87	54.50	2.83	4.42	6.62	8.73
199	7.26	5.43	15.85	54.43	2.78	4.38	6.67	8.71
203	7.20	5.43	16.02	54.49	2.83	4.47	6.62	8.68
207	7.33	5.38	1.64	54.57	2.84	4.48	6.63	8.70
213	7.37	5.31	16.22	54.47	2.84	4.53	6.68	8.59
217	7.38	5.31	16.28	54.52	2.81	4.58	6.63	8.63
221	7.62	5.34	16.44	54.43	2.82	4.56	6.59	8.53
225	7.30	5.31	16.55	54.31	2.81	4.61	6.55	8.51
229	7.71	5.33	16.65	54.29	2.83	4.65	6.54	8.48
233	7.54	5.36	16.86	54.27	2.83	4.67	6.45	8.51
237	7.55	5.30	16.84	53.99	2.80	4.69	6.51	8.36
249	7.31	5.16	17.38	53.83	2.84	4.84	6.49	8.40
253	7.86	5.25	17.37	53.85	2.81	4.83	6.46	8.39
257	7.57	5.30	17.48	53.92	2.84	4.89	6.41	8.45

Appendix 2

Table B22. 5% ZrO$_2$/TiO$_2$: Conversion, propene selectivity and yield from propane dehydrogenation by CO$_2$ (600 °C, CO$_2$/propane ratios of 2.6:1)

Reaction Time (h)	Propene Selectivity (%)	Ethene Selectivity (%)	Propane Conversion (%)	Propene Yield (%)	Ethene Yield (%)	Total olefins Yield (%)	CO Yield (%)	CO$_2$ Conversion (%)
0	48.9	26.3	48.1	23.5	12.7	36.2	21.3	26.3
3	50.0	25.1	50.9	25.4	12.8	38.2	18.8	24.8
6	48.6	23.8	52.9	25.7	12.6	38.3	17.8	24.0
8	47.2	22.5	54.9	25.9	12.4	38.3	17.0	24.3
11	45.9	21.6	56.8	26.0	12.3	38.3	16.8	23.9
13	44.0	20.4	58.4	25.7	11.9	37.6	16.0	25.1
15	44.7	20.0	59.2	26.4	11.8	38.3	15.3	24.9
17	44.2	19.9	59.4	26.3	11.8	38.1	13.9	25.0
20	44.6	19.7	60.4	26.9	11.9	38.8	14.2	24.8
21	42.5	18.7	62.0	26.3	11.6	37.9	13.9	27.1
26	43.8	19.3	62.6	27.4	12.1	39.5	14.6	25.5
29	43.9	18.9	63.3	27.8	11.9	39.7	14.7	25.5
32	43.6	18.6	64.2	28.0	11.9	39.9	14.5	25.1
35	42.7	18.0	65.0	27.8	11.7	39.5	14.4	25.0
39	40.3	16.8	65.9	26.6	11.1	37.6	14.1	27.6
42	40.4	17.0	65.9	26.6	11.2	37.8	13.3	27.7
45	40.9	17.1	66.1	27.1	11.3	38.4	13.6	27.2
48	40.3	16.9	67.0	27.0	11.3	38.3	13.9	27.9
51	40.0	16.7	66.9	26.8	11.2	38.0	13.9	27.8
54	39.7	16.8	67.0	26.6	11.3	37.9	13.7	27.4
57	39.7	16.6	67.2	26.7	11.2	37.9	13.8	26.7
60	39.3	16.4	67.6	26.6	11.1	37.6	12.7	27.0
63	38.8	16.2	67.4	26.2	10.9	37.1	12.0	27.8
67	39.2	16.7	66.6	26.1	11.2	37.3	11.9	26.2
71	40.8	16.6	66.7	27.2	11.1	38.3	12.4	24.6
75	40.7	16.9	66.2	26.9	11.1	38.1	11.9	22.8
79	38.7	15.7	67.7	26.2	10.6	36.9	11.5	23.0
83	37.7	15.5	68.0	25.6	10.6	36.2	11.2	23.3
86	38.9	16.0	67.4	26.2	10.8	37.0	11.2	21.7
89	38.9	16.0	67.2	26.1	10.7	36.8	10.8	21.7
93	38.9	16.1	66.9	26.0	10.8	36.8	10.5	21.7
96	38.5	16.1	67.0	25.8	10.8	36.6	10.4	22.1
100	38.6	15.9	67.4	26.0	10.7	36.7	10.3	22.4
104	38.1	15.8	67.4	25.6	10.6	36.3	10.1	22.6
108	38.1	16.0	67.6	25.8	10.8	36.6	10.1	22.7
111	37.8	15.7	67.6	25.5	10.6	36.1	9.8	23.1
129	37.2	15.5	67.8	25.2	10.5	35.7	9.2	23.1
145	36.7	15.5	67.7	24.9	10.5	35.4	8.7	22.7
149	36.8	15.3	68.2	25.1	10.5	35.6	8.8	22.7
153	36.5	15.3	68.2	24.9	10.4	35.4	8.5	22.7
157	36.1	15.4	67.9	24.5	10.4	35.0	8.5	22.6
161	36.4	15.3	68.0	24.7	10.4	35.2	8.1	22.8
165	36.2	15.3	68.0	24.6	10.4	35.0	8.2	23.0
169	36.0	15.3	68.1	24.5	10.4	34.9	8.3	23.0
173	36.3	15.2	68.1	24.8	10.4	35.1	8.1	23.2
177	36.0	15.2	68.2	24.6	10.4	34.9	8.0	23.2
181	35.2	15.1	68.2	24.0	10.3	34.3	7.9	23.1
191	35.4	15.0	68.5	24.3	10.3	34.6	7.7	23.2
195	35.1	15.0	68.3	24.0	10.2	34.3	7.7	23.2
199	35.4	14.7	68.4	24.2	10.1	34.3	7.7	23.3
203	35.1	15.0	68.5	24.0	10.3	34.3	7.6	23.2
207	35.2	15.1	68.4	24.1	10.3	34.4	7.6	23.1

Appendix 2

213	35.2	15.0	68.8	24.2	10.3	34.5	7.5	23.3
217	35.0	14.8	68.7	24.1	10.2	34.3	7.5	23.2
221	34.6	14.8	69.1	23.9	10.2	34.1	7.5	23.3
225	34.4	14.8	69.1	23.8	10.2	34.0	7.5	23.5
229	34.2	14.8	69.3	23.7	10.3	34.0	7.5	23.5
233	33.9	14.8	69.1	23.4	10.3	33.7	7.6	23.5
237	33.9	14.6	69.7	23.6	10.2	33.8	7.5	23.9
249	33.9	14.8	69.5	23.6	10.3	33.9	7.3	24.2
253	33.7	14.7	69.6	23.4	10.2	33.6	7.4	24.1
257	33.5	14.8	69.3	23.3	10.3	33.5	7.5	24.0

Appendix 2

Table B23. 5% ZrO_2/TiO_2: Gas concentrations produced from propane

dehydrogenation by CO_2 (600 °C at CO_2/propane ratio 12.2:1)

Time hours	H_2 mol%	CO mol%	methane mol%	CO_2 mol%	ethene mol%	ethane mol%	propene mol%	propane mol%
C_o				92.5				7.6
0	0.75	3.49	1.94	85.42	0.77	0.35	2.19	3.62
1	0.83	4.09	2.22	84.29	0.85	0.42	2.37	3.74
2	0.80	3.99	2.24	84.62	0.84	0.40	2.31	3.76
4	0.91	4.21	2.29	85.17	0.85	0.44	2.37	3.75
6	0.92	4.16	2.27	84.99	0.86	0.40	2.43	3.79
8	0.86	4.05	2.28	84.76	0.86	0.42	2.44	3.84
12	0.92	4.04	2.29	85.09	0.86	0.43	2.46	3.89
16	0.87	4.02	2.30	84.72	0.88	0.45	2.47	3.92
19	0.88	4.03	2.31	84.77	0.96	0.41	2.49	3.87
21	0.93	3.87	2.34	84.52	0.87	0.43	2.49	3.81
25	0.90	4.06	2.34	85.16	0.89	0.47	2.43	3.77
29	0.98	4.02	2.31	84.43	0.86	0.44	2.42	3.79

Table B24. 5% ZrO_2/TiO_2: Conversion, propene selectivity and yield of propane

dehydrogenation by CO_2 (600 °C at CO_2/propane ratio 12.2:1)

Reaction Time (h)	Propene Selectivity (%)	Ethene Selectivity (%)	Propane Conversion (%)	Propene Yield (%)	Ethene Yield (%)	Total olefins Yield (%)	CO Yield (%)	CO_2 Conversion (%)
0	55.1	19.3	52.4	28.9	10.1	38.9	3.8	7.7
1	61.3	22.1	50.8	31.1	11.2	42.3	4.4	8.9
2	60.1	21.9	50.5	30.4	11.1	41.4	4.3	8.5
4	61.5	22.2	50.6	31.1	11.2	42.4	4.6	7.9
6	63.6	22.6	50.1	31.9	11.3	43.2	4.5	8.1
8	64.8	22.8	49.5	32.1	11.3	43.4	4.4	8.4
12	66.1	23.3	48.9	32.3	11.4	43.7	4.4	8.0
16	67.1	23.9	48.4	32.5	11.6	44.0	4.3	8.4
19	66.7	25.8	49.1	32.7	12.7	45.4	4.4	8.4
21	65.8	23.0	49.9	32.8	11.5	44.3	4.2	8.6
25	63.4	23.3	50.4	31.9	11.7	43.7	4.4	7.9
29	63.6	22.7	50.1	31.9	11.4	43.2	4.3	8.7

Appendix 2

Table B25. 5% ZrO_2/TiO_2: Gas concentrations produced from propane dehydrogenation by CO_2 (600 °C at CO_2/propane ratio 24.2:1)

Time hours	H$_2$ mol%	CO mol%	methane mol%	CO$_2$ mol%	ethene mol%	ethane mol%	propene mol%	propane mol%
C$_o$				95.6				4.0
0	0.57	4.51	1.16	90.66	0.37	0.17	1.25	1.73
4	0.56	4.48	1.20	90.29	0.38	0.18	1.27	1.77
6	0.62	4.47	1.19	89.79	0.38	0.18	1.25	1.74
8	0.59	4.36	1.20	89.75	0.39	0.20	1.29	1.75
10	0.63	4.37	1.22	90.69	0.38	0.17	1.32	1.73
15	0.52	3.96	1.10	90.59	0.38	0.18	1.23	1.81
20	0.51	3.70	1.11	90.83	0.41	0.18	1.23	1.78
24	0.56	3.57	1.13	90.95	0.39	0.20	1.22	1.78
28	0.49	3.55	1.16	90.74	0.39	0.17	1.24	1.81
32	0.48	3.40	1.16	90.75	0.39	0.19	1.26	1.81
35	0.48	3.38	1.12	90.67	0.38	0.16	1.26	1.73
36	0.45	3.25	1.07	88.06	0.37	0.14	1.20	1.71
37	0.42	3.27	1.11	88.97	0.38	0.18	1.22	1.73

Table B26. 5% ZrO_2/TiO_2: Conversion, propene selectivity and yield of propane dehydrogenation by CO_2 at 600 °C at gas ratio 24.2:1 CO_2 to propane (Note: catalysts regenerated for 4 hours only via flow of air at 700 °C)

Reaction Time (h)	Propene Selectivity (%)	Ethene Selectivity (%)	Propane Conversion (%)	Propene Yield (%)	Ethene Yield (%)	Total olefins Yield (%)	CO Yield (%)	CO$_2$ Conversion (%)
0	56.4	16.5	56.2	31.7	9.3	41.0	4.7	5.2
4	58.2	17.2	55.2	32.1	9.5	41.6	4.7	5.6
6	56.7	17.3	55.8	31.6	9.7	41.3	4.7	6.1
8	58.3	17.7	55.8	32.5	9.9	42.4	4.6	6.1
10	59.4	17.0	56.2	33.4	9.6	43.0	4.6	5.1
15	57.8	17.9	54.1	31.2	9.7	40.9	4.1	5.2
20	56.6	18.9	55.0	31.1	10.4	41.6	3.9	5.0
24	56.4	18.1	54.9	30.9	9.9	40.8	3.7	4.9
28	57.8	18.2	54.3	31.4	9.9	41.2	3.7	5.1
32	59.0	18.1	54.1	31.9	9.8	41.7	3.6	5.1
35	56.7	17.0	56.3	31.9	9.6	41.5	3.5	5.2
36	53.8	16.5	56.6	30.5	9.4	39.8	3.4	7.9
37	55.1	17.3	56.3	31.0	9.7	40.7	3.4	6.9

Appendix 2

Table B27. 5% ZrO_2/TiO_2: Gas concentrations produced from propane dehydrogenation by CO_2 (600 °C at CO_2/propane ratio 34.3:1)

Time hours	H_2 mol%	CO mol%	methane mol%	CO_2 mol%	ethene mol%	ethane mol%	propene mol%	propane mol%
C_o				96.0				2.8
0	0.34	2.25	0.58	92.32	0.24	0.10	0.82	1.39
2	0.28	1.95	0.56	93.65	0.24	0.09	0.82	1.42
4	0.29	1.92	0.59	93.94	0.24	0.09	0.82	1.43
6	0.29	1.89	0.60	93.87	0.24	0.09	0.81	1.42
8	0.28	1.89	0.56	93.79	0.24	0.08	0.79	1.41
10	0.27	1.89	0.58	94.03	0.24	0.11	0.79	1.45
12	0.26	1.86	0.56	94.22	0.24	0.09	0.84	1.41
14	0.27	1.93	0.60	94.62	0.23	0.09	0.78	1.36
18	0.26	1.86	0.58	95.21	0.24	0.10	0.79	1.36
22	0.24	1.92	0.61	95.20	0.25	0.10	0.82	1.37

Table B28. 5% ZrO_2/TiO_2: Conversion, propene selectivity and yield of propane dehydrogenation by CO_2 at 600 °C at gas ratio 34.3:1 CO_2 to propane

Reaction Time (h)	Propene Selectivity (%)	Ethene Selectivity (%)	Propane Conversion (%)	Propene Yield (%)	Ethene Yield (%)	Total olefins Yield (%)	CO Yield (%)	CO_2 Conversion (%)
0	58.6	17.3	50.2	29.4	8.7	38.1	2.3	3.8
2	59.5	17.3	49.4	29.4	8.6	38.0	2.0	2.5
4	59.5	17.5	48.9	29.1	8.6	37.7	2.0	2.1
6	58.6	17.4	49.5	29.0	8.6	37.6	2.0	2.2
8	56.8	17.4	49.7	28.2	8.7	36.9	2.0	2.3
10	58.4	18.0	48.3	28.2	8.7	36.8	2.0	2.1
12	60.2	17.0	49.8	30.0	8.5	38.5	1.9	1.9
14	54.4	16.3	51.4	28.0	8.4	36.3	2.0	1.4
18	55.2	16.8	51.4	28.4	8.7	37.0	1.9	0.8
22	57.0	17.3	51.2	29.2	8.9	38.0	2.0	0.8

Table B29. Hydrogen content (mol%) produced from propane dehydrogenation by CO_2 at 600 °C at different gas ratio.

	without CO_2	CO_2/propane gas ratio 1:1.4	CO_2/propane ratio 1:3.1	CO_2/propane ratio 2.6:1	CO_2/propane ratio 12.2:1	CO_2/propane ratio 24.2:1	CO_2/propane ratio 34.3:1
H_2 content, mol%	14.79	8.92	11.20	7.49	0.88	0.60	0.53
Ratio of CO/H_2	-	1.1	0.5	1.1	4.6	7.3	7

Table B30. 1.3%BaO/5% ZrO_2/TiO_2, 2% BeO/5% ZrO_2/TiO_2 and 2% MgO/5% ZrO_2/TiO_2: Gas concentrations produced from propane dehydrogenation by CO_2 (at 600 °C)

Catalysts	Time hours	H_2 mol%	CO mol%	methane mol%	CO_2 mol%	ethene mol%	ethane mol%	propene mol%	propane mol%
C_o: (CO_2/Propane ratio: 19.7:1)					94.5				4.8
1.3%BaO/5%ZrO_2/TiO_2	0	0.83	12.02	1.19	82.70	0.41	0.12	0.25	1.33
1.3%BaO/5%ZrO_2/TiO_2	3	0.94	12.20	1.24	84.95	0.41	0.10	0.24	1.47
1.3%BaO/5%ZrO_2/TiO_2	6	1.04	11.91	1.08	85.21	0.41	0.09	0.26	1.53
1.3%BaO/5%ZrO_2/TiO_2	15	0.87	10.99	0.97	86.50	0.37	0.08	0.21	1.65
1.3%BaO/5%ZrO_2/TiO_2	18	0.83	10.80	0.90	86.65	0.39	0.08	0.21	1.67
1.3%BaO/5%ZrO_2/TiO_2	21	0.90	10.52	0.82	87.07	0.38	0.08	0.24	1.74
C_o: (CO_2/Propane ratio: 20.9:1)					96.2				4.6
2%BeO/5%ZrO_2/TiO_2	0	2.88	18.12	2.50	77.69	0.39	0.25	0.30	0.70
2%BeO/5%ZrO_2/TiO_2	3	2.70	17.81	2.40	78.57	0.40	0.25	0.29	0.73
2%BeO/5%ZrO_2/TiO_2	4	2.77	17.03	2.28	76.83	0.39	0.23	0.27	0.72
C_o: (CO_2/Propane ratio: 21.2:1)					95.6				4.5
2%MgO/5%ZrO_2/TiO_2	0	1.32	13.19	1.54	76.67	0.47	0.13	0.32	1.72
2%MgO/5%ZrO_2/TiO_2	2	1.21	12.65	1.63	76.77	0.47	0.14	0.28	1.80
2%MgO/5%ZrO_2/TiO_2	5	1.15	12.16	1.52	77.38	0.49	0.13	0.27	1.90
2%MgO/5%ZrO_2/TiO_2	6	1.10	11.63	1.51	75.43	0.49	0.13	0.25	1.84

Table B31. 1.3%BaO/5% ZrO_2/TiO_2, 2% BeO/5% ZrO_2/TiO_2 and 2% MgO/5% ZrO_2/TiO_2: conversion, propene selectivity and yield by propane dehydrogenation by CO_2 (at 600 °C)

Catalysts	Reaction Time (h)	Propene Selectivity (%)	Ethene Selectivity (%)	Propane Conversion (%)	Propene Yield (%)	Ethene Yield (%)	Total olefins Yield (%)	CO Yield (%)	CO_2 Conversion (%)
1.3%BaO/5%ZrO_2/TiO_2	0	7.3	11.9	72.4	5.3	8.6	13.9	12.7	12.5
1.3%BaO/5%ZrO_2/TiO_2	3	7.3	12.3	69.4	5.1	8.5	13.6	12.9	10.1
1.3%BaO/5%ZrO_2/TiO_2	6	8.0	12.5	68.1	5.5	8.5	14.0	12.6	9.8
1.3%BaO/5%ZrO_2/TiO_2	15	6.6	11.8	65.7	4.3	7.8	12.1	11.6	8.5
1.3%BaO/5%ZrO_2/TiO_2	18	6.8	12.5	65.2	4.4	8.2	12.6	11.4	8.3
1.3%BaO/5%ZrO_2/TiO_2	21	7.9	12.4	63.8	5.0	7.9	12.9	11.1	7.9
2%BeO/5%ZrO_2/TiO_2	0	7.8	9.9	84.7	6.6	8.4	15.0	97.9	18.8
2%BeO/5%ZrO_2/TiO_2	3	7.4	10.4	84.1	6.3	8.7	15.0	101.0	18.5
2%BeO/5%ZrO_2/TiO_2	4	7.1	10.1	84.3	6.0	8.5	14.5	87.9	17.7
2%MgO/5%ZrO_2/TiO_2	0	11.6	16.9	61.8	7.1	10.5	17.6	13.8	19.8
2%MgO/5%ZrO_2/TiO_2	2	10.6	17.3	59.9	6.3	10.4	16.7	13.2	19.7
2%MgO/5%ZrO_2/TiO_2	5	10.5	19.0	57.7	6.1	11.0	17.0	12.7	19.1
2%MgO/5%ZrO_2/TiO_2	6	9.6	18.5	59.1	5.7	10.9	16.6	12.2	21.1

Table B32. Effect of 2% Al_2O_3/5% ZrO_2/TiO_2 and 5.8% Al_2O_3/TiO_2: Gas concentrations produced from propane dehydrogenation by CO_2 (at 600 °C)

Appendix 2

Catalysts	Time hours	H_2 mol%	CO mol%	methane mol%	CO_2 mol%	ethene mol%	ethane mol%	propene mol%	propane mol%
C_o: (CO_2/Propane ratio: 18.3:1)					95.1				5.2
2%Al_2O_3/5%ZrO_2/TiO_2	0	1.64	11.93	2.18	79.72	0.50	0.16	0.44	1.63
2%Al_2O_3/5%ZrO_2/TiO_2	3	1.41	11.58	2.06	80.01	0.50	0.14	0.41	2.12
2%Al_2O_3/5%ZrO_2/TiO_2	6	1.89	11.39	1.93	79.97	0.50	0.11	0.34	2.19
2%Al_2O_3/5%ZrO_2/TiO_2	9	1.19	11.49	1.80	80.06	0.48	0.11	0.31	2.34
2%Al_2O_3/5%ZrO_2/TiO_2	12	0.96	11.41	1.75	80.53	0.50	0.12	0.27	2.39
C_o: (CO_2/Propane ratio: 21.3:1)					93.8				4.4
5.8%Al_2O_3/TiO_2	0	1.57	12.95	1.84	76.78	0.43	0.12	0.26	1.49
5.8%Al_2O_3/TiO_2	4	1.63	12.69	1.76	77.68	0.43	0.11	0.27	1.62
5.8%Al_2O_3/TiO_2	6	1.32	12.13	1.65	78.38	0.42	0.10	0.22	1.63

Table B33. Effect of 2% Al_2O_3/5% ZrO_2/TiO_2 and 5% Al_2O_3/TiO_2: Conversion,

propene selectivity and yield of propane dehydrogenation by CO_2 (at 600 °C)

Catalysts	Reaction Time (h)	Propene Selectivity (%)	Ethene Selectivity (%)	Propane Conversion (%)	Propene Yield (%)	Ethene Yield (%)	Total olefins Yield (%)	CO Yield (%)	CO_2 Conversion (%)
2%Al_2O_3/5%ZrO_2/TiO_2	0	12.2	14.1	68.6	8.4	9.7	18.1	12.5	16.2
2%Al_2O_3/5%ZrO_2/TiO_2	3	13.5	16.2	59.2	8.0	9.6	17.5	12.2	15.9
2%Al_2O_3/5%ZrO_2/TiO_2	6	11.3	16.6	57.8	6.5	9.6	16.2	12.0	15.9
2%Al_2O_3/5%ZrO_2/TiO_2	9	11.0	16.7	55.1	6.0	9.2	15.2	12.1	15.8
2%Al_2O_3/5%ZrO_2/TiO_2	12	9.6	17.8	54.0	5.2	9.6	14.8	12.0	15.3
5.8%Al_2O_3/TiO_2	0	8.8	14.6	66.1	5.8	9.7	15.5	76.1	13.8
5.8%Al_2O_3/TiO_2	4	9.7	15.5	63.2	6.1	9.8	15.9	78.7	13.5
5.8%Al_2O_3/TiO_2	6	7.9	15.3	63.0	5.0	9.6	14.6	78.7	12.9

Table B34. Effect of 2% $CuO/5\%ZrO_2/TiO_2$ and 2% $FeO/5\% ZrO_2/TiO_2$: Gas concentrations produced from propane dehydrogenation by CO_2 (at 600 °C)

Catalysts	Time hours	H_2 mol%	CO mol%	methane mol%	CO_2 mol%	ethene mol%	ethane mol%	propene mol%	propane mol%
C_o: (CO_2/Propane ratio: 19.7:1)					94.4				4.8
$CuO/5\%ZrO_2/TiO_2$	0	1.61	14.88	1.91	80.39	0.53	0.13	0.37	1.33
$CuO/5\%ZrO_2/TiO_2$	2	1.36	14.63	1.87	80.94	0.52	0.13	0.36	1.44
$CuO/5\%ZrO_2/TiO_2$	4	1.38	14.32	1.77	80.96	0.54	0.16	0.37	1.52
$CuO/5\%ZrO_2/TiO_2$	5	1.44	14.03	1.76	78.78	0.51	0.12	0.31	1.51
$CuO/5\%ZrO_2/TiO_2$	6	1.30	13.78	1.54	78.61	0.51	0.12	0.32	1.49
C_o: (CO_2/Propane ratio: 18.7:1)					95.6				5.1
$FeO/5\%ZrO_2/TiO_2$	0	3.98	24.78	3.07	63.83	0.02	0.08	0.09	0.16
$FeO/5\%ZrO_2/TiO_2$	2	3.65	24.72	3.11	61.94	0.02	0.08	0.07	0.14

Table B35. Effect of 2% $CuO /5\% ZrO_2/TiO_2$ and 2% $FeO/ 5\% ZrO_2/TiO_2$: conversion, propene selectivity and yield at 600 °C.

Catalysts	Reaction Time (h)	Propene Selectivity (%)	Ethene Selectivity (%)	Propane Conversion (%)	Propene Yield (%)	Ethene Yield (%)	Total olefins Yield (%)	CO Yield (%)	CO_2 Conversion (%)
$CuO/5\%ZrO_2/TiO_2$	0	10.6	15.2	72.2	7.7	11.0	18.6	15.8	14.8
$CuO/5\%ZrO_2/TiO_2$	2	10.6	15.6	70.1	7.4	10.9	18.4	15.5	14.3
$CuO/5\%ZrO_2/TiO_2$	4	11.4	16.6	68.4	7.8	11.3	19.1	15.2	14.2
$CuO/5\%ZrO_2/TiO_2$	5	9.4	15.5	68.5	6.4	10.6	17.0	14.9	16.5
$CuO/5\%ZrO_2/TiO_2$	6	9.6	15.4	68.9	6.6	10.6	17.2	14.6	16.7
$FeO/5\%ZrO_2/TiO_2$	0	1.8	0.5	96.9	1.7	0.5	2.2	25.9	33.2
$FeO/5\%ZrO_2/TiO_2$	2	1.8	0.5	96.9	1.7	0.5	2.2	25.9	35.2

Table B36. Effect of 7.4% VO/TiO$_2$, 6.9% NbO$_2$/TiO$_2$, 3.5% IrO$_2$/TiO$_2$ and 3.3% RhO$_2$/TiO$_2$ support: gas concentrations produced from propane dehydrogenation by CO$_2$

Catalysts	Temp. °C	Time hours	H$_2$ mol%	CO mol%	methane mol%	CO$_2$ mol%	ethene mol%	ethane mol%	propene mol%	propane mol%
C$_o$: (CO$_2$/Propane ratio: 22.3:1)						93.8				4.2
7.4% VO/TiO$_2$	550	0	4.50	21.52	3.49	67.60	0.06	0.22	0.27	0.28
7.4% VO/TiO$_2$	550	1	4.19	21.50	3.44	67.74	0.05	0.19	0.27	0.28
C$_o$: (CO$_2$/Propane ratio: 16.1:1)						94.8				5.9
6.9% NbO$_2$/TiO$_2$	600	0	1.50	9.84	1.44	87.08	0.50	0.16	0.52	1.65
6.9% NbO$_2$/TiO$_2$	600	1	2.01	15.37	1.87	78.90	0.44	0.18	0.56	1.55
C$_o$: (CO$_2$/Propane ratio: 18.3:1)						95.2				5.2
3.5 % IrO$_2$/TiO$_2$	575	0	3.51	16.43	0.96	78.40	0.05	0.09	0.31	1.25
3.5 % IrO$_2$/TiO$_2$	575	1	3.60	19.00	1.03	73.16	0.04	0.10	0.26	1.34
3.5 % IrO$_2$/TiO$_2$	575	2	3.66	19.62	1.05	72.83	0.05	0.09	0.21	1.71
C$_o$: (CO$_2$/Propane ratio: 17.2:1)						91.3				5.3
3.3 % RhO$_2$/TiO$_2$	600	0	4.32	14.43	1.42	61.87	0.00	0.00	0.00	0.06
3.3 % RhO$_2$/TiO$_2$	600	1	5.08	19.90	1.64	61.26	0.00	0.00	0.00	0.05

Table B37. Effect of 7.4%VO/TiO$_2$, 6.9%NbO$_2$/TiO$_2$, 3.5%IrO$_2$/TiO$_2$: conversion, propene selectivity and yield (at 600 °C)

Catalysts	Temp. °C	Reaction Time (h)	Propene Selectivity (%)	Ethene Selectivity (%)	Propane Conversion (%)	Propene Yield (%)	Ethene Yield (%)	Total olefins Yield (%)	CO Yield (%)	CO$_2$ Conversion (%)
7.4% VO/TiO$_2$	550	0	6.8	1.5	93.3	6.3	1.4	7.8	82.1	22.9
7.4% VO/TiO$_2$	550	1	6.8	1.4	93.4	6.4	1.3	7.6	82.5	22.9
6.9% NbO$_2$/TiO$_2$	600	0	12.2	11.8	72.0	8.8	8.5	17.3	10.4	8.1
6.9% NbO$_2$/TiO$_2$	600	1	13.0	10.0	73.7	9.6	7.4	16.9	16.2	16.8
3.5 % IrO$_2$/TiO$_2$	575	0	7.9	1.2	75.9	6.0	0.9	6.9	17.3	17.6
3.5 % IrO$_2$/TiO$_2$	575	1	6.8	1.0	74.3	5.1	0.7	5.8	20.0	23.2
3.5 % IrO$_2$/TiO$_2$	575	2	6.0	1.3	67.2	4.1	0.9	4.9	20.6	23.5
3.3 % RhO$_2$/TiO$_2$	600	0	0.0	0.0	99.0	0.0	0.0	0.0	15.8	32.2
3.3 % RhO$_2$/TiO$_2$	600	1	0.0	0.0	99.0	0.0	0.0	0.0	21.8	32.9

Appendix 2

Table B38. Effect of 7.9% HfO_2/TiO_2 and 2% PtO/TiO_2, 5% UO_3/TiO_2 and 5% ThO_2/TiO_2: gas concentrations produced from propane dehydrogenation by CO_2 (at 600 °C)

Catalysts	Temp. °C	Time hours	H_2 mol%	CO mol%	methane mol%	CO_2 mol%	ethene mol%	ethane mol%	propene mol%	propane mol%
C_o: (CO_2/Propane ratio: 20.5:1)						94.3				4.6
HfO_2/TiO_2	600	0	1.70	15.00	1.16	78.38	0.46	0.14	0.64	1.63
HfO_2/TiO_2	600	2	1.49	13.50	0.94	80.30	0.42	0.10	0.53	2.00
HfO_2/TiO_2	600	3	1.33	12.53	0.84	81.27	0.38	0.09	0.44	2.05
HfO_2/TiO_2	600	4	1.19	11.98	0.79	81.95	0.38	0.08	0.41	2.12
HfO_2/TiO_2	600	6	1.13	11.42	0.70	80.35	0.35	0.07	0.42	2.12
C_o: (CO_2/Propane ratio: 22.9:1)						96.3				4.2
PtO/TiO_2	600	0	1.56	11.76	1.19	84.30	0.43	0.11	0.30	2.08
PtO/TiO_2	600	3	1.43	10.77	1.10	85.09	0.45	0.11	0.34	2.17
PtO/TiO_2	600	5	1.33	10.31	1.04	85.50	0.47	0.11	0.35	2.30
C_o: (CO_2/Propane ratio: 22.3:1)						93.8				4.2
UO_3/TiO_2	600	0	0.70	7.34	0.45	83.83	0.29	0.05	0.24	2.69
UO_3/TiO_2	600	2	0.76	7.25	0.43	83.97	0.30	0.06	0.23	2.67
UO_3/TiO_2	600	6	0.71	7.24	0.44	84.07	0.29	0.05	0.23	2.69
C_o: (CO_2/Propane ratio: 19.5:1)						95.5				4.9
ThO_2/TiO_2	600	0	2.80	15.02	1.69	78.73	0.09	0.11	0.36	1.73
ThO_2/TiO_2	600	5	2.55	14.23	1.61	79.25	0.10	0.12	0.38	1.78

Table B39. Effect of 7.9% HfO_2/TiO_2 and 2% PtO/TiO_2, 5% UO_3/TiO_2 and 5% ThO_2/TiO_2: conversion, propene selectivity and yield by propane dehydrogenation by CO_2 (at 600 °C)

Catalysts	Temp. °C	Reaction Time (h)	Propene Selectivity (%)	Ethene Selectivity (%)	Propane Conversion (%)	Propene Yield (%)	Ethene Yield (%)	Total olefins Yield (%)	CO Yield (%)	CO_2 Conversion (%)
HfO_2/TiO_2	600	0	21.4	15.6	64.6	13.9	10.1	23.9	15.9	16.9
HfO_2/TiO_2	600	2	20.3	16.3	56.6	11.5	9.2	20.7	14.3	14.8
HfO_2/TiO_2	600	3	17.4	14.9	55.5	9.6	8.3	17.9	13.3	13.8
HfO_2/TiO_2	600	4	16.4	15.2	53.9	8.8	8.2	17.0	12.7	13.1
HfO_2/TiO_2	600	6	17.1	14.2	53.9	9.2	7.6	16.8	12.1	14.8
PtO/TiO_2	600	0	14.2	20.0	50.6	7.2	10.1	17.3	12.2	12.5
PtO/TiO_2	600	3	16.5	22.0	48.4	8.0	10.6	18.6	11.2	11.6
PtO/TiO_2	600	5	18.4	25.0	45.2	8.3	11.3	19.6	10.7	11.2
UO_3/TiO_2	600	0	16.0	19.3	35.9	5.8	6.9	12.7	7.8	10.6
UO_3/TiO_2	600	2	15.2	19.4	36.5	5.5	7.1	12.6	7.7	10.5
UO_3/TiO_2	600	6	15.3	19.2	36.1	5.5	6.9	12.4	7.7	10.4
ThO_2/TiO_2	600	0	11.3	2.9	64.8	7.3	1.9	9.2	15.7	17.6
ThO_2/TiO_2	600	5	12.3	3.1	63.6	7.8	2.0	9.8	14.9	17.0

Table B40. Effect of 10.5 % Tl_2O_3/TiO_2: Gas concentrations produced from propane dehydrogenation by CO_2 (CO_2/propane ratio 20.1:1 at 600 ^oC)

Time hours	H_2 mol%	CO mol%	methane mol%	CO_2 mol%	ethene mol%	ethane mol%	propene mol%	propane mol%
C_o				92.8				4.2
0	0.54	7.69	1.33	84.82	1.16	0.19	0.25	2.35
0.5	0.48	7.00	1.19	80.40	1.04	0.16	0.23	2.17
1	0.45	6.87	1.20	79.83	1.05	0.16	0.21	2.14
2	0.41	6.90	1.28	79.56	1.06	0.16	0.21	2.18
2.5	0.43	6.81	1.32	79.44	1.08	0.17	0.25	2.20
3	0.42	6.61	1.23	79.57	1.05	0.17	0.25	2.24
5	0.43	6.84	1.29	84.06	1.11	0.17	0.25	2.39
6	0.42	6.67	1.25	82.10	1.09	0.17	0.23	2.32
7	0.40	6.48	1.21	82.14	1.07	0.15	0.26	2.30
8	0.46	6.38	1.20	82.30	1.06	0.15	0.21	2.30

Table B41. Effect of 10.5% Tl_2O_3/TiO_2: CO_2 dehydrogenation of propane conversion, propene selectivity and yield of CO_2/propane ratio 22.1:1 at 600 ^oC

Reaction Time (h)	Propene Selectivity (%)	Ethene Selectivity (%)	Propane Conversion (%)	Propene Yield (%)	Ethene Yield (%)	Total olefins Yield (%)	CO Yield (%)	CO_2 Conversion (%)
0	13.6	63.1	44.0	6.0	27.7	33.7	8.3	8.6
0.5	11.3	51.1	48.3	5.5	24.7	30.2	7.5	13.4
1	10.3	50.8	49.1	5.1	24.9	30.0	7.4	14.0
2	10.3	52.2	48.2	5.0	25.2	30.1	7.4	14.3
2.5	12.6	54.2	47.5	6.0	25.8	31.7	7.3	14.4
3	12.7	53.5	46.7	5.9	25.0	30.9	7.1	14.3
5	13.9	61.3	43.1	6.0	26.4	32.4	7.4	9.4
6	12.0	58.1	44.8	5.4	26.0	31.4	7.2	11.5
7	13.7	56.6	45.2	6.2	25.6	31.8	7.0	11.5
8	10.9	56.0	45.2	4.9	25.3	30.3	6.9	11.3

Appendix 2

Table B42. 5.8% CrO/SiO_2 and 5.1% Ga_2O_3/Al_2O_3: Gas concentrations produced from propane dehydrogenation by CO_2 (at 600 ^oC)

Catalysts	Time hours	H_2 mol%	CO mol%	methane mol%	CO_2 mol%	ethene mol%	ethane mol%	propene mol%	propane mol%
C_o: (CO_2/Propane ratio: 22.9:1)					94.5				5.0
CrO/SiO_2	0	1.34	15.89	5.20	79.67	0.30	0.25	0.06	0.03
CrO/SiO_2	4	1.11	14.82	5.09	80.62	0.40	0.29	0.13	0.03
CrO/SiO_2	7	1.15	14.39	5.03	81.06	0.47	0.30	0.20	0.03
CrO/SiO_2	10	1.09	14.04	4.93	81.68	0.51	0.28	0.27	0.04
CrO/SiO_2	12	1.15	13.71	4.81	81.49	0.51	0.31	0.32	0.05
C_o: (CO_2/Propane ratio: 22.9:1)					94.5				5.1
Ga_2O_3/Al_2O_3	0	1.54	14.07	4.22	81.92	0.00	0.00	0.04	0.67
Ga_2O_3/Al_2O_3	1	1.62	14.66	4.26	81.42	0.00	0.00	0.03	0.61
Ga_2O_3/Al_2O_3	3	1.35	13.86	4.16	79.70	0.00	0.00	0.03	0.56
Ga_2O_3/Al_2O_3	4	1.19	13.81	4.19	79.73	0.00	0.00	0.03	0.53
Ga_2O_3/Al_2O_3	5	1.26	13.93	4.09	79.65	0.00	0.00	0.02	0.52

Table B43. 5.8% CrO_x/SiO_2 and 5.1% Ga_2O_3/Al_2O_3: conversion, propene selectivity and yield from CO_2 dehydrogenation of propane (at 600 ^oC)

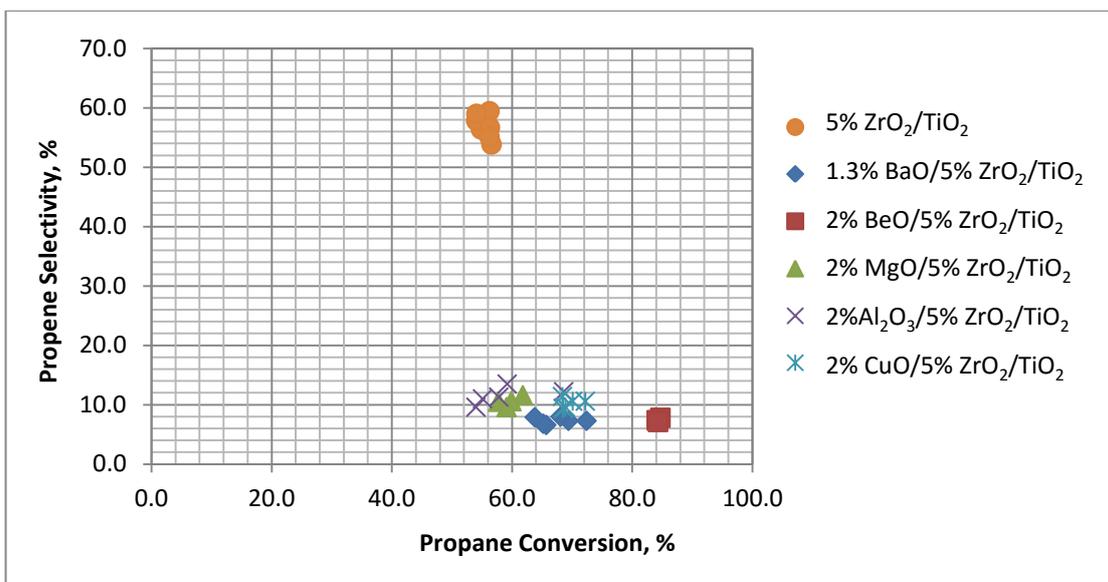| Catalysts	Reaction Time (h)	Propene Selectivity (%)	Ethene Selectivity (%)	Propane Conversion (%)	Propene Yield (%)	Ethene Yield (%)	Total olefins Yield (%)	CO Yield (%)	CO_2 Conversion (%)
CrO/SiO_2	0	1.1	6.0	99.5	1.1	6.0	7.1	16.8	15.7
CrO/SiO_2	4	2.6	8.1	99.4	2.6	8.0	10.6	15.7	14.7
CrO/SiO_2	7	4.1	9.5	99.3	4.0	9.5	13.5	15.2	14.2
CrO/SiO_2	10	5.5	10.2	99.3	5.4	10.1	15.5	14.9	13.6
CrO/SiO_2	12	6.5	10.4	99.1	6.4	10.3	16.7	14.5	13.8
Ga_2O_3/Al_2O_3	0	0.8	0.0	86.9	0.7	0.0	0.7	14.9	13.3
Ga_2O_3/Al_2O_3	1	0.7	0.0	88.0	0.6	0.0	0.6	15.5	13.8
Ga_2O_3/Al_2O_3	3	0.7	0.0	89.1	0.7	0.0	0.7	14.7	15.7
Ga_2O_3/Al_2O_3	4	0.6	0.0	89.5	0.6	0.0	0.6	14.6	15.6
Ga_2O_3/Al_2O_3	5	0.5	0.0	89.9	0.5	0.0	0.5	14.7	15.7

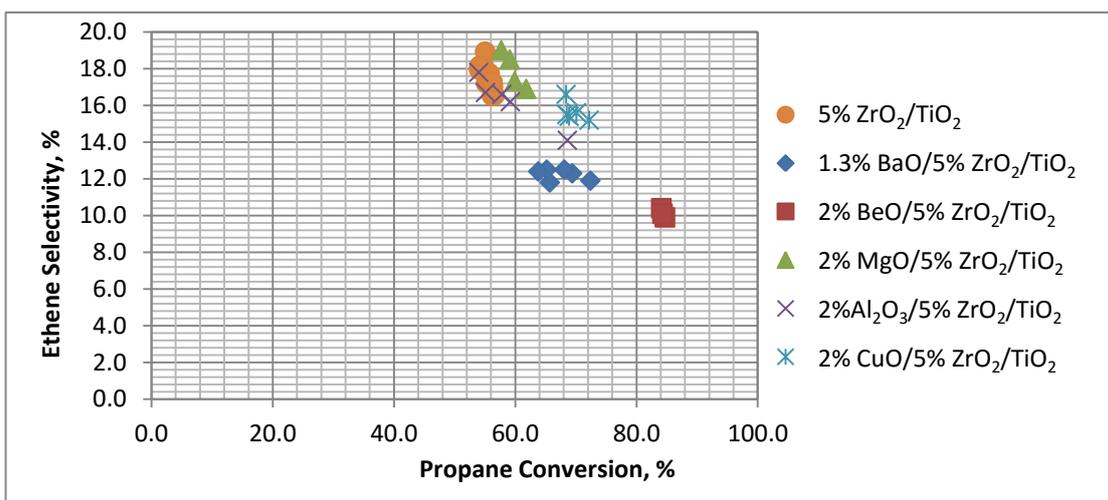Figure B1. Propene selectivity vs. propane conversion of the ternary oxides catalysts (at 600 ^{o}C)

Figure B2. Ethene selectivity vs. propane conversion of the ternary oxides catalysts (at 600 ^{o}C)
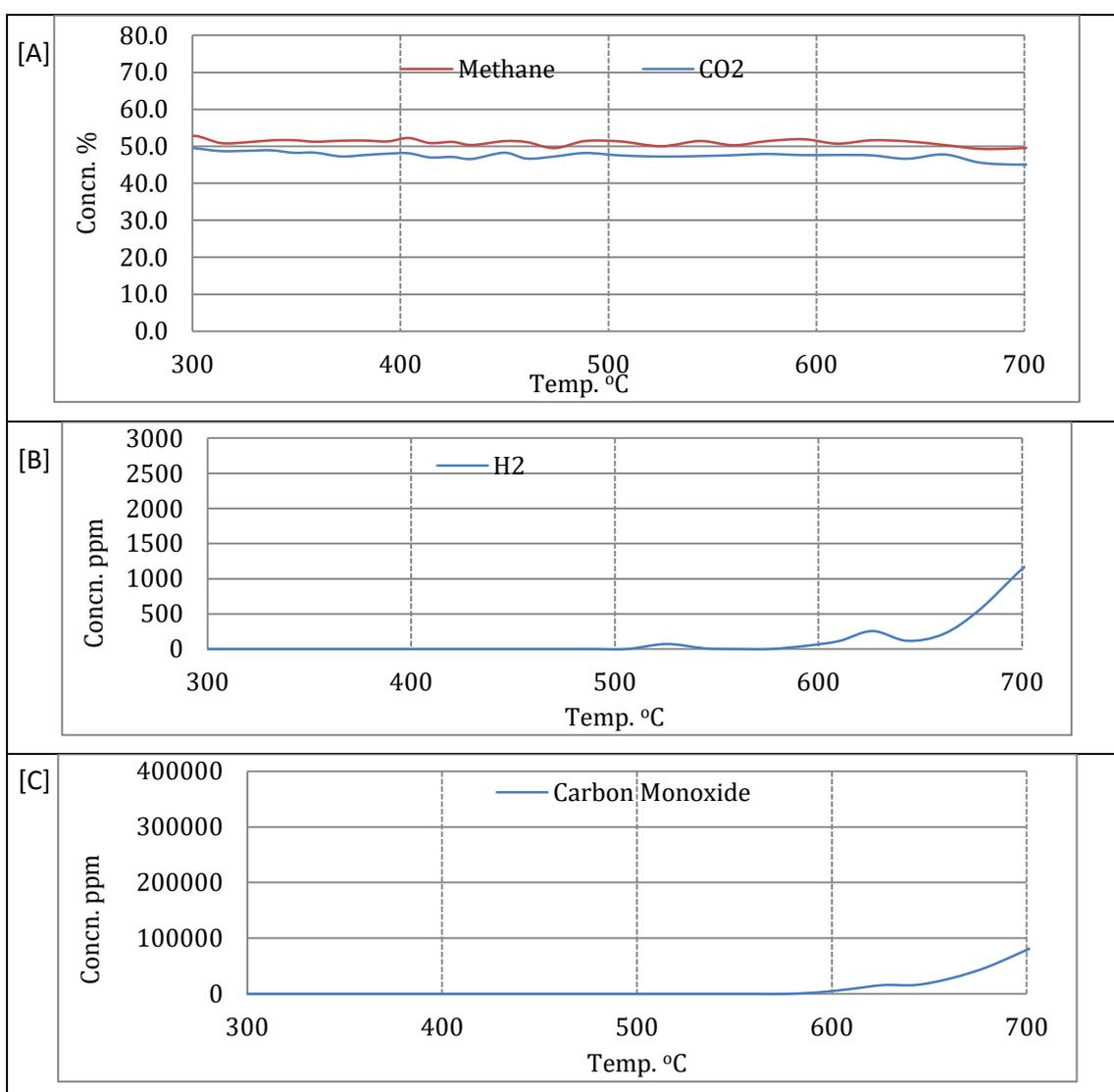
Appendix 3

Additional Results for Chapter-4

Figure C1. Reaction of CO_2 and CH_4 over catalyst 2% w/w Zr/Ti oxide made by

co-precipitation method-1 (CO_2/CH_4 1:1)
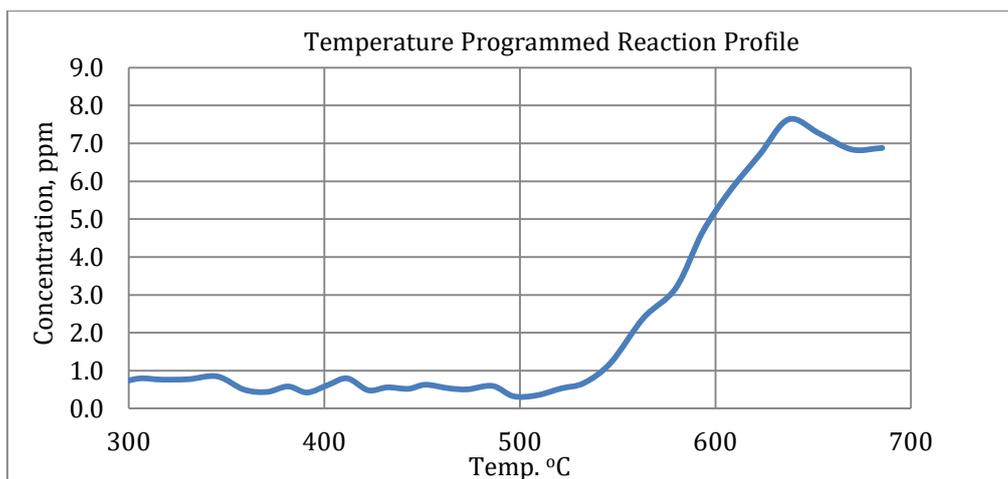
[A] Methane and CO_2 plot, [B] H_2 plot, [C] CO plot

Figure C2. Acetic acid formation over 50% w/w Zr/Ti oxide made by co-precipitation method-2, (CO_2:CH_4 1:1)

Figure C3. Acetic acid formation over 50% w/w Zr/Ti oxide made by co-precipitation method-3, (CO_2:CH_4 1:1)

Figure C4. Acetic acid formation during activity test of 50% w/w Zr/Ti oxide made by co-precipitation method-4, (CO_2:CH_4 1:1)

Figure C5. Activity test of 1% w/w Zr/Ti oxide made by impregnation method-1

$(CO_2:CH_4 \ 1:1)$: methane and CO_2 plot

Figure C6. Activity test of direct reaction of CO_2 and CH_4 on 5% w/w Zr/Ti oxide made by impregnation method-1 (CO_2:CH_4 1:1)

[A] CH_4 and H_2 plot, [B] CO_2 and CO plot, [C] methane and CO_2 plot

Figure C7. Activity test of direct reaction of CO_2 and CH_4 on 5% w/w Zr/Ti oxide made by impregnation method-2, (CO_2:CH_4 1:1)

[A] acetic acid plot, [C] H_2 plot

Figure C8. The comparison plots of ternary oxide of 2% w/w Al/ 5% w/w Zr/Ti
(CO_2:CH_4 1:1) [A] acetic acid and H_2 plot, [B] methane and H_2 plot

Figure C9. The comparison plots for ternary oxide of 3.4% w/w Co/ 5% w/w Zr/Ti
(CO_2:CH_4 1:1)

Figure C10. Overlay diagram of acetic acid of m/z 60 and the formation acetic acid and H_2 vs. reaction time over ternary oxide of 4% w/w Cu 5% w/w Zr/Ti catalyst (CO_2:CH_4 1:1)

Figure C11. The overlay diagram of acetic acid, ethane and ethylene formation at gas ratio CO_2/CH_4 1:9 on 5% w/w Zr/Ti oxide catalyst
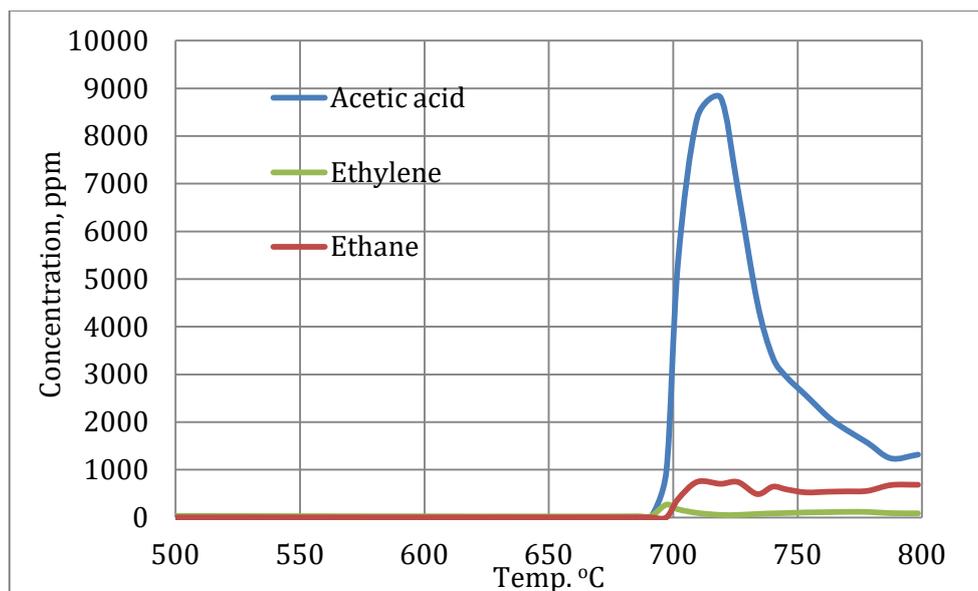
Figure C12. The overlay diagram of acetic acid, ethane and ethylene formation at gas ratio CO_2/CH_4 9:1 on 5% w/w Zr/Ti oxide catalyst
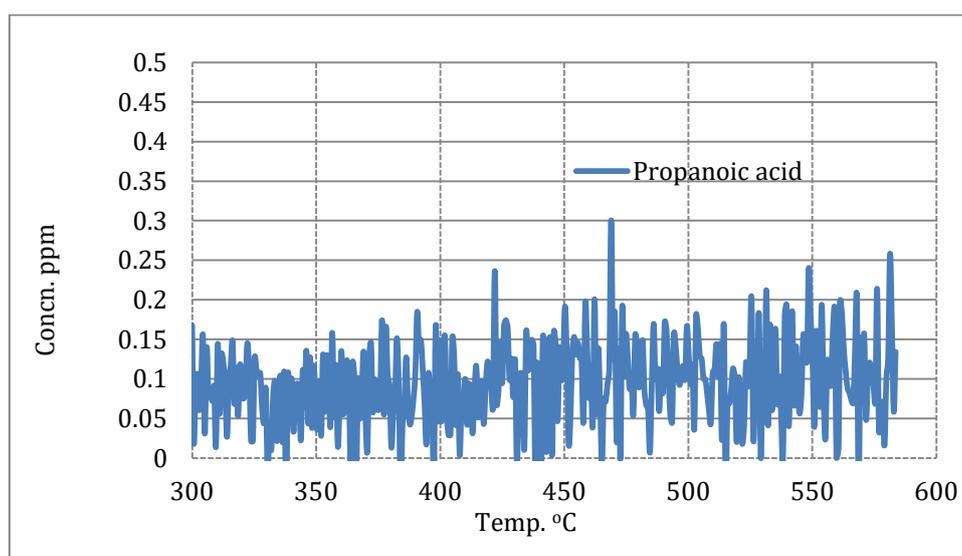

Figure C13. No detection of propanoic acid (CH_3CH_2COOH) from the direct reaction of ethane with CO_2 on 5% w/w Zr/Ti oxide catalyst (CO_2/ethane 1:1).
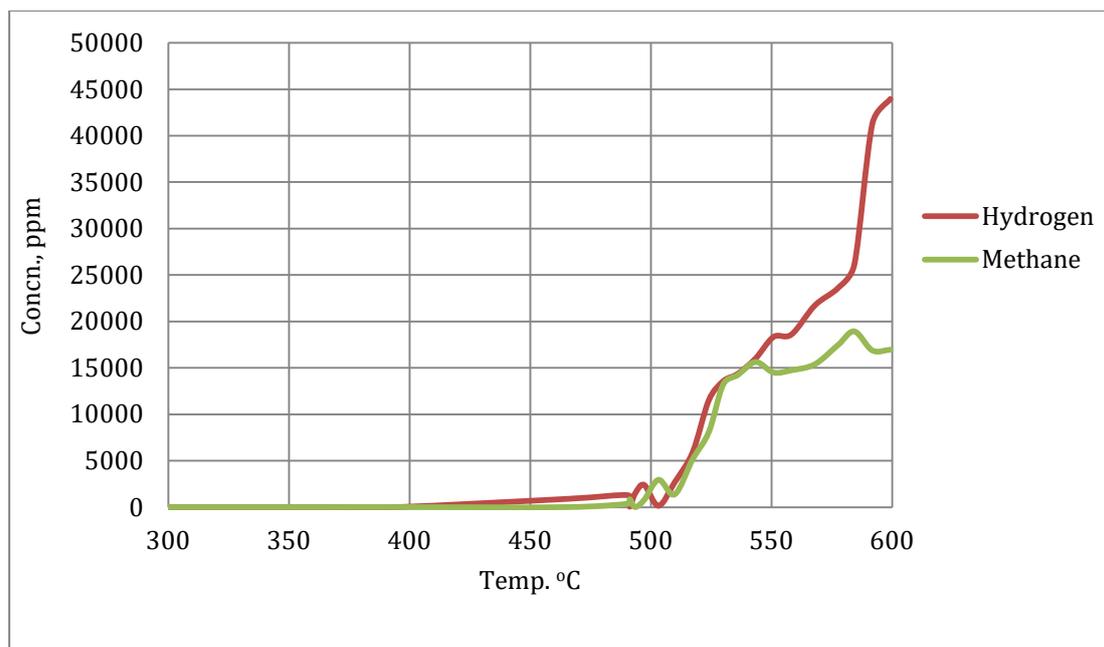
Appendix 3

Figure C14. Activity test of CO_2 with ethane was shown methane and H_2 made at the same temperature of the acetic acid formation on 5% w/w Zr/Ti oxide catalyst (CO_2/ethane 1:1).
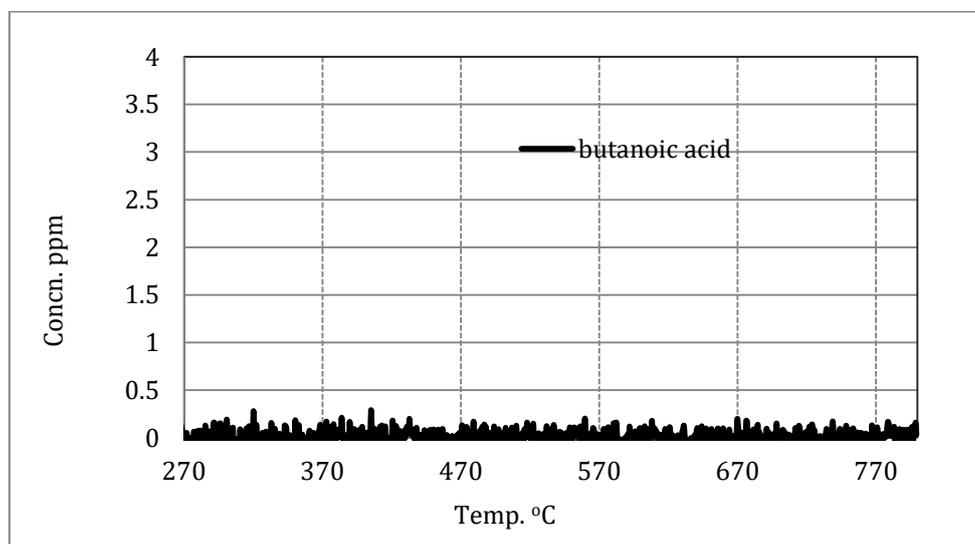

Figure C15. No detection of butanoic acid ($CH_3CH_3CH_2COOH$) from the direct reaction of propane with CO_2 on 5% w/w Zr/Ti oxide catalyst (CO_2/propane 1:1).